# Temporal variability of meltwater and sediment transfer dynamics at an Arctic glacier, Storglaciären, northern Sweden

by

Richard David Gravelle

A Doctoral Thesis

submitted in partial fulfillment of the requirements for the award of

Doctor of Philosophy of Loughborough University

December 2013

# *Abstract*

In glacierised regions, suspended sediment fluxes are highly responsive to climate-driven environmental change and can provide important information regarding the relationships between glacier variations, climate and geomorphic change. As a result, understanding patterns of suspended sediment transport and their relationship with meltwater delivery is of critical importance. However, studies of glacial suspended sediment transport are often limited by interpreting patterns of suspended sediment transfer based on whole-season data, allowing precise patterns to become masked. This thesis aims to contribute to the understanding of suspended sediment transfer in glacierised basins through the investigation of patterns of suspended sediment delivery to the proglacial area of Storglaciären, a small polythermal valley glacier located in the Tarfala valley, Arctic Sweden. High temporal resolution discharge and suspended sediment concentration data were collected during two summer field campaigns at Storglaciären. Interpretations of suspended sediment transport data were made using diurnal hysteresis and sediment availability data, combined with suspended sediment 'shape' and 'magnitude' data classified by applying principal component and hierarchical cluster analyses. Analysis of the dominant discharge generating processes at Storglaciären was also conducted using principal component analysis, allowing patterns of discharge to be better understood. This was complemented by analysis of the structure and evolution of the glacier drainage system by linear reservoir modelling and flow recession analysis. The results suggest that patterns of discharge and suspended sediment transport at Storglaciären are complex, with distinct processes and magnitudes of transport evident at both proglacial outlet streams, Nordjåkk and Sydjåkk. These processes are intrinsically linked to meteorological variables, with both ablation-driven and precipitation-driven discharge exerting influence over patterns of suspended sediment transport in the proglacial area of Storglaciären.

# *Acknowledgements*

Firstly I would like to thank my supervisors, Dr. Richard Hodgkins and Professor Steve Rice. I am extremely grateful for the continued advice and support you have given me during this study and for always being available to answer my questions. Thank you also to my director of research, Dr. David Ryves for your guidance and insightful comments.

The help of support staff at Loughborough University Department of Geography has been invaluable during this study, and thanks are therefore due to Stuart Ashby, Barry Kenny, Fengjuan Xiao and Mark Szegner.

I have been fortunate to be part of a great group of postgraduate students during my time at Loughborough. Whilst there are too many names to mention here, I would like to specifically thank Jonathan Lewis, Matthew Johnson, Sally Little, Tom Matthews and Joseph Pomeroy.

Nick Martin from SonTek/YSI has been a great help and source of information regarding the Argonaut-SL H-ADCPs used in this study and always happy to offer advice whether equipment or software based.

The Tarfala Research Station has been a very welcoming field base in my two seasons there, and I gratefully thank Peter Jansson, Ninis Rosqvist, Henrik Törnberg, Andreas Bergström and Torbjörn Bergelv for their generosity and for logistical support. Peter Jansson also kindly provided discharge data from the Rännan and Lillsjön gauging stations, meteorological data from Tarfala, and time-lapse photographs of Storglaciären.

No field based study can be completed without the help of field assistants, and this study is no exception! Many thanks are therefore due to Tom Matthews, Alessio Gusmeroli, Adam Booth, Joseph Pomeroy, Stuart Cameron, Alex Wilmore, Ylva Sjöberg, Mattias Lindh, and Andrea Rücker.

This project was supported by a Loughborough University Faculty Development Studentship. Additional funding was gratefully received from the Royal Geographical Society, the Dudley Stamp Memorial Fund, the John Guest Phillips Memorial Travelling Scholarship, and the British Society for Geomorphology.

Finally, thank you to my wife Gina to whom I owe so much.

# *Table of Contents*

# *List of Tables*

# *List of Figures*

*Chapter 1*

# Introduction and Context

## 1.1. Introduction

The rapid change in the energy balance at the Earth's surface during the last century that has resulted in increased global temperatures has been correlated to a significant thinning, mass loss and retreat of the world's glaciers (Haeberli *et al*., 2000; Oerlemans, 2000). The perennial ice of glaciers is an important part of the water cycle in cold regions and their downstream river catchments. It represents a storage component with strong effects on river discharge and fresh water supply. As populations within or in proximity to glaciated basins continue to rise, glacier hydrology increasingly has important implications for water resource management (Carrivick and Brewer, 2004). For instance, up to 2 billion people living downstream of the Himalayas, the European Alps and the Cordilleran mountain chains of the Americas depend on snow- and ice-fed rivers for subsistence, power and livelihoods (Blyth *et al*., 2002). Therefore, the need to understand processes and change in snow- and ice-fed river basins is of key importance.

Glacial meltwater is also an important medium for sediment transport. For example, during the last 100,000 years, 25% of all oceanic sedimentation has occurred in glacier-fed fjords (Syvitski, 1991), despite glaciers accounting for only about 10% of total land surface cover. Sediment fluxes are difficult to predict, because of the variable effects of sediment storage and release, but further glacial retreat is likely to increase their volatility. Such changes will result in reduced river channel capacity through deposition, increased flood risk and influencing landscape change. Furthermore, negative impacts are likely to be observed in river ecology and the transfer of sediment and nutrients to oceanic margins. Snow- and ice-fed river systems are typical of high altitudes and high latitudes,

and are generally characterised by major seasonal and diurnal discharge variability, steep gradients and high hydraulic roughness. Given the efficacy of mechanical denudation in mountain environments and the ready availability of stored, finely-comminuted sediment at the margins of retreating ice masses, fluvial sediment is an important environmental parameter. For example, suspended sediment can impact on water and habitat quality via its influence on light transmission in the water column, and through deposition on river bed gravels, negatively affecting fish spawning. Sedimentation may also reduce channel capacity and exacerbate flood risks. Aside from the general delivery of sediment to the continental margins, sediment-associated transport also dominates the flux of many nutrients and contaminants to the oceans. Suspended sediment fluxes are also highly responsive to climate-driven environmental change and provide important information regarding the relationships between glacier variations, climate and geomorphic change (Hodgkins *et al.,* 2003). As a result, the significance of meltwater as a control on sediment transport and patterns of suspended sediment delivery is of great interest not only to glaciologists and hydrologists, but also to policy makers with regards to sea level rise and potential anthropogenic impacts. Whilst it is therefore imperative that drainage and sediment transport from non-temperate glaciers are better understood, studies of subglacial suspended sediment transfer (e.g. Hodson and Ferguson, 1999; Swift *et al*., 2002; 2005) typically interpret patterns of suspended sediment transfer based on whole-season data. Particularly in Arctic catchments, where significant contributions to the total suspended sediment yield are made from ice-marginal sources, this approach can lead to precise patterns of suspended sediment transport becoming 'smothered' by analyses on a coarse temporal scale (Irvine-Fynn *et al*., 2005a). A number of recent studies (e.g. Orwin and Smart, 2004; Irvine-Fynn *et al*., 2005a) have employed statistical methodologies in an attempt to 'break-down' the complexities of subglacial suspended sediment transfer, and this study aims to utilise similar techniques to assess detailed changes in patterns of suspended sediment delivery to the proglacial area of a relatively low-latitude Arctic glacier.

The following sections represent the conceptual transit of meltwater through the

glacial drainage system from ice surface to the subglacial environment to provide a background for the study.

## 1.2. Glacial Meltwater Generation

The hydrology of glacierised catchments differs from that of non-glacierised catchments due to the presence of snow and ice, and the lack of vegetation and soil cover (Willis, 2005). Whereas rainfall provides the dominant water input in non-glacierised areas, snow and ice melt are key contributors to the hydrology of non-glacierised areas (Röthlisberger and Lang, 1987; Chen and Ohmura, 1990). Understanding the effects of glaciers on catchment hydrology is of key theoretical and practical importance (Østrem, 1973; Fountain and Tangborn, 1985). It is therefore, the aim of this review to expand the complex nature of catchment hydrology in order to more fully understand the influential nature of glaciers in the hydrological cycle.

### 1.2.1. Energy Balance

Glacierised basins have relatively abundant meltwater sources, and the quantity of melt produced is limited only by the available energy (Fountain and Tangborn, 1985; Röthlisberger and Lang, 1987). However, the hydrometeorological and glaciological processes that control the production of meltwater are highly complex. The quantity of water made available by glacier melt is a function of variations in atmospheric conditions, and the energy balance at the glacier surface (Hock, 2005). Such conditions are extremely influential in this respect, controlling the intensity of surface runoff from ice and snowmelt, the intensity and physical state of precipitation and ultimately, yearly changes in glacier mass balance (Rutter, 2002). However, there are a number of individual physical processes which cause ablation to occur, making glacier-atmosphere interactions complex (Hock, 2005). Melting of ice and snow is calculated by assessing energy fluxes to and from a glacier surface. For this purpose, energy balance is commonly

calculated in melt models (e.g. Richards *et al*., 1996; Hock, 2005). The energy balance at a glacier surface can be expressed as:

$$Q_N + Q_H + Q_L + Q_G + Q_R = Q_M \quad (1.1)$$

where: $Q_N$ = net radiation; $Q_H$ = sensible heat flux; $Q_L$ = latent heat flux; $Q_G$ = ground heat flux; $Q_R$ = sensible heat flux supplied as rain; and $Q_M$ = energy consumed as melt (Oerlemans, 2000; Hock, 2005; Andreassen *et al*., 2008). The relative importance of each energy component varies over time and depending on location (Paterson, 1994; Hock, 2005), although it has been suggested (Munro and Young, 1982; Willis and Bonvin, 1995) that the energy available for ice melt in a glacierised basin is derived primarily from net radiation and sensible heat transfer. However, Sawada and Johnson (2000) observed that variations in air temperature were more strongly correlated to variations in discharge than net radiation during a period of study at the Slims River, Yukon. Sawada and Johnson also noted however, that during this study, neither net radiation or air temperature were strongly correlated to seasonal discharge variations.

The energy balance at a glacier surface is also influenced by surface albedo, particularly given the suggested importance of radiation inputs. Albedo is defined as the average reflectivity of a surface over a spectrum of between 0.35 and 2.8 μm (Jonsell *et al*., 2003; Hock, 2005). Glacier surfaces typically exhibit an albedo of between <0.1 for sediment-rich 'dirty' snow or ice, to >0.9 for fresh snow (Brock *et al*., 2000; Hock, 2005), although albedo varies spatially and temporally over a surface (Jonsell *et al*., 2003). Controls on changes in albedo can be largely divided into two categories: firstly, processes related to surface layer characteristics (e.g. grain size, surface roughness); secondly, processes related to radiation and atmospheric factors (e.g. wavelength) (Jonsell *et al*., 2003). Van de Wal *et al*. (1992) in a study of albedo at Hintereisferner, Austria, found that spatial differences in ablation correlated significantly with variations in albedo.

From the energy available at the glacier surface-air interface, melt rates can be calculated by:

$$M = \frac{Q_M}{\rho_W L_f} \quad (1.2)$$

where: $\rho_W$ = water density; and $L_f$ = latent heat of fusion (Hock, 2005; Andreassen *et al*., 2008).

### 1.2.2. Mass Balance

Glacier mass balance is concerned with changes in glacier mass through net input and output of ice (Braithwaite, 2002). Typically, mass balance is measured in yearly intervals, providing a spatial and temporal record of mass change (Paterson, 1994). The mass balance of a glacier is controlled by two processes not directly related to one another (Huss *et al*., 2008): accumulation as a result of snowfall; and ablation as a result of surface melting and, in some cases, terminal calving (Braithwaite, 2002). The annual mass balance of a glacier is therefore defined by the difference between accumulation and ablation over the period of a year. A glacier experiencing a great amount of accumulation and little ablation is described as having a positive mass balance. Conversely, a glacier experiencing little accumulation and high levels of ablation is described as having a negative mass balance. A glacier with no differences between accumulation and ablation is said to be in equilibrium.

Although annual mass balance can be calculated simply, a greater understanding of spatial and temporal variability of accumulation and ablation can be observed by calculating the net mass balance (Dyurgerov and Meier, 1999). Net mass balance is a function of two seasonal mass changes: winter balance and summer balance (Braithwaite, 2002). The winter balance is the net change in glacier mass between autumn and spring, and mainly consists of snow accumulation. Summer balance is the net change in mass between consecutive years, and consists mainly of snow and ice ablation.

Measurements of glacier mass balance can be achieved both directly and indirectly (Barry, 2006). Direct methods of mass balance calculation typically involve glaciological techniques, using snow pits and ablation stakes on a glacier surface as

a simple means to determine variations in surface thickness over the course of the measurement period. However, these techniques are not without drawbacks. Changes in surface ice thickness assumes an ice density of 900 kg $m^{-3}$ (Braithwaite, 2002), and snow covered surfaces require additional measurement of snow density to be obtained (Braithwaite, 2002). Indirect methods of calculating mass balance may include geodetic and photogrammetric, or hydrological methods. Haakensen (1986) found that a correlation between cumulative mass balance and glacier volume change could be observed by comparing maps of Hellstugubreen, Norway between 1968 and 1980. However, a similar study by Østrem and Haakensen (1999) shows that a comparison between maps of Ålfotbreen, Norway from 1968 to 1988, and traditional directly measured mass balance during the same period has significant discrepancies. Whereas the mass balance calculated from maps indicates a mass loss of 5.8 m water equivalent (w.e.), traditionally measured mass balance indicates a mass gain of 3.4 m w.e. over the study period. The hydrological method of mass balance analysis involves the calculation of the glacier water balance, making it the least direct of the three methods (Tangborn *et al*., 1975). The water balance of a glacier can be expressed as:

$$P(l) - E(l) - R(l) + F(il) = B(l) \qquad (1.3)$$

where $P$ = precipitation; $E$ = net evaporation and/or condensation; $R$ = net runoff (defined as the difference between outflow and inflow); $F$ = the melting of ice and snow; $B$ = the liquid water balance; ($l$) = liquid water; and ($il$) = changes from ice to liquid water (Tangborn *et al*., 1975). In order to calculate mass balance using this method, the above parameters must be measured for the glacier drainage basin as a whole.

### 1.2.3. Glacier Water Storage

Prediction of the rate and quantity of water flow through glaciers is complicated by a number of different hydrological processes (Fountain, 1996). This includes

the initiation of 'temporary storage' (Theakstone and Knudson, 1981) which helps to maintain river levels during periods of low meltwater production. A number of authors have described modes of water storage within glaciers (Theakstone and Knudsen, 1981; Collins, 1982; Östling and Hooke, 1986; Hodgkins, 2001; Jansson *et al*., 2003). However, the term glacier storage is widely and loosely used to describe a number of glaciological and hydrological processes over varying temporal scales (Jansson *et al*., 2003). Studies of glacier storage have often been associated with seasonal variations in the delay of runoff by glaciers (Tangborn *et al*., 1975; Collins, 1982; Chen and Ohmura, 1990). Nonetheless, it should be considered that glacier ice itself is a form of storage (Jansson *et al*., 2003) given that glacier ice accounts for ~ 75% of the Earth's available freshwater (IPCC, 1996; 2001). However, as well as water in solid state (i.e. ice), glaciers are also effective stores of liquid water. Collins (1982) suggests a number of ways and locations in which this occurs including, for instance, surface snow, supraglacial pools, within crevasses and englacial conduits, and at the ice-bed interface. Jansson *et al*. (2003) subdivide such sources of storage into three general storage time-scales: long-term storage; intermediate-term storage; and short-term storage, each having a different influence on catchment hydrology.

The amount of water stored by glaciers can be defined as the difference between water input by surface melting and precipitation, and water output by discharge (Hodgkins, 2001). However, the exact residence time of glacially stored water can range from hours to thousands of years, depending on the size and type of glacier, the location of the glacier, and the season during which precipitation occurred (Fountain and Tangborn, 1985). Storage of water by glaciers can generally be attributed to greater water inputs than the glacier drainage system is able to transmit (Jansson *et al*., 2003), for instance during high precipitation events, or during the beginning of the melt season when the glacial drainage system is under developed. This water can then be released during the later stages of the melt season, although some may also be released during the winter (Jansson *et al*., 2003). Such is the seasonal variation in glacier storage, many of the studies relating to this area have focused on seasonal patterns of storage and release of water. For instance, Östling and Hooke (1986) observed that in Storglaciären,

Northern Sweden, storage of water began in May, and lasted until July, when net loss started. Storglaciären exhibited a positive net storage balance during the period of storage, suggesting that release of water during the winter months was required to balance summer storage. Östling and Hooke calculated that ~0.2 x $10^6$ $m^3$ of water remained in storage at the end of the melt season, based on discharges from the proglacial streams Nordjåkk and Sydjåkk which drain from Storglaciären, and have been observed to flow in winter (Östling and Hooke, 1986; Jansson *et al*., 2003). Hodgkins (1997) and Hodgkins *et al*. (1999) provide evidence for over-winter water storage in Scott Turnerbreen, Svalbard, where water collects and freezes in ice-marginal drainage channels, contributing to proglacial icing. It is suggested (Hodgkins, 1999) that this occurs as a result of the glacier drainage system not adjusting (or being unable to adjust) rapidly enough to cope with the volume of meltwater transmitted towards the end of the melt season. Given that Scott Turnerbreen is an entirely non-temperate glacier, and is frozen to its bed (Hodgkins 1997; 1999; Hodgkins *et al*., 1999), the lack of subglacial drainage may increase the potential for over-winter storage, with release occurring during the following melt season. Water storage, and subsequent release by glaciers contributes to seasonal and annual variations in discharge. However, the processes which control the rate of meltwater production, and hence, release from storage are complex.

### 1.2.4. Proglacial Runoff

Proglacial fluvial systems receive water from a variety of sources, and vary in discharge over a range of frequencies and magnitudes (Marren, 2005). Primarily, discharge in proglacial rivers is the product of supraglacial runoff, runoff redirected through englacial and subglacial systems, and in some cases, groundwater (Röthlisberger and Lang, 1987). However, precipitation and downstream tributary inputs also have a significant role (Marren, 2005). Brabets *et al*. (2004) observed that of the 2001 water year runoff for the glacially fed Tlikakila River, Alaska, 86% was attributable to either ice or snow melt. In comparison, only 14% was attributable to rainfall runoff, and 1% to groundwater.

The nature of these components means that discharge in rivers draining glaciers is mainly driven by the diurnal temperature cycle, which also controls rates of meltwater production (Lang, 1967; Hannah and Gurnell, 2001). Lawler *et al*. (2003) also observed that glacier-fed river discharges in two southern Icelandic catchments increased in January over a 20 year study period. These increases are consistent with increases in local daily mean air temperatures observed during the study period. Similarly, decreased daily mean air temperatures during March and April correlate strongly with lowered spring discharges at the same catchments (Lawler *et al*., 2003). However, Hannah *et al*. (1999) observed during the 1996 melt season at Taillon Glacier, France, that a typical melt season trend in proglacial discharge did not occur, most likely due to a lack of climatic variation. It is suggested that persisting snow cover may have been a factor in the occurrence of sub-seasonal streamflow variations, although frequent, heavy rainfall events are also considered (Hannah *et al*., 1999).

## 1.3. Glacial Drainage System Structure

The ability to quantify the movement of water through glaciers is fundamental to several critical issues in glaciology. Both the spatial distribution and the rate of infiltration of water through the glacial system control glacier dynamics, water storage, glacier-induced flooding, and the prediction of runoff from glacierised drainage basins (Fountain and Walder, 1998; Fountain *et al*., 2005). Understanding the outflow hydrograph of a glacier can facilitate resource planning in areas dependent on glacial meltwater for consumption, agricultural irrigation, and hydropower. Having discussed the generation of meltwater at the glacier surface in Section 1.2, this section outlines the routing of meltwater from the glacier surface to the subglacial drainage system.

### 1.3.1. Supraglacial Drainage

Supraglacial water is derived principally from surface melt and precipitation, although it can be supplemented by spillover of water from crevasses or moulins, or by the frictional melting of existing supraglacial channel walls through stream action (Marston, 1983). Furthermore, supraglacial drainage can be supplemented by the release of water from supraglacial storage, such as the seasonal snowpack, and firn layers. The rate at which runoff from a glacier occurs can depend largely on surface cover, particularly whether the surface is snow-covered, firn-covered or ice covered. Each of these media have differing hydrological properties, and changes in any of these surfaces can impact melt rates and runoff rates (de Woul *et al*., 2006).

#### 1.3.1.1. Snow and Firn Drainage

The significance of glacier snowpacks is such that the seasonal removal or decay of snowpack results in the evolution of meltwater sources and pathways (Willis *et al*., 2002; Swift *et al*., 2005) as water is able to drain into the glacier body. Similarly, studies of snow hydrology in non-glacial environments suggest that snow dampens and delays the passage of diurnal meltwater within catchments (Colbeck, 1972; Campbell *et al*., 2006). The rate of water flow through a snowpack is largely determined by snow grain size, pressure and snow permeability (Marsh, 2005). In the case of permeability, ice layers within the snow can have a strong impact on water flow rates (Marsh and Woo, 1984; Campbell *et al*., 2006). Such layers can prevent water from flowing vertically, resulting in areas of water ponding, and the initiation of lateral water flow (Fountain, 1996). This continues until a gap in the ice layer is found, and water flow downwards can continue (Colbeck, 1973). On reaching the bottom of a snowpack, water can continue to follow the same flow pathways as water on a non-snow covered surface (e.g. overland flow, open channel flow etc.). On snow-covered ice, the presence of snow greatly decreases the rate at which water can flow, compared with that of flow over bare ice surfaces (Fountain, 1996). As in snowpack percolation, the rate of water flow is

determined, not only by the vertical transit time through the snow, but also the lateral transit time to the nearest crevasse or moulin. Willis *et al*., (2002) propose from the results of a surface melt model based on data from Haut Glacier d'Arolla, Switzerland, that the removal of supraglacial snow not only increases peak diurnal discharges at catchment outlets, but also reduces minimum diurnal discharges entering the glacier system through moulins. This corresponds to the suggestion that the thickness of a snowpack may determine the timing of the 'spring event', a period of enhanced subglacial water pressure resulting from an influx of early-season melt water into the subglacial drainage system, and responsible for glacial uplift and increased ice velocity (Röthlisberger and Lang, 1987; Nienow, 1997; Campbell *et al*., 2006).

Following percolation through the snowpack, water then encounters the firn layer (Fountain, 1996), a metamorphic transition between snow and glacier ice. The term firn is applied generally to partially compacted, wetted snow, which has survived at least one melt season (de Woul *et al*., 2006). Firn is found abundantly in the accumulation area of a glacier, where ice is often overlain by several tens of metres of firn (Fountain, 1989; Fountain and Walder, 1998; de Woul *et al*., 2006). Firn layers are known to significantly delay water transport by temporarily storing water in the firn aquifer (de Woul *et al*., 2006), a zone of water saturation situated above the impermeable ice-firn transition. The rate of water flow through the firm aquifer depends largely on the thickness of the saturated layer, and the effective porosity of the firn (Fountain, 1996). Fountain (1989) found that ~11 cm of water was stored within the firn layer of South Cascade Glacier, USA, averaged across the accumulation area as a whole ($1.78 \times 10^5$ m$^3$). In comparison with Tangborn *et al*.'s (1975) study at South Cascade Glacier, this volume of water represents approximately 12% of the total spring water storage (Fountain, 1996).

#### 1.3.1.2. Supraglacial Channelised Drainage

At the end of the melt season, the surface of a glacier consists of ice in the lower ablation area, and snow and firn at higher elevations in the accumulation area (Fountain and Walder, 1998). On the bare ice of a glacier surface, surface meltwater and rainfall are able to flow across the ice surface (Fountain, 1996). This water can be redirected into the body of the glacier as it is intercepted by crevasses or moulins (Stenborg, 1973). The limitation of storage sites, combined with a lack of potential obstructions (e.g. snowpack) means that water is able to flow rapidly across bare ice, increasing the rate of runoff (Fountain, 1992; 1996). Where this type of overland flow occurs, and the rate of down cutting by supraglacial water exceeds surface ablation, this water will typically carve a supraglacial stream channel (Marston, 1983). Supraglacial channels have been studied and reviewed both in Norway (Hambrey, 1977; Knighton, 1981; Knighton, 1985) and Alaska (Marston, 1983) and are reported to evolve in a similar manner to alluvial channels, but just over a much more rapid timeframe with incision occurring at rates in excess of the seasonal ablation rate. The persistence and stability of supraglacial channels over several decades on non-temperate glaciers is readily explained by the greater volumes of supraglacially routed runoff which results in high rates of channel incision compared to ice surface ablation, and the low rates of ice creep ensure channel forms are not subject to lateral closure during the winter months (Irvine-Fynn, 2008).

### 1.3.2. Supraglacial-Englacial Interface

In temperate and polythermal glaciers, precipitation and surface runoff reach the englacial drainage system through drainage structures such as crevasses and moulins (Fountain and Walder, 1998). These structures form the interface between the supraglacial and englacial drainage systems, and are critical in routing water into the glacier, particularly in temperate glaciers where the majority of runoff is derived from meltwater generated at the glacier surface (Nienow *et al*., 1998).

Shreve (1972) theorised the onset of englacial drainage through percolation of surface meltwater through permeable, temperate ice based on a study by Nye and Frank (1973). This study suggested a network of water-filled passages (~ 1 cm in diameter) occurring along three-grain intersections in polycrystalline ice under hydrostatic stress. However, a number of studies suggest that the amount of water drained through this network is likely to be negligible, due to the passages being too small for water to effectively pass through (Raymond and Harrison, 1975), and to water passages becoming blocked by air bubbles (Lliboutry, 1971). Lliboutry (1996) also suggested that the permeability of near surface ice may be lower than englacial ice, and may therefore hinder drainage via this method. This is also true of polythermal glaciers exhibiting a cold-surface layer, which acts as an 'aquiclude' (Hodgkins, 1997) and prevents water percolation through the surface layer into temperate ice beneath. In the absence of percolation, the most efficient means for water to enter the englacial system is through larger drainage structures, such as moulins or crevasses (Figure 1.1).

#### 1.3.2.1. Moulins

The term moulin (or glacial mill; Stenborg, 1968) refers to a single vertical, cylindrical shaft which penetrates into a glacier, connecting the glacial surface with the englacial drainage system. Stenborg (1968) investigating the internal drainage of Storglaciären and Mikkaglaciären, Sweden, suggested that the formation of moulins is dependent on two conditions being fulfilled. Firstly, sufficient meltwater must be produced at the glacier surface to enable meltwater and precipitation to collect and form surface rills. Secondly, there must be opportunity for surface water to penetrate into the ice, often via crevasses. Holmlund (1988a) supports this theory, and concludes that on Storglaciären, both of Stenborg's (1968) conditions for moulin formation are fulfilled. However, Holmlund (1988b) also concluded that the likelihood of moulin formation is enhanced by the presence of an impermeable cold surface layer, which prevents water from entering the glacier by percolation as suggested by Shreve (1972).

Despite this limitation, water is still able to access the englacial drainage system through crevasses. When these crevasses close, water flowing into them is able to keep a channel open, thus maintaining the connection to the englacial drainage system, and forming a moulin (Holmlund and Hooke 1983). This does suggest however that inputs into the englacial drainage system are restricted to areas of the glacier where high extending strain rates occur near the surface, and hence where crevasses are able to form (Holmlund, 1988b).

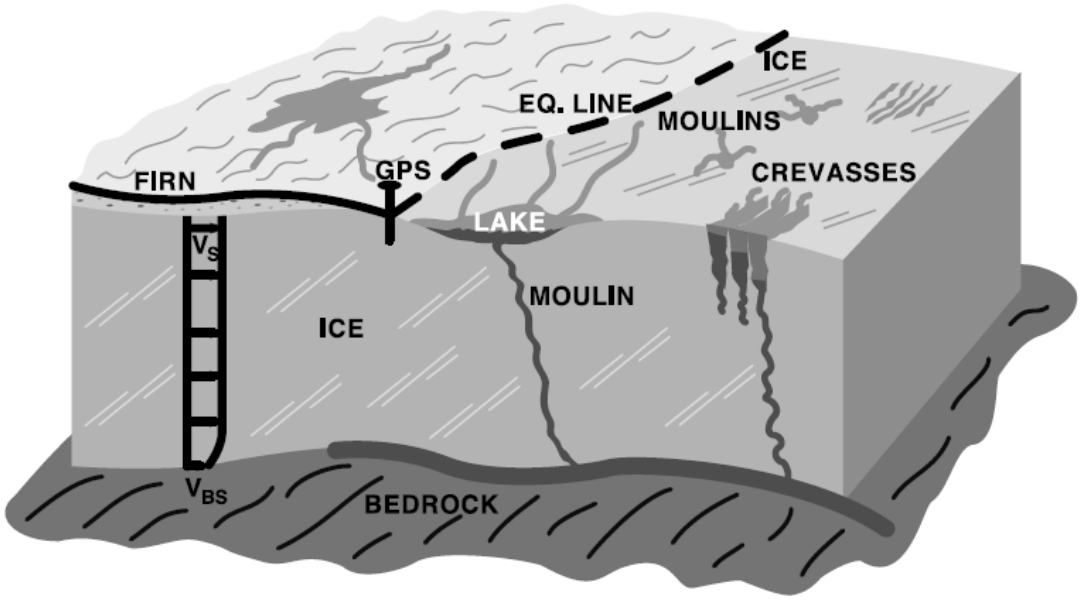


**Figure 1.1. Diagrammatic representation of the influence of moulins and crevasses in routing water to the bed of the Greenland Ice Sheet (Zwally *et al.*, 2002)**

Observations of the internal geometry or structure of moulins are rare, and where they do exist, often lack detail. Dewart (1966) described moulins on Kaskawulsh Glacier, Yukon Territory as vertical shafts with prominent shelves at approximately 20 m depth. Although corkscrew shaped moulins were also mentioned, these were thought to be less common than moulins with vertical passageways. Speleological exploration of a number of moulins during the winter season by Holmlund (1988b) allowed the internal structure of the moulins on Storglaciären to be observed and mapped. These descents into the glacier showed that the first 25 – 30 m of each moulin consisted of a straight, vertical shaft. Below this level, the responsiveness of temperate ice has a greater influence on the

geometry and width of the moulins. The moulins mapped ended (or became inaccessible to further exploration) around 40 m in depth, and in shafts with a shallower angle, frequently contained a plunge pool. From this point on, the moulins are drained by a downward dipping channel (between 0 and 45°), following the direction of the original crevasse. These conduits meander with an amplitude of 1 – 1.5 m, suggesting that during the melt season, meltwater in the conduit flowed at high velocity, and with a Froude number in excess of unity (Holmlund, 1988b).

Recent studies have linked moulins to an acceleration mechanism of glaciers and ice sheets, whereby meltwater that reaches the glacier bed has a lubricating effect. The theory of subglacial water lubrication was first presented by Weertman (1969) who suggested that the initiation of glacier surges occurs when subglacial water becomes deep enough to 'drown' bed obstacles which hinder sliding. This phenomena has since been linked with the rapid demise of the Laurentide Ice Sheet circa 10,000 years ago, during a period of increased surface melting. More recently, Zwally *et al*. (2002) observed a correlation between surface ice melt intensity and changes in ice velocity on the western Greenland Ice Sheet, and suggested that water draining to the bed of the ice sheet via moulins may induce acceleration near the ice sheet equilibrium zone.

#### 1.3.2.2. Crevasses

The importance of crevasses in the supraglacial-englacial drainage interface has been demonstrated in their role in moulin formation. However, it has also been suggested that crevasses are able to transmit large volumes of water from the surface to the bed of glaciers through the phenomena of fracture propagation. Crevasses form according to the principles of fracture mechanics, where tensile stress in glacier ice exceeds the tensile strength of the ice, exploiting weaknesses which affect the load bearing capacity of the ice. Near such weaknesses, concentration of high stresses may lead to propagation of the weakness, resulting, ultimately in the fracture of the material (van der Veen, 1998). Based on these

principles, both Weertman (1973) and Robin (1974) suggested that the greater density of water compared with ice may allow water filled crevasses to propagate downwards until they ultimately reach the glacier bed. This is supported by van der Veen (1998), who, using a model of tensile stresses in individual and multiple crevasses found that increased net stress intensity in water filled crevasses theoretically allows penetration to the bed of the glacier. This however, occurs on the condition that the water level remains sufficiently close to the ice surface (~10 – 20 m), and that a tensile stress of greater than 100 – 150 kPa is maintained at the fracture tip. Alley *et al*. (2005) argue that glaciogenic stresses are often insufficient to propagate fractures of less than a few tens of metres deep, although conclude that inflow from supraglacial lakes may help to drive the process. Hooke (1989) indicated that no field evidence had (at the time) been found to support evidence of this process. However, several more recent studies have observed in the field what are thought to be examples of hydrologically driven fracture propagation.

During a period of study at John Evans Glacier, Canada, Boon and Sharp (2003) observed the water filling of a crevasse, causing meltwater to back up and pond in a supraglacial stream channel. Over an eleven day period, the water level rose to a maximum depth of 6.9 m above the channel bed, forming a supraglacial pond which extended approximately 200 m upstream of the crevasse. Thirteen days after the start of the monitoring period, the pond drained abruptly and completely within one hour. However, previously observed negative changes in water level suggest that drainage was occurring before this time, albeit less abruptly, indicating that drainage was initiated and not sustained (Boon and Sharp, 2003). It is believed that the pond drainage event established a permanent hydrological connection between the glacier surface and the subglacial drainage system due to the observation of turbid, solute-rich water in front of the glacier terminus three days following the drainage. Similarly, Das *et al*. (2008) observed the rapid drainage of a supraglacial lake on the western margin of the Greenland Ice Sheet. Although the lake covered a surface area of ~5.6 $km^2$ at its maximum extent, it was able to fully drain within 1.4 hours at an average rate of 8700 $m^3s^{-1}$. The drainage event was found to coincide with horizontal and vertical movement of the ice

sheet, as well as increased seismic activity in the 30 minutes preceding the onset of rapid drainage. In both studies, a number of fresh crevasses and fractures perpendicular to ice flow direction were found following the drainage events (Boon and Sharp, 2003; Das *et al*., 2008). This, combined with the abruptness of the lake drainage, suggest that drainage in both studies occurred as a result of hydrologically driven ice fracture.

### 1.3.3. Englacial Drainage

Collins (1979a) defined englacial flow as water passing through sediment-free, ice walled conduits on or within the glacier. This suggests that although water may pass through subglacial conduits, it is distinguishable from subglacial flow by its dilute nature. This is due to a combination of high flow rates and volumes of meltwater limiting contact time between the water and the ion-rich material of the glacier bed. This is in contrast with subglacial flow, where water acquires solutes as it moves in contact with bedrock, sediments and sediment-laden basal ice and is therefore relatively concentrated (Vatne *et al*., 1996). Tranter and Raiswell (1991) used the terms 'quick flow' and 'delayed flow' rather than englacial and subglacial to describe the two components of water movement, which better identify the different residence times of the water in the subglacial drainage system (Vatne *et al*., 1996).

Much of the current understanding of englacial drainage system structure in temperate glaciers has been influenced by the theoretical model of Shreve (1972). The model assumes that the behaviour of englacial conduits is the result of three characteristics: (1) that the capacity of the drainage system continually adjusts to changes in the supply of meltwater (i.e. remains in a steady state); (2) that under steady state conditions, pressure within the system is governed primarily by the ambient pressure in the surrounding ice, and secondarily by the rate of melting of the conduit walls; and (3) that the network of conduits becomes arborescent over time, expanding into ever-larger trunk-passages. According to Shreve's (1972) model, water will tend to flow steeply downwards towards areas with gentler

surface slopes, but will become almost parallel as the steepness of the surface increases.

Shreve's (1972) model makes a number of critical assumptions. It is assumed that the drainage system is in steady state, that englacial water will flow along the steepest hydraulic gradient in cylindrical conduits, and also that water pressure in such conduits is approximately equal to the surrounding ice pressure. This last assumption stems from the idea that englacial conduits expand and contract in response to differences in pressure between water in conduits and in surrounding ice. This causes englacial conduits to adopt a geometry which equalises these pressures (Gulley *et al*., 2009), suggesting that conduit water pressure is self-regulating in response to overburden pressure. This theory has been used as the basis to explain a number of glacio-hydrological processes, including glaciohydraulic supercooling (Alley *et al*., 1997; 1998; 2003), tunnel valley formation (Shreve, 1985) and subglacial lake formation (Pattyn, 2008), as well as being widely adopted in glacier hydrological models (Pälli *et al*., 2003; Rippin *et al*., 2003; Bindschadler and Choi, 2007). However, a number of studies have challenged many of the assumptions in Shreve's model. Firstly, the assumption of steady state englacial drainage does not apply to systems which are fed by surface meltwater, or which undergo significant diurnal, seasonal or annual fluctuations (Gulley *et al*., 2009). Secondly, Shreve's model requires that the drainage system be recharged evenly across the glacier surface. However, this is often not the case, as recharge is concentrated at a small number of discrete points such as large moulins and crevasses (Gulley *et al*., 2009). Thirdly, the assumption that water pressure is equal to ice overburden pressure has been contested by Fowler (1984) and Lliboutry (1996) who contend that no other evidence of this type of pressure balance exist in other deformable media.

#### 1.3.3.1. Englacial Conduits

Fountain and Walder (1998) suggest that near-horizontal englacial conduits originate from the action of water flowing along the bottom of crevasses. This is

supported by the work of Pohjola (1994), who used down-borehole imaging and found that englacial conduits occur in close proximity to bands of bubble-free ice, believed to be the result of water refreezing in crevasses, and Harper and Humphrey (1995), who found a similar relationship between blue (bubble-free) ice bands and conduits. Hagen *et al*. (2003) suggest a different means of englacial conduit formation, whereby supraglacial meltwater channels in polythermal glaciers evolve to form englacial channels. This is caused largely by the lack (or reduced number) of crevasses, inhibiting drainage of meltwater into the glacier, and hence resulting in a greater number of meltwater channels forming on the glacier surface. Sustained high discharges in these supraglacial channels, combined with water flowing over a surface slope of between 0.1 and 0.2 $mm^{-1}$ dissipate enough mechanical energy in the meltwater to cause down-cutting of the channels into the ice surface (Vatne, 2001). The deepest of these channels are preserved over the winter season, and continue to act as meltwater pathways during the melt season (Vatne, 2001). Over time, ice and snow gradually close the top of the channel, forming a completely englacial conduit.

Although Fountain and Walder (1998) suggest that pre-existing crevasses give conduit formation a 'head-start', Gulley *et al*. (2009) argue that since a conduit will only form where incision rates are greater than ablation rates, a crevasse is not a necessary condition for conduit formation. Furthermore, it is suggested that such 'cut-and-closure' crevasses are more likely to form in uncrevassed areas of a glacier, since supraglacial water is less likely to be diverted into the glacier, and hence, more likely to incise a channel (Gulley *et al*., 2009). In terms of conduit closure, Gulley *et al*. (2009) suggest that ice creep is less important than snow accumulation over a conduit in the early stages of closure, and that ice deformation is more critical in the later stages. The process of 'cut-and-closure' englacial conduit formation is similar to another suggested by Pohjola (1994), whereby englacial drainage structures originate in the accumulation area by preservation of conduits which exist at the base of the seasonal snowpack. Over time, accumulation and reduced ice deformation may allow advection of the conduit into the glacier, thus forming an englacial conduit. However, unlike the process described by Hagen *et al*. (2003) this process is likely to require year

round drainage through the snowpack, and is therefore unlikely to form within a single defined ablation season.

Observations made within glacier marginal caves and moulin networks have resulted in the widespread belief that englacial water flow occurs in tubular (cylindrical) conduits (Shreve, 1972; Röthlisberger, 1972; Holmlund, 1988b), and several theories regarding water flow in englacial conduits have been based on this premise (Shreve, 1972; Röthlisberger, 1972; Weertman, 1972; Lliboutry, 1983; Hooke, 1984). Each of these theories is based on the concept that the size of an englacial conduit is governed by the rate of melting of the conduit walls by frictional heating from flowing water, and the rate of conduit closure as a result of overburden pressure exceeding the pressure of water inside the conduit. Röthlisberger (1972) suggested that under steady state conditions and constant discharge, a conduit of given length will remain at a given size and pressure if the effects of ice deformation are offset by the melting of the conduit walls by heat transfer.

Whilst the above discussed theories have adopted the concept that englacial conduits are circular in cross section, a study of englacial water pathways in Storglaciären, Sweden, conducted by Fountain *et al*. (2005) found evidence to suggest that not all englacial conduits are tubular. Using a combination of tracer injections, ground penetrating radar (GPR), and down-borehole camera imaging, the study found that of the englacial water pathways intercepted by boreholes, 80% (n=44) were fracture-like features with near-vertical dip (~70%) subparallel walls. Furthermore, images taken of the features appear identical to images taken within water-filled surface crevasses, leading the authors to consider the features englacial fractures (Fountain *et al*., 2005). The fractures were found to hydraulically link small holes within the ice to form an integrated hydrological network. The fractures ranged in width from 0.3 to 20 cm, and did not correlate with depth. Water flows only occurred within ten of the fractures, and ranged in velocity from 0.5 to 4 cm $s^{-1}$. These velocities are slow compared with theoretical models of water flow within tubular conduits (Shreve, 1972; Röthlisberger, 1972). Importantly, the findings of Fountain *et al.* (2005) are in agreement with earlier

work conducted at Aletschgletscher, Switzerland by Hock *et al*. (1999) that englacial systems are not dominated by circular conduits.

### 1.3.4. Subglacial Drainage

Reconstructing the configuration and dynamics of subglacial drainage systems has represented a research focus for glaciologists for a number of decades (Hubbard and Nienow, 1997). The structure of the subglacial drainage system reflects the ability of individual flow pathways to attract and capture meltwater from competing hydraulic configurations, whilst the size of the channels reflects the counteracting effects of enlargement by turbulent heating, and closure by ice deformation (Hubbard and Nienow, 1997). However, whilst a number of characteristics of the subglacial drainage system are shared with the englacial drainage system, some factors differ in their relative importance and influence. For example, the hydraulic roughness of an unconsolidated gravel bed will have roughness factors ten times that of an ice enclosed conduit (Röthlisberger and Lang, 1987; Lawson, 1993). Furthermore, whilst the concept of an englacial conduit displaying a circular cross section is well established in englacial hydrology, subglacial conduits can differ considerably from this idealized configuration, depending on ice deformation rates, bed composition and bed roughness (Lawson, 1993).

#### 1.3.4.1. Subglacial Tunnel System

Nye (1953) suggests that an isolated, water-filled void in glacial ice will be closed by inward ice flow unless the ice overburden pressure is equal to the water pressure within the void. However, a conduit within or beneath a glacier may remain open even if water pressure is lower than the overburden pressure, providing that water flowing within the conduit dissipates enough energy to keep the conduit open through heating. This idea was adopted by Röthlisberger (1972), who theorised that subglacial tunnels are able to exist at the glacier bed. These channels (later termed Röthlisberger, or R-channels) were proposed to be semi-

circular in cross section, and remain open due to water flowing within the channel remaining at the pressure-melting temperature by gaining or losing energy. Röthlisberger concluded that the largest subglacial channels capture the drainage of smaller channels, resulting in an arborescent drainage network similar to that described in englacial systems by Shreve (1972). Hooke (1984) theoretically assessed the extent of channelised flow beneath a glacier, and predicted that open channel flow is dependent on ice thickness, and should be common beneath steeply sloping alpine glaciers with an ice thickness of less than a few hundred metres. This conclusion is partly supported by Fountain (1993) and Kohler (1995), who inferred through use of dye tracing that open channel flow occurs beneath thinner marginal glacier ice, but is not as extensive as proposed by Hooke (1984).

Nye (1973) suggested that R-channels must be transient features, and are forced shut as they are advected against the upglacier side of bed obstacles. Furthermore, Nye maintained that continuous subglacial meltwater drainage requires the presence of channels incised into the bed, since these provide a more permanent drainage structure. So-called Nye (or N-) channels are therefore formed by the downwards incision of meltwater into bedrock (Figure 1.2), or through the creation of protochannels. Studies of former subglacial beds by Walder and Hallet (1979) and Hallet and Anderson (1980) have revealed a large number of N-channels typically 0.1 m deep, and preferentially orientated with the former direction of ice flow. It is therefore thought that N-channels constitute a morphologically distinct part of the drainage system of small alpine glaciers (Fountain and Walder, 1998). However, their hydraulic behaviour is simply that of elongated orifices in a cavity network (Fountain and Walder, 1998).

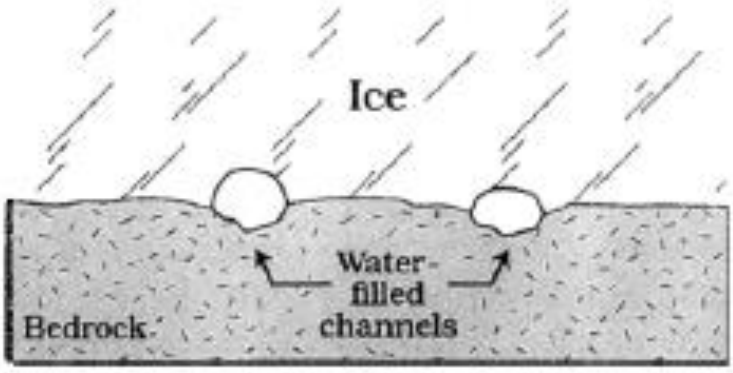


**Figure 1.2. A diagrammatic example if Nye-channel configuration (Fountain and Walder, 1987)**

### 1.3.4.2. Linked Cavity System

Subglacial cavities form as a result of sliding ice becoming separated from the glacier bed (Fountain and Walder, 1998). This occurs as a result of high bed roughness, high water pressures and rapid sliding (Lliboutry, 1968; Nye, 1970). Stresses generated on the stoss side of a bed obstruction are greater than those generated on the lee side, and cause ice to become separated from the bed in the lee of the obstacle. Such cavities are typically less than 1 metre in height, with variable lengths of up to several metres (Walder and Hallet, 1979). Kamb (1987) proposed a subglacial linked cavity drainage system based on the 1982-1983 surge of Variegated Glacier, Alaska. During the surge, subglacial water pressure was observed to be high (often equalling the ice overburden pressure) (Kamb *et al*., 1985), and subglacial water flow showed low velocities compared with non-surge periods (Brugman, 1986). These observations conflict with the work of Rothlisberger (1972) who theorised that increasing water flux should cause subglacial water pressure to decrease. Furthermore, dye-tracing experiments during the surge revealed that the dye used was dispersed across the width of the glacier, and not confined to a single outflow stream (as observed post-surge) (Kamb, 1987). Kamb (1987) suggested that during non-surge periods Variegated Glacier exhibits a subglacial tunnel system (Rothlisberger, 1972; Weertman, 1972; Nye, 1976). However, the system evolves during surge events to form a glacier wide network of linked cavities with a cross sectional area of $\sim$ 200 $m^2$ (Figure 1.3).

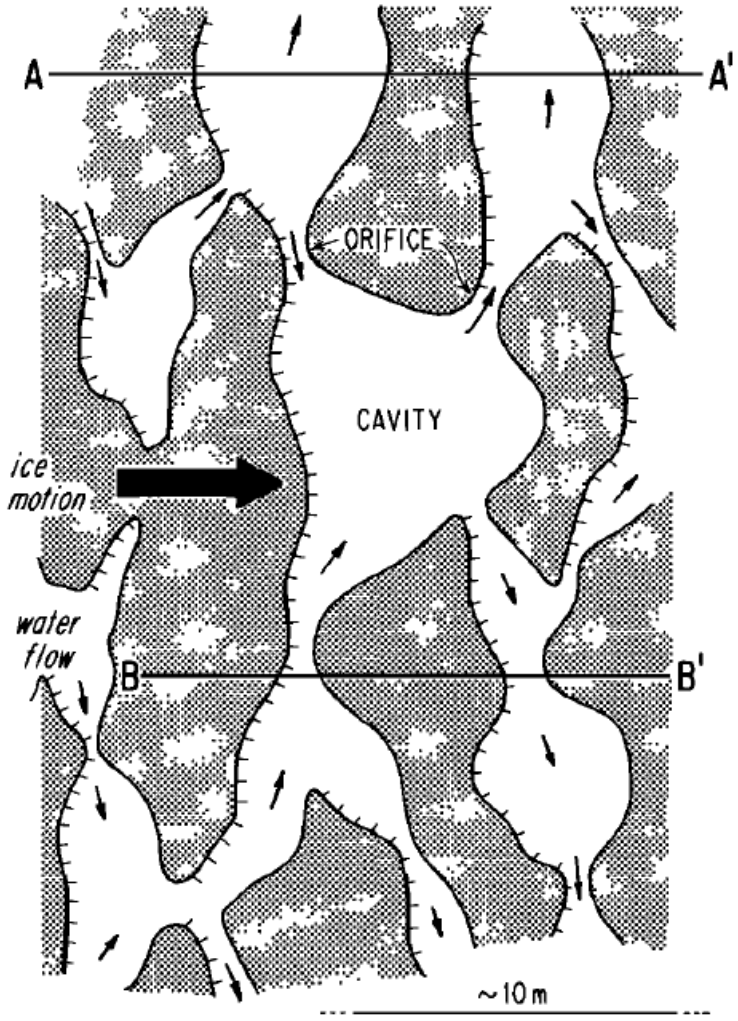


**Figure 1.3. Idealised downwards looking view of a subglacial linked cavity drainage system (Kamb, 1987).**

The system is characterised by large cavities (with an average height of 0.2 m) caused by ice separation from the bed in the lee of bed obstacles, and linked by smaller conduits. The size and interconnection of the cavities (referred to by Kamb as orifices) prevents unique flow paths from being established, and explains the high dispersion of tracers observed by Brugman (1986). The interconnecting 'orifices' display a much smaller surface area than the main cavities, explaining the reduced velocity of subglacial water as flow is restricted (Kamb, 1987). The nature of a linked cavity drainage system is dependent on the topography of the bed, much in the same way as Nye channels. The dimensions and spatial distribution of bed roughness elements, water pressure and ice overburden pressure all influence the pattern of flow within the system (Kamb, 1987).

## 1.4. Fluvial Suspended Sediment Transfer in Glacierised Basins

In glacierised basins, temporal variability in suspended sediment transport by glacial meltwater is largely influenced by changes in the rate of meltwater production at the glacier surface and changes in the behaviour of two or more hydraulically distinct reservoirs within and beneath the glacier (Collins, 1979b; Fountain, 1992; Gurnell *et al*., 1992; Clifford *et al*., 1995; Willis *et al*., 1996; Richards *et al*., 1996; Hodson and Ferguson, 1999). Having observed in previous sections the processes which generate glacial discharge, and the routing of meltwater into the subglacial drainage system, this section aims to outline the geomorphic roles of meltwater at the glacier bed, and the processes which control suspended sediment evacuation over seasonal and sub-seasonal scales.

### 1.4.1. Suspended Sediment Entrainment

Basal sediment evacuation by meltwater has often been observed to dominate sediment budgets (Hallet *et al*. 1996; Alley *et al*., 1997), and is often assumed to indicate direct glacial denudation (Hallet *et al*., 1996; Orwin and Smart, 2004). As a result, the majority of basal sediment is transported to the ice-margin by the subglacial drainage system (Evensen and Clinch, 1987; Kirkbride, 1995; Swift *et al*., 2002). Upon reaching the glacier bed, the erosive capacity of subglacial streams is extremely high. Mechanical erosion is able to take place, although Alley *et al*. (1997) suggest that the rate of abrasion by glacial meltwater is dependent on the concentration of suspended sediment in the water prior to reaching the bed.

### 1.4.2. Seasonal Controls on Subglacial Suspended Sediment Transport

Suspended sediment transport in subglacial streams has been widely observed to fluctuate seasonally, and largely reflects the increased availability of meltwater during the melt season (Collins, 1990; Gurnell, 1995).

During the winter months, increased snow cover and reduced air temperature substantially reduces the volume of melt produced at the glacier surface, and as a result, little or no surface meltwater is able to access the glacier bed. For example, Hodgkins *et al*. (1998) estimated that the mean winter discharge of Scott Turnerbreen, Svalbard in 1993 was approximately 0.01 $m^3$ $s^{-1}$. Low discharges limit suspended sediment entrainment and transport at the glacier bed, resulting in widespread sediment accumulation in the subglacial drainage system (Collins, 1989, 1990; Leistøl, 1967; Vatne *et al*., 1992; Hooke *et al*, 1985). Upon the commencement of summer ablation, the subglacial drainage system evolves quickly with increasing volumes of meltwater reaching the bed through crevasses and moulins. As a result, Collins (1989) suggested that the distributed subglacial drainage system reaches its maximum spatial extent early in the ablation season. Increasing ablation and meltwater generation throughout the season results in the development of a more channelised subglacial drainage system which is able to transmit meltwater more efficiently, facilitating high discharges (Richards *et al*., 1996). Sediment accumulated during the winter months is easily entrained in response to such rising discharges, and a number of studies have suggested that the seasonal maximum suspended availability of sediment occurs early in the ablation season (Collins, 1989, 1990; Leistøl, 1967; Vatne *et al*., 1992; Hooke *et al*, 1985). However, following this early maximum, suspended sediment concentration has been widely observed to decrease during the melt season (Østrem, 1975; Bogen, 1996; Collins, 1990; Hammer and Smith, 1983; Leistøl, 1967; Hooke *et al*., 1985). This has been related to decreased sediment availability due to depletion of the subglacial sediment store (Hooke *et al*., 1985) or relatively immobile channelised flowpaths having limited access to sediment sources (Collins, 1989; 1990; Gurnell *et al*., 1992). However, it has also been suggested that cold and polythermal glaciers do not follow this trend, with suspended sediment concentrations exhibiting an increasing trend through the ablation season (Repp, 1988; Bogen, 1991; Hodgkins, 1996; Hodson and Ferguson, 1999). This may reflect the increased dominance of ice-marginal sediment sources in polythermal glacier basins (e.g. Lukas *et al*., 2005; Porter *et al*., 2010).

### 1.4.3. Diurnal Controls on Subglacial Suspended Sediment Evacuation

Temporal variability in proglacial suspended sediment transport, especially at temperate glaciers, is largely forced by changes in the rate of meltwater production at the glacier surface and changes in the behaviour of two or more hydraulically distinct flow reservoirs within and beneath the glacier (Collins, 1979b; Fountain, 1992; Gurnell *et al*., 1992; Clifford *et al*., 1995; Willis *et al*., 1996; Richards *et al*., 1996; Hodson and Ferguson, 1999). As a result, the diurnal variability of suspended sediment transport in glacierised basins is closely linked to variability in patterns of discharge (Walling, 1974; Gurnell, 1987; Willis *et al*., 1996). The relationship between discharge and suspended sediment evacuation is hysteretic and changes more or less continuously during a runoff season (Østrem, 1975). Hysteresis implies a bivariate relationship in which values of the dependent variable for a given value of the independent variable differ according to whether the independent variable is increasing or decreasing (Hodgkins, 1996). In this case, discharge is the independent variable, and suspended sediment concentration is the dependent variable. Due to the constantly changing nature of discharge and suspended sediment delivery in glacierised basins, hysteresis loops take on a pattern of constantly changing loops, each associated with a period of high water discharge (Leistøl, 1967). When suspended sediment concentration and discharge are non-synchronous, hysteresis loops will be clockwise (i.e. suspended sediment concentration peaks before discharge), and anticlockwise when discharge peaks before suspended sediment concentration (Hodgkins, 1996; Stott and Mount, 2007). This is exemplified in Figure 1.4.

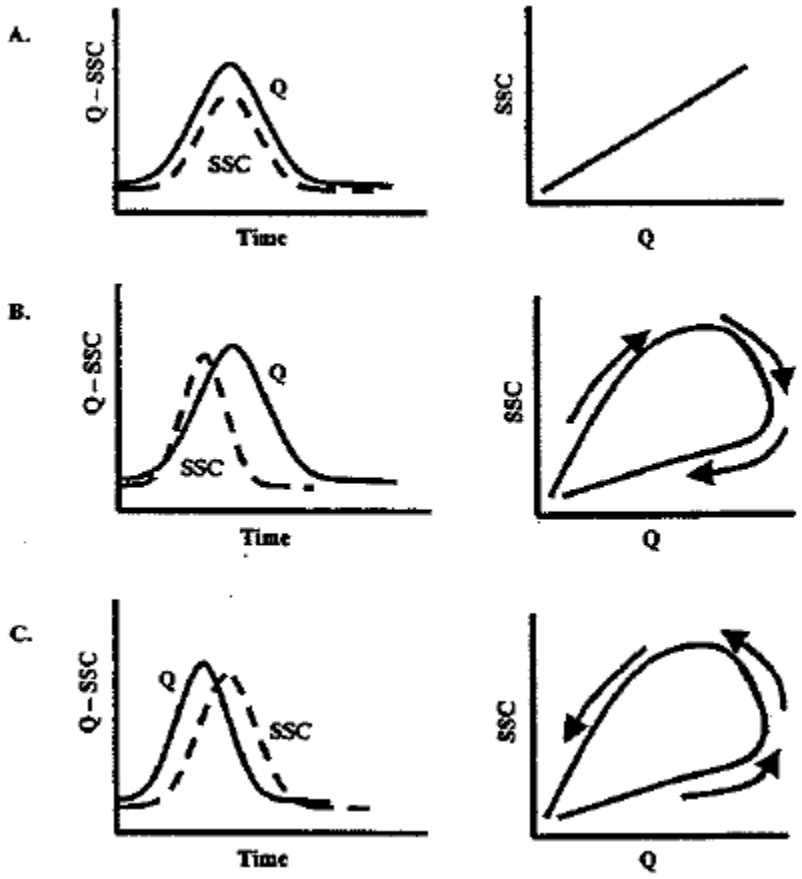


**Figure 1.4. Common relationships between discharge (Q) and suspended sediment concentration (SSC). (A) Coincident peaks of Q and SSC have equal values on the receding limb of the hydrograph resulting in a linear relationship. (B) SSC peaks before Q, and SSC values are lower on the receding limb of the hydrograph resulting in a clockwise (positive) hysteresis relationship. (C) SSC peaks after Q, and SSC values are higher on the receding limb of the hydrograph resulting in an anticlockwise (negative) hysteresis relationship. After: Hudson (2003).**

A number of studies have identified short-term variations in suspended sediment evacuation that appear independent of changes in discharge (e.g. Gurnell and Warburton, 1990; Hodson and Ferguson, 1999). It has been suggested that such 'pulses' or 'flushes' of suspended sediment can form a significant component of the total sediment transport over a given period. For example, Gurnell and Warburton (1990) estimated that during a 22 day monitoring period, 1891 tonnes (46%) of the total suspended sediment load at Glacier de Tsidjiore Nouve was transported during flush events, of which 369 tonnes (9%) occurred as part of a flush peak. A number of mechanisms have been suggested through which increases in

suspended sediment availability are able to occur independently of discharge. Willis *et al*. (1996) suggest that short term pulses of high suspended sediment concentration may be indicative towards increased sediment supply to the subglacial hydrological system by processes of glacier motion. The pulses themselves are then generated by the subsequent transport of such sediment to the proglacial zone (Willis *et al*., 1996). Similarly, it has been suggested that short-term shifts reflect changes to the subglacial drainage system as channels become more efficiently connected or migrate across the glacier bed (e.g. Collins, 1989, 1990; Gurnell, 1982; 1995; Gurnell *et al*., 1991, 1992; Hodson *et al*., 1997, Swift *et al*., 2002; 2005).

## 1.5. Thesis Aims and Structure

This study aims to contribute to the understanding of fluvial suspended sediment transfer in glacierised basins through the investigation of patterns of suspended sediment and meltwater delivery to the proglacial area of Storglaciären, a small polythermal valley glacier located in the Tarfala valley, arctic Sweden. Fulfilment of this aim will be achieved through the following objectives:

i. To identify key meteorological drivers of discharge generation in the Storglaciären basin

ii. To assess the variability of discharge between two proglacial outlet streams of Storglaciären: Nordjåkk and Sydjåkk.

iii. To assess seasonal-scale variability in suspended sediment delivery to the proglacial area of Storglaciären

iv. To investigate the nature of the drainage system of Storglaciären and identify periods of drainage system evolution.

v. To understand the underlying factors which influence suspended sediment transport at Storglaciären.

vi. To assess the applicability of physically based sediment transfer model in predicting suspended sediment delivery in the Storglaciären basin.

The structure of this thesis from this point forward is as follows:

Chapter 2 provides an overview of the field site, and outlines previous hydrological research focused on Storglaciären. Chapter 3 details the collection and analysis of discharge data collected over two summer field campaigns at Storglaciären concerned with Objective 1. Chapter 4 explains the collection and subsequent analysis of suspended sediment data in the proglacial area of Storglaciären in the context of Objective 2. Chapter 5 details the statistical techniques used to explore patterns of suspended sediment delivery at Storglaciären in greater detail, based on Objective 3. Chapter 6 explains the use of linear-reservoir and suspended sediment entrainment models to simulate meltwater routing and suspended sediment transfer in the Storglaciären basin. Each chapter contains a methods and results section, and provides a brief discussion of the major findings of the chapter. A broader discussion of the results, linking all three chapters together is included in Chapter 7. Concluding remarks are included in Chapter 8.

*Chapter 2*

# Field Site

## 2.1. Introduction

This chapter introduces the field site of the study in the Tarfala valley, northern Sweden. This includes the glacial history and geology of the area before focusing on the glacier used during the investigation, Storglaciären.

## 2.2. Geographical Setting of the Tarfala Valley

The Tarfala valley (Figure 2.2) is located on the eastern side of the Kebnekaise massif in northern Sweden (Figure 2.1), ca. 160 km north of the Arctic Circle (67° 55' N, 18° 35' E). The valley is a typical sub-arctic high alpine environment with a total area of 20.6 $km^2$, and encompassing an altitudinal range of between 800 and 2103 m a.s.l. The Tarfala basin is well defined by the surrounding steep mountain ridges of the Kebnekaise massif. The valley contains four glaciers, with a total glacierised area of 30% (Dahlke *et al*., 2012).

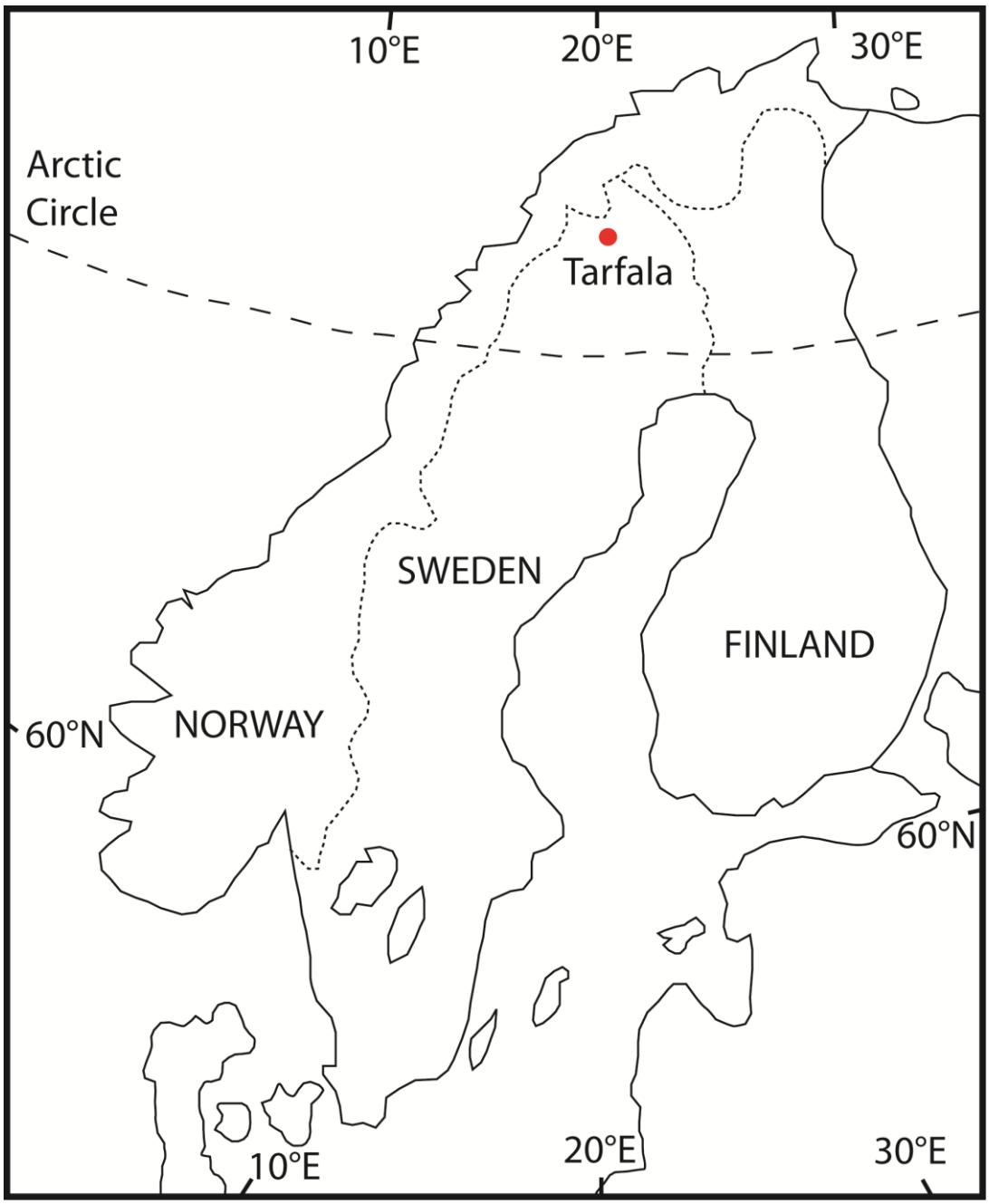


**Figure 2.1. Map of Scandinavia showing the location of the Tarfala valley (adapted from Etienne *et al.*, 2003).**

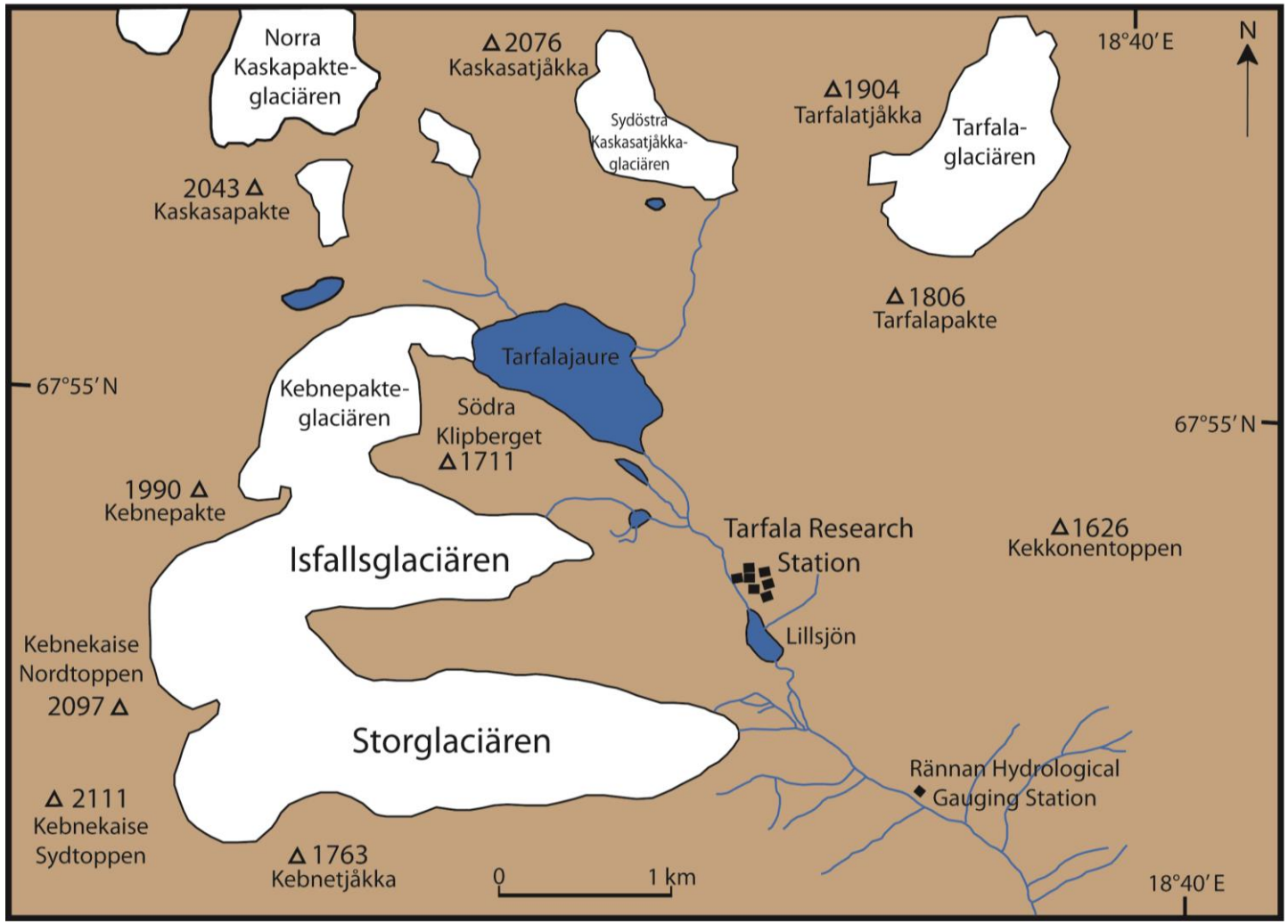


**Figure 2.2. Map of the Tarfala valley including major peaks and glaciers, as well as hydrological gauging sites managed by the Tarfala Research Station.**

## 2.3. Geology and Glacial History

Similar to other Swedish mountain ranges, the Kebnekaise massif belongs to the 1000 km long Seve belt of the Scandinavian Caledonides (Andréasson and Gee, 1989). It has been suggested that the Seve belt originated in the outer part of the Late Precambrian rifted margin of the Early Palaeozoic continent Baltica, and may also include fragments of the early floor of the Iapetus Ocean (Gee, 1975; Solyom *et al*., 1979). During the closure of the Iapetus suture (ca. 420 Ma) the collision between the continents Laurentia and Baltica thrust this margin several hundreds of kilometres eastwards onto the Baltoscandian platform (Andréasson and Gee, 1989) into its current position.

Detailed geological mapping of the Tarfala valley (Andréasson and Gee, 1989; Baird, 2005) has revealed eight major lithologies, thought to represent the Autochthon-Parautochthon, Middle Allochthon and Upper Allochthon tectonostratigraphic units of the Scandinavian Caledonides (Bhattacharyya and Hudleston, 2001)

The basin of Storglaciären itself is dominated by three major tectonic units (Andréasson and Gee, 1989). The geology of the lower ablation area and proglacial zone of the glacier are defined by the presence of Tarfala Amphibolite, and it is this lithology which is present at both stream gauging sites used in this study. Up-glacier, a band of Storglaciären Mylonite Gneiss underlies the area in which a subglacial ridge (or riegel) is believed to occur, and which strongly influences the dynamics of the glacier (Hooke *et al*., 1987; Jansson, 1997). The accumulation and upper ablation areas of the glacier are underlain by bedrock of the Kebne Dyke Complex and Kebne Amphibolite respectively, with the approximate position of the glacier Equilibrium Line Altitude (ELA) marking the divide.

Contemporary glacierisation in northern Sweden is confined to cirque and valley glaciers in the higher massifs (e.g. Kebnekaise, Sarek). Under present

climatic conditions, Kleman and Stroeven (1997) estimate that approximately 50% of well-developed cirques in the area contain glaciers. However, the region has undergone repeated glaciation during the Quaternary, with widespread cirque glaciation and mountain ice sheets inferred to have been dominant between 0.7 and 2 Ma, corresponding to an interglacial – warm interstadial cycle (Kleman and Stroeven, 1997). The last 0.7 Ma have seen the area dominated by successive Fennoscandian ice sheets during the Weichselian period, in particular during the formation of an ice sheet corresponding to marine isotope stage 5d (ca. 110-120 kyr BP) which is believed to have formed much of the moraine morphology in northern Sweden (Kleman and Stroeven, 1997; Goodfellow *et al*., 2008).

## 2.4. Storglaciären

Storglaciären (Figures 2.3 and 2.4) is a small polythermal valley glacier situated in the Tarfala valley on the eastern side of the Kebnekaise massif (Jansson, 1996). The glacier is ~ 3 km in length and ranges in altitude from ~ 1120 m a.s.l at the terminus to ~ 1730 m a.s.l at the headwall beneath the southern Kebnekaise peak. In total, Storglaciären covers an area of ~ 3 $km^2$ (Jansson, 1996; Holmlund and Jansson, 2002). Radio echo surveys conducted in 1981 (Björnsson, 1981) and 1993 (Eriksson *et al*., 1993) revealed that the bed of the glacier contains four overdeepenings separated by rock bars (Bjornsson, 1981), the largest of which is located in the upper reaches of the ablation area (Jansson, 1996). On average, Storglaciären reaches a depth of ~95 m, with a maximum depth of ~ 250 m corresponding to the upper ablation area overdeepening (Jansson, 1996). The closure of this overdeepening results from the occurrence of the transverse subglacial riegel (as mentioned in the 'geology and glacial geology' section above) and occurs approximately 130 m up-glacier from the terminus of Storglaciären (Jansson, 1997). The dynamic behaviour of Storglaciären is strongly controlled by hydrologic conditions influenced by the riegel (Jansson, 1995; Jansson *et al*., 1999), and studies have found that the glacier experiences diurnal fluctuations in surface velocity both

up-glacier and down-glacier of the riegel as a result of longitudinal coupling (Jansson and Hooke, 1989; Jansson, 1995; 1997).

The proglacial area of Storglaciären consists of a till sheet ~ 0.3 km$^2$ in area which has been exposed by the retreat of Storglaciären since 1910 (Bronge, 1996; Holmlund *et al.*, 1996a). The proglacial area of Storglaciären has been studied in detail by Etienne *et al.* (2003) who identified seven sediment lithofacies within the proglacial area. These lithofacies have enabled several stages in the evolution of the proglacial sedimentary system to be identified, which are of considerable value in the inference of past glacier dynamics (Etienne *et al.*, 2003).

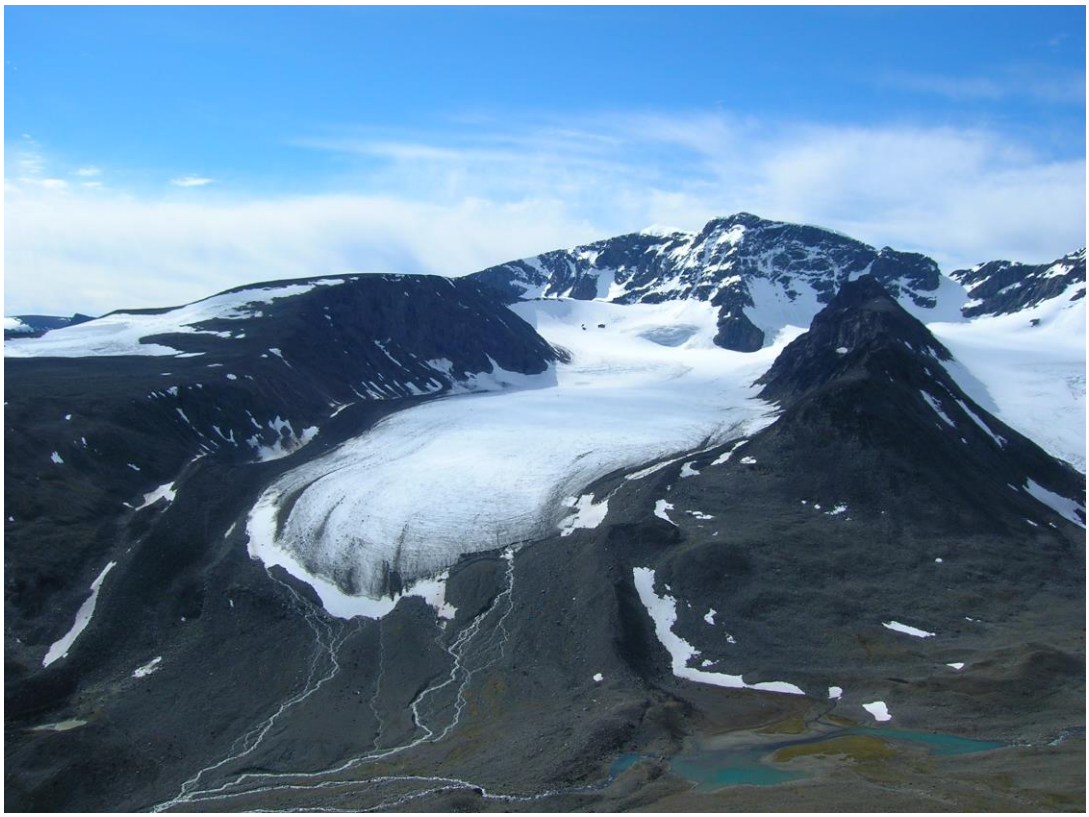

**Figure 2.1. Photograph of Storglaciären taken from Kekkonentoppen**

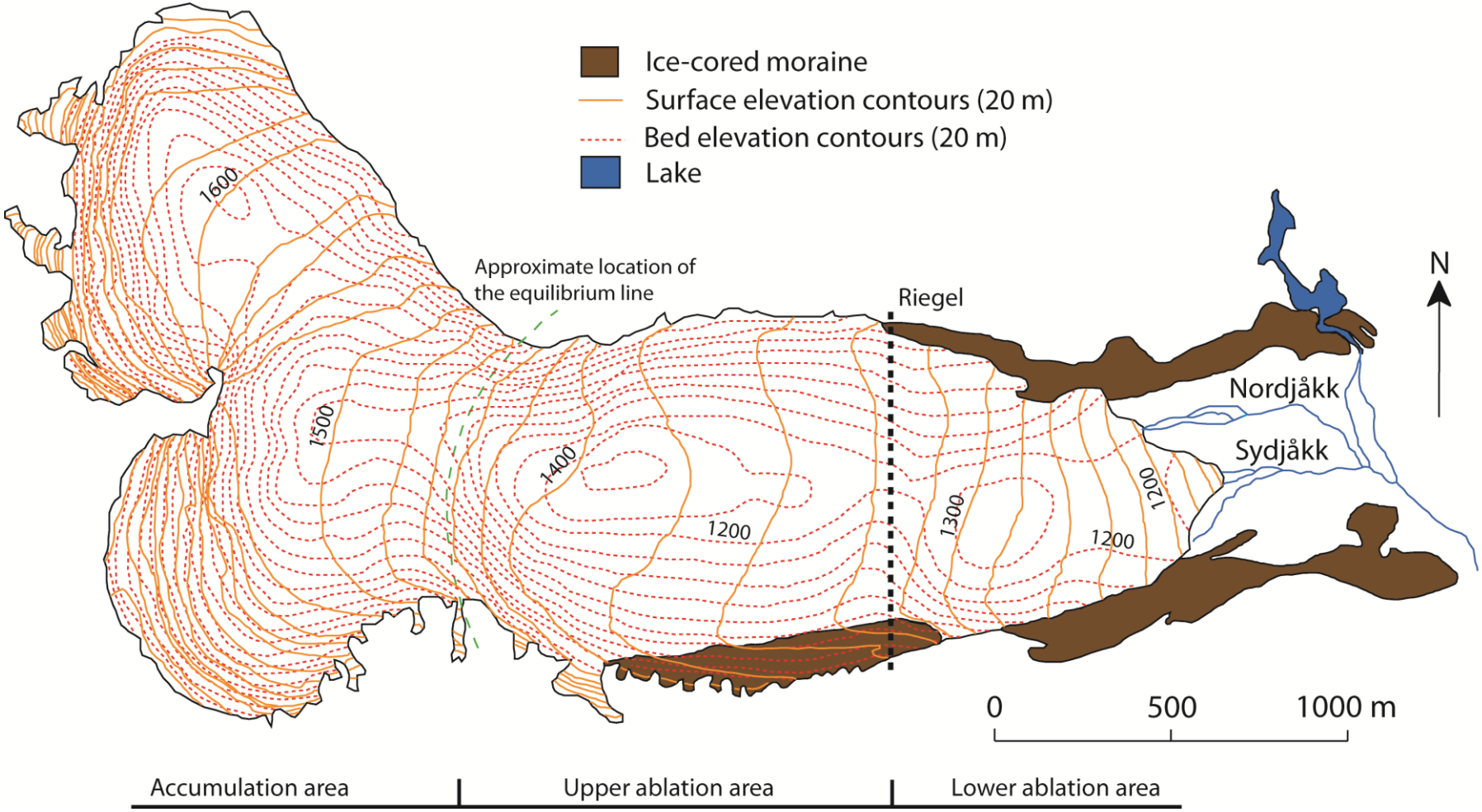


**Figure 2.2. Map of Storglaciären showing both surface (solid contours) and bed topography (dashed contours) (adapted from Jansson and Ove Näslund, 2009)**

### 2.4.1. Mass Balance

Storglaciären has been widely studied in terms of its mass balance, and has been the subject of an ongoing mass balance monitoring programme since 1945; the longest for any glacier worldwide (Schytt, 1947; Holmlund 1987; Holmlund and Jansson, 1999; Holmlund *et al*., 1996b; Holmlund *et al*., 2005; Jansson and Pettersson, 2007). These physical measurements have allowed the glacier mass balance to be estimated by regression back to 1878 (Holmlund 1987; Holmlund and Jansson, 1999; Holmlund *et al*., 1996b; Holmlund *et al*., 2005). The monitoring programme is maintained by the Tarfala Research Station, and mass balance is established using the direct glaciological method (Østrem and Brugman, 1991): snow depth and density measurements for the winter balance, and ablation stake measurements for summer balance (Jansson and Pettersson, 2007). The value of these measurements is enhanced by the high spatial resolution of the data: Snow depth is measured at ~ 300 points (~ 100 points $km^{-2}$) and ~ 50 ablation stakes are distributed across the entire glacier surface (~15 stakes $km^{-2}$) (Jansson and Pettersson, 2007). The quality of snow depth measurements has been increased in recent years by the use of snow radar, which allows depth measurements to be collected to an accuracy of ±10 cm (Holmlund *et al*. 1996a).

The long term mass balance record of Storglaciären shows that since between 1945 and 1970, the glacier experienced a significant loss of volume, resulting in a thinning of ~16 m (Holmlund, 1988c). Between 1970 and 1985 the net mass balance remained in equilibrium, although large annual variability was observed. The period between 1985 and 1996 has seen an increase in glacier volume as a result of increased precipitation (Holmlund, 1987; Holmlund *et al*., 1996b). Reanalysis of multi temporal aerial images by Zemp *et al*. (2010) showed that over the period 1959 to 1999, Storglaciären lost an ice volume of $19x10^6 m^3$. Averaged over the total glacier surface area, this corresponds to a decrease in thickness of 5.7 m, and an annual ice loss of 0.14 m (Koblet *et al*., 2010; Zemp *et al*. 2010). Temperature index mass balance modelling of Storglaciären based on ERA-40 data

calculates that the static mass balance sensitivity of the glacier to an increase in temperature varies around the mean value of -0.48 m $yr^{-1}$ $K^{-1}$ (Radić and Hock, 2006). This result agrees closely with previous estimates of static mass balance sensitivity: de Woul and Hock (2005) estimated a sensitivity of -0.46 m $yr^{-1}$ $K^{-1}$ using modelled observational data, and Braithwaite and Zhang (1999) estimated a sensitivity of -0.48 m $yr^{-1}$ $K^{-1}$ using a degree-day model (Radić and Hock, 2006). Radić and Hock also modelled the volume loss of Storglaciären based on the IPCC B2 emission scenario (IPCC, 2001). These results suggest that the glacier will lose between 50-90% of its volume by the end of 2100 (Radić and Hock, 2006).

### 2.4.2. Thermal Regime

The polythermal structure of the glacier has been identified and mapped using both direct temperature measurements (Schytt, 1968; Hooke *et al*., 1983) and Ground Penetrating Radar (GPR) (Holmlund and Eriksson, 1989; Pettersson *et al*., 2003). The glacier is mostly temperate (~85%) except for a cold (subfreezing) surface layer in the ablation area (Hooke *et al*., 1983; Holmlund and Eriksson, 1989; Jansson, 1996; Gusmeroli *et al*., 2010). This is typical of glaciers exhibiting a Scandinavian-type (or Svalbard-type) thermal regime (Aschwanden and Blatter, 2009). The cold layer is thickest at the glacier terminus with a maximum thickness of approximately 60-70 m (Gusmeroli *et al*., 2010; Moore *et al*., 2011) and a minimum thickness of approximately 25 m towards the approximate position of the glacier equilibrium line (Jansson, 1996; Moore *et al*., 2011). Pettersson *et al*. (2003; 2007) estimate that the layer thinned by ~8.3 m between 1989 and 2001, corresponding to a total average decrease of 22%. This and continued thinning has been attributed to short-tem increases in winter temperatures, reduction in temperature gradients, and ice emergence velocities (Pettersson *et al*., 2007). Based on the thickness of the cold surface layer, Moore *et al*. (2011) estimate that the rim of cold ice around the glacier margins and terminus is approximately 50 – 200 m wide. Radar and thermistor measurements collected by Moore *et al*. (2011) suggest that the cold layer meets the glacier bed ~ 100 m from the terminus (referred to as the basal thermal transition), with basal freezing occurring where

the layer thins at the glacier margin. It is estimated that around 16% of the total glacier area is frozen to the bed (Holmlund *et al*., 1996a).

### 2.4.3. Hydrology

Studies of proglacial hydrology at Storglaciären are relatively few compared with the extensive literature covering other areas of glaciological study undertaken in the Tarfala valley. Nonetheless, a number of studies have involved the collection of hydrological data, often in the context of glacier dynamics and surface energy balance. These studies provide valuable information concerning the hydrological behaviour of Storglaciären, and hence, meltwater delivery into the proglacial zone. The scarcity of studies of proglacial hydrology has largely been attributed to the difficulties of collecting discharge data in the Tarfala valley as a result of frequent changes in size and position of proglacial streams (Bronge, 1996; Bronge and Openshaw, 1996; Schneider and Bronge, 1996). The Tarfala Research Station has nonetheless maintained a hydrological measurement programme in the valley, with pressure transducer measurements recorded at the entrance to the Storglaciären proglacial area (Lillsjön), and further down valley at the Rännan gauging station where a permanent flume has been in place since 1968. These data allow a rough estimation of runoff from Storglaciären to be calculated. However since spring 2010, no hydrological data have been available down valley from Storglaciären due to the destruction of the gauging station by a slush avalanche (Jansson, *pers. comm*.).

### 2.4.4. Englacial Hydrology

The internal drainage of Storglaciären was first studied by Stenborg (1965; 1969; 1973). Using salt tracer measurements, Stenborg (1973) concluded that Storglaciären conformed to a 'two-system model' of glacier drainage, where a division of internal drainage occurs between areas of different drainage behaviour. This division coincides with the boundary between the main areas of oblique

crevasses of different strike orientation (Stenborg, 1973), suggesting that drainage behaviour is dictated, at least in part, by ice structural features. As a result, a tracer injected into crevasses and moulins on the south side of the glacier emerges in the proglacial stream Sydjåkk. Similarly, a tracer injected into crevasses on the north side of the glacier emerges in the proglacial stream Nordjåkk (Stenborg, 1969; 1973; Hooke *et al*., 1988). These conclusions are supported by Kohler (1995), who used salt tracing to demonstrate similar input-to-stream connections, despite changes in terminus position and exact moulin locations since Stenborg's (1969) study. This also suggests that the internal drainage structure of Storglaciären has changed very little over several decades. The distinction in drainage areas of the glacier has also been suggested by Jansson (1996) who concluded that Storglaciären consists of three distinct hydrological regimes operating in different areas of the glaciers. These can be defined based on the hydrological properties of each: (1) the lower ablation area (down-glacier from the riegel) where subglacial water pressure varies between close to zero and overburden pressure, and is closely correlated to ice velocity; (2) the upper ablation area (up-glacier from the riegel) where water pressure remains at around 80-100% of overburden pressure; and (3) the firn area, where local diurnal velocity variations have been observed, possibly as a result of water influx into the glacier bergschrund (Jansson, 1996).

Holmlund and Hooke (1983) documented the occurrence of high water-pressure events in August 1978 and September 1981, during which water levels in a number of moulins rose rapidly (> 7 m $h^{-1}$) and unexpectedly. In these cases, water levels reached, or were close to the glacier surface, and were sustained for between one and two days before declining at a rate slower than that of the increase. The 1978 event also resulted in an increase in the proglacial discharge and turbidity of Nordjåkk, usually noted for transmitting low sediment loads (Hooke and Pohjola, 1994).

Östling and Hooke (1986) applied salt and dye tracing during the 1984 melt season to calculate glacial runoff and to investigate the role of water storage at Storglaciären. During the study period, Östling and Hooke (1986) estimated that

water inputs to the glacier (including surface melting, precipitation, geothermal and strain energy driven melt, and meltwater from ice-marginal sources) totalled $7.91\pm0.26\times10^6 m^3$. Conversely, runoff and the refreezing of meltwater resulted in a total loss of $8.12\pm0.56\times10^6 m^3$. According to these values, the glacier exhibited a negative water balance at the end of the melt season, suggesting that approximately $0.2\times10^6 m^3$ of water was stored in the glacier at the beginning of the 1984 melt season (Östling and Hooke, 1986). Cumulative storage curves indicate that the maximum volume of storage during the melt season is approximately $0.6x10^6 m^3$, occurring during late May and early June. Although this value is in good agreement with the maximum volume of subglacial cavities ($\sim0.5\times10^6 m^3$ ) suggested by Hooke *et al*. (1983), it is suggested that this volume is reached in early to mid August (Hooke *et al*., 1983). Östling and Hooke (1986) therefore concluded that water is stored in englacial reservoirs (e.g. firn and crevasses) early in the melt season and moves into the subglacial drainage system later.

Holmlund (1988a; 1988b) carried out a thorough investigation of the internal geometry and evolution of moulins in the centre of the ablation area of Storglaciären. Holmlund (1988a) observed that the top 25-30 m of the moulins studied were typically straight and vertical as a result of the cold surface layer. After this, the moulins widen and their geometry becomes more complex as melting and closure rates vary. The moulins mapped during the study reached 30-40 m depth and exhibited a distinct bottom, from which a channel drains water away from the moulin. These streams have an inclination of 0-45° and trend in the direction of the original crevasse (Holmlund, 1988a). However, based on the theory of Shreve (1972), such streams should drain downglacier in a direction normal to equipotential planes. As this does not appear to be the case at Storglaciären, Holmlund (1988a) concluded that the internal drainage system of Storglaciären does not follow Shrevian theory (Shreve, 1972). This may be the result of atmospheric or near-atmospheric pressure in englacial conduits, causing the hydrostatic pressure of the glacier ice to have little effect on the geometry of the drainage system.

A study of englacial water pathways in Storglaciären conducted by Fountain *et al*. (2005) found evidence to suggest that the englacial hydrology of Storglaciären is not dominated by circular englacial conduits, as suggested by the theories of Shreve (1972) and Röthlisberger (1972). Using a combination of tracer injections, ground penetrating radar (GPR), and down-borehole camera imaging, the study found that of the englacial water pathways intercepted by boreholes, 80% (n=44) were fracture-like features with near-vertical dip (~70%) and subparallel walls. Furthermore, images taken of the features appear identical to images taken within water-filled surface crevasses, leading the authors to consider the features englacial fractures (Fountain *et al*., 2005). The fractures were found to hydraulically link small holes within the ice to form an integrated hydrological network. The fractures ranged in width from 0.3 to 20 cm, and did not correlate with depth. Water flows only occurred within ten of the fractures, and ranged in velocity from 0.5 to 4 cm $s^{-1}$. These velocities are slow compared with theoretical models of water flow within tubular conduits (Shreve, 1972; Röthlisberger, 1972).

### 2.4.5. Subglacial Hydrology

Hooke (1984) attempted to demonstrate that subglacial conduits at Storglaciären are predominantly open (not completely water filled) by applying a theoretical model based on the works of Shreve (1972), Röthlisberger (1972), and Lliboutry (1983). Both Shreve (1972) and Röthlisberger (1972) theorised that the closing of circular subglacial conduits by plastic deformation (e.g. Nye, 1953) and the opening of such conduits by melting (e.g. Haefeli, 1970) were balanced under steady-state conditions. However, although both theories make reference to the possibility of unfilled or semi-filled conduits, the models are only valid when conduits are completely water filled (Hooke, 1984). Hooke (1984) developed a new model considering conduit gradient, ice thickness, conduit diameter and friction within a given conduit. In testing the model at Storglaciären, Hooke (1984) estimated meltwater input from the glacier surface and from ice-marginal sources (~ 2 $m^3$ $s^{-1}$), and the estimated spacing of input points around the 8 km glacier perimeter (~ every 100 m). Using these data, Hooke (1984) suggested that

subglacial conduits transmitting water at a velocity of ~ 0.025 $m^3$ $s^{-1}$ would be open (i.e. unfilled), providing that either: (1) the slope of the bed is greater than 1° under 100 m of ice, or (2) the slope of the bed is greater than 2.5° under 150 m of ice.

Between 1984 and 1989, a number of tracer studies were undertaken at Storglaciären in order to develop understanding of the geometry and behaviour of the englacial and subglacial drainage systems (Zimmerer, 1987; Hooke *et al*., 1988; Seaberg *et al*., 1988; Hooke, 1991, Hock and Hooke, 1993; Kohler, 1995). Stenborg (1969) theorised that the drainage system of Storglaciären consisted of a network of branched conduits, rather than fewer large conduits. This theory is supported by Hooke *et al*. (1988), Seaberg *et al*. (1988), and Hock and Hooke (1993) who all concluded that drainage occurs through a multi-branched, 'arborescent' network of conduits. During high discharge events low-level conduit anabranches fill with water, increasing both the hydraulic gradient and velocity of water within the conduits. At the same time, overall sinuosity of the conduits decreases as water overflows bends in more sinuous anabranches, and as higher-level conduits are occupied (Seaberg *et al*., 1988). The character of this network was described as 'homogenous braiding' by Seaberg *et al*. (1988), a situation where enough conduit anabranches of varying size and length exist, increasing dye dispersion, and causing dye return peaks to merge indistinguishably (Hock and Hooke, 1993). This is supported by the results of Hooke *et al*. (1988) who observed that dye at the sampling location was detected in a number of discrete pulses. Hooke *et al*. (1988) inferred that this occurred as a result of the injected dye becoming split into separate 'parcels' by a distributary conduit network. Such behaviour is also suggestive of drainage through a subglacial linked cavity network (Lliboutry, 1983; Iken and Bindschadler, 1986), although Hooke *et al* (1988) concluded that drainage from the injection site (a crevasse slightly above the glacier equilibrium line) to the sampling location had occurred englacially and not in contact with the glacier bed. Hock and Hooke (1993) further supported the theory of a multi-branched drainage network, hypothesizing that the tracer transit times observed during their study and the number of moulins providing meltwater input to the drainage system, indicated a branched network of wide and low passages

occurring beneath the lower ablation area, providing direct drainage from large areas of the glacier bed (Hock and Hooke, 1993). The nature of these passages was disputed however by Cutler (1998), who applied a model of subglacial tunnel evolution using data from Holmlund and Hooke (1983), Holmlund (1988b) and field observations from the 1992 and 1993 melt seasons to estimate the surface area of crevasse reservoirs. Although the model suggests that subglacial tunnels evolve on a time scale of days as a response to fluctuating inflow, a single summer melt season is insufficient time for a channel to develop to the dimensions suggested by Hock and Hooke (1993) (height ~0.1 m, width > 10 m). Kohler (1995) concluded that an 'appreciable length' of the subglacial drainage network at Storglaciären occurs in pressurised conduits. This is in contrast with the work of Hooke (1984) who predicted an open channel system using Röthlisberger's (1972) unmodified expression for semi-circular basin conduits.

### 2.4.6. Proglacial Hydrology

Hock and Noetzli (1997) monitored proglacial discharge as part of a comprehensive glacio-meteorological monitoring programme to model areal glacier melt and discharge. Artificial weirs were constructed on both Nordjåkk and Sydjåkk ~300 m downstream of the glacier terminus and mechanical stage recorders were used to monitor water level. Stage-discharge measurements were obtained using salt dilution techniques (Hock and Noetzli, 1997). It is noted in the study that the relationship between stage and discharge is well established for discharges up to 2 $m^3s^{-1}$ at the Nordjåkk gauging station, and 1 $m^3s^{-1}$ at the Sydjåkk gauging station (Hock and Noetzli, 1997).

## 2.5. Suspended Sediment Transport within the Storglaciären Drainage Basin

Despite a large number of hydrological studies focused on Storglaciären, very little research has been carried out on the nature of suspended sediment transport within the Storglaciären drainage basin.

Schneider and Bronge (1996) investigated long term suspended sediment transport in the Storglaciären drainage basin, concluding that between the years 1980 to 1990, the average suspended sediment leaving the basin was ~$5.74\times10^{6}$ kg $yr^{-1}$. As Schneider and Bronge (1996) concluded that Storglaciären was the primary source of sediment entering the Tarfalajåkk, this equates to a specific suspended sediment yield of $1.85\times10^{6}$ kg $km^{-2}$ $yr^{-1}$. These data correspond to a predicted rate of subglacial erosion of 0.65 mm $yr^{-1}$, and a total value of subglacial erosion for the duration of the study period of between 0.9-1.3 mm yr-$^{1}$. Hydrological gauging during this study was carried out at Rännan, although depth integrated suspended sediment measurements in 1986 were collected at semi-permanent gauging stations established at the Nordjåkk and Sydjåkk in the proglacial area and assumed to be comparable to those collected at Rännan.

Using repeat aerial photogrammetric surveys of the proglacial area of Storglaciären obtained in 1980 and 1990, Holmlund *et al*. (1996b) identified changes in the topography of the proglacial till layer and inferred patterns of sediment erosion and sedimentation. Focusing specifically on areas of the proglacial area directly affected by meltwater streams, Holmlund *et al*. (1996b) calculated an annual volume of erosion from runoff of ~$1.0\times10^{3}m^{3}$, and an annual sedimentation volume of ~$1.3\times10^{3}m^{3}$. These values constitute approximately 50% and 65% respectively of the annual suspended sediment load, and 25%-32% of the total sediment transport recorded at the Rännan gauging station. The study also suggested that the proglacial area of Storglaciären functions as a sediment source, releasing sediment into the proglacial streams. Holmlund *et al*. (1996b) estimated that mass exchange of sediment between the proglacial area and proglacial streams in the first kilometre from the glacier terminus accounts for approximately 30% of the total annual sediment transport (assuming that bedload and suspended sediment are each evenly represented) both contributing 50% to the overall sediment transport budget.

*Chapter 3*

# Patterns of Proglacial Discharge Variability

## 3.1. Introduction

Diurnal glacier outflow hydrographs provide an integrated response to the climatic processes generating surface meltwater and the physical mechanisms controlling the flow of water within the intervening glacier drainage system (Röthlisberger and Lang, 1987; Hannah and Gurnell, 2001). Detailed analysis of proglacial discharge records (e.g. Oerter *et al*., 1981; Hannah *et al*., 1999; 2000) has revealed that the form of the diurnal hydrograph changes throughout the melt season. Such changes may reflect fluctuations in bulk meltwater inputs and the increased efficiency of the glacier drainage system as it evolves over the ablation period (Gurnell, 1995; Richards *et al*., 1996). Given the inaccessibility of sub- and englacial environments, analysis of such fluctuations in proglacial stream discharge can provide valuable information on the hydrology of a glacier which would otherwise be unobtainable and which can contribute significantly to understanding the glacial drainage system (Fountain, 1992). As a result, effective stream monitoring is essential in elucidating the hydrological regime of a glacier and understanding patterns of interannual variability.

This chapter describes the design and implementation of stream gauging sites and subsequent data collection and analysis undertaken at Storglaciären over both the 2009 and 2010 melt seasons. The data presented in this chapter will also provide a basis for subsequent chapters which will investigate the relationship between discharge and suspended sediment transport.

### 3.1.1. Aims of the Chapter

This chapter aims to investigate discharge patterns in the proglacial area of Storglaciären and the factors which influence these. There are two specific objectives:

- To identify the role of meteorological variables in discharge generation at Storglaciären.
- To assess the variability of discharge between two proglacial outlet streams of Storglaciären: Nordjåkk and Sydjåkk.

## 3.2. Proglacial Stream Descriptions

The proglacial drainage of Storglaciären is characterised by two outlet streams, reflecting the division of internal drainage suggested by Stenborg (1973). These streams, Nordjåkk and Sydjåkk are situated laterally on opposing sides of the glacier terminus (Figure 3.1 and 3.2) and divide the area between the terminus and the LIA terminal moraine. Both streams converge with the larger Tarfalajåkk in the proglacial area ~ 400 m downstream of Storglaciären (Schneider and Bronge, 1996). There is a lack of consensus regarding the ratio by which total glacier discharge is divided between the two streams. Several authors have suggested that both streams transmit similar levels of discharge (e.g. Holmlund, 1988b). However it has also been proposed that Nordjåkk carries a greater amount of discharge, reflecting the fact that Nordjåkk primarily transmits meltwater from the accumulation area (Östling and Hooke, 1986; Hock and Hooke, 1993). This may also result in a difference in the amplitude of diurnal discharge variations between the two streams (Hock and Hooke, 1993). The nature of the drainage regime at Storglaciären results in the bulk of surface meltwater being routed through either Nordjåkk or Sydjåkk with very little meltwater transmitted by other transport pathways.

The northern outlet stream, Nordjåkk, initially emerges on a section of lateral moraine on the northern side of the glacier, approximately 50 m up glacier from the terminus. At this location, the stream is shallow with a relatively flat bed. The stream remains exposed for approximately 10-20 m before disappearing beneath a semi-permanent snowpack. The stream re-emerges at the glacier terminus onto a raised section of the proglacial area. Observations later in the melt season suggest that as the snowpack melts and Nordjåkk becomes re-exposed, the stream follows the boundary between the glacier margin and the lower part of the lateral moraine. Upon reaching the terminus, the stream converges with subglacial meltwater which appears to be routed from the centre of the glacier terminus.

The southern outlet stream, Sydjåkk, emerges from Storglaciären approximately 10 m from the glacier margin onto a raised section of the proglacial area. Unlike Nordjåkk, Sydjåkk is not visible prior to this, possibly as a result of a greater degree of subglacial routing. At the point of emergence from Storglaciären and for approximately 25-30m downstream, the topography of the proglacial area is relatively flat before descending steeply over an area of exposed bedrock.

The flat topography exhibited in the upper reaches of both Nordjåkk and Sydjåkk has resulted in these sections becoming characterised by the presence of large in-stream boulders and, during low flow conditions, mid-stream bars consisting of fine silt. These in-stream obstacles have resulted in a step-pool channel configuration (Zimmerman and Church, 2001; Chin, 2002) becoming evident in both streams. Along these reaches, channel stability is considerably higher than in downstream sections where the angle of slope increases, increasing stream power and erosive potential. In these areas stream bifurcation causes a number of sub-streams to form and large areas of braiding are common.

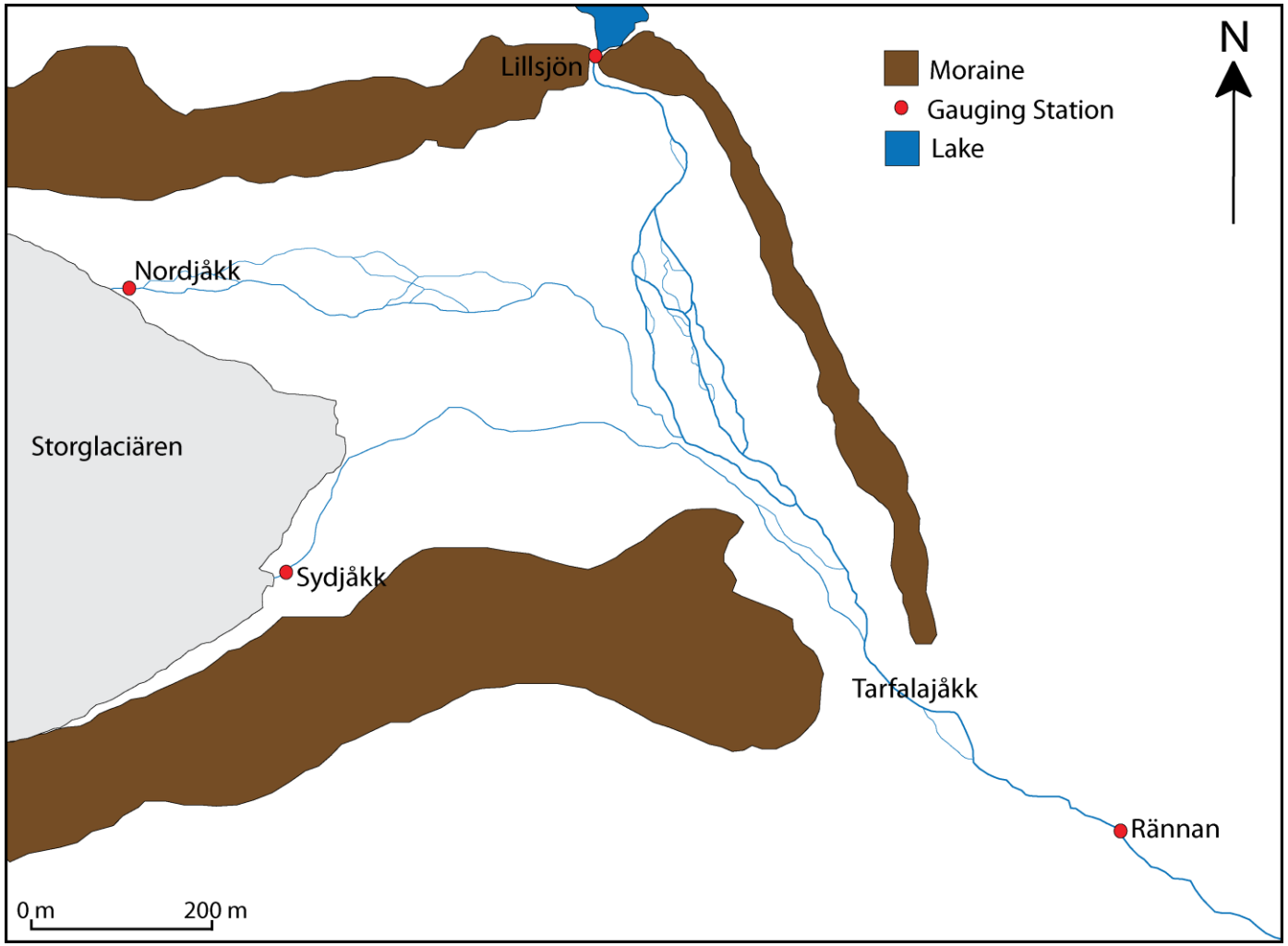


**Figure 3.1. Map of the proglacial area of Storglaciären encompassing the locations of the Nordjåkk and Sydjåkk gauging stations used in this study, and the Lillsjön and Rännan gauging stations managed by Stockholm University.**

**Figure 3.2. Photograph of the terminus of Storglaciären looking south. Both proglacial streams are visible with Sydjåkk at the top of the photograph, and Nordjåkk at the bottom.**

## 3.3. Methods

### 3.3.1. Introduction

Proglacial stream discharge data were collected during two field seasons conducted between July 11th and August 18th (day of year 192-230) 2009, and between July 11th and August 19th (day of year 192-231) 2010.

### 3.3.2. Deployment of Instrumentation

Discharge data were collected using Horizontal Acoustic Doppler Current Profiling (H-ADCP) systems deployed at each gauging site (Figure 3.3). These systems measure the horizontal velocity profile across the width of a river channel from a fixed location on the channel bank (Le Coz *et al*., 2008; Nihei and Kimizu, 2008). Two SonTek/YSI Argonaut-SL H-ADCP systems were installed during both field campaigns – an SL1500 and an SL3000. A summary of the specifications of each unit is listed in Table 3.1.

**Figure 3.3. Photograph of a SonTek/YSI Argonaut-SL prior to deployment at Nordjåkk. Model shown is the SL1500.**

**Table 3.1. Summary of Argonaut-SL specifications**

| Specification | SL1500 (Nordjåkk) | SL3000 (Sydjåkk) |
|---|---|---|
| Frequency | 1500 kHz | 3000 kHz |
| Sampling Volume Size | 0.2 m - 20 m | 0.1 m - 5 m |
| Water Velocity | Range: ± 6 m $s^{-1}$<br>Resolution: 0.1 cm $s^{-1}$<br>Accuracy: ± 1% of measured velocity, ± 0.5 cm $s^{-1}$ | |
| Stage Measurement | Min depth: 0.15 m<br>Max depth: 10 m<br>Accuracy: ± 0.1%, ± 0.3 cm | Min depth: 0.10 m<br>Max depth: 5 m<br>Accuracy: ± 0.1%, ± 0.3 cm |
| Operating Temperature | -5°C - 60°C | |
| Pressure Rating | 30 m | |
| Power Consumption | 0.7 - 1.3 W | |
| Recorder Size | 4 MB (over 500,00 samples) | |
| Multi Cell Profiling | 10 Cells | |
| Temperature Sensor | Resolution: ± 0.01°C<br>Accuracy: 0.5°C | |

The frequency of the unit has implications for both the measurement range of the unit, and the depth at which the system can be deployed. However, given the relatively modest stream dimensions of Nordjåkk and Sydjåkk, the difference between the two units has little consequence for the comparison of data recorded by each unit. In the interest of continuity, the units were deployed at the same site each field season. As observations in the field suggested that Sydjåkk was the narrower and shallower of the two streams, it was decided that the smaller blanking distance and sampling range of the SL3000 would better suit the stream characteristics and allow a greater volume of water to be sampled. Conversely, the SL1500 unit was deployed at Nordjåkk, the wider and deeper of the two streams. Both H-ADCP units were deployed at gauging stations located approximately 20 m downstream from the glacier terminus at sites displaying stable cross sections (Figure 3.4). Each station was constructed from either scaffolding or Dexion

slotted angle in an A-frame configuration and secured to the channel bank using large rocks and sandbags. Instruments were mounted to the gauging station frame using Aluminium drilled strip and cable ties. The two horizontal velocity beams on each H-ADCP unit are angled at 25° off the axis of the unit: one beam facing up stream, and one facing downstream. Therefore, each station was positioned away from large in-channel obstacles that may not only influence the downstream velocity distribution, but also physically obstruct either beam. Both units contain solid-state recorders capable of storing up to 4 MB of data, thus eliminating the need for an external data logger. Power to both units was supplied by a 12 V battery connected to a solar panel to allow trickle charging and prevent data loss through battery failure.

Two important considerations were made regarding the depth at which each unit was deployed within the stream. Firstly, each unit required installation below the minimum water level of the stream in order to maintain a continuous immersion of the unit. Secondly, each unit needed to be mounted high enough from the stream bed to prevent the influence of bedload transport in the data collected. Although every effort was made to fulfil both of these criteria, it is believed that some loss of data was experienced late at the end of each season as extremely low discharges were observed in both streams and caused the H-ADCP units to become exposed. Both units were mounted parallel to both the stream bed, and the direction of water flow and secured tightly to prevent subsequent movement of the unit. Tilting of the unit (at an angle of greater than approximately 3-5° in either the horizontal or vertical plane of the unit) can affect both velocity and stage measurements by reducing the reliability of the vertical beam and by potentially causing the horizontal beams to interact with either the channel bed or the water surface (SonTek/YSI, 2007). However, given that the internal compass of the Argonaut-SL continuously records the orientation and tilt of the unit, it is easy to establish whether any movement of the unit occurred during the deployment period. As there is no evidence to suggest that either of the units tilted either in the vertical or horizontal plane by an increment of greater than 0.5°, it can be concluded that no adverse effect on the data collected was experienced as a result of changes to the plane of the H-ADCP unit.

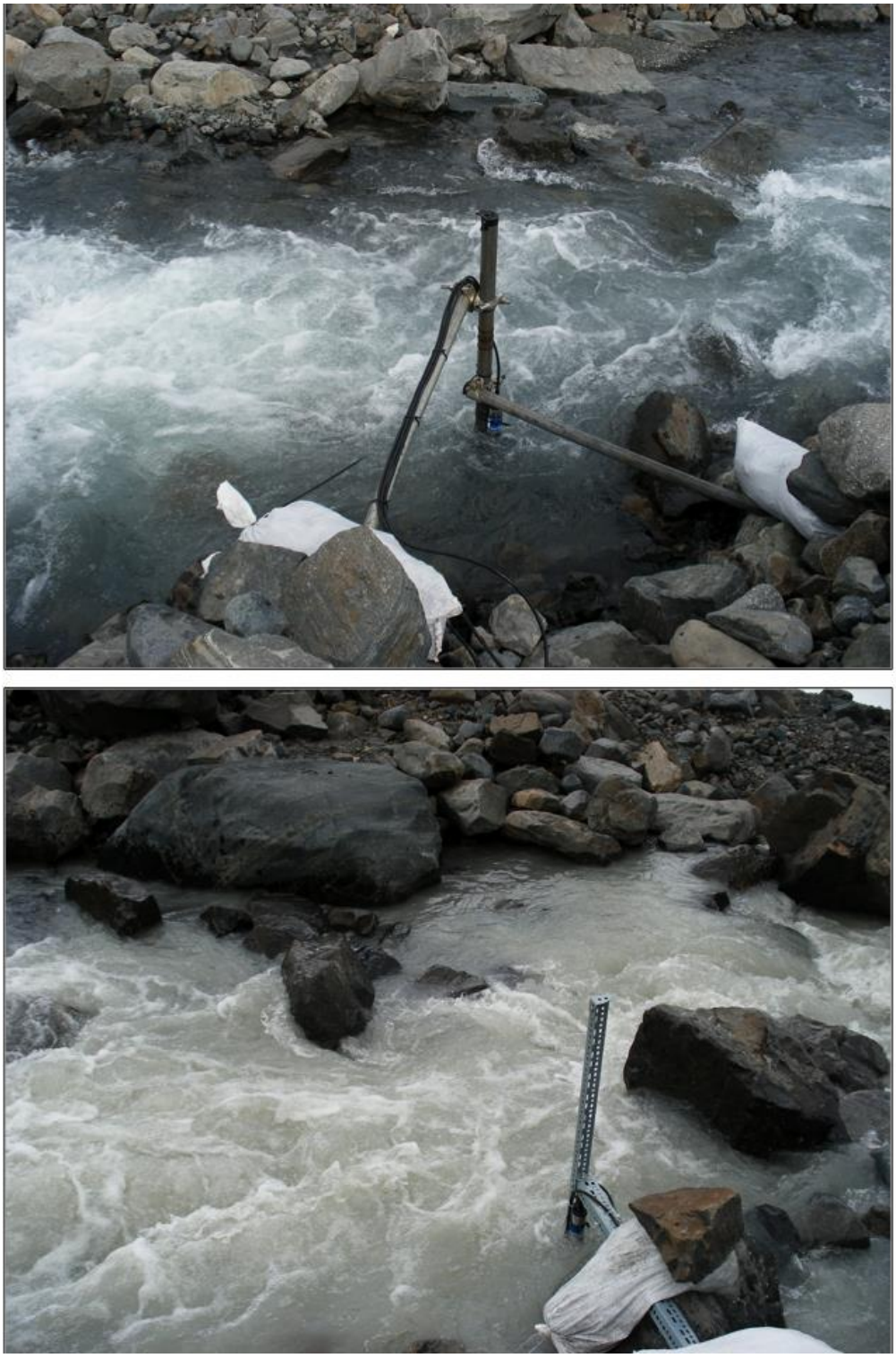

**Figure 3.4. Photographs of deployed gauging stations at Nordjåkk (top) and Sydjåkk (bottom). Flow direction in both photographs is from left to right.**

The final stage of H-ADCP deployment requires a survey of the channel cross section to be conducted in order to provide the Argonaut-SL with the channel geometry data required to calculate discharge. These were undertaken prior to each deployment, and encompassed a detailed survey of the channel width (obtained at 0.1 m resolution), the elevation of the Argonaut-SL within the channel, and the depth of water above the Argonaut-SL. However, unlike traditional surveying where heights are measured relative to the surveyor, these surveys were measured relative to the Argonaut unit. This allows changes in depth or channel area to be detected in relation to the location of the Argonaut-SL within the system. Survey data were programmed into the Argonaut using the SonTek/YSI Argonaut Deployment Software (v.3.30), which also allows measurement variables such as sampling interval, cell width and the number of cells to be specified by the user. Once the requisite data is entered, deployment can be completed, and data collection begins.

### 3.3.3. Measurement of Stream Discharge

Stage and velocity data were collected at intervals of 60 seconds in order to obtain as high a resolution time series as possible. Discharge is estimated using a ⅙ power law relationship (Chen, 1991) which converts measured velocity into mean channel velocity and subsequently, discharge (SonTek/YSI, 2007). Since the H-ADCP units only measure at one depth within the water column, an estimation of the relationship between measured velocity and mean channel velocity is achieved by comparing measured depth with total channel depth (SonTek/YSI, 2002) as demonstrated in Equation 3.1:

$$\frac{V}{u} = \frac{1}{m+1}\left(\frac{h}{y}\right)^{m} \qquad (3.1)$$

where: $V$ is mean channel velocity; $u$ is measured velocity; $m$ is an exponential power law of ⅙ (Gonzales *et al*., 1996), $h$ is channel depth, and $y$ is the distance to the channel boundary (Figure 3.5). Discharge is obtained as the product of $V$ and channel cross-sectional area (SonTek/YSI, 2002). These calculations are inbuilt

into the SonTek/YSI software which accompanies the H-ADCP units (ViewArgonaut v.3.72) and are performed following the recovery of collected data.

The Argonaut-SL units allow a user defined sampling volume to be chosen in order that the most appropriate area of the channel cross section is measured. SonTek/YSI (2007) suggest that whilst it is ideal to obtain as large a sampling volume as possible, it is not necessary to measure the full channel width. This is due to the fact that a smaller section based on the flow distribution of the channel can provide more accurate velocity measurements. Nonetheless, given the relatively small cross sections of the two stream channels and the dynamic nature of glacial streams, each H-ADCP unit was programmed to sample the full width of the channel cross section (Figure 3.5). As well as a single channel averaged velocity and discharge measurement, the units also recorded a multiple cell velocity profile. This allows the instrument to measure velocity in a number of individual cells or 'bins' across the channel width. The channel dimensions of Nordjåkk and Sydjåkk mean that ten cells were profiled and allow specific flow characteristics for different areas of the channel to be investigated.

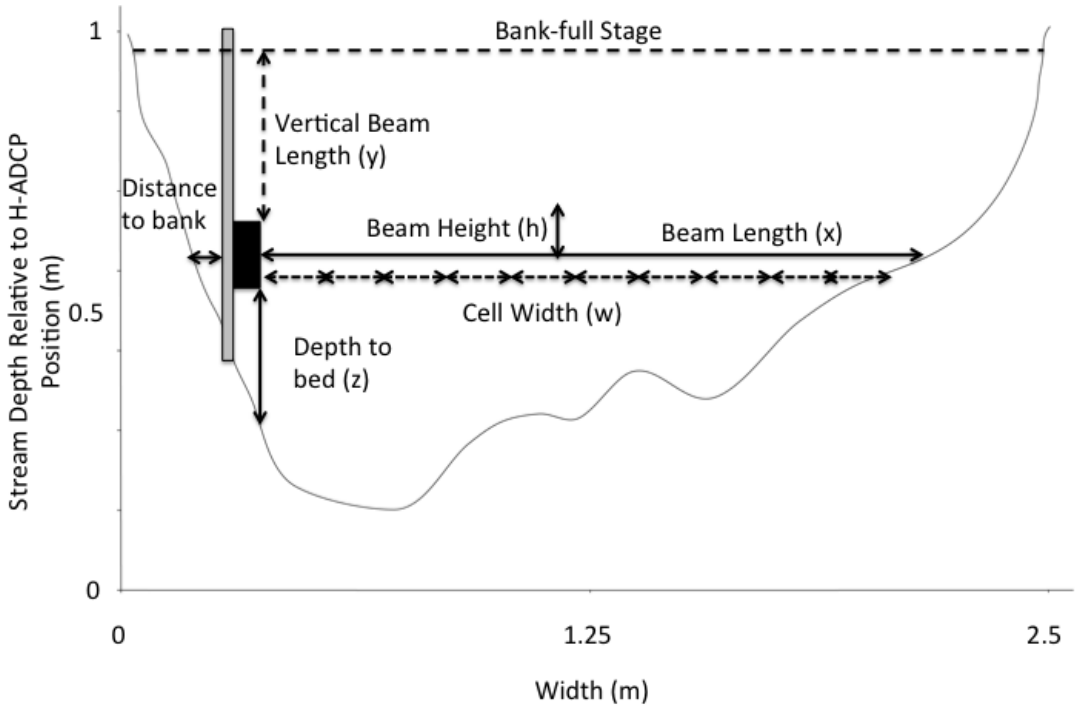


**Figure 3.5. Measured cross-sectional diagram of Sydjåkk showing positioning of H-ADCP unit and channel geometry used in the theoretical discharge calculation.**

### 3.3.4. Synthesis of Discharge Data

As described in the section above, the Argonaut-SL H-ADCP units utilise an upward facing acoustic beam in the calculation of discharge. This beam allows the distance from the unit to the water surface and subsequently the total water depth to be defined using the survey data described in the section above. During extremely low flow events, the upward beams of the Argonaut units were sometimes unable to correctly detect the water surface and calculate stage in spite of continually recording cross sectional stream velocity, and therefore were prevented from calculating discharge. In these cases, data from manual stream depth surveys (conducted at a resolution of 0.1 m width and 0.01 m depth) were used to manually provide estimates of stream depth and channel area. Stream area measurements derived from these surveys were plotted in a time series and a line fitted closely to the points using the 'Interpolate' function of Synergy Software's Kaleidagraph™ v. 4.1.2 (Synergy, Software, 2010). This allowed a continuous time series of stream channel area to be synthesised. Multiplication of these area values allowed discharge to be calculated simply using the standard discharge equation Q = VA. Plots of the cross-sectional area values used during this process are presented in Figures 3.6 (2009) and 3.7 (2010).

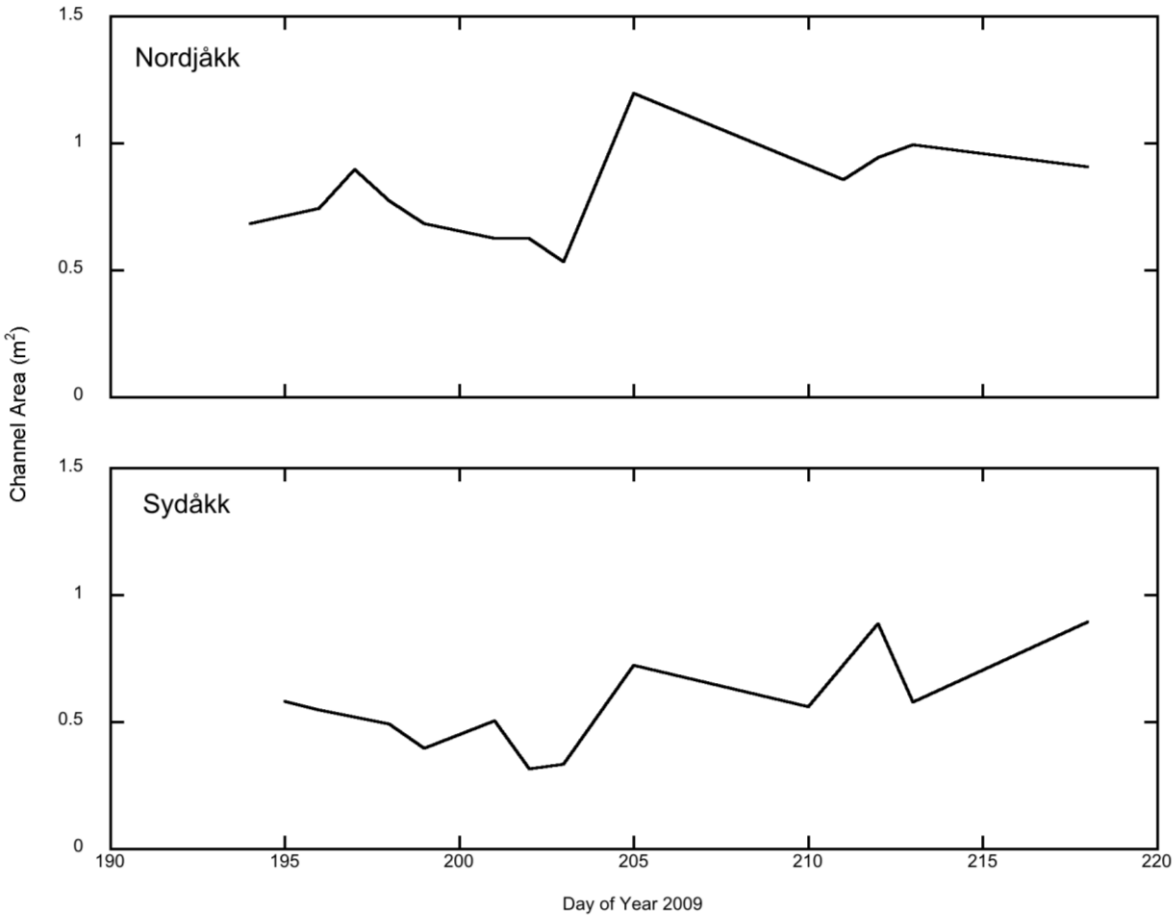


**Figure 3.6. Plots showing channel area data used in the synthesis of discharge data during the 2009 ablation season at Nordjåkk and Sydjåkk**

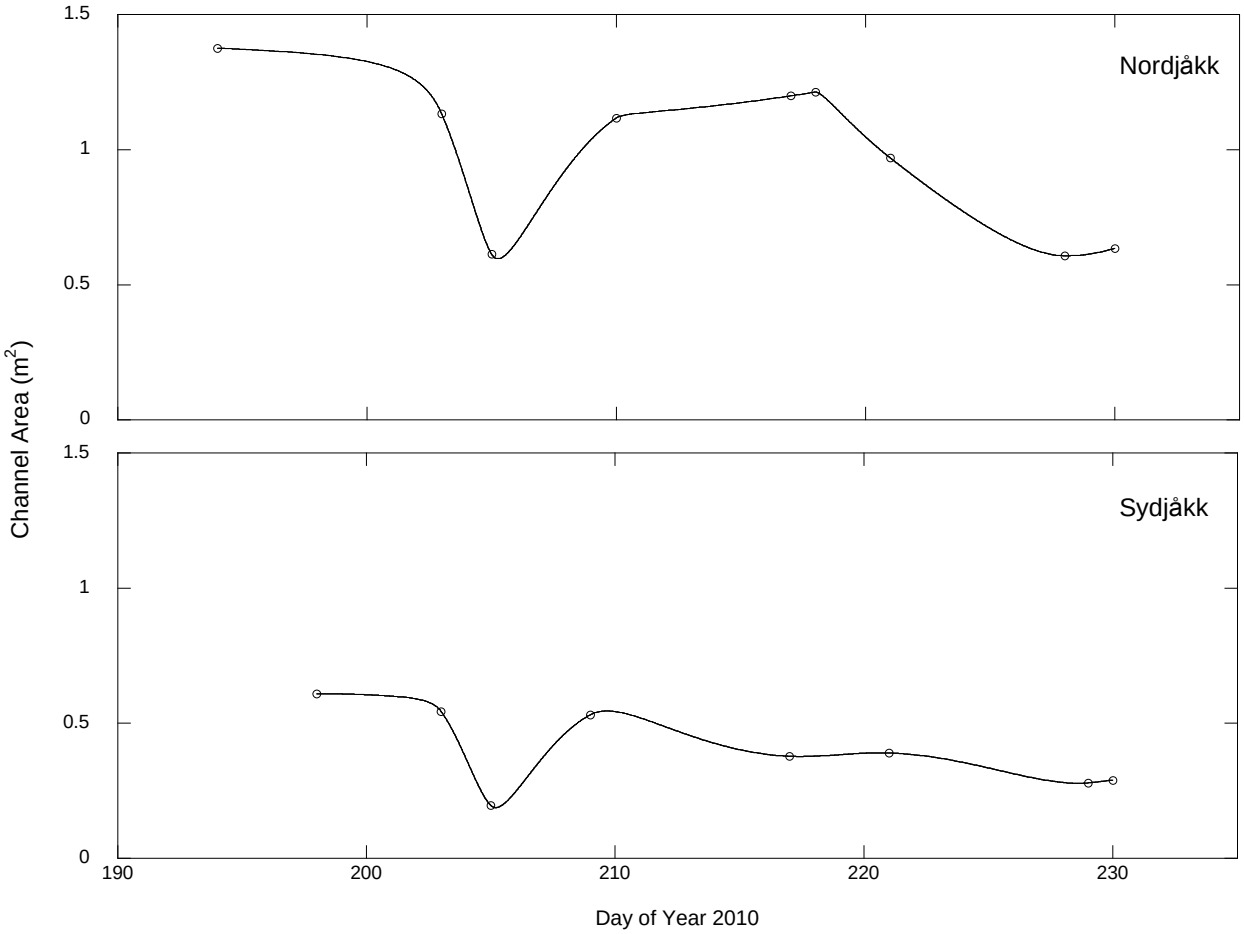


**Figure 3.7. Plots showing channel area data used in the synthesis of discharge data during the 2010 ablation season at Nordjåkk and Sydjåkk**

### 3.3.5. Missing Data

During the field campaign, data were downloaded from the units periodically in case of recorder failure or damage to the units. However, some gaps in the data still exist in both seasons, albeit mainly in the 2009 time series during which no solar panels were used and battery failure was more common. Although such problems are typical in unstable glacifluvial systems (Cooper, 2003) they present significant problems where continuous data are required. Therefore, statistical methods were required in order to fill missing data periods and provide a continuous data record.

Short periods of missing data of up to approximately one day were predicted using the geometric function 'Interpolate' of Synergy Software's Kaleidagraph™ v. 4.1.3 (Synergy Software, 2010). This function fits a curve to a time series which passes through acquired data points and predicts missing data from preceding and succeeding angles of slope (Cooper, 2003). This method is advantageous as it predicts missing data points conservatively when traversing inflections in a time series (Cooper, 2003; Synergy Software, 2010). Longer periods of missing data (> 1 day) were predicted deterministically using least-squares linear regression of the continuous record of discharge recorded at Stockholm University's Rännan gauging station, approximately 1 km downstream from the glacier terminus (see Figure 3.1). A summary of the periods of missing data is presented in Table 3.2 and Figures 3.8 to 3.10.

**Table 3.2. Summary of discharge data missing from raw time series. Percentage values reflect the total number of missing data days, the number of days filled by interpolation techniques, and the number of days filled using regression.**

| | 2009 | | 2010 | |
|---|---|---|---|---|
| | Nordjåkk | Sydjåkk | Nordjåkk | Sydjåkk |
| % Data Missing | 45.4 | 15.1 | 51.9 | 28.2 |
| % Data Interpolated | 5.0 | 15.1 | 10.4 | 11.8 |
| % Data Gap Filled | 40.4 | 0 | 41.4 | 16.3 |

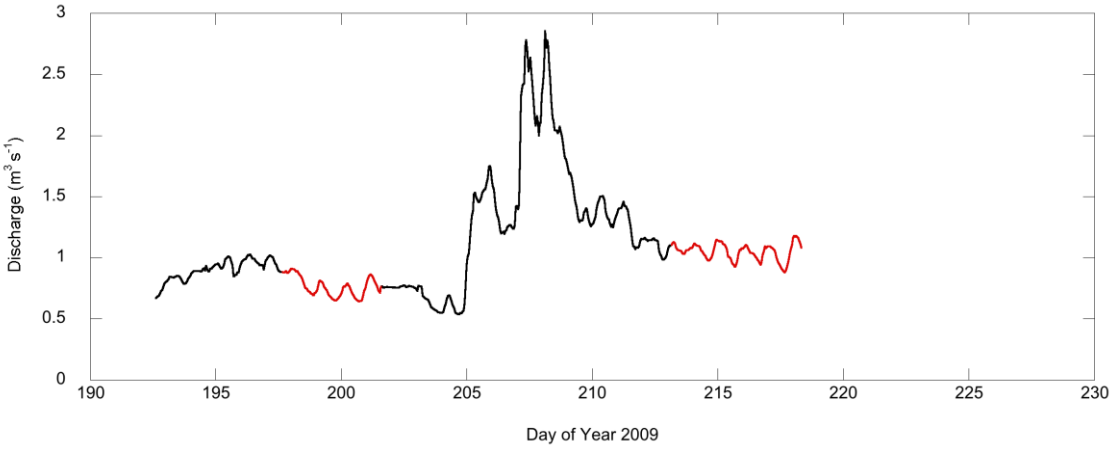


**Figure 3.8. Discharge data recorded at the Nordjåkk gauging station during the 2009 melt season. Period of missing data filled using linear regression are shown in red.**

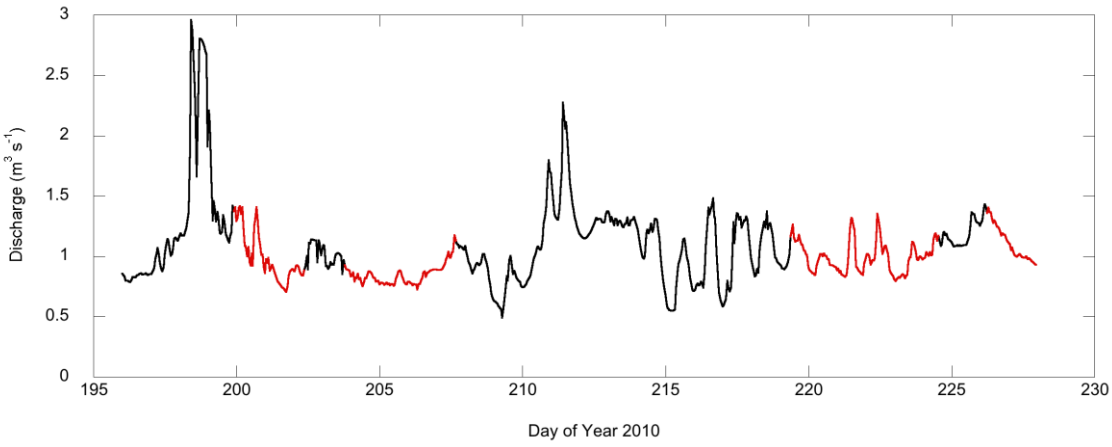


**Figure 3.9. Discharge data recorded at the Nordjåkk gauging station during the 2010 melt season. Period of missing data filled using linear regression are shown in red.**

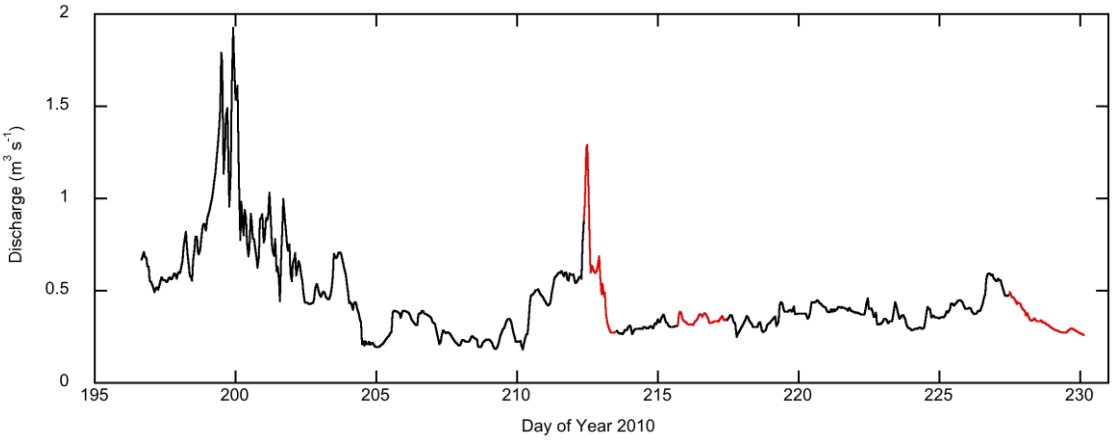


**Figure 3.10. Discharge data recorded at the Sydjåkk gauging station during the 2010 melt season. Period of missing data filled using linear regression are shown in red.**

In spring 2010, the Rännan gauging site was destroyed by a slush avalanche, so data from the station was not available for the 2010 field season. However, analysis of a number of years of discharge data collected by the Tarfala Research Station (P. Jansson, pers. comm.) revealed that a close pattern exists between data collected at Rännan and at the Lillsjön gauging station located approximately 1 km upstream of both the glacier terminus and Rännan (see Figure 3.1). Modelling this relationship by least squares linear regression allowed a record of discharge at Rännan to be estimated and facilitated missing time series data analysis for the 2010 melt season. This regression takes the form: $Q_R = 1.987Q_L - 1.904$ ($r^2 = 0.95$) where $Q_R$ is discharge at the Rännan gauging station, and $Q_L$ is the discharge at the Lillsjön gauging station. This relationship was obtained through analysis of discharge data collected at Rännan and Lillsjön during the 2005, 2006, 2007 and 2009 melt seasons. Although data from other years were available, these were excluded from the analysis for a variety of reasons. Both 2002 and 2007 were discarded as no Lillsjön data were available, and data from 2003 was considered unsuitable as the Rännan time series was already the product of data reconstruction (Schneider, 1996). Data from 2004 were also considered unreliable due to the use of a new pressure transducer and discharge rating curve that year, as well as suffering from missing data as a result of sediment obstructing the pressure transducer inlet pipe (Hubacher, 2006). Relationships from each year were plotted individually using data collected between Julian days 195 and

231 (July 14th – August 19th) in order to match the monitoring period used within this study. The data from each year was then merged into a single composite data set and re-plotted to give a regression equation which represents a multi-year relationship between Rännan and Lillsjön. Given the strength of the relationships represented by $r^2$ in each of the analysed years, and in the final composite data set, the relationship between the two gauging stations is considered reliable, and appropriate for use reconstructing discharge at the Rännan gauging station.

Data from each of the four years used are presented in Figure 3.11, and the final composite linear relationship is presented in Figure 3.12. The reconstructed Rännan discharge data is presented in Figure 3.13 alongside the Lillsjön discharge data used in the reconstruction. By subtracting the discharge of Lillsjön from the discharge of Rännan, the discharge of Storglaciären can be calculated, and this is also presented. Descriptive statistics of these time series are presented in Table 3.3, and a range of published mean discharges of Storglaciären presented in Table 3.4.

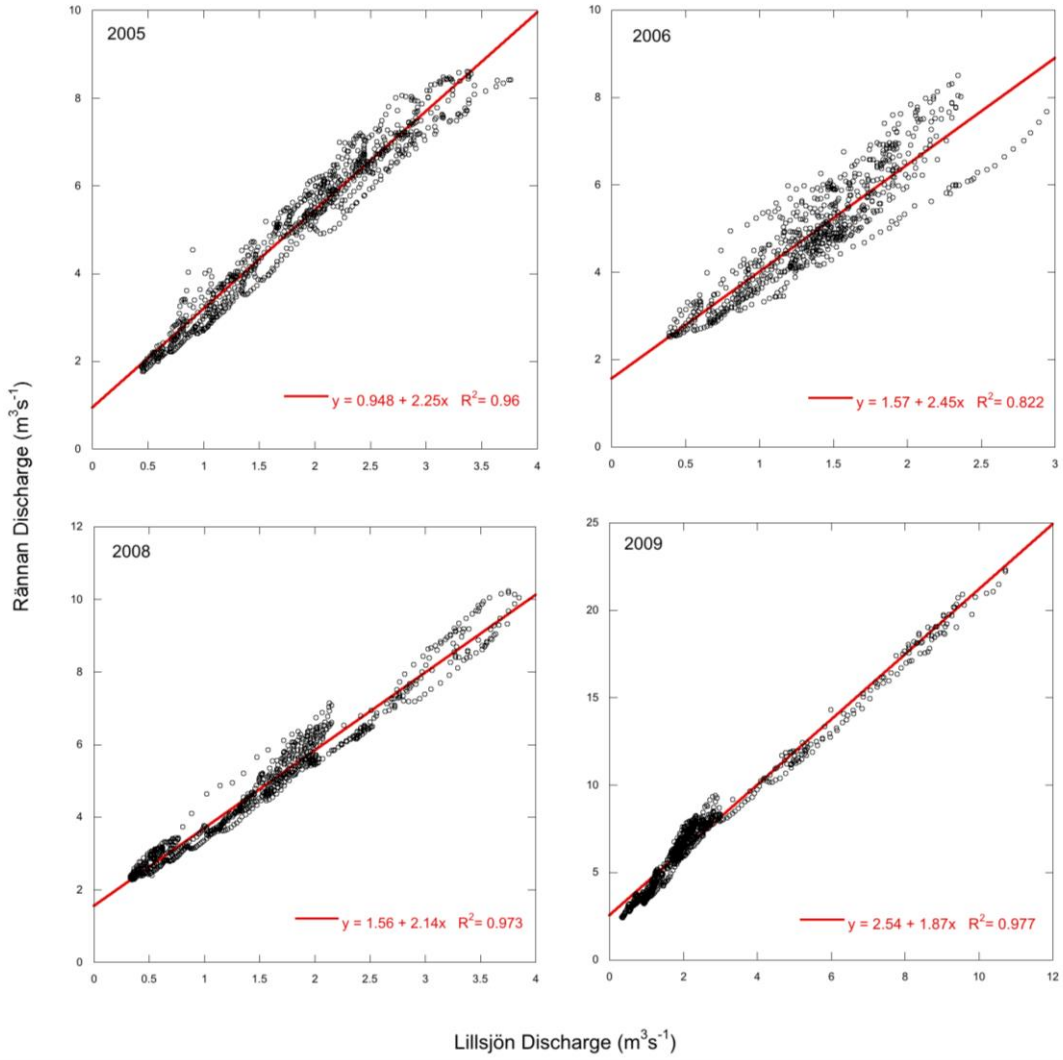


**Figure 3.11. Relationships between discharge data collected at the Rännan and Lillsjön gauging stations over the period July 14th – August 19th (Julian days 195-231)**

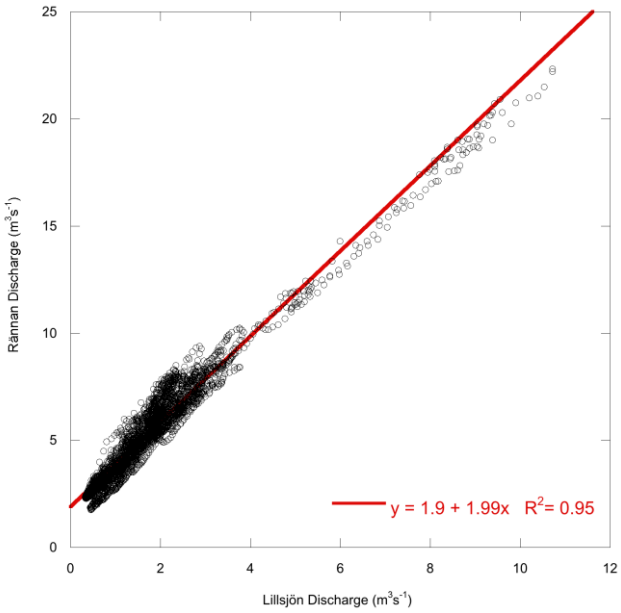


**Figure 3.12. Composite relationship between discharge data collected at the Rännan and Lillsjön gauging stations over the period July 14th – August 19th (Julian days 195-231). Formed using data collected during the 2005, 2006, 2008 and 2009 melt seasons.**

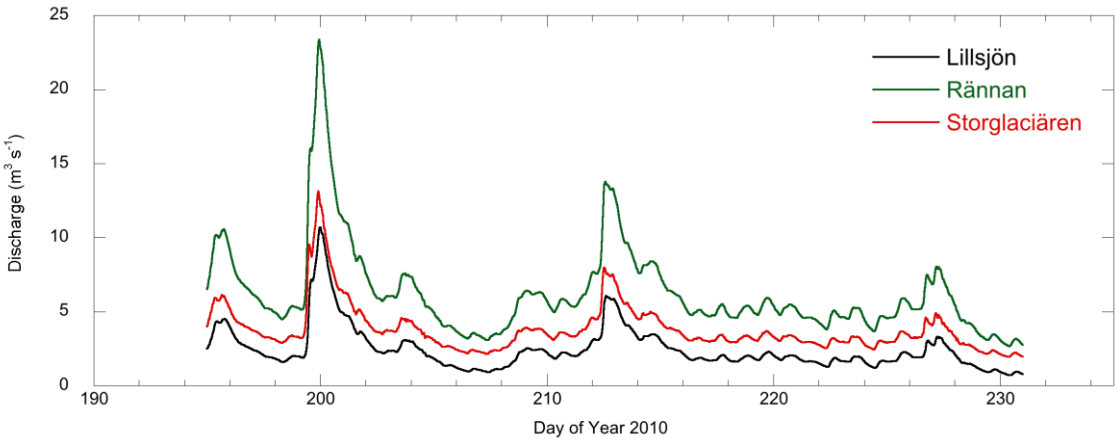


**Figure 3.13. Discharge at Rännan during the 2010 melt season reconstructed using discharge data from the Lillsjön gauging station. The regression model used is presented in Figure 3.12. Estimated discharge of Storglaciären (calculated by subtracting Lillsjön discharge from Rännan discharge) is also shown.**

**Table 3.3. Descriptive statistics of discharge data from Rännan, Lillsjön and Storglaciären for the 2010 monitoring period.**

| | Lillsjön | Rännan | Storglaciären |
|---|---|---|---|
| Mean Discharge ($m^3 s^{-1}$) | 2.44 | 6.25 | 3.81 |
| Maximum Discharge ($m^3 s^{-1}$) | 10.68 | 23.35 | 13.13 |
| Minimum Discharge ($m^3 s^{-1}$) | 0.72 | 2.67 | 1.95 |

**Table 3.4. Mean discharge values for Storglaciären**

| Study | Monitoring Period | Mean Discharge ($m^3 s^{-1}$) |
|---|---|---|
| Nilsson & Sundblad (1975) | 1-17th Aug 1969 | 2.07 |
| Östling & Hooke (1986) | May-Sept 1984 | 2.26 |
| Hock & Hooke (1993) | Jul 26th - Aug 23rd 1989 | 0.70 |
| Jansson (1995) | Jul 14th - Aug 18th 1987 | 1.64 |
| Schneider & Bronge (1996) | Jun 15th - Sept 3rd 1981 | 4.18 |
| Hock & Jansson (2005) | Aug-Sept 1994 | 1.19 |

A summary of linear regression models used to fill data gaps at both gauging sites is shown in Table 3.5 and Figures 3.14 to 3.16.

**Table 3.5. Summary of linear regression models used to predict missing discharge data at the Nordjåkk and Sydjåkk gauging stations during the 2009 and 2010 ablation seasons. Dates and times are given in the hour-day format. In the regression column, $Q_R$ is the discharge ($m^3 s^{-1}$) of Storglaciären calculated using the Rännan and Lillsjön gauging stations, $Q_N$ is the discharge ($m^3 s^{-1}$) at the Nordjåkk gauging station and $Q_S$ is the discharge ($m^3 s^{-1}$) at the Sydjåkk gauging station. In the final three columns, $r^2$ is the coefficient of determination, *se* is the standard error of the curve (±%), and *F* is the *F*-test statistic (given in italics where values are not significant at the 0.01 significance level).**

| Year | Gauging Station | Missing Data Period | Regression Model | $r^2$ | *se* | *F* |
|---|---|---|---|---|---|---|
| 2009 | Nordjåkk | 17:00 195 - 13:00 201 | $Q_N = 0.463 + 0.177Q_R$ | 0.87 | 0.28 | 920.52 |
| 2009 | Nordjåkk | 05:00 213 - 09:00 220 | $Q_N = 0.353 + 0.164Q_R$ | 0.75 | 0.30 | 751.12 |
| 2010 | Nordjåkk | 23:00 199 - 08:00 202 | $Q_N = -1.330 + 1.410Q_R$ | 0.87 | 0.16 | 2341.31 |
| 2010 | Nordjåkk | 20:00 203 - 15:00 207 | $Q_N = -0.664 + 0.359Q_R$ | 0.78 | 0.16 | 959.19 |
| 2010 | Nordjåkk | 10:00 219 - 12:00 224 | $Q_N = -0.190 + 0.282Q_R$ | 0.67 | 0.18 | 570.48 |
| 2010 | Nordjåkk | 07:00 226 - 00:00 229 | $Q_N = 0.328 + 0.204Q_R$ | 0.79 | 0.16 | 779.60 |
| 2010 | Sydjåkk | 10:00 212 - 12:00 213 | $Q_S = -1.090 + 0.903Q_R$ | 0.60 | 0.20 | 462.97 |
| 2010 | Sydjåkk | 18:00 215 - 10:00 217 | $Q_S = -0.941 + 0.800Q_R$ | 0.61 | 0.09 | 362.73 |
| 2010 | Sydjåkk | 12:00 227 - 03:00 230 | $Q_S = -0.019 + 0.113Q_R$ | 0.80 | 0.17 | 819.49 |

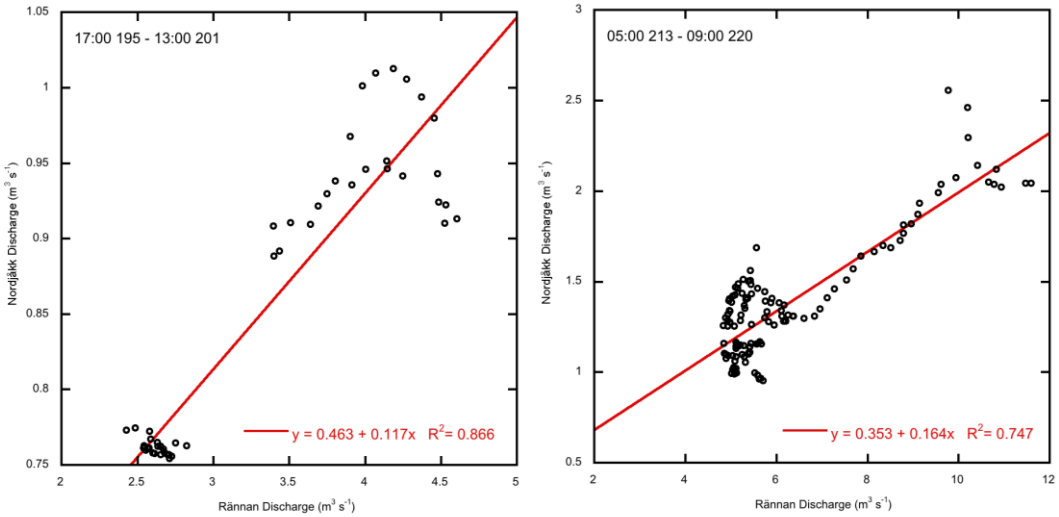


**Figure 3.14. Plots showing data used to construct linear regression models in order to fill missing data gaps during the 2009 season at Nordjåkk. Full details of each model are presented in Table 3.3.**

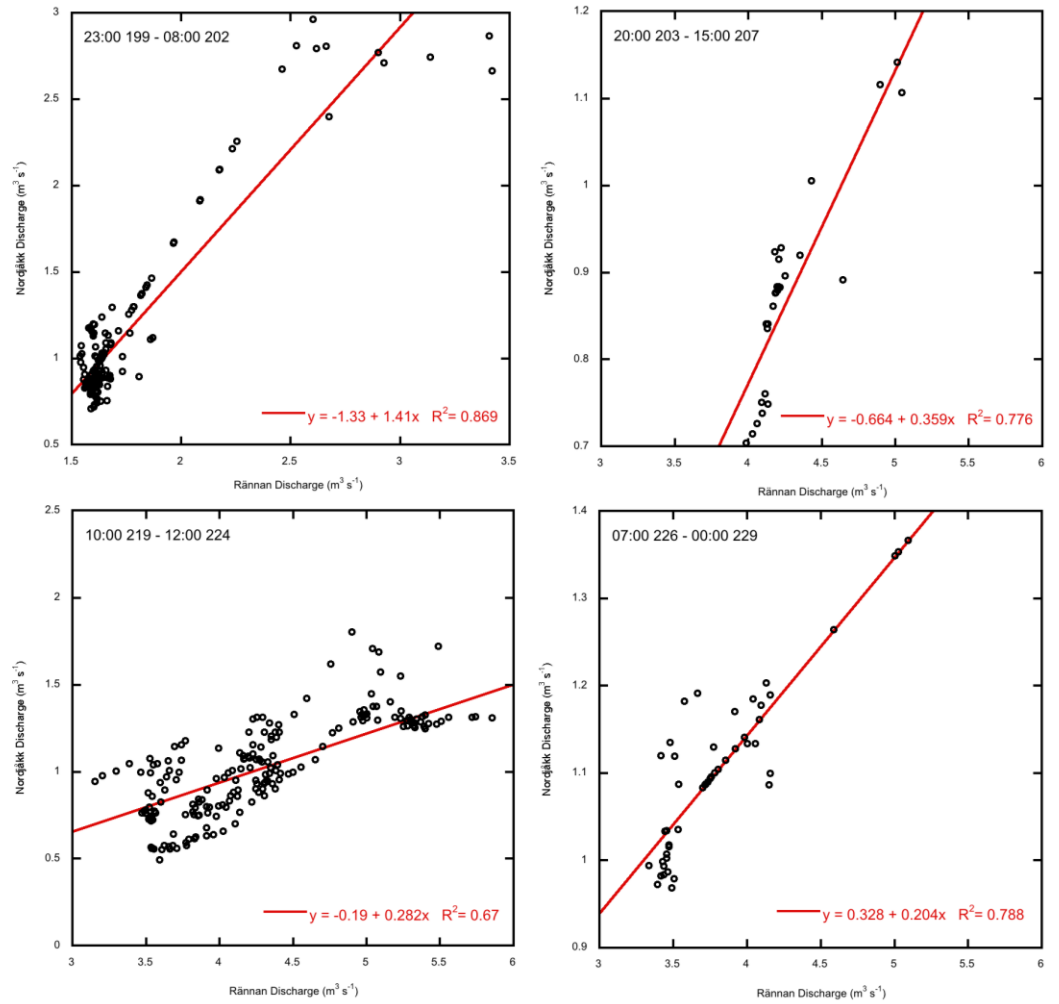


**Figure 3.15. Plots showing data used to construct linear regression models in order to fill missing data gaps during the 2010 season at Nordjåkk. Full details of each model are presented in Table 3.3.**

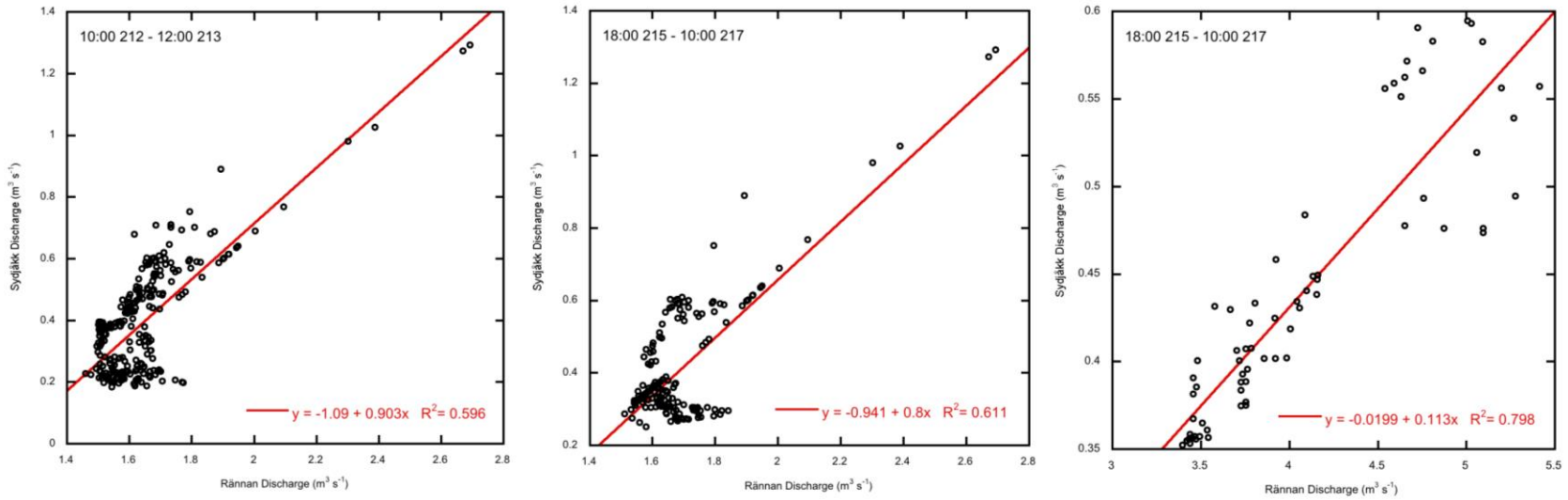


**Figure 3.16. Plots showing data used to construct linear regression models in order to fill missing data gaps during the 2010 season at Sydjåkk. Full details of each model are presented in Table 3.3.**

### 3.3.5.1. Validation of Gap-filling Techniques

As observed in the above section, high incidences of missing data in the discharge time series have necessitated the use of techniques to fill such gaps. It is important therefore, that the consequences of simulating missing data are understood so that the completed data set can be treated with confidence. This section aims to accomplish this through the use of an experimental technique. This involves the creation of a gap within a period of raw discharge data which is subsequently filled using interpolation. The two data sets (original and gap-filled) can then be compared in order to ascertain the effect that gap filling has on the data.

Testing was carried out using discharge data collected at the Sydjåkk gauging station during the 2010 season, and which had been used in analysis of discharge-sediment hysteresis. Hysteresis describes this relationship between discharge and sediment transport (Gregory and Walling, 1973; Walling, 1974; Church and Gilbert, 1975; and Statham, 1977) and implies a bivariate relationship in which values of the dependent variable for a given value of the independent variable differ according to whether the independent variable is increasing or decreasing (Hodgkins, 1996). A more complete description of hysteresis is given in Chapter 4 where it is used in the analysis of suspended sediment dynamics. These data were used due to the fact that hysteresis analysis is performed individually on each day of the monitoring period, allowing a number of results to be accumulated, rather than over a more coarse time period. Furthermore, hysteresis analysis produces a distinctive pattern which facilities easy comparison between the original and gap-filled data sets.

Testing the effects of gap filling was carried out in two stages. Firstly, a gap nine hours long was created in the discharge time series. This length was selected as it represents the mean duration of periods of missing data observed during the study. Analysis of periods of missing data at Sydjåkk during the 2010 melt season suggest that most gaps occur overnight and especially between the hours of 05:00 and 09:00 (as shown in Figure 3.17). The missing data was therefore established

to encompass this period, as well as a three hour gap between 02:00 and 06:00, and a two hour gap between 09:00 and 11:00 which are also frequently afflicted with missing data.

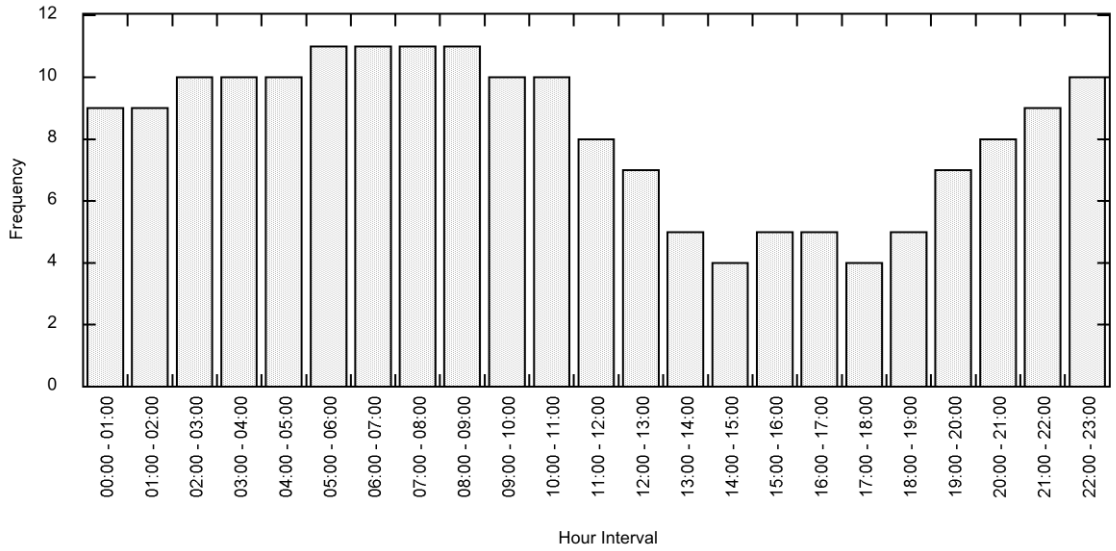


**Figure 3.17. Frequency of missing discharge data during one hour time intervals during the 2010 melt season at Sydjåkk.**

The second stage involved the filling of the created period of missing data. This was accomplished using the geometric function 'Interpolate' of Kaleidagraph™ v. 4.1.3 (Synergy Software, 2010) as described in Section 3.3.5. Hysteresis analysis was then carried out on both the original and gap filled data sets and differences between the two analyses recorded. Least squares linear regression was also carried out, as this is used as a proxy for suspended sediment availability in Chapter 4. Evaluation of the influence of gap filling was based on four factors: changes in the direction of the hysteresis loop (either clockwise or anticlockwise), the slope of linear regression, the intercept of linear regression, and the regression coefficient of determination ($r^2$). These factors allow assessment of both the pattern of the data set, and any quantitative changes which may occur. Examples of 'before and after' hysteresis loops of three days are presented in Figure 3.18, and statistics of the full analysis are presented in Table 3.6.

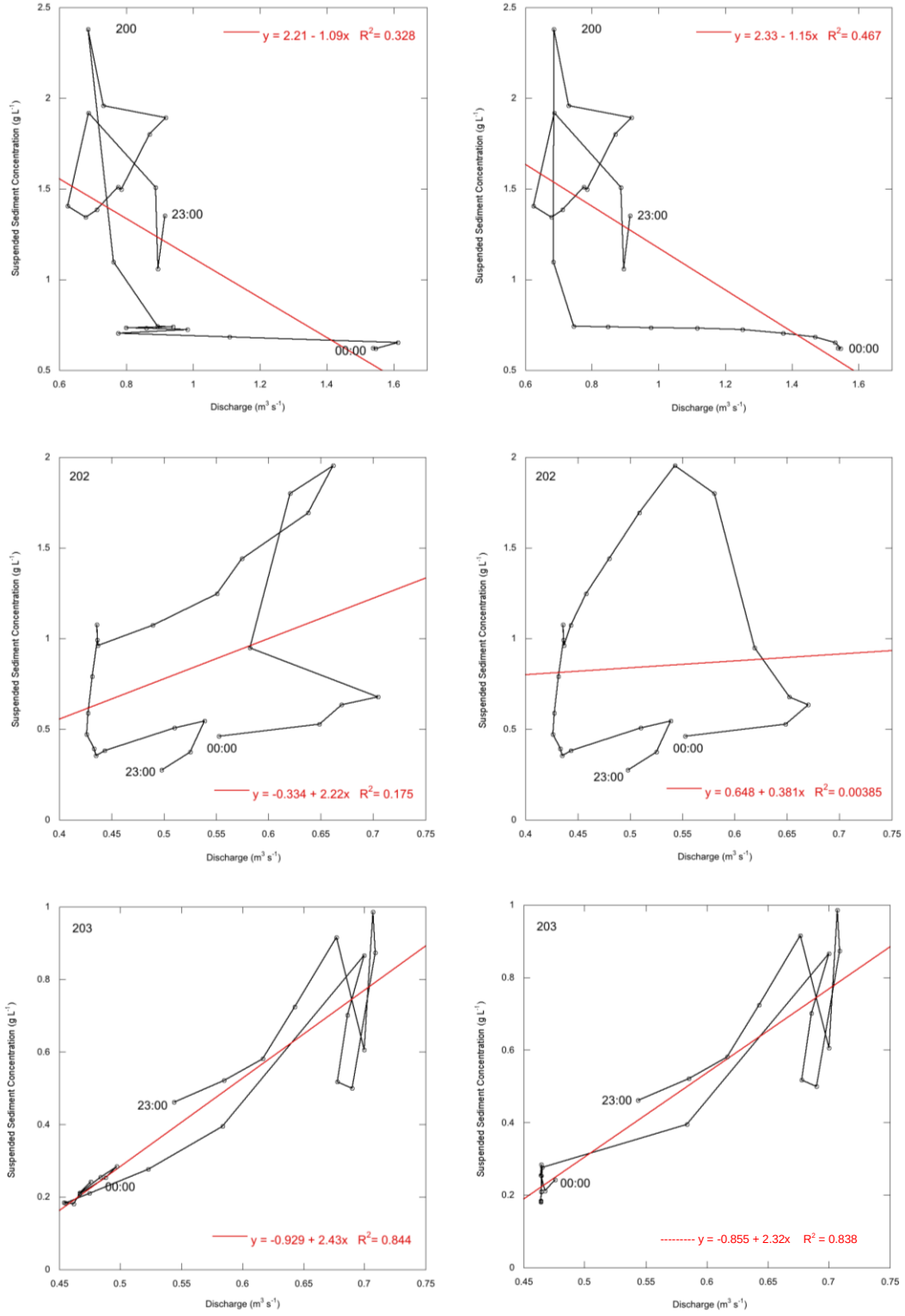


**Figure 3.18. Examples of hysteresis analysis carried out on both original data (left), and gap-filled data (right) on days 200, 202 and 203. Linear regression lines and equations are shown in red.**

**Table 3.6. Differences in regression statistics between original and gap-filled discharge data following hysteresis analysis. N.B. As several of the results of these analyses contain negative data, these have been corrected to positive to demonstrate relative change.**

| | Slope | Intercept | $r^2$ |
|---|---|---|---|
| Mean Change | 2.583 | 0.824 | 0.080 |
| Maximum Change | 22.284 | 6.658 | 0.311 |
| Minimum Change | 0.007 | 0.000 | 0.001 |

It is clear from observing the hysteresis loops in Figure 3.18. that the shape of the loop in generally well maintained. In Day 202 the gap filling results in the removal of a small clockwise loop, although the overall directional trend of the loop is maintained. None of the days tested showed a change in the overall hysteresis direction. As a result, it can be concluded that gap filling does not significantly affect the main trend of the data, although as shown in Day 202, the resolution of the data may be slightly coarsened. Table 3.6. shows the differences in regression statistics between original and gap-filled data. In each statistic, the mean change is small suggesting that gap filling has very little effect on the regression. Although the maximum change in slope is high, the maximum intercept and $r^2$ are considerably smaller, suggesting that this may be an anomaly. Overall, it appears that differences in all four of the factors tested are small and that therefore gap filling is unlikely to adversely affect data analysis or interpretation.

### 3.3.5.2. Reproducibility of Time Series

An important advantage of the least squares linear regression gap-filling technique used during this study is the ability for missing data periods of 1 day or longer to be filled deterministically using discharge data collected at the Rännan gauging station. As a result, it is possible to present continuous data even where gaps are too long to fill using interpolation techniques. The influence of gap filling on the

results of data analysis has been assessed in Section 3.3.5.1. However, this section aims to further test the effectiveness of gap filling by using least squares linear regression to reproduce a period of discharge data in the same way as if it was a period of missing data. In this way the original and replicated discharge time series can be compared, allowing the discrepancy between the data to be used as an assessment of the technique.

In order to carry out the assessment, two periods of discharge data collected during the 2010 melt season were reproduced, one from Nordjåkk (Days 215-219), and one from Sydjåkk (Days 222-227). These periods were selected as they fit two essential criteria: (i) the length of the period was appropriate to justify gap-filling (i.e. > 1 day); and (ii) the data were continuous and free from gaps or periods filled by interpolation. Time series reproduction was performed using the least square linear regression technique described in Section 3.3.5. The details of the regression models used for each reproduction are presented in Table 3.7, and in Figures 3.19 and 3.20.

**Table 3.7. Summary of linear regression models used to predict missing discharge data at the Nordjåkk and Sydjåkk gauging stations during tests on the reproducibility of time series. Dates and times are given in the hour-day format. In the regression column, $Q_R$ is the discharge ($m^3 s^{-1}$) of Storglaciären calculated using the Rännan and Lillsjön gauging stations, $Q_N$ is the discharge ($m^3 s^{-1}$) at the Nordjåkk gauging station and $Q_S$ is the discharge ($m^3 s^{-1}$) at the Sydjåkk gauging station. In the final three columns, $r^2$ is the coefficient of determination, *se* is the standard error of the curve (±%), and *F* is the *F*-test statistic (given in italics where values are not significant at the 0.01 significance level).**

| Year | Gauging Station | Missing Data Period | Regression Model | $r^2$ | *se* | *F* |
|---|---|---|---|---|---|---|
| 2010 | Nordjåkk | 17:00 215 - 04:00 219 | $Q_N = -0.177 + 0.278Q_R$ | 0.69 | 0.21 | 213.52 |
| 2010 | Sydjakk | 13:00 222 - 11:00 227 | $Q_S = -0.013 + 0.110Q_R$ | 0.71 | 0.04 | 341.67 |

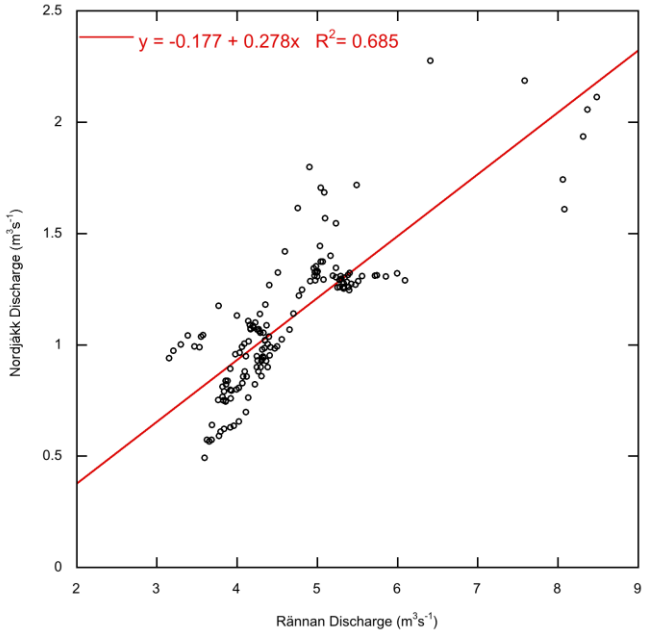


**Figure 3.19. Plot showing data used to construct linear regression models in order to test the reproducibility of data during the 2010 season at Nordjåkk. Full details of each model are presented in Table 3.7.**

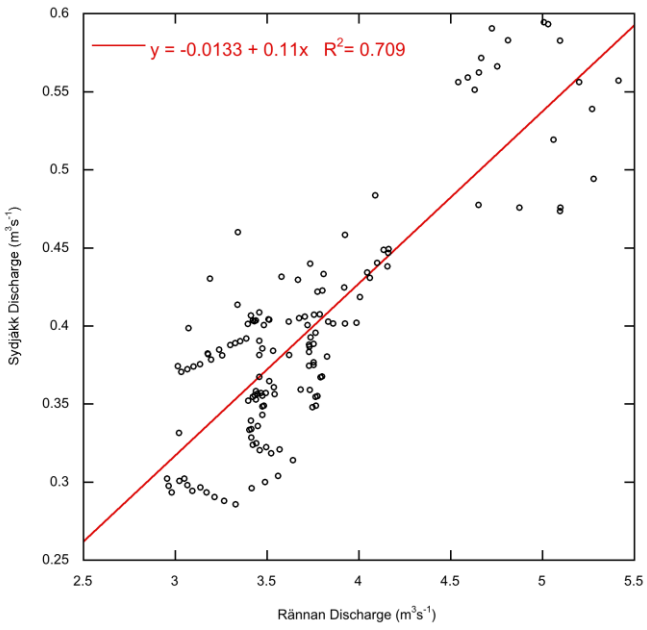


**Figure 3.20. Plot showing data used to construct linear regression models in order to test the reproducibility of data during the 2010 season at Sydjåkk. Full details of each model are presented in Table 3.7.**

The reproduced Nordjåkk discharge data (Figure 3.21) suggests that gap-filling produces a conservative approximation of the original data. Whilst the pattern of discharge appears to match the original time series, changes in magnitude are inadequately represented, producing a narrow range of data. Figures 3.21. and 3.22. suggest that this results in the reproduced data underestimating the original data, although overestimation is also apparent (e.g. Days 216 and 218). This is also evident in Table 3.8, where the original data is underestimated by a maximum of approximately 0.57 $m^3s^{-1}$. Comparatively, the original data is overestimated by a maximum of approximately 0.30 $m^3s^{-1}$ (presented in Table 3.8 as minimum difference). However, in spite these inconsistencies, the difference between the mean original and reproduced data is small, ~ 0.1 $m^3s^{-1}$. This suggests that the fit between the two data sets is closer than that suggested by the range of over or underestimation presented in Figure 3.22 and Table 3.8.

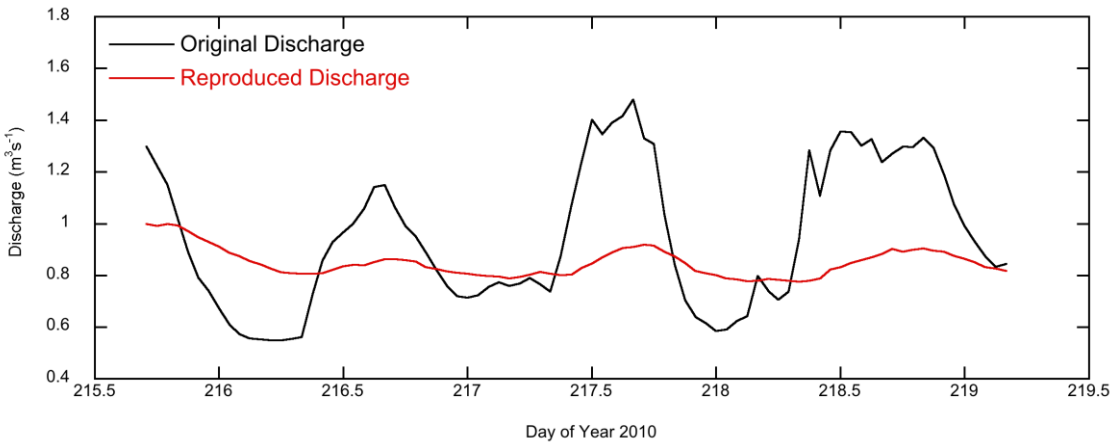


**Figure 3.21. Plot showing a period of discharge data collected at the Nordjåkk gauging station during the 2010 season (black), and a reproduction of the data using least squares linear regression (red).**

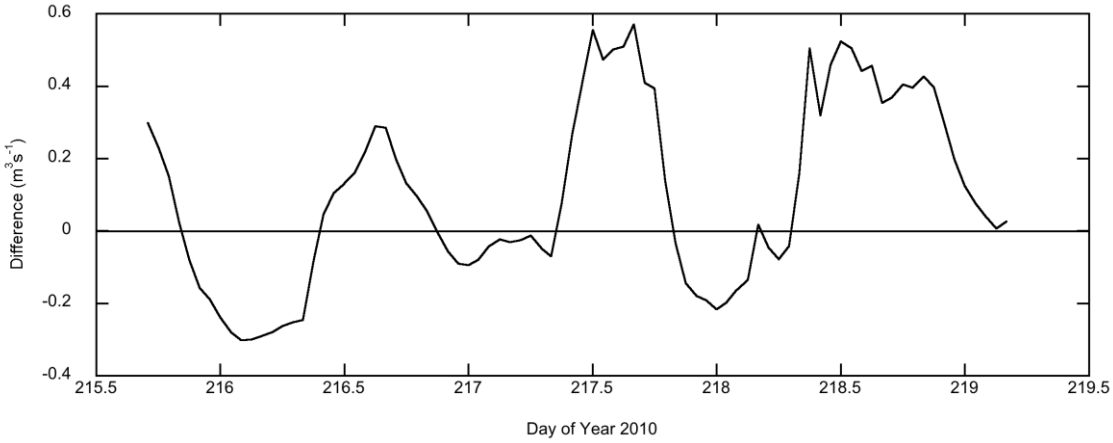


**Figure 3.22. Plot showing the difference between the original data collected at Nordjåkk during the 2010 season, and the time series produced using least squares linear regression.**

**Table 3.8. Summary of descriptive statistics comparing discharge data collected at Nordjåkk, and data reproduced using least squares linear regression. Difference refers to statistical analysis performed on the calculated difference between the original and reproduced data. These data are graphically represented in Figure 3.22. Differences are relative to zero, i.e. negative values indicate that the reproduced data is less than the original data.**

| | Nordjåkk | | |
|---|---|---|---|
| | Original Discharge | Reproduced Discharge | Difference |
| Mean ($m^3s^{-1}$) | 0.948 | 0.849 | 0.099 |
| Maximum ($m^3s^{-1}$) | 1.480 | 0.999 | 0.570 |
| Minimum ($m^3s^{-1}$) | 0.548 | 0.777 | -0.301 |
| Range ($m^3s^{-1}$) | 0.931 | 0.222 | 0.871 |
| St. Dev. ($m^3s^{-1}$) | 0.273 | 0.055 | 0.251 |
| Variance | 0.075 | 0.003 | 0.063 |

The reproduced Sydjåkk discharge data (Figure 3.23) indicates a much closer fit between the original and replicated data. As observed in the Nordjåkk data (Figure 3.21), the temporal pattern of the reproduced time series matches that of the original data. The reproduced data appears to lag the original data, although this is to be expected given the distance downstream of the Rännan gauging

station (~ 1 km). The fit between the two time series is considerably closer than that observed between the Nordjåkk data with a maximum deviation of approximately 0.08 $m^3s^{-1}$ (Table 3.9; Figure 3.24). Similarly to the Nordjåkk time series, the mean difference between the Sydjåkk time series is very small, ~0.01 $m^3s^{-1}$ suggesting that the reproduced data closely fits the original data.

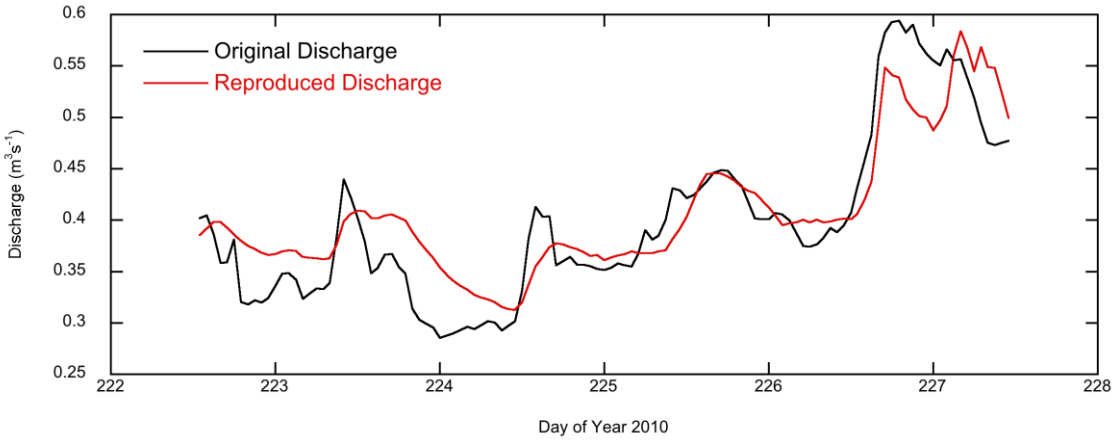


**Figure 3.23. Plot showing a period of discharge data collected at the Sydjåkk gauging station during the 2010 season (black), and a reproduction of the data using least squares linear regression (red).**

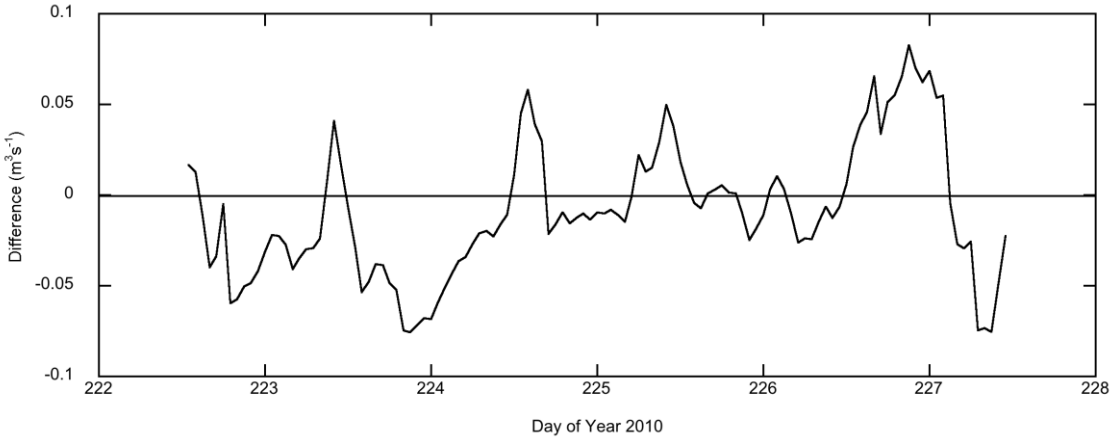


**Figure 3.24. Plot showing the difference between the original data collected at Sydjåkk during the 2010 season, and the time series produced using least squares linear regression.**

**Table 3.9. Summary of descriptive statistics comparing discharge data collected at Sydjåkk, and data reproduced using least squares linear regression. Difference refers to statistical analysis performed on the calculated difference between the original and reproduced data. These data are graphically represented in Figure 3.24. Differences are relative to zero, i.e. negative values indicate that the reproduced data is less than the original data.**

| | Sydjåkk | | |
|---|---|---|---|
| | Original Discharge | Reproduced Discharge | Difference |
| Mean ($m^3s^{-1}$) | 0.398 | 0.407 | 0.009 |
| Maximum ($m^3s^{-1}$) | 0.594 | 0.584 | 0.083 |
| Minimum ($m^3s^{-1}$) | 0.286 | 0.313 | -0.076 |
| Range ($m^3s^{-1}$) | 0.309 | 0.271 | 0.158 |
| St. Dev. ($m^3s^{-1}$) | 0.080 | 0.063 | 0.036 |
| Variance | 0.006 | 0.004 | 0.001 |

It is clear from the data presented above that Nordjåkk and Sydjåkk both differ in terms of the reproducibility testing of discharge data. Whilst the reproduced Nordjåkk time series presents a narrow range of data, both widely over and underestimating the original time series, the Sydjåkk time series fits closely, with very fine margins of discrepancy between the original and reproduced data (< 0.1 $m^3s^{-1}$). However, in both cases, the difference between the mean original and reproduced data is small (< 0.1 $m^3s^{-1}$ at Nordjåkk, and < 0.01 $m^3s^{-1}$ at Sydjåkk). It is these values that provide confidence in the effectiveness of the least squares linear regression technique, as they suggest that the mean discharge of a period of missing data can be reproduced accurately. As observed in the Nordjåkk replication, one adverse effect of the gap filling technique may be the loss of resolution in the data, resulting in periods of over or underestimation. This may however be a function of the difference between the high resolution data collected in the proglacial are of Storglaciären, and the comparatively lower resolution data collected at Rännan which is used to reproduce it.

### 3.3.6. Validation of Monitoring Period

In order to validate the length of the monitoring period (JD 192 to 231), discharge data collected at the Rännan gauging station between 2002 and 2009 was used to better understand the hydrological dynamics of the Storglaciären basin during July and August. These data are presented in Figures 3.25 – 3.32 The start of the Storglaciären melt season varies from year to year (Hubacher, 2006), although Östling and Hooke (1986) suggest that it typically occurs in mid to late June.

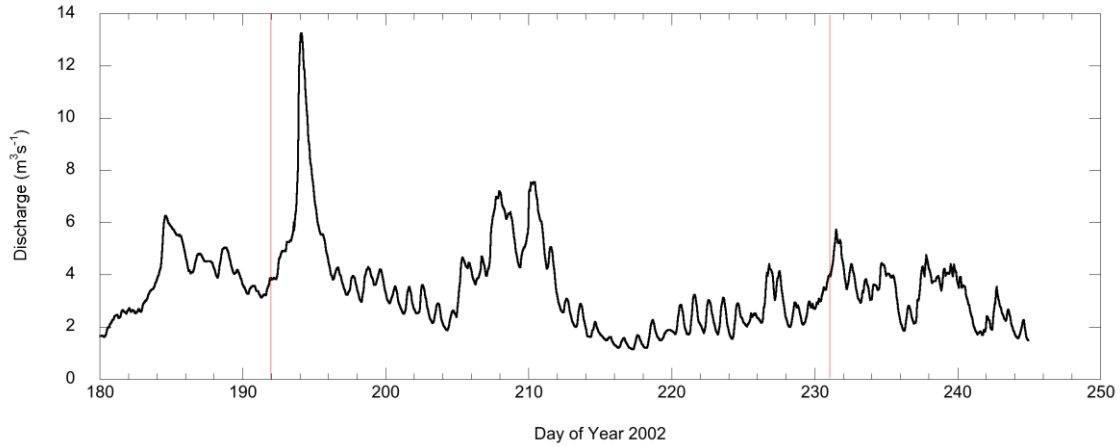


**Figure 3.25. Discharge time series from the Rännan gauging site during the 2002 ablation season. The red lines indicate the span of the monitoring period in this study (JD 192-231).**

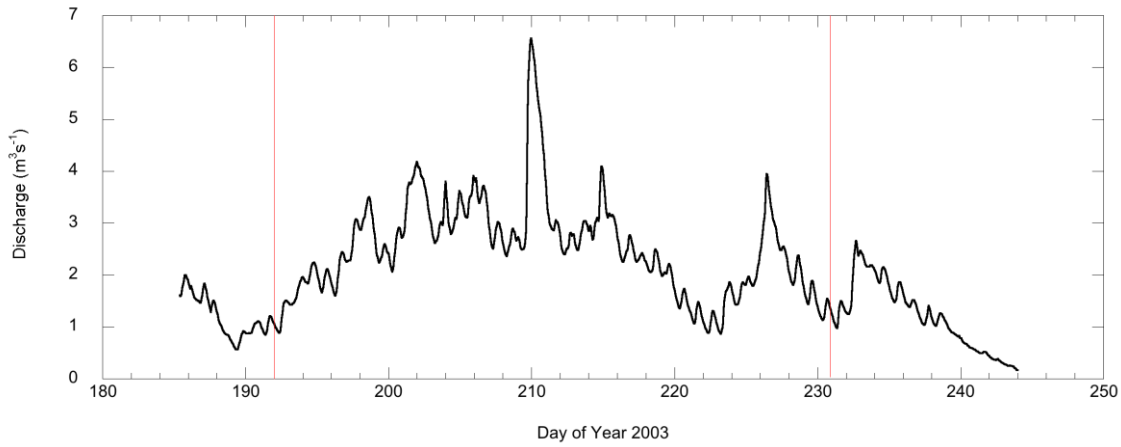


**Figure 3.26. Discharge time series from the Rännan gauging site during the 2003 ablation season. The red lines indicate the span of the monitoring period in this study (JD 192-231).**

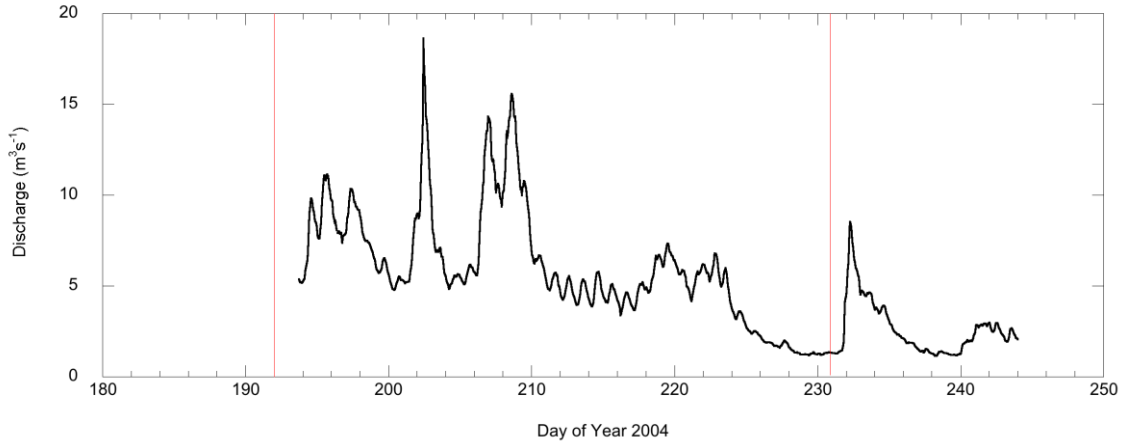


**Figure 3.27. Discharge time series from the Rännan gauging site during the 2004 ablation season. The red lines indicate the span of the monitoring period in this study (JD 192-231).**

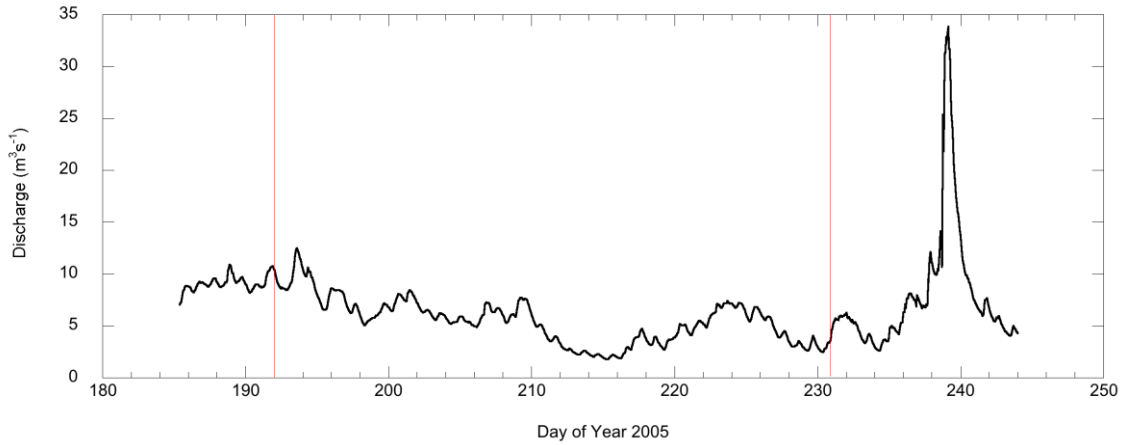


**Figure 3.28. Discharge time series from the Rännan gauging site during the 2005 ablation season. The red lines indicate the span of the monitoring period in this study (JD 192-231).**

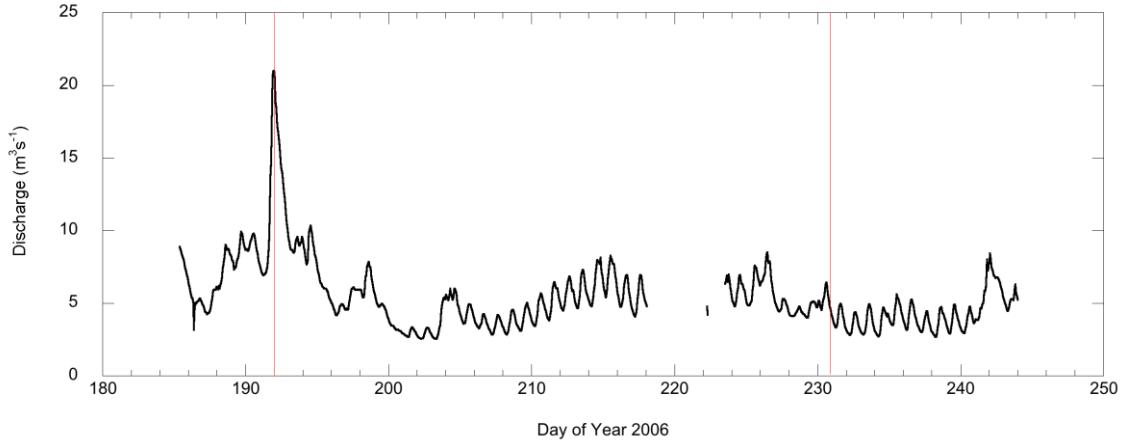


**Figure 3.29. Discharge time series from the Rännan gauging site during the 2006 ablation season. The red lines indicate the span of the monitoring period in this study (JD 192-231).**

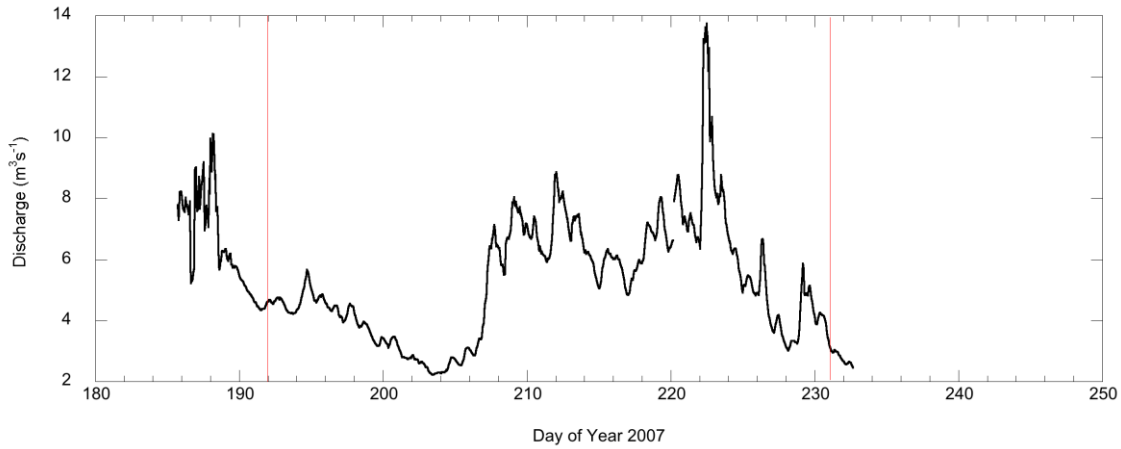


**Figure 3.30. Discharge time series from the Rännan gauging site during the 2007 ablation season. The red lines indicate the span of the monitoring period in this study (JD 192-231).**

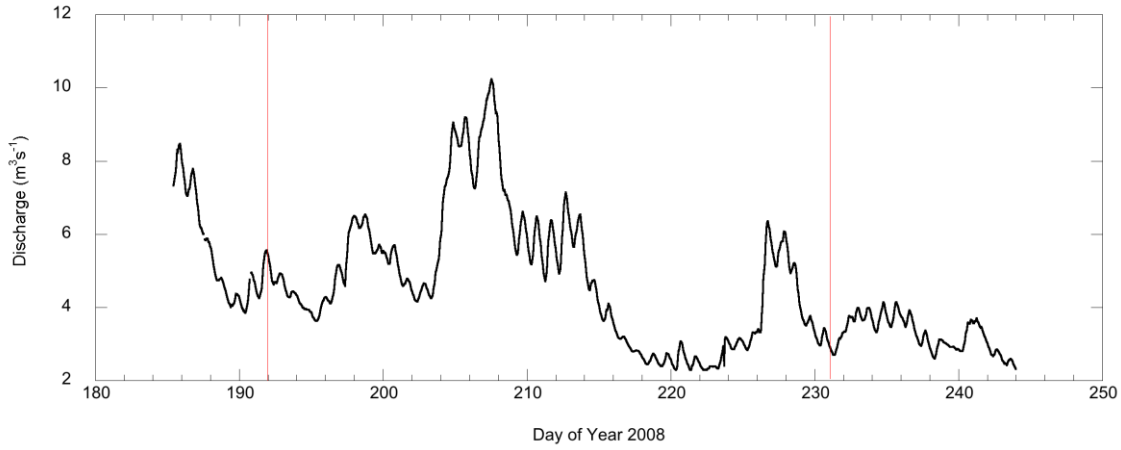


**Figure 3.31. Discharge time series from the Rännan gauging site during the 2008 ablation season. The red lines indicate the span of the monitoring period in this study (JD 192-231).**

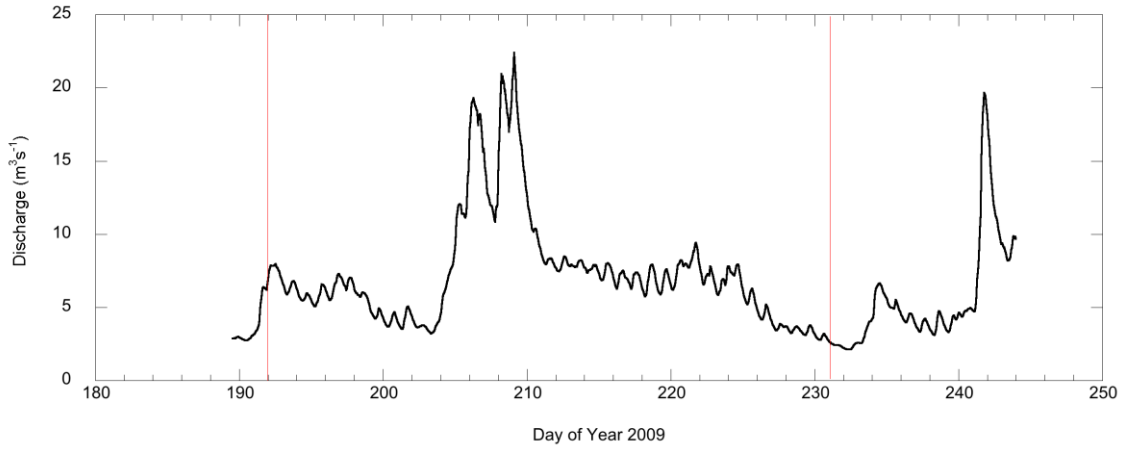


**Figure 3.32. Discharge time series from the Rännan gauging site during the 2009 ablation season. The red lines indicate the span of the monitoring period in this study (JD 192-231).**

Unfortunately, in many cases, the available data does not extend far beyond the monitoring period of this study, making a full analysis difficult. However based on the data presented above (and summarised in Table 3.10.) it is apparent that in seven of the eight years analysed, the seasonal maximum discharge occurs between days 192 and 231. Furthermore, in all eight years, mean discharge over the period 192 to 231 is within 1 $m^3 s^{-1}$ of the mean discharge over the period 185 to 244. A number of years (2004, 2005 and 2009) suggest that large discharge peaks occur outside of the monitoring period. However as it appears that discharge is otherwise in decline before these peaks occur, these are likely the results of heavy rainfall rather than any significant glaciological activity.

Whilst the start date of the study monitoring period (11th July, JD 192) means that the beginning of the glacier melt season is likely to have been missed, the data presented in Figures 3.25 – 3.32 and in Table 3.10. suggest that the bulk of the melt season hydrological activity does occur between JD 192 and 231. As a result, it is felt that the study monitoring period can be considered representative of the wider melt season, and an appropriate indicator of the hydrological regime of Storglaciären.

**Table 3.10. Mean and maximum discharges recorded at the Rännan gauging station between 2002 and 2009 during the equivalent study monitoring period (JD 192 -231), and the wider melt season (JD 185 – 244).**

| Year | Rännan Mean Discharge ($m^3 s^{-1}$) | Rännan Mean Discharge 192-231 ($m^3 s^{-1}$) | Rännan Maximum Discharge ($m^3 s^{-1}$) | Rännan Maximum Discharge 192-231 ($m^3 s^{-1}$) |
|---|---|---|---|---|
| 2002 | 3.48 | 3.50 | 13.25 | 13.25 |
| 2003 | 2.07 | 2.47 | 6.56 | 6.56 |
| 2004 | 5.11 | 5.87 | 18.62 | 18.62 |
| 2005 | 6.43 | 5.48 | 33.86 | 12.48 |
| 2006 | 5.44 | 5.44 | 21.00 | 21.00 |
| 2007 | 5.33 | 5.20 | 13.75 | 13.75 |
| 2008 | 4.55 | 4.77 | 10.24 | 10.24 |
| 2009 | 6.78 | 7.25 | 22.40 | 22.40 |

### 3.3.7. Identification of Discharge-Generating Processes

Discharge-generating processes at Storglaciären were inferred using principal component analysis (PCA). Principal component analysis is a multivariate statistical technique which explores the variance of a data set. This allows a data set to be subdivided and specific patterns examined which may otherwise be 'smothered' by the general trend of the data (Irvine-Fynn, 2005a). Employing principal component analysis to a data set reduces the data into a smaller number of principal components (PC). These are uncorrelated, and can be seen as measures of the underlying 'dimensions' in the data set (Irvine-Fynn, 2005a). Each component identified represents a large proportion of the total variability of the data set, allowing physically based interpretation of the principal component loading scores (Jolliffe, 1990; 1993; Orwin and Smart, 2004).

Following the methods of Orwin and Smart (2004), classification of discharge-generating processes was carried out using an input matrix combining hourly discharge data and hourly meteorological variables from both proglacial streams. The input matrix was generated using *n* rows of days by *N* columns of average daily discharge for each gauging station, average maximum and minimum air temperature, total daily rainfall, and total daily solar radiation. Principal component analysis was run using a Varimax orthogonal rotation in order to maximise loadings on the variables. and to simplify the columns of the input matrix. This allows the maximum simplification of data patterns to be achieved. Components with an Eigenvalue of >1 were retained, and the loading scores for each variable plotted. The strength of each loading score was used to infer the relative importance of each variable in influencing discharge generation, and hence, patterns of proglacial runoff.

### 3.3.8. Meteorological Data

All meteorological data presented in this and subsequent chapters were collected by automatic weather station (AWS) at the Tarfala research station. This station has been operating since 1987 and hourly records a number of meteorological parameters (including wind speed, relative humidity and global radiation) although only air temperature and precipitation are employed in this study. The Tarfala AWS is located approximately 1 km north of the terminus of Storglaciären at an elevation of 1135 m.a.s.l. (approximately 50 m lower than the glacier terminus). Due to the difference in elevation and surface cover between the glacier terminus and the AWS, a certain degree of care is required in applying these data to glaciological analyses. Jansson and Näslund (2009) estimate deviations in air temperature between the Tarfala AWS and measurements obtained on the glacier of between 2°C and 3°C during the summer months, based on an adiabatic lapse rate of 0.6-1°C/100 m. As a result, air temperature collected at the Tarfala AWS is likely to reflect the overall melt occurring on the surface of Storglaciären, although this may vary at higher elevations, and as a result of localised shading. Similar care is also required in interpreting precipitation data, especially as rain gauges under normal conditions underestimate rainfall by as much as 10% (Jansson and Näslund, 2009). As high wind speeds are also a factor in the Tarfala valley, the total error of the gauge is unknown. However, Jansson and Näslund (2009) suggest that precipitation data obtained by the Tarfala AWS accurately reflect the timing and intensity of rainfall events, although not the absolute magnitude.

This study utilizes the data obtained by the Tarfala AWS to reflect general changes in air temperature and rainfall as drivers of melt and suspended sediment transport. As melt is not directly estimated using data from the Tarfala AWS, it is felt that the use of these data is acceptable and not likely to introduce excessive error into the study.

## 3.4. Description of Hydrological Time Series

### 3.4.1. 2009 Ablation Season Observations

Discharge data from both Nordjåkk and Sydjåkk during the 2009 ablation season are presented in Figure 3.33. Descriptive statistics of the discharge time series of both streams are presented in Table 3.11. Time series of air temperature and rainfall during the 2009 ablation season are presented in Figure 3.34.

**Nordjåkk**

The discharge hydrograph recorded at the Nordjåkk gauging station during the 2009 season is characterised by long periods of relatively stable discharge, albeit with a pronounced diurnal cyclicity. Discharge in the early stages of the season (until Day 205) is relatively low with a distinct diurnal pattern. A large, multi-peaked discharge event occurs around the middle of the season (between Days 205 and 210) yielding the seasonal maximum discharge (2.85 $m^3 s^{-1}$). Following this event, and until the end of the season, discharge resumes its previous diurnal pattern. However, average discharge is higher during this period compared with the period prior to the high discharge event (1.13 $m^3 s^{-1}$ compared with 0.81 $m^3 s^{-1}$).

**Sydjåkk**

The discharge hydrograph recorded at the Sydjåkk gauging station during the 2009 season is characterised by high variability and a pronounced diurnal pattern. Similarly to the Nordjåkk time series, peak discharge was recorded during a mid-season high discharge event (~1.3 $m^3 s^{-1}$), although several periods of high discharge both earlier and later in the season exhibit similar magnitudes. The overall trend of the season is negative, with discharge steadily declining throughout the season.

**Table 3.11. Discharge time series descriptive statistics for Nordjåkk and Sydjåkk during the 2009 ablation season ($m^3$ $s^{-1}$)**

| | 2009 | |
|---|---|---|
| | Nordjåkk | Sydjåkk |
| Mean | 1.08 | 0.77 |
| Maximum | 2.85 | 1.29 |
| Minimum | 0.53 | 0.25 |
| St. Dev. | 0.42 | 0.25 |

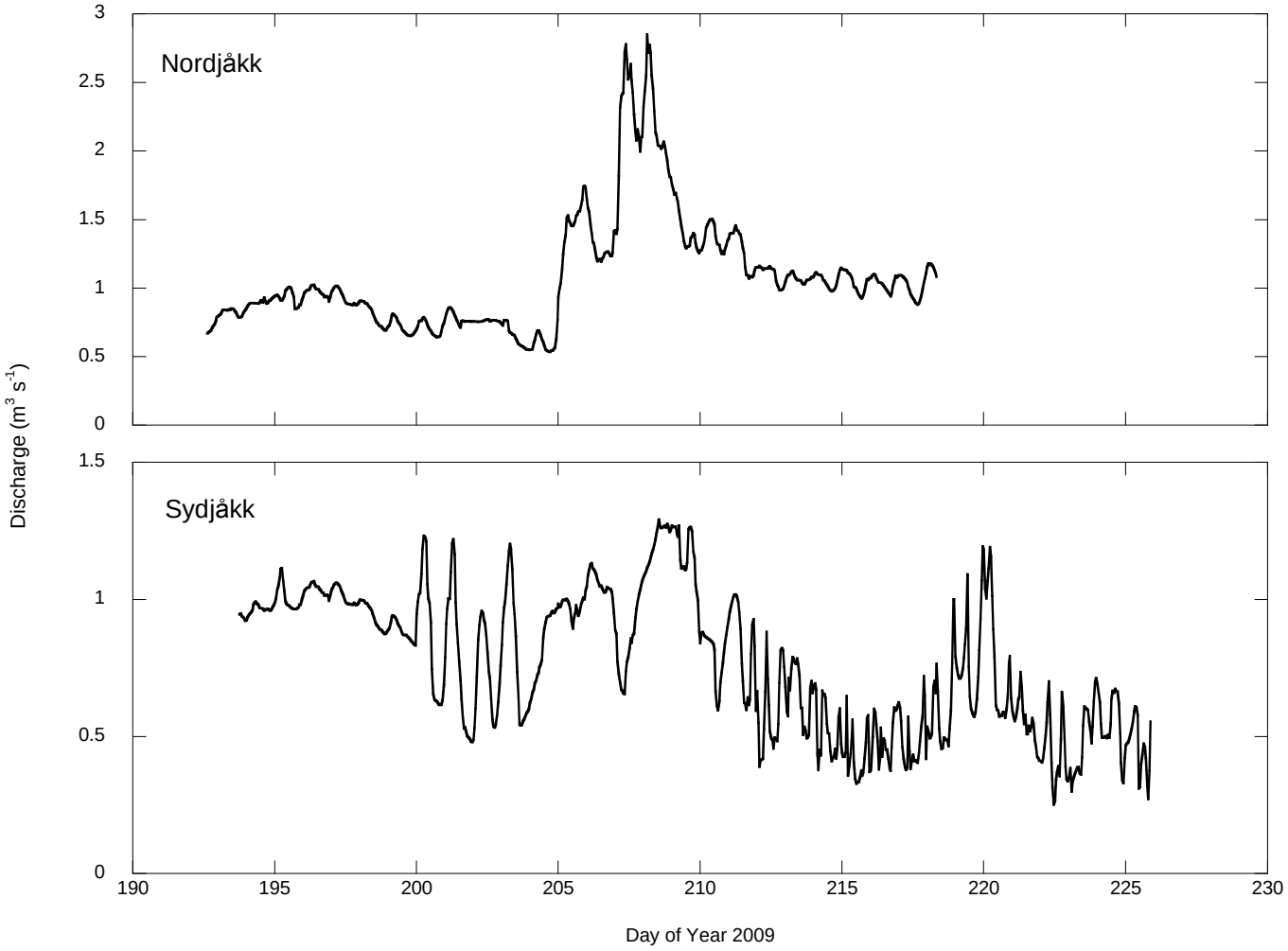


**Figure 3.33. Discharge time series from the Nordjåkk and Sydjåkk gauging site during the 2009 ablation season. Note that the *y*-axes of both graphs use different scales.**

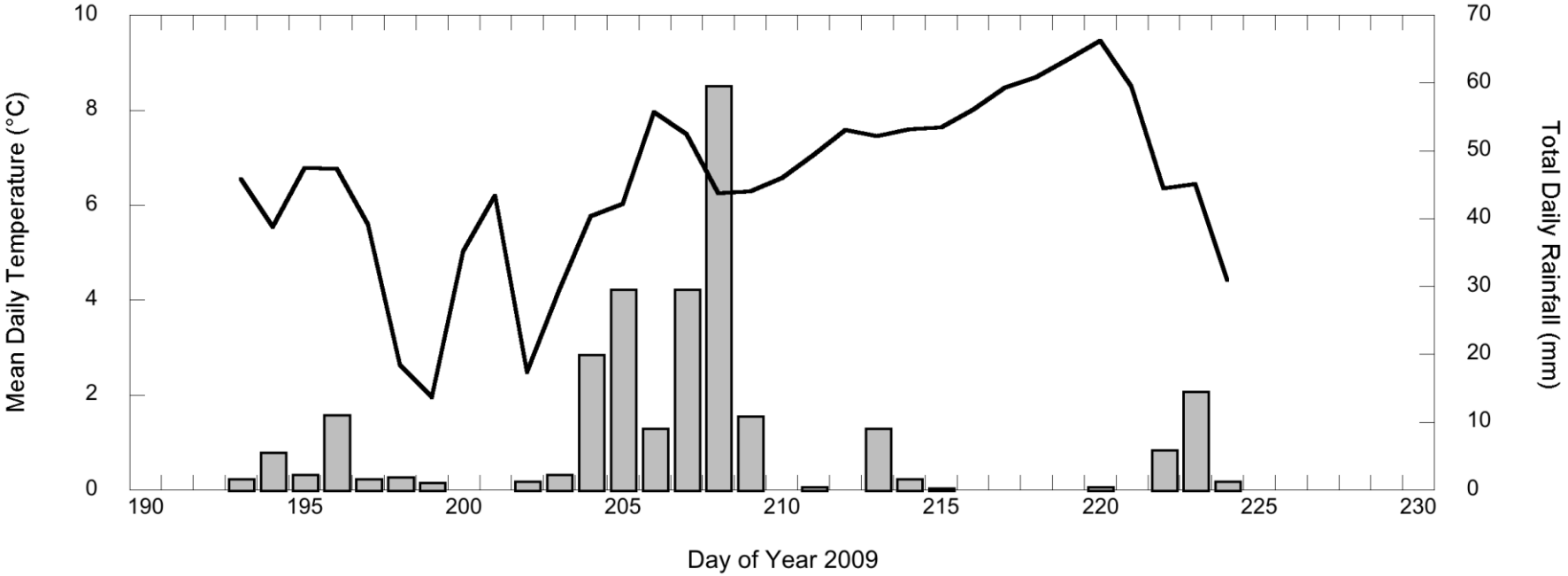


**Figure 3.34. Time series of air temperature (°C) and rainfall (mm) recorded at the Tarfala Research Station during the 2009 ablation season.**

### 3.4.2. 2010 Ablation Season Observations

Discharge data from both Nordjåkk and Sydjåkk during the 2010 ablation season are presented in Figure 3.35. Descriptive statistics of the discharge time series of both streams are presented in Table 3.12. Time series of air temperature and rainfall during the 2010 ablation season are presented in Figure 3.36.

#### Nordjåkk

The discharge hydrograph recorded at the Nordjåkk gauging station during the 2010 melt season (Figure 3.35) is characterised by relatively low discharges recorded throughout (~ 1.2 $m^3 s^{-1}$ average). The time series does however contain three high discharge events. These events are approximately evenly spaced, occurring at the beginning, middle and end of the measured period. Event 1 occurs between days 198 and 199, reaching a maximum discharge of 3.0 $m^3 s^{-1}$. Event 2 occurs between days 211 and 212, peaking at 2.2 $m^3 s^{-1}$. Event 3 occurs between days 226 and 227, with a similar peak discharge as event 2, around 2.1 $m^3 s^{-1}$. Between days 215 and 221 the hydrograph shows a more pronounced diurnal rhythm, with greater variability between daily maximum and minimum discharges, often between 0.5 and 1 $m^3 s^{-1}$.

#### Sydjåkk

The discharge hydrograph recorded at the Sydjåkk gauging station is relatively stable for the majority of the season (Figure 3.35). Although high discharge events occur early and towards the middle of the season, these are typically short-lived events, resulting in low variability of discharge during periods of recession. High discharge event 1 occurs between days 199 and 201, peaking on day 200. This event exhibits the highest recorded seasonal discharge, ~ 1.9 $m^3 s^{-1}$. Event 2 occurs on day 213, although a short period of rising discharge is observed prior to this from ~ day 210. The peak discharge during this event is significantly lower than that observed during event 1, peaking at around 1.3 $m^3 s^{-1}$. A third event

observed in the 2010 Nordjåkk discharge record is distinguishable in the Sydjåkk hydrograph, although the peak discharge is markedly lower in magnitude than that of Nordjåkk (~ 0.6 $m^3$ $s^{-1}$ compared to ~ 2.1 $m^3$ $s^{-1}$) and is therefore not considered a high discharge event here.

**Table 3.12. Discharge time series descriptive statistics for Nordjåkk and Sydjåkk during the 2010 ablation season ($m^3$ $s^{-1}$)**

| | 2010 | |
|---|---|---|
| | Nordjåkk | Sydjåkk |
| Mean | 1.06 | 0.45 |
| Maximum | 2.96 | 1.92 |
| Minimum | 0.49 | 0.18 |
| St. Dev. | 0.33 | 0.23 |

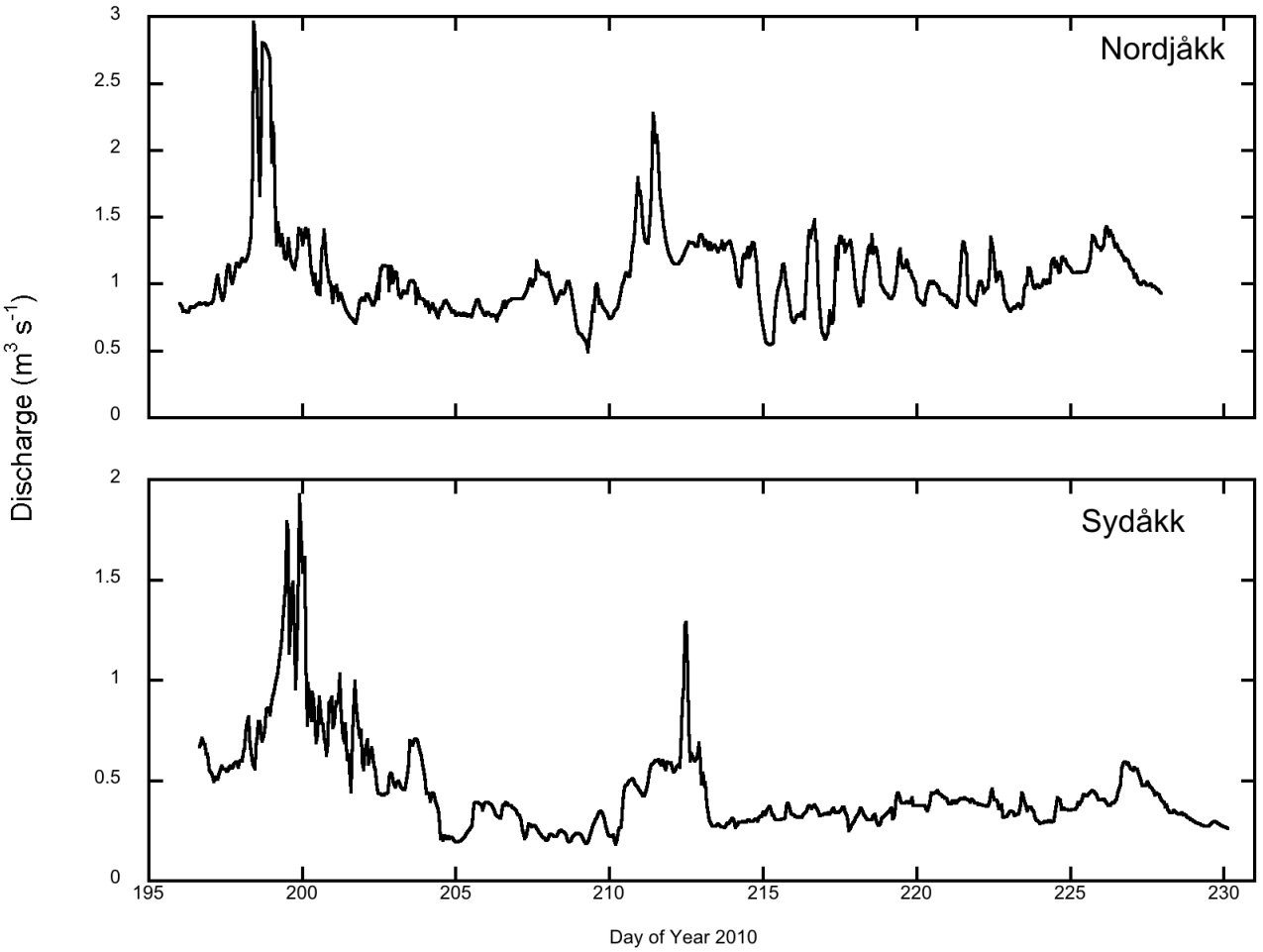


**Figure 3.35. Discharge time series from the Nordjåkk and Sydjåkk gauging sites during the 2010 ablation season**

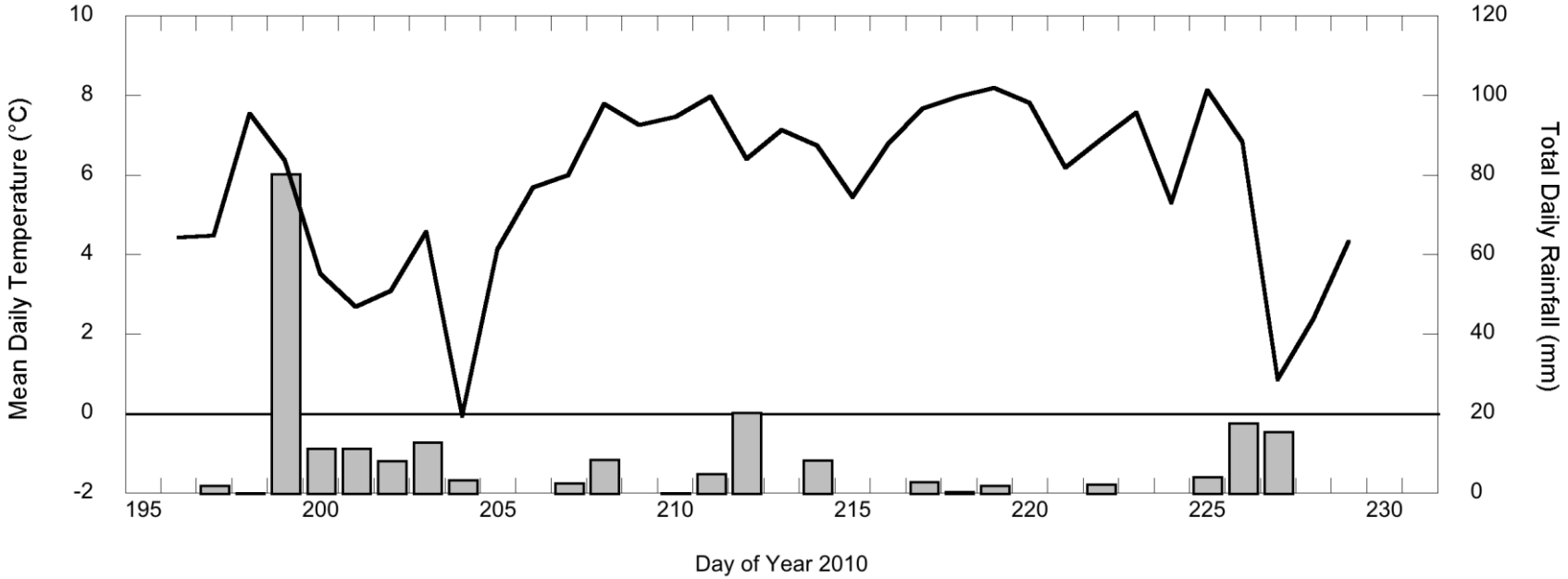


**Figure 3.36. Time series of air temperature (°C) and rainfall (mm) recorded at the Tarfala Research Station during the 2010 ablation season.**

## 3.5. Classification of Discharge-Generating Processes

In both 2009 and 2010, a principle component analysis of combined hourly discharge and meteorological data retained two discrete components related to the generation of discharge (Table 3.13). Explaining ca. 75% of each data set, these data suggest the dominant meteorological factors which exert control on discharge patterns. Components making up the remaining ca. 25% of variability were discarded on account of having eigenvalues less than 1. The first component exhibits a strong, positive loading with all three of the temperature variables (maximum, minimum and mean temperature), and a weak (often negative) loading with both the precipitation and solar radiation variables. The second component exhibits a strong, positive loading with daily precipitation, and a relatively strong, negative loading with solar radiation. The three temperature variables exhibit very weak (and in some cases negative) loading. The loadings for each meteorological variable during the 2009 and 2010 ablation seasons are presented in Tables 3.14 and 3.15, and plotted in Figures 3.37 and 3.37 for ease of visual interpretation.

**Table 3.13. Percentage of total variance given for each discharge generating process identified by principal component analysis**

| Year | Component 1 | Component 2 |
|---|---|---|
| 2009 | 45.05 % | 32.71 % |
| 2010 | 41.63 % | 34.11 % |

**Table 3.14. Principal component loadings for meteorological variables and both the Nordjåkk and Sydjåkk gauging stations during the 2009 ablation season.**

| | Component | |
|---|---|---|
| | 1 | 2 |
| Nordjåkk Discharge | 0.429 | 0.797 |
| Sydjåkk Discharge | -0.435 | 0.631 |
| Average Hourly Temperature | 0.992 | 0.029 |
| Maximum Daily Temperature | 0.927 | -0.095 |
| Minimum Daily Temperature | 0.937 | 0.191 |
| Total Daily Precipitation | 0.031 | 0.927 |
| Daily Total Solar Radiation | -0.013 | -0.671 |

**Table 3.15. Principal component loadings for meteorological variables and both the Nordjåkk and Sydjåkk gauging stations during the 2010 ablation season.**

| | Component | |
|---|---|---|
| | 1 | 2 |
| Nordjåkk Discharge | 0.466 | 0.591 |
| Sydjåkk Discharge | -0.203 | 0.908 |
| Average Hourly Temperature | 0.981 | 0.006 |
| Maximum Daily Temperature | 0.906 | -0.082 |
| Minimum Daily Temperature | 0.900 | 0.010 |
| Total Daily Precipitation | -0.186 | 0.845 |
| Daily Total Solar Radiation | -0.164 | -0.703 |

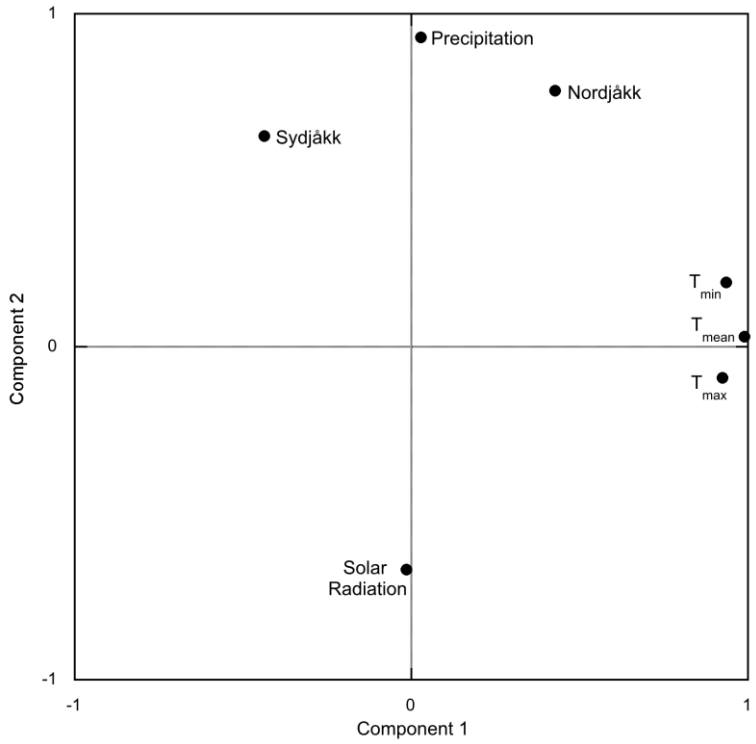


**Figure 3.37. Principal component loadings for meteorological variables and gauging stations during the 2009 ablation season**

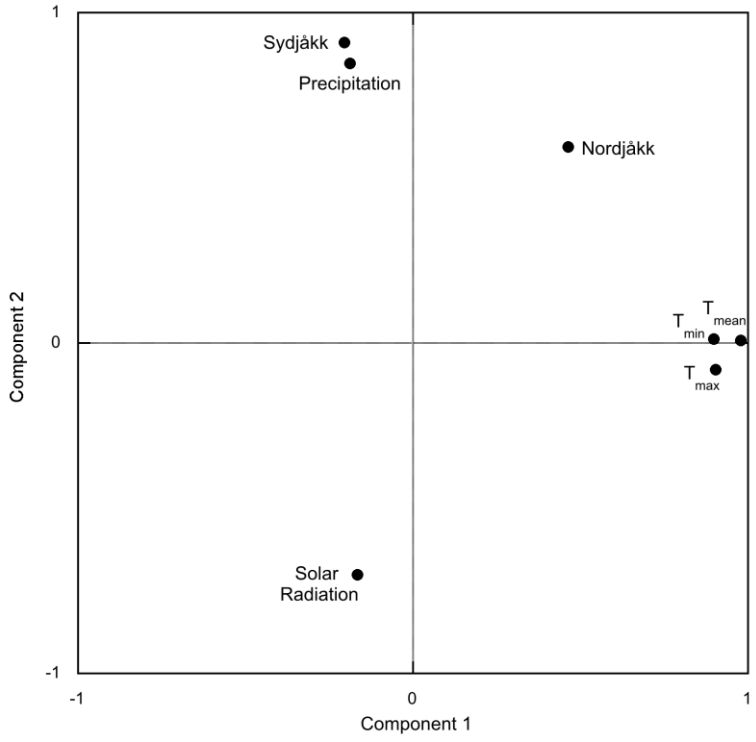


**Figure 3.38. Principal component loadings for meteorological variables and gauging stations during the 2010 ablation season**

## 3.6. Discussion

### 3.6.1. Discharge Generating Processes at Storglaciären

The principal component loadings for Nordjåkk and Sydjåkk during both the 2009 and 2010 ablation seasons are described in Section 3.5, and presented in Figures 3.37 and 3.38, and in Tables 3.13, 3.14 and 3.15.

Due to the fragmented nature of the 2009 time series, the interpretation and discussion below is based solely on the 2010 time series. Given the extensive missing data in the 2009 time series, it is difficult to assess the representativeness of the data in the context of a full glacier melt season, and to make firm interpretations. However the data has been presented throughout the chapter for thoroughness and openness.

Based on the strength of loading with temperature variables in the 2010 ablation season, the first component is interpreted as showing the dominance of ablation on discharge patterns. The strength of loading with both precipitation and solar radiation variables allows the second component to be interpreted as showing the dominance of precipitation (specifically rainfall events) on discharge patterns. The relative dominance of each component is even across both ablation seasons, with ablation explaining the greatest variance in the data set in both years. It is interpreted therefore, that ablation has a greater influence on discharge generation at Storglaciären than precipitation.

However, as observed by Orwin and Smart (2004) in a similar study at Small River Glacier, Canada, the dominant discharge-generating processes at Storglaciären differ between the two gauging stations, suggesting that each stream is hydrologically distinct from the other. Both Nordjåkk and Sydjåkk load relatively strongly with precipitation (Nordjåkk 0.591; Sydjåkk 0.908) but only modestly with ablation (Nordjåkk 0.466; Sydjåkk -0.203). As Sydjåkk is loaded positively with precipitation, but negatively with ablation, it is interpreted that precipitation has a greater influence on discharge patterns in Sydjåkk than ablation. Whilst it is

clear therefore that precipitation dominates patterns of discharge at Sydjåkk, it is possible that Nordjåkk is not entirely dominated by either ablation or precipitation patterns. Instead, discharge patterns at Nordjåkk are influenced more-or-less equally by both ablation and precipitation.

The interpretation above suggests that precipitation (specifically rainfall) is extremely influential upon discharge regimes at Storglaciären despite ablation driven discharge accounting for a greater variability of the data set. However it is suggested that this is a result of discontinuous patterns of rainfall. Dahlke *et al*. (2012) have suggested that increases in the mean summer discharge and magnitude of flood peaks in the Tarfala valley are a result of large precipitation events. Similar results in other arctic and subarctic glacierised catchments (Kane *et al*., 2003; Cunderlik and Ouarda, 2009) support this conclusion, and suggest that rainfall related runoff magnitude can exceed those of ablation related runoff by a factor of three (Kane *et al*., 2003). This increasing influence of precipitation as a driver of discharge in the Tarfala valley has been linked to firn and snow cover loss on Storglaciären, providing areas of bare ice which provide fast runoff pathways (Collins, 1998; Hock *et al*., 2005; Dahlke *et al*., 2012). It is inferred that a similar process is responsible for the results observed during this study, and that the dominant discharge drivers of both Nordjåkk and Sydjåkk are influenced by the individual routing characteristics of each stream.

Since Nordjåkk is postulated to be fed mainly by englacial or supraglacial meltwater originating from ice and snow melt in the accumulation area (Hooke *et al*., 1988; Seaberg and *et al*., 1988; Kohler, 1992; Hock and Hooke, 1993; Hooke and Pohjola, 1994), it is likely to respond rapidly to periods of increased ablation. During both study years, melting of spring snow cover in the northern ablation area occurred relatively quickly, resulting in large bare ice areas which would be expected to rapidly route water, either ablation or rainfall derived into Nordjåkk (Hock *et al*., 2005). The relatively equal influence of ablation and precipitation as discharge drivers at Nordjåkk are therefore interpreted as the result of water routing through one or both of the above mentioned runoff pathways.

The dominance of precipitation as a driver of discharge generation in Sydjåkk is interpreted based on the same principle, reflecting the routing characteristics of

the stream. It has been suggested that Sydjåkk is fed by water routed through crevasses and moulins in the upper ablation and lower accumulation areas of Storglaciären (Hooke *et al*., 1988; Seaberg *et al*., 1988; Kohler, 1992; Hock and Hooke, 1993; Hooke and Pohjola, 1994). This water is routed to the glacier bed and therefore has an increased residence time and as such, a greater sediment load than Nordjåkk (Hock and Hooke, 1993).

Subglacially routed discharge is well known to be modulated with transport times through snow and firn typically damping the variations in water input to the system (e.g. Collins, 1979a; Flowers, 2008; Schuler and Fischer, 2009; Gulley *et al*., 2012), increasing residence time. Given the subglacial nature of Sydjåkk, it is possible that the correlation between ablation and discharge is diminished, reducing the direct influence of ablation. Precipitation however, is able to enter the Sydjåkk channel rapidly through supraglacial and/or ice marginal slope runoff, resulting in a stronger influence on stream discharge.

## 3.7. Summary

Based on the interpretations made in Section 3.6, the following conclusions can be drawn regarding patterns of proglacial discharge at Storglaciären:

- Principal component analysis of proglacial discharge and meteorological variables indicates that ablation is the dominant control upon generation of discharge at Storglaciären.
- The meteorological drivers of discharge generation differ at each of the two proglacial streams at Storglaciären: Sydjåkk is dominated by precipitation driven discharge, whilst discharge generation varies at Nordjåkk, influenced equally by precipitation and ablation. This reflects the routing characteristics of each stream, and suggests that supraglacial runoff may be a key runoff pathway at Storglaciären.

*Chapter 4*

# Temporal Patterns of Suspended Sediment Transfer

## 4.1. Introduction

The supply-controlled nature of suspended sediment concentrations in fluvial systems makes them sensitive indicators of climate-driven environmental change (Walling, 1995; Hodgkins *et al*., 2003). In glacierised basins, temporal variability in suspended sediment transport by glacial meltwater is largely influenced by changes in the rate of meltwater production at the glacier surface and changes in the behaviour of two or more hydraulically distinct reservoirs within and beneath the glacier (Collins, 1979b; Fountain, 1992; Gurnell *et al*., 1992; Clifford *et al*., 1995; Willis *et al*., 1996; Richards *et al*., 1996; Hodson and Ferguson, 1999). Monitoring the spatial and temporal patterns of sediment storage and release in glacierised basins can provide valuable information on sediment transfer processes within a glacier basin (Hodson *et al*., 1998), as well as the relationships between climate, glacier variations and landscape change (Hodgkins, 2003).

This chapter describes the collection and analysis of suspended sediment concentration data undertaken at Storglaciären over both the 2009 and 2010 melt seasons. The data presented in this chapter will allow inferences to be made as to the nature of sediment transport at Storglaciären, and provide a basis for further chapters which will investigate the form of the suspended sediment time series.

### 4.1.1. Aims of the Chapter

This chapter aims to assess seasonal suspended sediment delivery to the proglacial area of Storglaciären through analysis of the diurnal relationship between stream discharge and suspended sediment concentration. There are two specific objectives:

(i) To identify periods in the suspended sediment time series which are suggestive of changes in the availability at Storglaciären.

(ii) To identify factors which may influence the delivery of suspended sediment to the proglacial area of Storglaciären on a seasonal scale.

## 4.2. Methods

### 4.2.1. Instrumented Monitoring of Suspended Sediment Transport

Continuous monitoring of proglacial stream turbidity was carried out during two field seasons conducted between July 11th and August 18th (day of year 192 – 230) 2009, and between July 11th and August 19th (day of year 192-231) 2010. Turbidity data were collected using Greenspan TS100 infrared turbidity probes deployed at each gauging site (Figure 4.1). The TS100 uses a high gain infra-red system to detect the backscatter intensity of suspended particles, transmitting a beam of 800 nm wavelength and measuring the intensity of reflected light (Greenspan Analytical, 2007).

Each probe was securely mounted to its gauging station in order to prevent movement of the probe during operation, and also to protect it in the event of damage to the gauging station. Both probes were mounted ~ 0.25 m from the bed. This distance is recommended by Greenspan (Greenspan Analytical, 2007) in order to reduce reflection from the stream bed, since reflection errors increase the closer the probe transmitter is to a reflective surface. However, this distance also protected the probe head from potential damage as a result of bedload movement, and ensured that the probe head remained submerged even during low discharge events. As recommended by Greenspan (Greenspan Analytical, 2007), the probe was directed face downwards (rather than mounted at an angle, e.g. facing away from the direction of flow) and submerged sufficiently to prevent interference from solar radiation. Turbidity was measured at intervals of 60 seconds and averaged every 10 minutes in order to obtain as high a resolution time series as possible.

**Figure 4.1. Photograph of the Greenspan TS100 turbidity probe prior to deployment at the Sydjåkk gauging station**

### 4.2.2. Suspended Sediment Sampling

Calibration of turbidity data was achieved through the use of sediment rating curves formed using discrete, depth-integrated water samples. Details of these curves are outlined in Table 4.1 and presented in Figures 4.3 to 4.6.

**Table 4.1. Summary of linear regression models used to predict continuous suspended sediment concentration data from discrete depth-integrated suspended sediment samples. *n* is the number of data points used, $r^2$ is the coefficient of determination, *se* is the standard error of the curve (±%), *F* is the *F*-test statistic (given in italics where values are not significant at the 0.01 significance level), a is the linear-regression slope, and b is the linear regression intercept**

| Stream/Year | *n* | $r^2$ | *se* | *F* | *a* | *b* |
|---|---|---|---|---|---|---|
| Nordjåkk 2009 | 17 | 0.86 | 0.01 | 38.92 | 0.03 | 0.12 |
| Sydjåkk 2009 | 15 | 0.81 | 0.02 | 37.34 | 0.02 | 0.75 |
| Nordjåkk 2010 | 27 | 0.62 | 0.01 | 40.91 | 0.03 | 0.09 |
| Sydjåkk 2010 | 54 | 0.84 | 0.21 | 508.39 | 0.14 | 1.03 |

Samples of 0.5 L were obtained using a USDH-48 depth-integrating sediment sampler at regular intervals of between 15 minutes and 1 hour over the course of a single sampling period. This allowed samples to be obtained during a range of different flows and sediment loads. Samples were collected in line with the turbidity probe, approximately 0.1 m downstream. This allowed samples to more closely represent the turbidity recorded by the probe upstream, without disturbing either the flow of water around the probe or the stream bed, thus artificially entraining sediment. Immediately following collection, each sample was filtered through pre-weighed Whatman Grade 40 (8 μm) filter papers of 110 mm diameter (Figure 4.2). The filtration apparatus employed during the study consisted of an airtight chamber beneath which the filter paper was affixed. Each sample was loaded into the chamber from above and a bicycle pump was used to introduce air into the chamber, impelling the sample through the filter paper.

Following filtration, each filter paper was wrapped securely in foil to preserve both the paper and the retained sediment until further laboratory analysis could be carried out. In order to prevent contamination of samples, the USDH-48, sample bottle, and filtration apparatus were each rinsed three times with stream water immediately prior to sampling and filtration.

**Figure 4.2. Photographs of the filtration apparatus used in the study (left), and a Whatman-Grade 40 filter paper following sample filtration (right)**

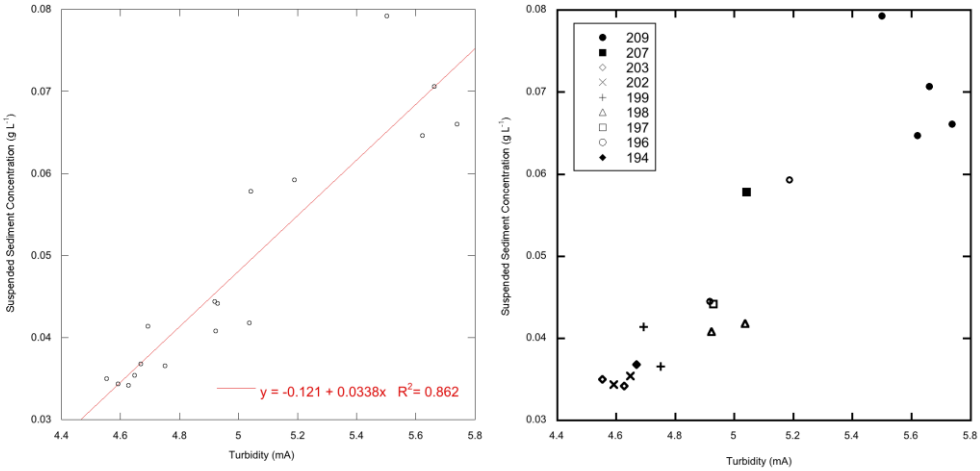


**Figure 4.3 Suspended sediment rating curve constructed for the 2009 season at Nordjåkk using depth- integrated suspended sediment samples. Dates on which suspended sediment samples were collected are indicated in the right-hand plot.**

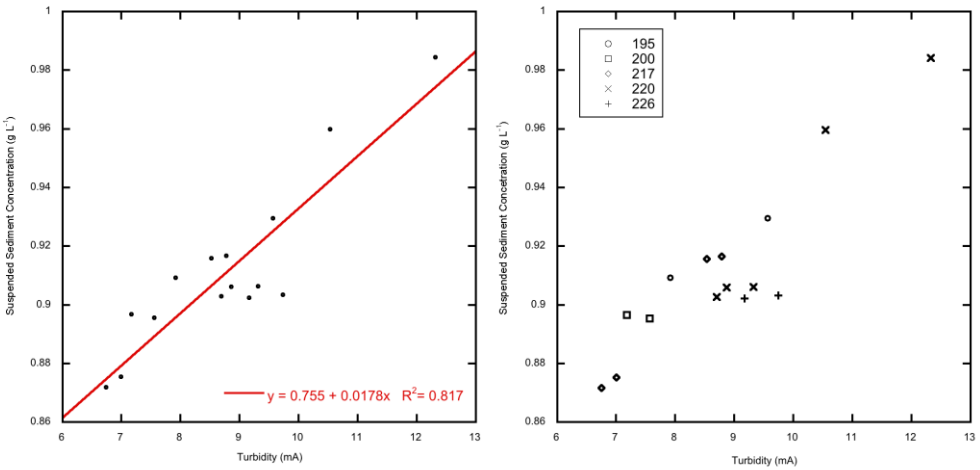


**Figure 4.4 Suspended sediment rating curve constructed for the 2009 season at Sydjåkk using depth- integrated suspended sediment samples. Dates on which suspended sediment samples were collected are indicated in the right-hand plot.**

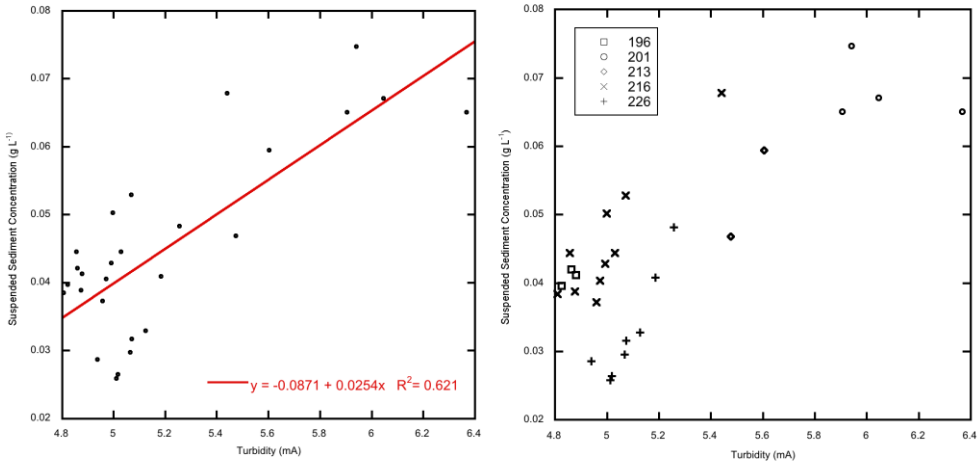


**Figure 4.5 Suspended sediment rating curve constructed for the 2010 season at Nordjåkk using depth- integrated suspended sediment samples. Dates on which suspended sediment samples were collected are indicated in the right-hand plot.**

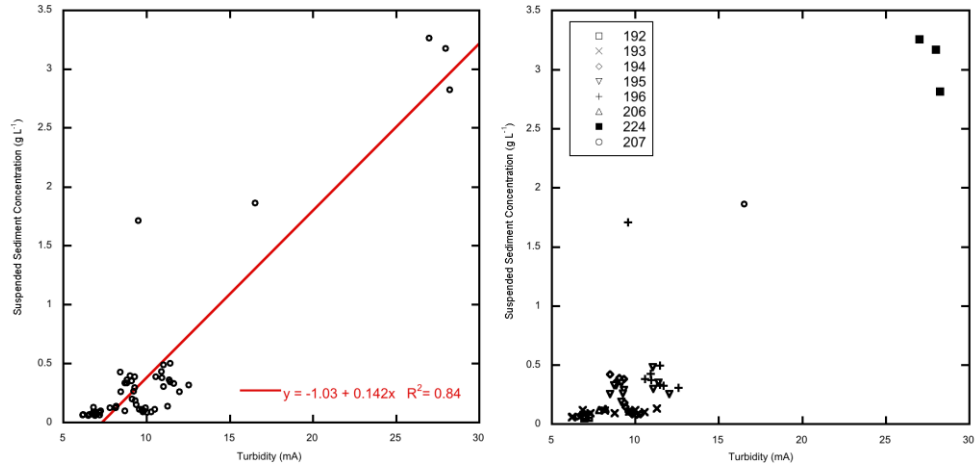


**Figure 4.6 Suspended sediment rating curve constructed for the 2010 season at Sydjakk using depth- integrated suspended sediment samples. Dates on which suspended sediment samples were collected are indicated in the right-hand plot.**

### 4.2.3. Laboratory Analysis of Suspended Sediment

At the end of each of the field seasons, the papers were air dried and re-weighed in a laboratory setting in order to provide suspended sediment concentration (SSC) in g $L^{-1}$. Each paper was weighted to a tolerance of 0.01 g on a calibrated digital balance. In order to maintain continuity, this balance was also used to originally weigh the filter papers prior to use in the field.

Based on Hodgkins (1999) error determination in suspended sediment monitoring, each individual sediment sample collected and analysed has an accuracy of ±2.8%. This includes inaccuracies introduced in the sample collection and weighing stages, whereby the greatest source of error occurs as a result of hygroscopic moisture absorption by each individual filter paper. Gurnell *et al*. (1992) estimated this error to be ±0.16% of the mean suspended sediment concentration. Hodgkins (1999) and Gurnell *et al*. (1992) both suggest that the loss of sub-8 μm particles during filtration contributes around 1% underestimation of the mean suspended sediment concentration. Although Hodgkins (1999) disregarded this as a significant source of error due to the rapid clogging of filter paper pores, filter paper saturation in this study only occurred during especially high sediment transport, notably at the end of the 2010 field season. Underestimation of suspended sediment concentration may therefore be greater than that calculated by Gurnell *et al*. (1992) and Hodgkins (1999).

### 4.2.4. Missing Data

Although care was taken during both field seasons to prevent data loss by battery or other technical failure, periods of missing data were still present in the time series of both study years (Table 4.2). Although in most cases these periods were short, missing data limits effective analysis and present significant problems where continuous time series are required. Therefore, statistical methods were necessary in order to fill missing data periods and provide a continuous time series.

Short periods of missing data of up to approximately one day were predicted using the geometric function 'Interpolate' of Synergy Software's Kaleidagraph™ v. 4.1.2 (Synergy, Software, 2010). This function fits a curve to a time series which passes through acquired data points and predicts missing data from preceding and succeeding angles of slope (Cooper, 2003). This method is advantageous as it predicts missing data points conservatively when traversing inflections in a time series (Cooper, 2003; Synergy Software, 2010). Only one missing data period of longer than one day existed in both seasons. In this case, suspended sediment concentration was predicted deterministically using least-squares linear regression of the continuous discharge record of Storglaciären calculated using data from the Rännan and Lillsjön gauging sites. This technique was evaluated in Section 3.3.5.2 in order to assess its effectiveness in filling periods of missing data. This analysis suggests that gaps filled using least squares linear regression accurately simulate the mean of the missing data. However, it is possible that a loss of data resolution may be observed, resulting in a more conservative time series. A summary of the linear regression model used to fill data gaps is shown in Table 4.3 and in Figures 4.7 and 4.8.

**Table 4.2. Summary of suspended sediment concentration data missing from raw time series. Percentage values reflect the total number of missing data days, the number of days filled by interpolation techniques, and the number of days filled using regression.**

| | 2009 | | 2010 | |
|---|---|---|---|---|
| | Nordjåkk | Sydjåkk | Nordjåkk | Sydjåkk |
| % Data Missing | 30.8 | 41.7 | 15.2 | 2.4 |
| % Data Interpolated | 0 | 0 | 0.9 | 2.4 |
| % Data Gap Filled | 0 | 0 | 14.3 | 0 |

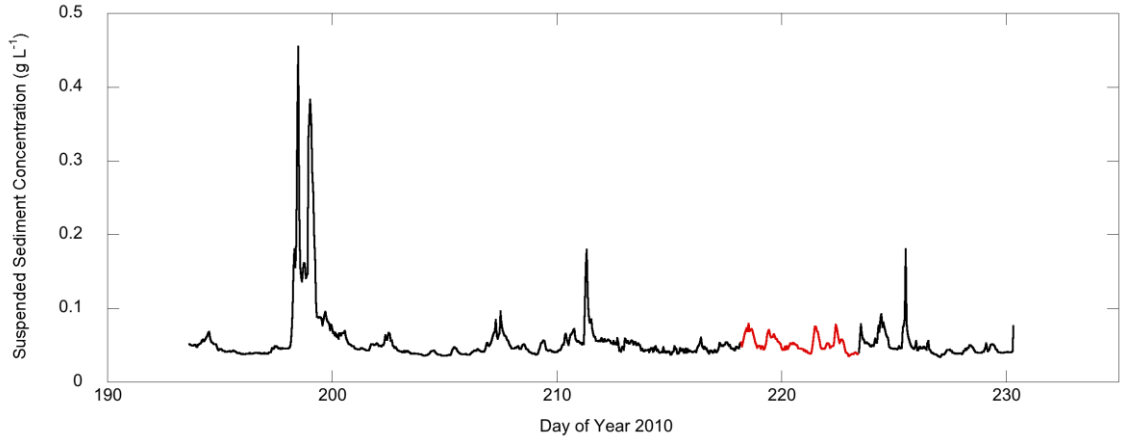


**Figure 4.7. Suspended sediment concentration data recorded at the Nordjåkk gauging station during the 2010 melt season. Period of missing data filled using linear regression are shown in red.**

**Table 4.3. Summary of linear regression models used to predict missing turbidity data during the 2010 ablation season. Dates and times are given in the hour-day format. In the regression column, $Q_R$ is discharge ($m^3s^{-1}$) at the Rännan gauging station and $SSC_N$ is the suspended sediment concentration ($g\ L^{-1}$) at the Nordjåkk gauging station. In the final three columns, $r^2$ is the coefficient of determination, *se* is the standard error of the curve (±%), and *F* is the *F*-test statistic (given in italics where values are not significant at the 0.01 significance level)**

| Year | Gauging Station | Missing Data Period | Regression Model | $r^2$ | se | F |
|---|---|---|---|---|---|---|
| 2010 | Nordjåkk | 05:00 218 – 10:00 223 | $SSC_N$ =-0.0019 – 0.0087$Q_R$ | 0.49 | 0.27 | 476.14 |

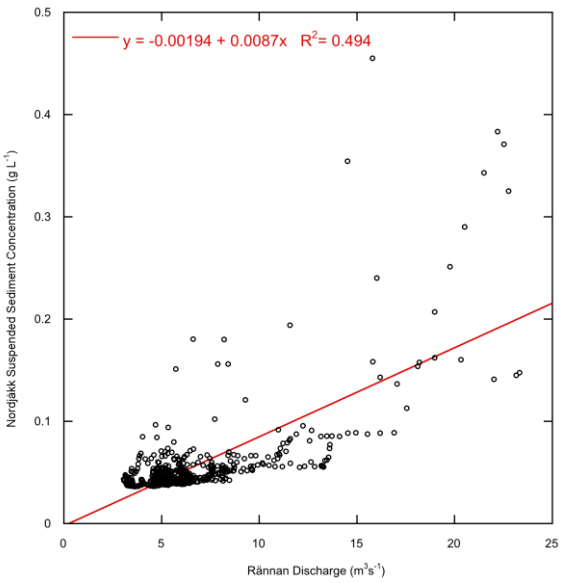


**Figure 4.8. Plot showing data used to construct linear regression models in order to fill missing data gaps during the 2010 season at Nordjåkk. Full details of each model are presented in Table 4.3.**

### 4.2.5. Hysteresis Analysis

During a given runoff season, the relationship between meltwater discharge and sediment transport in glacial streams changes more or less continuously (Østrem, 1975). In this regard, a pattern of constantly changing loop-shaped relationships is frequently observed, each associated with a period of high water discharge (Bogen, 1980). A number of studies have applied the term 'hysteresis' to describe this relationship between discharge and sediment transport (Gregory and Walling, 1973; Walling, 1974; Church and Gilbert, 1975; and Statham, 1977). Hysteresis implies a bivariate relationship in which values of the dependent variable for a given value of the independent variable differ according to whether the independent variable in increasing or decreasing (Hodgkins, 1996). Clockwise hysteresis implies that suspended sediment concentration is higher on the rising limb of the diurnal hydrograph than at the equivalent discharges on the falling limb. Therefore, the diurnal suspended sediment concentration peak leads the diurnal discharge peak. Conversely, anticlockwise hysteresis implies that suspended sediment concentration is higher on the falling limb of the diurnal

hydrograph and therefore, the diurnal suspended sediment concentration lags behind the diurnal discharge peak (Hodgkins, 1996).

In order to ascertain temporal changes in the relationship between discharge and suspended sediment transport, hysteresis loops were obtained by plotting hourly discharge (independent variable) against hourly suspended sediment concentration (dependent variable) for each day of the study period. Days containing partial data (e.g. at the start/end of the season, or in the case of missing data) were discarded from the analysis to ensure that only full hysteresis loops were compared. Since diurnal hysteresis loops often contain several shifts between clockwise and anticlockwise hysteresis throughout the 24-hour period, each day was analysed based on the overall directional trend in order to simplify analysis of sediment dynamics. Examples of diurnal discharge and suspended sediment time series and hysteresis loops exhibiting clockwise and anticlockwise hysteresis are presented in Figure 4.9.

This technique is temporally coarse and risks disregarding otherwise imperceptible changes in the nature of suspended sediment transport. Nonetheless, this form of analysis facilitates a more effective seasonal-resolution interpretation and is therefore sufficient for use in this study.

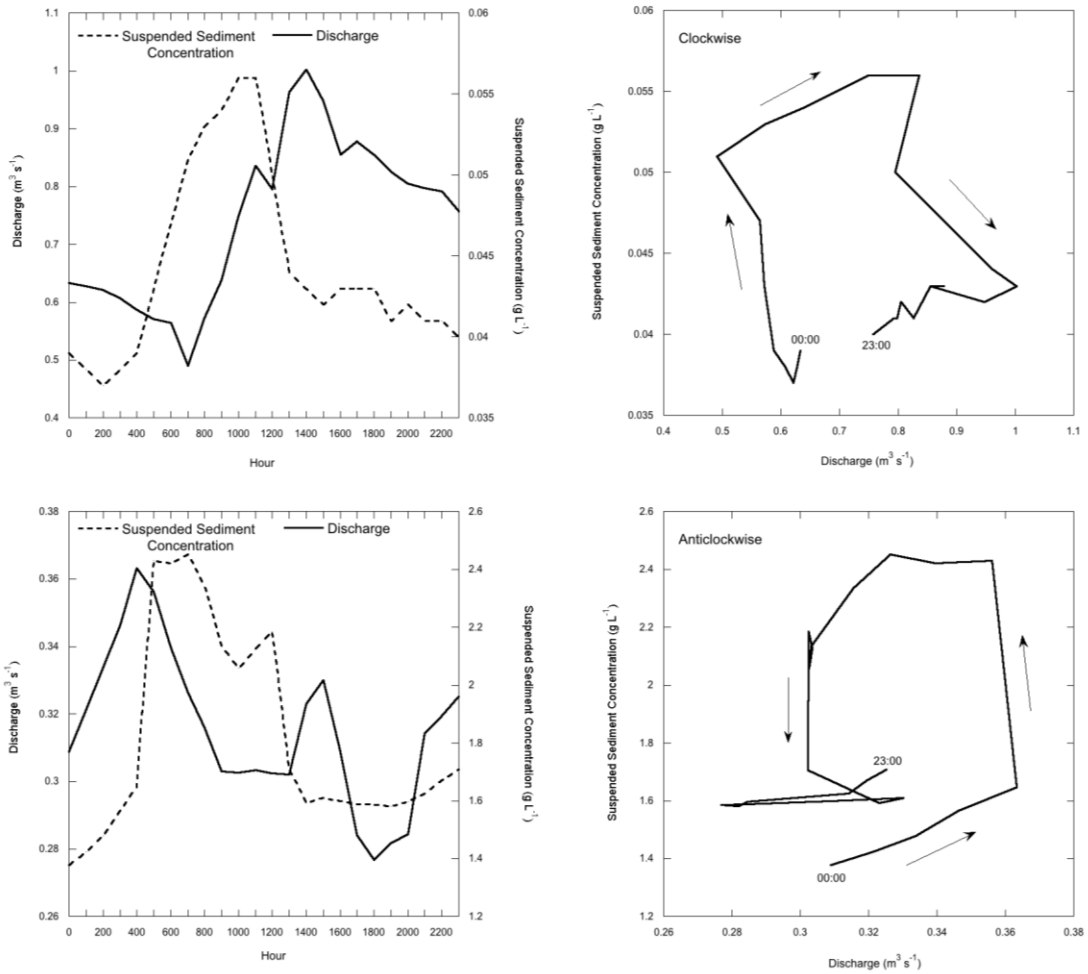


**Figure 4.9. Examples of mean diurnal variation of discharge and suspended sediment concentration (left-hand column) and corresponding hysteresis plots (right-hand column). Clockwise hysteresis direction (Nordjåkk, Day 209 2010) is shown top, and anticlockwise hysteresis direction shown bottom (Sydjåkk, Day 218 2010).**

### 4.2.6. Suspended Sediment Availability

Whilst hysteresis is a useful tool in characterising the changing relationship between discharge and suspended sediment concentration, investigation of the strength of association between the two variables can provide useful information upon which process inferences can be drawn (Hodson *et al*., 1998).

Gurnell *et al*. (1994) and Hodgkins (1996; 1999) inferred seasonal changes in the processes of proglacial suspended-sediment transfer at glaciers in Svalbard on the basis of changes in the parameters of simple regression and time series models.

In particular, and in both cases, a consistent increase in the slopes of linear regression models, predicting SSC from discharge, was interpreted to indicate an increase in the availability of sediment for fluvial transport: a fixed increment in discharge yielded progressively greater increments in SSC. Following the methods of Hodgkins (1996), regression models between suspended sediment concentration and discharge were created for each of the days used in the hysteresis analysis. Least squares linear regression (where discharge was the independent variable and suspended sediment concentration the dependent variable) was applied to each diurnal hysteresis loop, corresponding to the form $Q = aSSC^b$. The relative change in regression slope between days was used to infer the availability of sediment in the glacial drainage system, and thereby determine temporal changes in sediment transfer processes.

## 4.3. Results

### 4.3.1. Description of Suspended Sediment Time Series

#### 4.3.1.1. 2009 Ablation Season Observations

**Nordjåkk**

Suspended sediment concentration data from both Nordjåkk and Sydjåkk during the 2009 ablation season is presented in Table 4.4 and Figure 4.10. Comparable with the discharge hydrograph, the 2009 suspended sediment concentration record obtained at Nordjåkk shows a similar pattern of pronounced diurnal cyclicity. However these data show much greater variability with a number of small peaks evident, particularly at the start of the season. The seasonal maximum suspended sediment concentration (0.14 g $L^{-1}$) occurs around day 205 during the first peak of a sustained period of high discharge. However suspended sediment concentration data is unfortunately unavailable during the highest discharge period, although the responsiveness of suspended sediment concentration to increasing discharge during the first peak suggests that an even greater suspended sediment concentration peak during this event is likely. The remainder of the suspended sediment concentration data until the end of the recorded time series is largely fragmented with little in the way of prolonged data periods. However the available data does suggest an increasing suspended sediment concentration trend towards the end of the season, possibly in connection with the increased end of season discharge as described above.

**Sydjåkk**

Unfortunately, the 2009 suspended sediment concentration record obtained from Sydjåkk is highly fragmented with only limited periods of continuous data present.

The beginning of the season appears to be relatively stable with little variability in suspended sediment concentration. Later in the season, the suspended sediment concentration time series appears to be more variable with a number of peaks evident, and strong diurnal patterns obvious. The seasonal maximum suspended sediment concentration occurs during this period (2.80 g $L^{-1}$), although gaps in the data series make it unclear whether this was superseded at another point in the season.

**Table 4.4. Descriptive statistics of suspended sediment data collected during the 2009 ablation season.**

| | Nordjåkk | Sydjåkk |
|---|---|---|
| Mean (g $L^{-1}$) | 0.06 | 1.87 |
| Maximum (g $L^{-1}$) | 0.14 | 2.80 |
| Minimum (g $L^{-1}$) | 0.02 | 1.62 |
| St. Dev. (g $L^{-1}$) | 0.02 | 0.22 |

**Table 4.5. Descriptive statistics of suspended sediment data collected during the 2010 ablation season.**

| | Nordjåkk | Sydjåkk |
|---|---|---|
| Mean (g $L^{-1}$) | 0.06 | 1.17 |
| Maximum (g $L^{-1}$) | 0.45 | 4.34 |
| Minimum (g $L^{-1}$) | 0.03 | 0.01 |
| St. Dev. (g $L^{-1}$) | 0.04 | 0.87 |

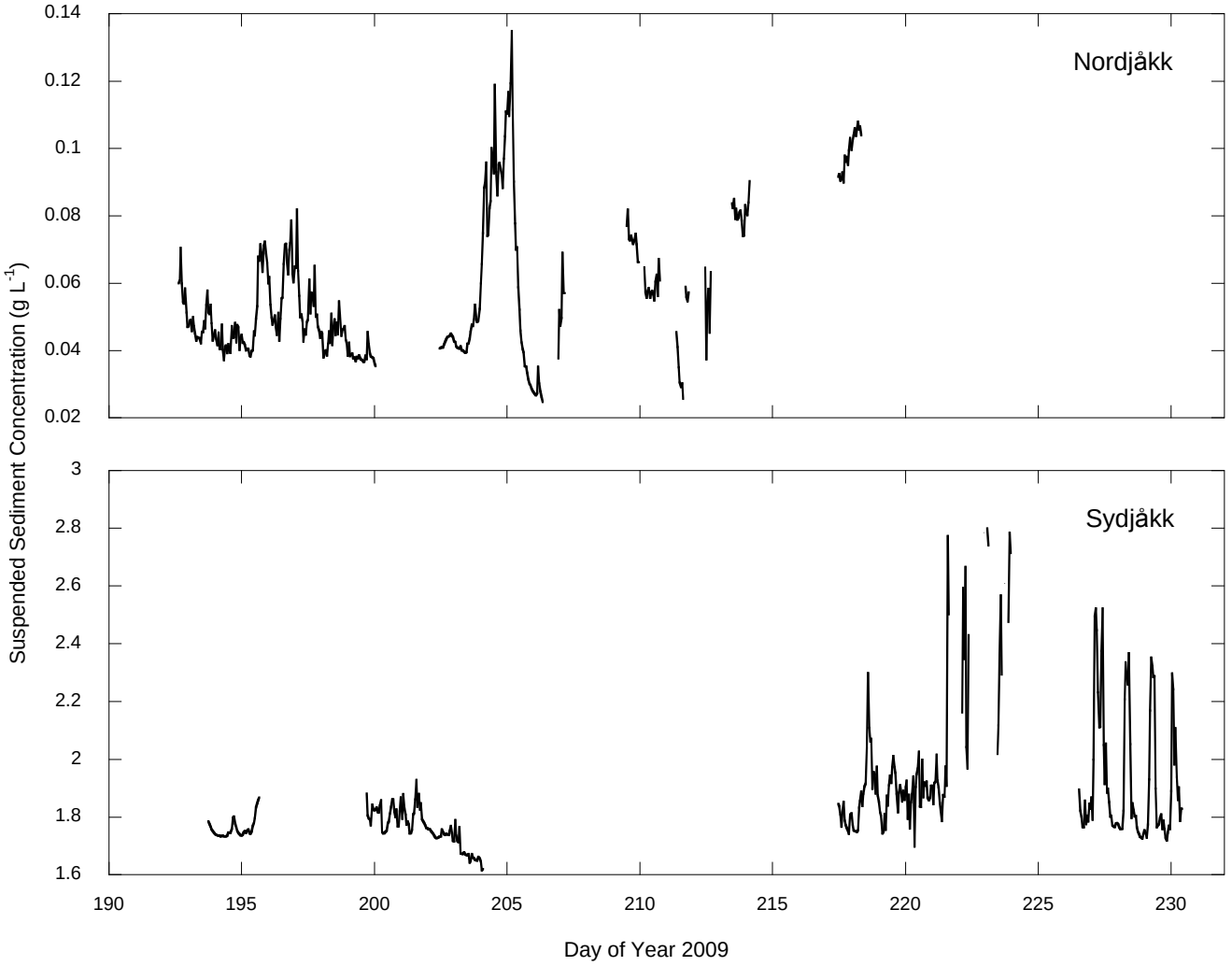


**Figure 4.10. Hourly suspended sediment time series from Nordjåkk and Sydjåkk during the 2009 ablation season**

#### 4.3.1.2. 2010 Ablation Season Observations

**Nordjåkk**

Suspended sediment concentration data from both Nordjåkk and Sydjåkk during the 2010 ablation season is presented in Figure 4.11 and Table 4.5 (section 4.3.1.1). Suspended sediment concentration recorded at the Nordjåkk gauging station during the 2010 melt season is largely characterised by a limited responsiveness to the hydrological behaviour of the stream. Peak suspended sediment concentration was recorded during a high discharge event between days 189 and 199, reaching a maximum suspended sediment concentration of 0.45 g $L^{-1}$. Similar responses to high discharge events are evident during events 2 and 3, although peak suspended sediment concentration in both events only reaches ~ 0.18 g $L^{-1}$. The remainder of the suspended sediment time series show little variability in suspended sediment concentration, with an average concentration of ~ 0.05 g $L^{-1}$.

**Sydjåkk**

Unlike the relatively stable discharge hydrograph, the suspended sediment concentration data recorded at the Sydjåkk gauging station during the 2010 melt season exhibits high variability and a number of peaks in suspended sediment concentration apparently independent of the hydrological behaviour of the stream. At the beginning of the season, suspended sediment concentration peaks at ~3.6 g $L^{-1}$ on day 199 during high discharge event 1 (as described above) and is followed by a number of smaller peaks during the falling limb of the discharge hydrograph. A seemingly independent suspended sediment concentration peak occurs on day 208, followed by a period of highly variable suspended sediment concentration between days 212 and 215 during which the seasonal high suspended sediment concentration is observed (~4.2 g $L^{-1}$). Two suspended sediment concentration peaks occur at the end of the season on days 224 and 226 (both ~ 3.9 g $L^{-1}$).

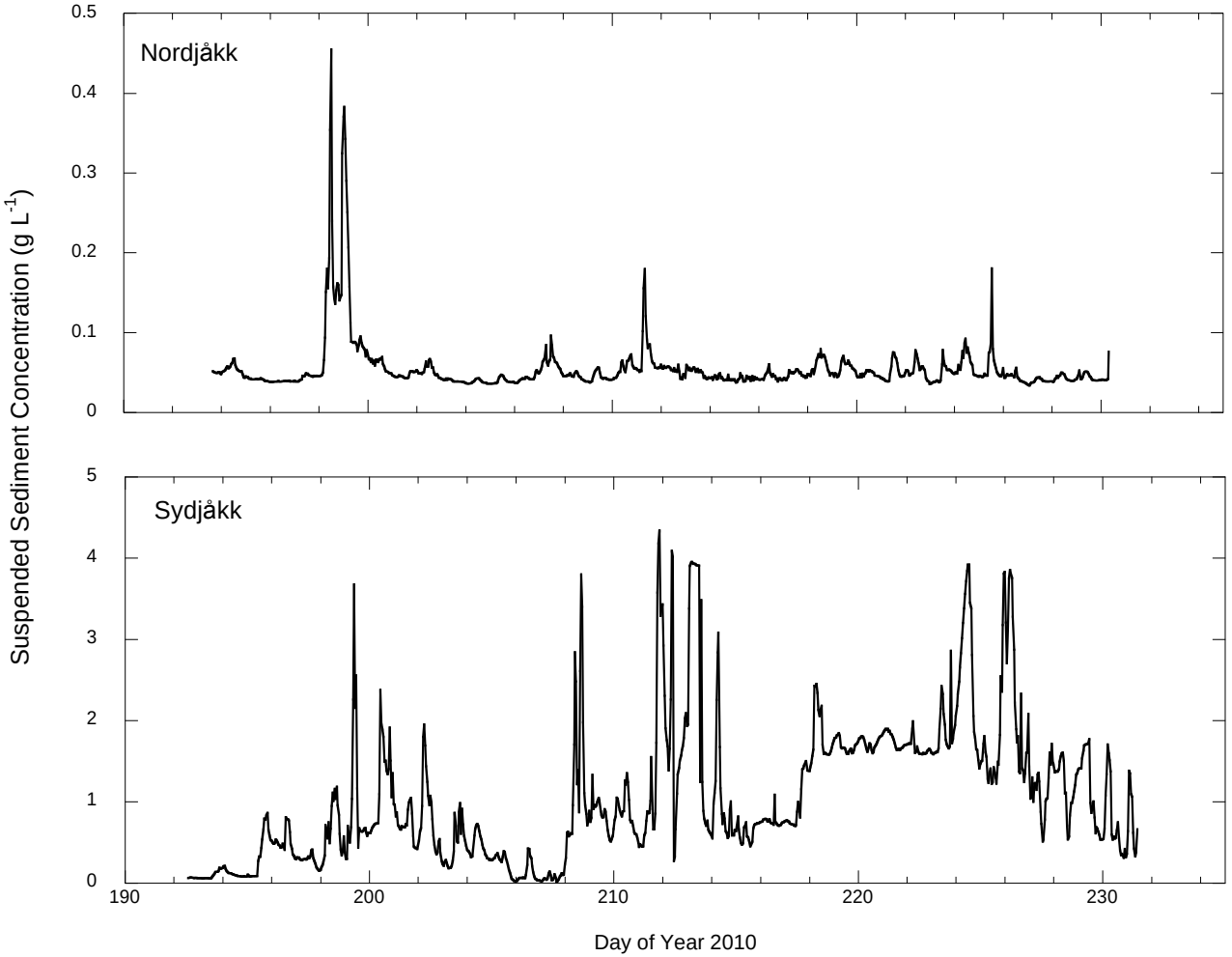


**Figure 4.11. Hourly suspended sediment time series from Nordjåkk and Sydjåkk during the 2010 ablation season**

### 4.3.2. Description of Seasonal Suspended Sediment Transfer

#### 4.3.2.1. 2009 Observations of Hysteresis Direction

**Nordjåkk**

Due to the fragmented nature of the data obtained from the Nordjåkk gauging station during the 2009 field season, hysteresis analysis was only possible for a limited number of days due to the need for complete 24-hour days to be analysed. Nonetheless, analysis of ten days was possible, yielding valuable insights into sediment transport dynamics at Nordjåkk (Figure 4.12).

The available data begins on day 193, exhibiting an anticlockwise hysteresis direction which is also repeated on day 194. A shift to a clockwise direction is observed on day 195, lasting until day 196. This marks the start of a period of a relatively strong diurnal rhythm within the suspended sediment time series, and to a lesser extent, the discharge hydrograph. Day 197 exhibits an anticlockwise direction, coinciding with a small peak in suspended sediment concentration but this is short-lived and shifts quickly back to clockwise on day 198. An anticlockwise direction is resumed on day 199, but this marks the beginning of a gap in the data, so it is unknown whether this pattern continues over the following days. The hysteresis data resumes on day 203, with a pattern of three consecutive anticlockwise days. All three of these days coincide with the rising limb, subsequent peak, and falling limb of a high discharge event, unfortunately marking the end of the available hysteresis data.

**Sydjåkk**

The season begins on day 194, exhibiting an anticlockwise pattern of hysteresis (Figure 4.13). Unfortunately a gap in the suspended sediment concentration time series prevents hysteresis analysis between day 194 and day 200 when

analysis is resumed. A period of clockwise hysteresis occurs between day 200 and day 204, coinciding with a period of highly variable discharge. Following another data gap, a clockwise pattern is continued on day 218 but shifts to an anticlockwise pattern on days 219 and 220, ending the season.

#### 4.3.2.2. 2009 Observations of Suspended Sediment Availability

**Nordjåkk**

At the beginning of the season, sediment availability rises rapidly between days 193 and 194 (Figure 4.12). Suspended sediment availability on day 193 is shown to be significant at the 95% confidence level using regression p-values, although not on day 194, suggesting that the limited availability prior to day 194 is significant, but that the increase in availability is not. Sediment availability decreases between days 194 and 195, with day 195 shown to be statistically significant. Another significant decrease in availability is observed on day 196, although this is relatively modest and suggests only a small change in availability. A sudden increase is observed on day 197, followed by a considerable, rapid and statistically significant decrease in availability between days 197 and 198. This coincides with a period of variable suspended sediment concentration and may suggest exhaustion of the subglacial sediment supply. Sediment availability increases on day 199, although this is not significant. Following a gap in the data, day 203 shows that sediment availability has decreased since day 199, although no inferences can be made as to the nature of this decrease due to the lack of data. However the limited availability on day 203 is shown to be significant. Availability increases considerably between day 203 and 204 before decreasing significantly again on day 205, coinciding with the falling limb of both the discharge hydrograph and suspended sediment concentration time series.

**Sydjåkk**

An isolated data point (day 194) makes it difficult to infer sediment availability at the beginning of the season (Figure 4.13). However, following a gap in the time series, the data resumes on day 200 at a greater slope value (~ -0.05) than observed on day 194. This suggests that sediment availability has increased during the missing data period, although the exact nature of this increase is impossible to infer. Days 200 and 201 indicate a slight decrease in availability, although this is followed by a slight increase on day 202, and a greater, more rapid increase on day 203. Suspended sediment availability on both days 202 and 203 are shown to be statistically significant suggesting an important link between increasing sediment availability and a period of high discharge variability evident in the discharge hydrograph. A change in slope following a second data gap suggests that availability has again decreased, although this quickly increases between days 218 and 219. The season ends with another decrease in availability on day 220.

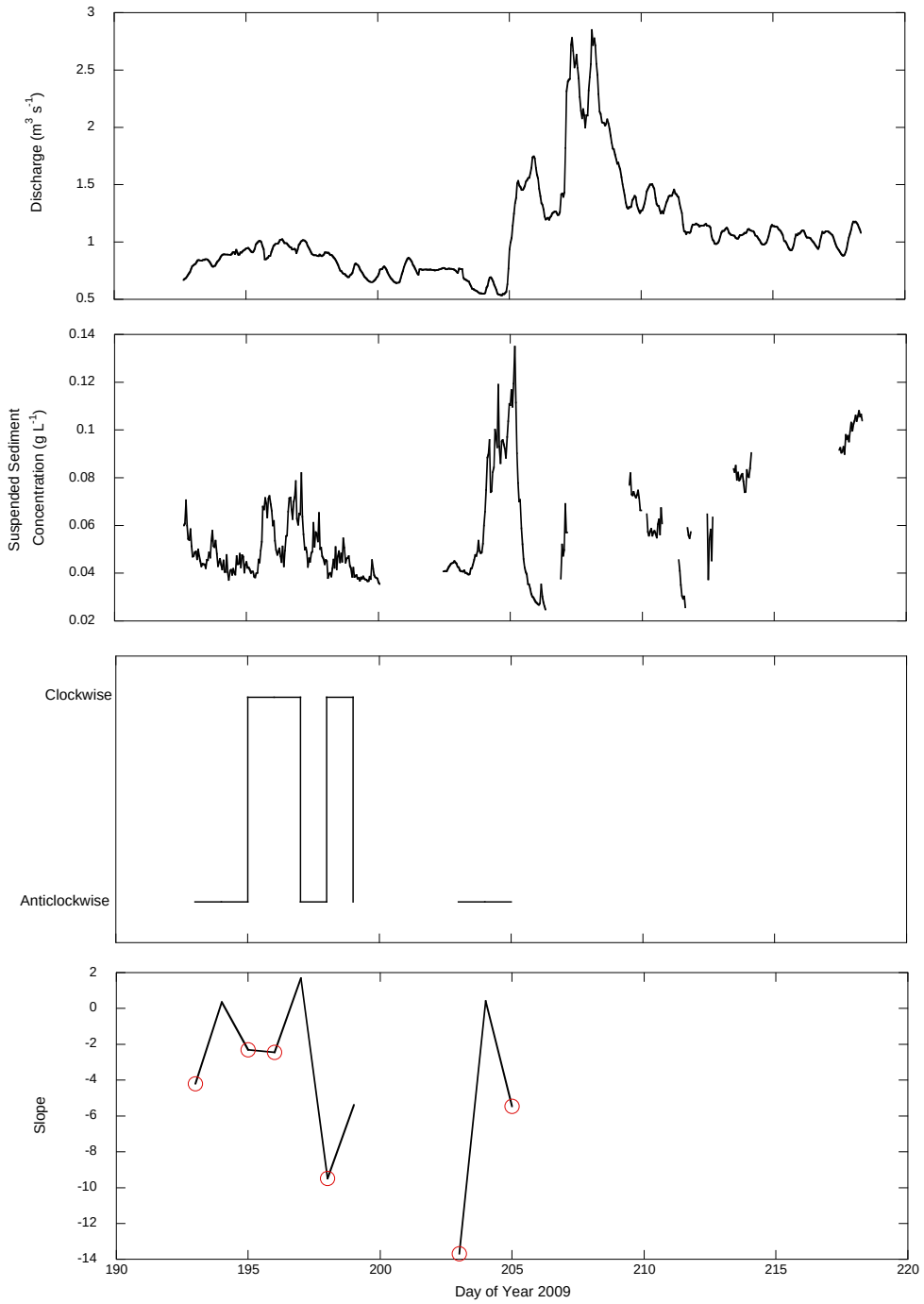


**Figure 4.12. Data for Nordjåkk collected during the 2009 ablation season. From top: mean hourly discharge; mean hourly suspended sediment concentration; step plot of diurnal hysteresis direction; linear-regression slope values of Q-SSC hysteresis loops representing suspended sediment availability. Red circles days on which suspended sediment availability is shown to be statistically significant (p =<0.05).**

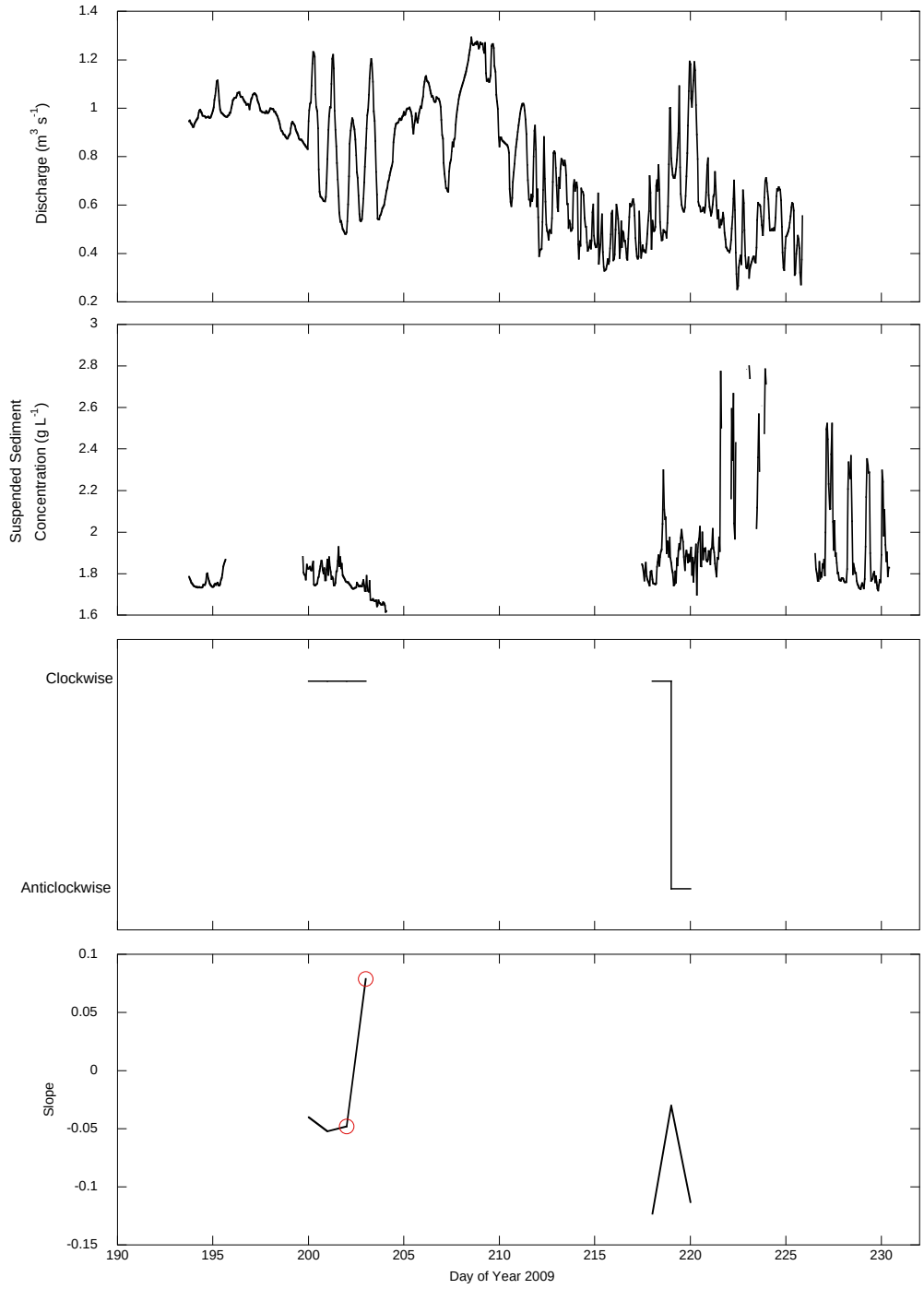


**Figure 4.13. Data for Sydjåkk collected during the 2009 ablation season. From top: mean hourly discharge; mean hourly suspended sediment concentration; step plot of diurnal hysteresis direction; linear-regression slope values of Q-SSC hysteresis loops representing suspended sediment availability. Red circles days on which suspended sediment availability is shown to be statistically significant (p =<0.05).**

#### 4.3.2.3. 2010 Observations of Hysteresis Direction

**Nordjåkk**

Diurnal hysteresis direction recorded at the Nordjåkk gauging station during the 2010 field season show a largely clockwise pattern with only 7 days exhibiting anticlockwise hysteresis (Figure 4.14).

The beginning of the 2010 season experiences an early shift from clockwise to anticlockwise hysteresis, coinciding with the rising limb of a high discharge event on day 198. However, a clockwise pattern resumes on day 199, and continues uninterrupted until day 205. Day 206 displays anticlockwise hysteresis although but this is short-lived, a relatively extended period of clockwise hysteresis returning on day 207. Days 212 to 217 exhibit the most variable period of the season, with hysteresis direction changing daily. Day 213 marks the start of this pattern, with two consecutive anticlockwise days coinciding with the falling limb of the second high discharge event of the season (peaking on day 212). This is followed by three rapid direction changes: clockwise on day 215, anticlockwise on day 216, and clockwise on day 217. Following a gap between days 217 and 224, the data resume on day 224 with two consecutive anticlockwise days, shifting to clockwise on day 226 to end the season on day 227.

**Sydjåkk**

Diurnal hysteresis direction recorded at the Sydjåkk gauging station during the 2010 field season (Figure 4.15) show a marginally clockwise pattern with 19 days exhibiting clockwise hysteresis, compared with 14 which exhibit anticlockwise hysteresis. Unlike the hysteresis patterns observed at the Nordjåkk gauging site however, the direction of hysteresis switches continuously through the monitoring period with only relatively short (3-4 days) periods exhibiting a constant direction at any time.

Although the season starts with an anticlockwise pattern on day 197, this shifts to a clockwise pattern on day 198, coinciding with a period of high discharge. This pattern continues uninterrupted until day 201, before shifting into a three-day period of anticlockwise hysteresis between days 202 and 204. Between days 205 and 207, during a period of extremely low observed discharge and suspended sediment concentration, the pattern returns to clockwise, but switches to anticlockwise on day 208 in conjunction with the rising limb of a peak in suspended sediment concentration. During the peak of this event on day 209, the hysteresis direction assumes a clockwise pattern, returning to anticlockwise on day 211. Days 212 to 215 exhibit both a period of increased discharge, and high variability in suspended sediment concentration values. This is reflected in the pattern of hysteresis direction, with day 212 exhibiting a clockwise direction to coincide with peak suspended sediment concentration, and day 213 returning to an anticlockwise direction as suspended sediment concentration falls rapidly. Days 214 to 216 exhibit a clockwise pattern as suspended sediment concentration peaks for the final time during this period of variability. Days 217 to 220 display an anticlockwise pattern of hysteresis during a period of relatively stable discharge and suspended sediment concentration behaviour. Days 220 to 224 return to a clockwise pattern with day 224 coinciding with the rising limb of a high suspended sediment concentration event. The remainder of this event however is characterised by anticlockwise hysteresis, through days 225 to 227. Hysteresis direction returns to clockwise on day 228, and continues to the end of the season on day 229.

#### 4.3.2.4. 2010 Observations of Suspended Sediment Availability

**Nordjåkk**

At the beginning of the season, sediment availability rises rapidly from day 196 and peaks on day 199, coinciding with the peak of a high discharge event and a period of increased suspended sediment concentration (Figure 4.14). This

increase in availability is significant at the 95% confidence interval. Immediately following the peak, sediment availability between days 199 and 200 exhibits a sudden and rapid decrease, although this is not shown to be significant. Days 200 to 205 show a relatively steady pattern of availability with only slight slope changes occurring day to day. A relatively modest, but statistically significant increase in availability is observed on day 206, although this appears to be short-lived since availability immediately decreases between days 206 and 207. Significant increases in availability are observed on days 208 and 210, although both of smaller magnitude than that observed on day 206. Like day 206, both peaks in availability are immediately followed by a decrease in availability the following day. Day 211 shows a slight increase in availability from day 210, although this is not statistically significant. A rapid and significant decrease in availability is observed on day 212, coinciding with a high discharge and event. This is again short-lived, although the subsequent increase in availability over the next two days occurs more slowly than the original day 212 decrease. Days 214 to 217 show a steady pattern of availability with only a very slight increasing trend discernible. Of these four days, only day 217 is shown to be statistically significant. Following a gap in the time series, the data resume on day 224. This is the last significant day of the time series and shows an elevated level of sediment availability, the second highest of the season. This decreases considerably on day 225, although the gap in data preceding day 224 conceals whether this was part of a larger decrease in sediment availability, or a discrete event. The final days of the season (days 226 and 227) show a constant level of availability, with no substantial change in pattern.

**Sydjåkk**

At the beginning of the melt season, sediment availability displays relatively little variability, increasing only slightly during the rising limb of the highest discharge event of the season (Figure 4.15). A slight but marked decrease in availability coincides with the peak of this event on day 200, and this is shown to be significant ($p<0.05$). This decrease in availability is short lived however, and

availability begins to increase from day 201, peaking on days 202 and 203, during a period of increased suspended sediment concentration. Both of these days are shown to be statistically significant. Decreased availability is observed on days 204 and 205, although only day 205 is shown to be statistically significant. This coincides with the lowest measured values of both discharge and suspended sediment concentration. Day 206 exhibits a brief, although not significant increase in availability, but is immediately followed by a rapid and relatively sudden decrease in availability, coinciding with a peak in suspended sediment concentration. Days 207 and 208 reflect this change with availability increasing again on day 209. Each of these days are statistically significant. From day 210, availability increases relatively rapidly, coinciding with a period of high variability in suspended sediment concentration. This variability is reflected in the pattern of sediment availability, with a sudden decrease evident on day 214, and frequent changes in availability occurring until day 218. Although this period is variable, none of the data is shown to be significant. A decrease in availability on day 219 is shown to be significant, and is followed by a further significant decrease on day 221. From here availability increases rapidly, peaking on day 223, again statistically significant in spite of a period of stability in both discharge and suspended sediment concentration records. Availability once again decreases on day 224 during a high suspended sediment concentration event and despite increasing slightly on day 225 in conjunction with falling suspended sediment concentration, continues to decrease relatively quickly on day 226 as suspended sediment concentration peaks for a second time. This low availability is shown to be significant on day 226, although this is the last significant day of the season. The final days of the monitored period show a marked increase in availability on day 227, although a decrease in availability commences on day 228, lasting until the final monitored day, 229.

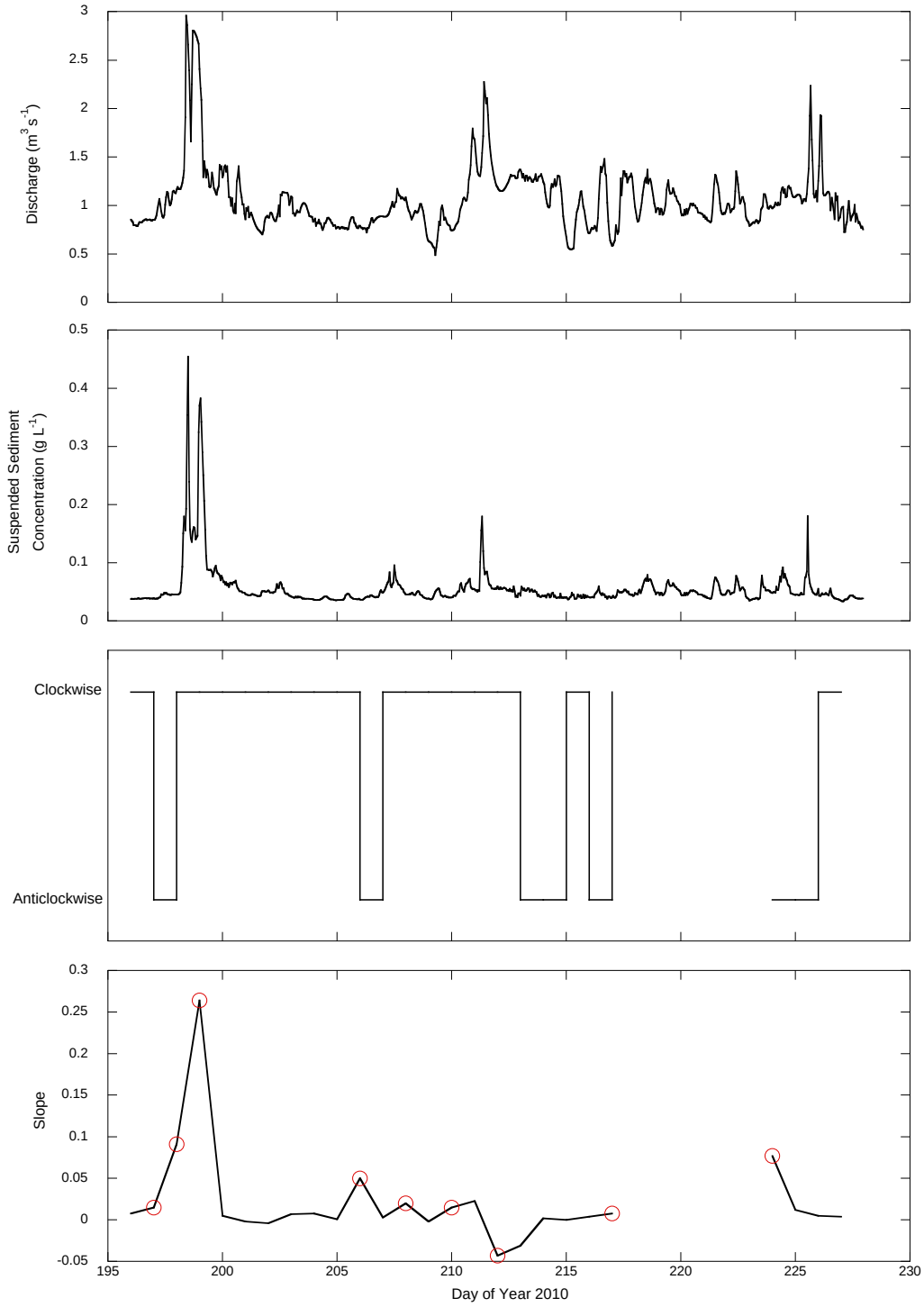


**Figure 4.14. Data for Nordjåkk collected during the 2010 ablation season. From top: mean hourly discharge; mean hourly suspended sediment concentration; step plot of diurnal hysteresis direction; linear-regression slope values of Q-SSC hysteresis loops representing suspended sediment availability. Red circles days on which suspended sediment availability is shown to be statistically significant (p =<0.05). Due to the use of similar techniques to fill gaps in both the discharge and suspended sediment time series, no analysis was attempted between day 218 and day 224 as these data would be statistically invalid.**

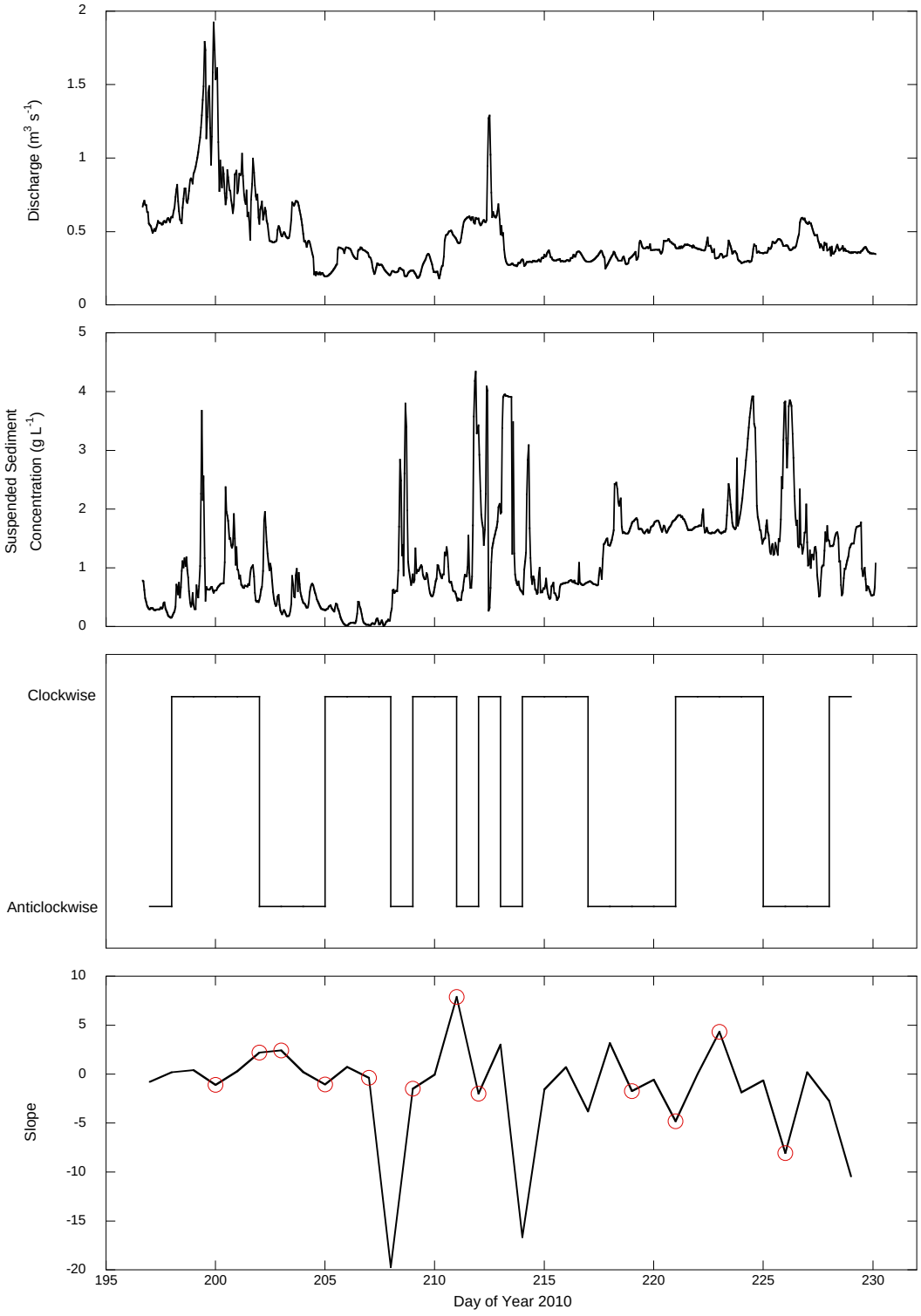


**Figure 4.15. Data for Sydjakk collected during the 2010 ablation season. From top: mean hourly discharge; mean hourly suspended sediment concentration; step plot of diurnal hysteresis direction; linear-regression slope values of Q-SSC hysteresis loops representing suspended sediment availability. Red circles days on which suspended sediment availability is shown to be statistically significant (p =<0.05).**

## 4.4. Discussion

### 4.4.1. Comparing Suspended Sediment Transfer at Nordjåkk & Sydjåkk

Having described observations of suspended sediment transfer at Storglaciären in Section 4.3, this section compares and contrasts changes in suspended sediment data at Nordjåkk and Sydjåkk.

As in Chapter 3 the interpretation and discussion below is based solely on the 2010 time series. Given the extensive missing data in the 2009 time series, it is difficult to assess the representativeness of the data in the context of a full glacier melt season and to make firm interpretations. However the data has been presented throughout the chapter for thoroughness and openness.

#### 4.4.1.1. 2010 Ablation Season

During the early stages of the ablation season, both Nordjåkk and Sydjåkk exhibit relatively long periods of clockwise diurnal hysteresis throughout and following a high discharge event (day 198). This suggests that both streams have abundant suspended sediment supplies at this stage of the season, although Sydjåkk does exhibit evidence of sediment supply exhaustion five days later. Diurnal hysteresis direction is also clockwise during two other high discharge events, even at a late stage in the season. This suggests a relatively consistent sediment supply throughout the season, albeit possibly decreasing in responsiveness to discharge. Hysteresis direction at Sydjåkk, whilst briefly clockwise during the middle season discharge event, exhibits an anticlockwise pattern during the end of season discharge peak.

Towards the end of the season, Sydjåkk is characterised by an increase in the suspended sediment concentration baseline, and a number of suspended sediment peaks independent of stream discharge. Missing data gaps at Nordjåkk during this period make comparison between the two streams difficult. However, the Nordjåkk suspended sediment time series appears to remain

closely related to discharge, albeit with reduced responsiveness, as suggested above. This suggests a fundamental difference in suspended sediment transfer at both streams.

The greatest variation between the two streams occurs around the middle of the season (between days 207 and 214). During this period, the suspended sediment time series at Nordjåkk remains stable with clockwise diurnal hysteresis direction and relatively modest changes in suspended sediment availability. However, the suspended sediment time series at Sydjåkk shows little connection with the discharge time series and is characterised by large transient suspended sediment peaks, rapid shifts in hysteresis direction, and abrupt changes in sediment availability.

### 4.4.2. General Patterns and Controls Influencing Suspended Sediment Transfer at Storglaciären

Based on the data presented in Section 4.3, and the comparisons of sediment transport in Nordjåkk and Sydjåkk in Section 4.4.1, this section makes inferences on patterns and controls of suspended sediment transfer to the proglacial area of Storglaciären.

Seasonally, both Nordjåkk and Sydjåkk exhibit an overall clockwise pattern of diurnal hysteresis. This supports the conclusion of Schneider and Bronge (1996) that suspended sediment concentration peaks before discharge at both Nordjåkk and Sydjåkk at diurnal and seasonal timescales. Both streams exhibit hysteresis and sediment availability data which suggest an abundance of suspended sediment during the early stages of the season. Jansson *et al*. (2005) suggest that this may occur as a result of extensive local lifting of Storglaciären in response to early season high discharge. Such events would expose previously unavailable unconsolidated sediments, resulting in large scale flushing of suspended sediment sources. Subsequent discharge events will not encounter the same quantities of sediment, resulting in reduced suspended sediment concentrations, in spite of high discharge (Jansson *et al*., 2005). This is also alluded to by

Schneider and Bronge (1996), who suggest that high discharge 'floods' early in the season are accompanied by higher suspended sediment concentrations than those late in the season. Although no 'floods' were observed during either ablation season, data from Nordjåkk during the 2010 season suggests that suspended sediment response to high discharge gradually declines as the season progresses. This is exemplified by the difference in suspended sediment response to high discharge events early in the season (day 196) and later in the season (days 212 and 227). Whilst suspended sediment concentration on day 196 peaks at 0.45 g $L^{-1}$, response during the two subsequent discharge events is more subdued, yielding a maximum suspended sediment concentration of ~ 0.18 g $L^{-1}$. This is suggestive of diminishing suspended sediment availability, and is supported by decreasing regression slopes. Therefore, this is interpreted as the result of the gradual removal of unconsolidated sediment along transport pathways.

Periods of anticlockwise hysteresis do occur however, which, combined with sediment availability data suggest the occurrence of suspended sediment supply exhaustion at both streams as observed in other studies (e.g. Collins, 1979a; Humphrey *et al*., 1986; Hodgkins, 1996; Hodson and Ferguson, 1999). These occur principally at Sydjåkk and are less frequent at Nordjåkk, occurring predominantly towards the middle of the season following a peak in discharge. The longest supply exhaustion inferred from both diurnal hysteresis direction and sediment availability data at Nordjåkk lasted for two days, suggesting that the supply of suspended sediment is recharged relatively rapidly. Conversely, supply exhaustion episodes at Sydjåkk (for instance, between days 218 and 221) are prolonged, lasting for up to four days. This may occur as a result of the fundamental differences in the routing of the two streams, with Sydjåkk having a greater subglacial residence time, and therefore relying more heavily on subglacial processes to supply suspended sediment.

Data from the 2010 ablation season suggest that the relationship between discharge and suspended sediment transfer differs between Nordjåkk and Sydjakk. Whilst suspended sediment concentration remains largely stable at

Nordjåkk and responds closely to discharge, Sydjåkk exhibits a dynamic suspended sediment time series. Large fluctuations in suspended sediment concentration are therefore frequently observed, often as large as ~ 4 g $L^{-1}$, often independent of discharge. Such episodic suspended sediment peaks occur predominantly during the middle of the ablation season, although several also occur towards the end of the season. Similar episodic events have been observed at both temperate (e.g. Gurnell and Warburton, 1990; Willis *et al*., 1996) and non-temperature (e.g. Hodgkins, 1999; Porter *et al*., 2010) glaciers and have been attributed to both subglacial and ice-marginal sediment delivery processes. During the mid-season period of high suspended sediment concentration, peaks independent of discharge are interpreted as representing shifts in the subglacial drainage system in response to relatively high discharge, and resulting in increased suspended sediment delivery to the proglacial area. Later in the season, the increased suspended sediment concentration baseline suggests a more constant process, rather than episodic subglacial drainage system rationalisation. Field observations during this period suggest that Sydjåkk was characterised by low discharges and an extremely high sediment load, peaking above 3 g $L^{-1}$. Furthermore, large volumes of pebble sized bedload material were observed in the stream channel which did not appear to originate on the stream banks. The size of material entrained combined with the volume of material at such a late stage in the season suggest an ice-marginal source. It is therefore speculated that suspended sediment from the ice-cored southern lateral moraine has been mobilised, possibly as the result of fluvial undercutting at the glacier margin.

## 4.5. Summary

Based on the interpretations made in Section 4.4, the following conclusions can be drawn regarding suspended sediment transport at Storglaciären.

- Suspended sediment transport differs greatly between the two proglacial streams at Storglaciären: suspended sediment concentrations at Nordjåkk are typically low and respond closely to discharge. Conversely, Sydjåkk carries a much greater suspended sediment concentration which is often independent of discharge, and exceed concentrations at Nordjåkk by an order of magnitude. Episodic suspended sediment events during the middle of the 2010 ablation season suggest rationalisation of the subglacial drainage system, possibly in response to the retreat of the glacier snow line.
- Seasonally, suspended sediment is abundant early in the ablation season at both streams. There is some evidence of reduced suspended sediment responsiveness to discharge later in the season, although these are short-lived, suggesting that sediment sources are recharged rapidly.
- High variability in suspended sediment delivery late in the 2010 ablation season at Sydjåkk suggest that ice-marginal processes may contribute greatly to the fluvial suspended sediment load. However, this is not evident at Nordjåkk.

Finally, although the use of a sediment transfer model did not allow accurate predictions of suspended sediment concentration to be made, revisiting this technique may enable little understood processes such as sediment exhaustion to be investigated further. Short-term sediment availability can influence the delivery of suspended sediment, although it is not accounted for in models such as the one applied here, which assume constant sediment availability. Knowledge of suspended sediment availability at Storglaciären may allow related processes to be parameterized, enabling more accurate predictions of suspended sediment transfer.

*Chapter 5*

# Drivers of Suspended Sediment Transport

## 5.1. Introduction

Short-term storage and release of suspended sediment transfer in proglacial channels vary spatially and temporally in response to fluctuations in sediment sources, diurnal discharge variations, and rates of transfer processes (Gurnell and Warburton, 1990; Orwin and Smart, 2004). Given the likelihood of sediment storage and remobilisation along a channel reach, traditional monitoring of suspended sediment at a single gauging location provides only coarse approximations of proglacial suspended sediment transfer patterns (Harbor and Warburton, 1993; Collins, 1998; Orwin and Smart, 2004). Principal component analysis is able to overcome such limitations by reducing the variance of a complex data set into several components, allowing more detailed interpretations of suspended sediment transfer to be made. Furthermore, hierarchical cluster analysis can be employed to objectively identify periods of similar response amongst components, revealing otherwise masked patterns. Principal component analysis is a common tool in studies of water quality (e.g. Haag and Westrich, 2002) but until recently has been used relatively infrequently in glaciological studies. Hannah *et al*. (1999; 2000) and Swift *et al*. (2005) have both employed principal component analysis and hierarchical cluster analysis in classifying discharge hydrographs, whilst Orwin and Smart (2004) and Irvine-Fynn *et al*. (2005a; 2005b) applied similar analyses to identify patterns of suspended sediment transfer in glacier basins.

### 5.1.1. Aims of the Chapter

The aim of this chapter is to utilise techniques of principal component analysis and hierarchical cluster analysis to more closely examine patterns in the suspended sediment time series collected at Storglaciären during the 2009 and 2010 ablation seasons. There are two specific objectives:

(i) To identify patterns of suspended sediment delivery using suspended sediment response shape and magnitude.

(ii) To identify factors which influence suspended sediment delivery to the proglacial area of Storglaciären.

## 5.2. Methods

### 5.2.1. Classification of Daily Suspended Sediment Response Shape

Classification of suspended sediment response shape was achieved in two stages. Firstly, principal component analysis was used to identify underlying components which explained sediment transfer processes. A more detailed explanation of the background to this procedure is given in Chapter 3. The analysis used an input matrix of *N* columns of days by *n* rows of hourly suspended sediment concentration. As with the discharge-generating processes analysis, PCA was performed using a VARIMAX orthogonal rotation to maximise loadings on the variables. Components with an Eigenvalue of >1 were retained. Principal component scores were plotted against time to reveal the underlying 'shape' of the retained components. Secondly, Hierarchical Cluster Analysis (HCA) was performed on the retained PCA components to identify periods of comparable hydrograph 'shape'. Cluster analysis is a method of data analysis which provides classification in data sets. Patterns or groups within the data set are clustered so that the degree of association is strong between members of the same cluster, and weak between members of different clusters. Hierarchical cluster analysis is a method of cluster analysis which forms groups by means of a hierarchy. This occurs either through agglomeration, whereby each observation starts in a unique cluster and is merged with others as they move up the hierarchy, or though division whereby all observations start in one cluster, and are split as individual clusters move down the hierarchy. Effectively, each can be described more simply as either a 'top down', or a 'bottom up' approach.

Prior to running HCA, principal component loadings were standardized to z-scores (mean = 0, standard deviation = 1) to remove major variations in the magnitude of observations (Orwin and Smart, 2004). Hierarchical cluster analysis was run using Ward's (1963) method, as this allowed more physically interpretable clusters (Orwin and Smart, 2004). Ward's (1963) method is a method of agglomerative hierarchical cluster analysis which treats cluster analysis as an

analysis of variance problem, rather than using distance metrics or measures of association. Therefore, Ward's method attempts to minimize the variance of the differences between attributes within a cluster based on the sum of squares of the difference of the attributes. Interpretation of clusters was performed visually, with each cluster assigned an appropriate 'shape' title according to their structure (Hannah *et al*., 2000; Orwin and Smart, 2004).

### 5.2.2. Classification of Daily Suspended Sediment Magnitude

The method of classifying suspended sediment 'magnitude' was developed by Orwin and Smart (2004) based on the cluster analysis of bulk discharge indices proposed by Hannah *et al*. (2000). In this case, daily bulk sediment indices were used, including mean daily suspended sediment concentration; daily suspended sediment concentration range; daily suspended sediment concentration standard deviation, daily maximum and minimum suspended sediment concentration; and total suspended sediment load. All daily indices were calculated in grams per litre, except for total suspended sediment load, which was calculated in kilograms per day. Observations were standardised to z-scores (mean = 0, standard deviation = 1) and clustering performed using Ward's method. Like 'magnitude' clusters were visually identified using the cluster agglomeration schedule and assigned classes based on the raw data contained within each cluster (Orwin and Smart, 2004).

### 5.2.3. Composite Daily Suspended Sediment Shape and Magnitude Response

Following the methods of Orwin and Smart (2004), suspended sediment shape and magnitude data for each gauging station were plotted alongside meteorological, discharge and suspended sediment concentration data. This enables events which produce distinctive suspended sediment shape and magnitude responses at each gauging site to be identified.

### 5.2.4. Classification of Daily Meteorological Data

This final analysis was used to identify comparable periods of meteorological conditions in order to infer meteorological controls on suspended sediment transfer. Hierarchical cluster analysis was applied to daily indices of average, maximum and minimum temperature; average relative humidity, total daily global solar radiation; and total daily rainfall. As in previous cluster analyses, observations were standardised to z-scores in order to remove major differences in magnitude. Cluster analysis was performed using Ward's method (Ward, 1963) and clusters identified visually using the cluster agglomeration schedule.

## 5.3. Results

### 5.3.1. Description of Daily Suspended Sediment Response Shape

In both years, principal component analysis of daily suspended sediment data retained three shared discrete components related to suspended sediment shape. These components were classified into 'building', 'peaked' and 'recessional' classes, reflecting recurring shapes in the seasonal sedigraph. In addition, principal component analysis carried out on 2009 data retained a further component, interpreted as 'variable' response. This component does not occur within both data series, hence 'variable' response is observed exclusively at Nordjåkk. Each component shape can be rationalised as follows:

- 'Peaked' days show the most pronounced diurnal pattern with a clear peak during the afternoon.
- 'Recessional' days exhibit a distinct decline in suspended sediment concentration throughout the day.
- 'Building' days are similar in shape to 'peaked' days, but may peak overnight or during the evening, having increased gradually throughout the day.
- 'Variable' days show frequent changes in suspended sediment response throughout the day, albeit at a small magnitude. Suspended sediment concentration may build towards a diurnal maximum, but this is not pronounced enough to classify as 'peaked'.

The distribution of each response shape at both stream gauging sites is outlined in Tables 5.1 and 5.2: Examples of each shape response are presented in Figure 5.1.

**Table 5.1. Distribution of sediment response shapes at Nordjåkk and Sydjåkk during the 2009 ablation season.**

| Sediment Response Shape | Nordjåkk (n) | Nordjåkk (%) | Sydjåkk (n) | Sydjåkk (%) |
|---|---|---|---|---|
| Recessional | 2 | 30.00 | 2 | 25.00 |
| Peaked | 1 | 10.00 | 3 | 37.5 |
| Building | 5 | 50.00 | 3 | 37.5 |
| Variable | 1 | 10.00 | - | - |

**Table 5.2. Distribution of sediment response shapes at Nordjåkk and Sydjåkk during the 2010 ablation season.**

| Sediment Response Shape | Nordjåkk (n) | Nordjåkk (%) | Sydjåkk (n) | Sydjåkk (%) |
|---|---|---|---|---|
| Recessional | 8 | 25.00 | 18 | 52.94 |
| Peaked | 18 | 56.25 | 5 | 14.71 |
| Building | 6 | 18.75 | 10 | 29.41 |

Although comparison of data from the 2009 ablation season is difficult due to periods of missing data at both gauging sites, it is clear that Nordjåkk and Sydjåkk exhibit vastly different occurrences of individual suspended sediment response shapes. At Nordjåkk, 'building' response shapes are dominant (n= 5; 50%), whilst at Sydjåkk, both 'peaked' and 'building' response shapes are equally prevalent (n=3; 37.5%). This is considerably greater than the occurrence of 'peaked' response at Nordjåkk (n=1; 10%). 'Recessional' response shapes are least prevalent at Sydjåkk (n=2; 25%), although this value is similar to that observed at Nordjåkk (n=2; 30%). 'Variable' response is only observed during one day at the Nordjåkk gauging site, accounting for 10% of the total variability of suspended sediment response, matching 'peaked' response.

During the 2010 ablation season, both Nordjåkk and Sydjåkk are dominated by different sediment response shapes. At Nordjåkk, 'peaked' sediment response is dominant (n=18; 56.25%), whereas at Sydjåkk, 'recessional' response is dominant (n=18; 52.94%). The streams differ even further in terms of the least prevalent response shapes. 'Building' sediment response shapes are least prevalent at Nordjåkk accounting for only 18.75% (n=6) of the total variability of sediment response, whereas 'peaked' sediment response shapes are least prevalent (n=5; 14.71%) at Sydjåkk. 'Building' sediment response shapes at Sydjåkk accounted for 29.41% of the total variability of the data set (n=10).

In terms of interannual variability between the two streams, only 'recessional' response at Nordjåkk is similar during both ablation seasons. Neither stream is dominated by the same response shape during both seasons.

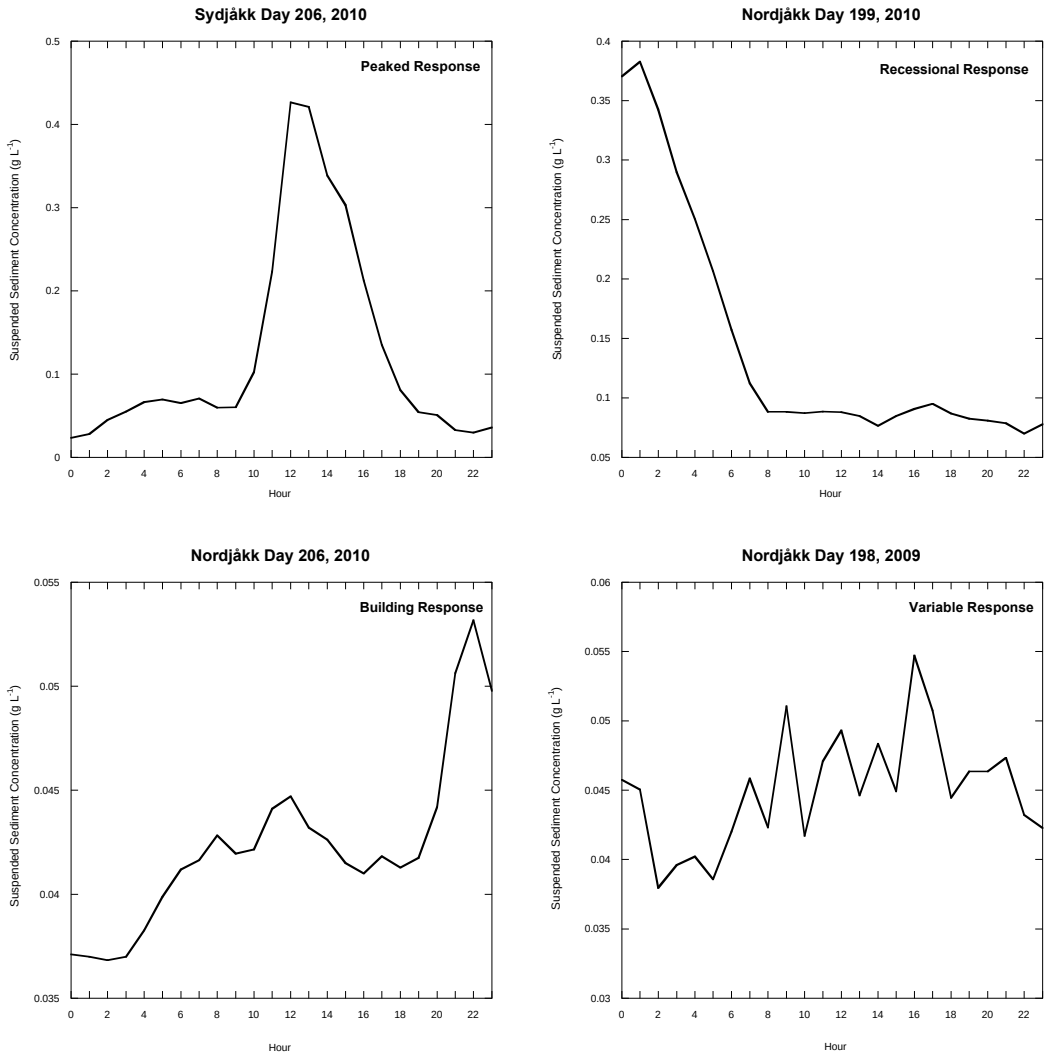


**Figure 5.1. Examples of suspended sediment response shapes classified using Principal Component Analysis**

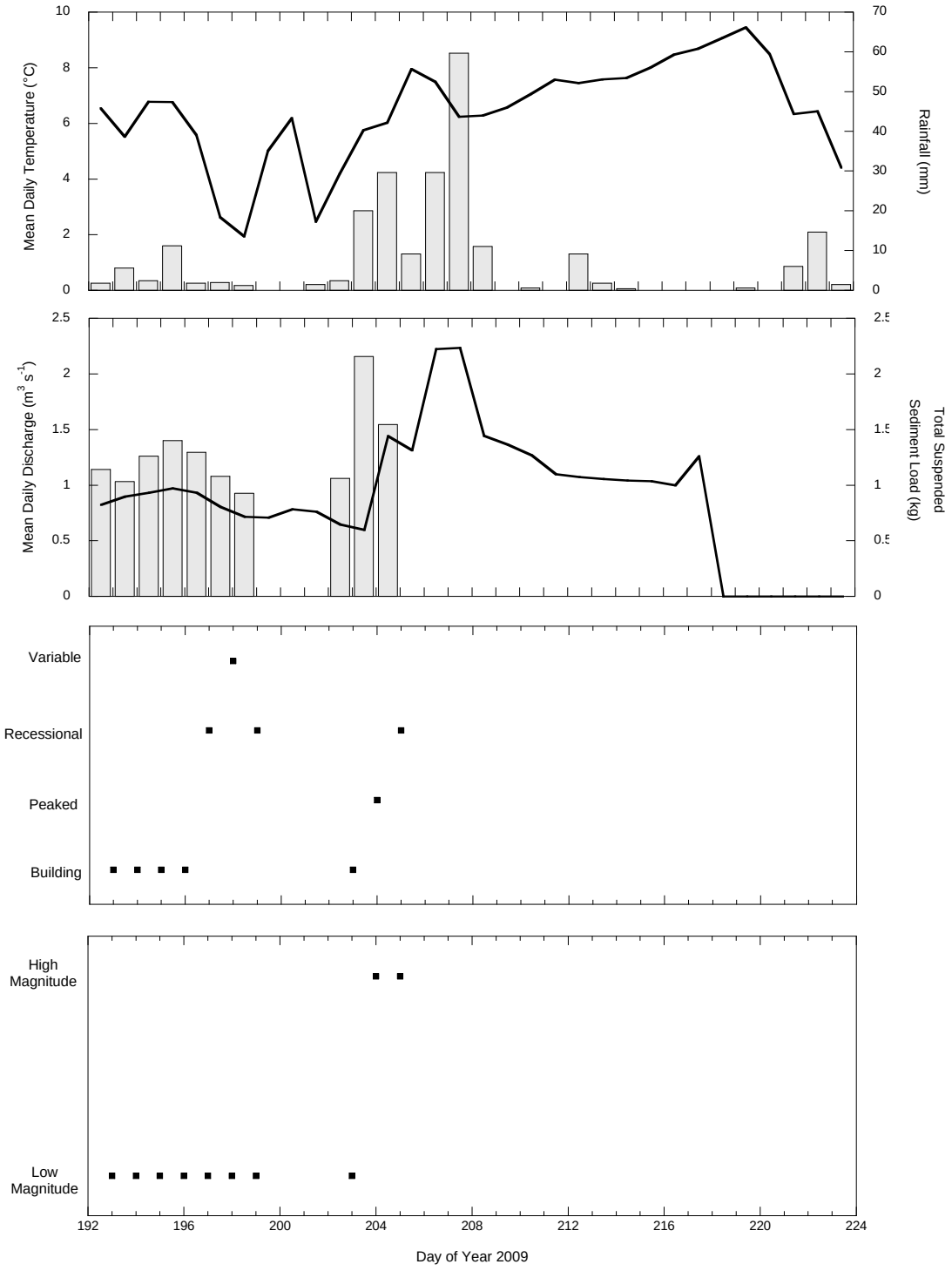


**Figure 5.2. Composite daily suspended sediment response shape and magnitude plot for the Nordjåkk gauging site during the 2009 ablation season. N.B. Gaps in the total daily suspended sediment load plot are the result of missing data and do not indicate an absence of suspended sediment transport.**

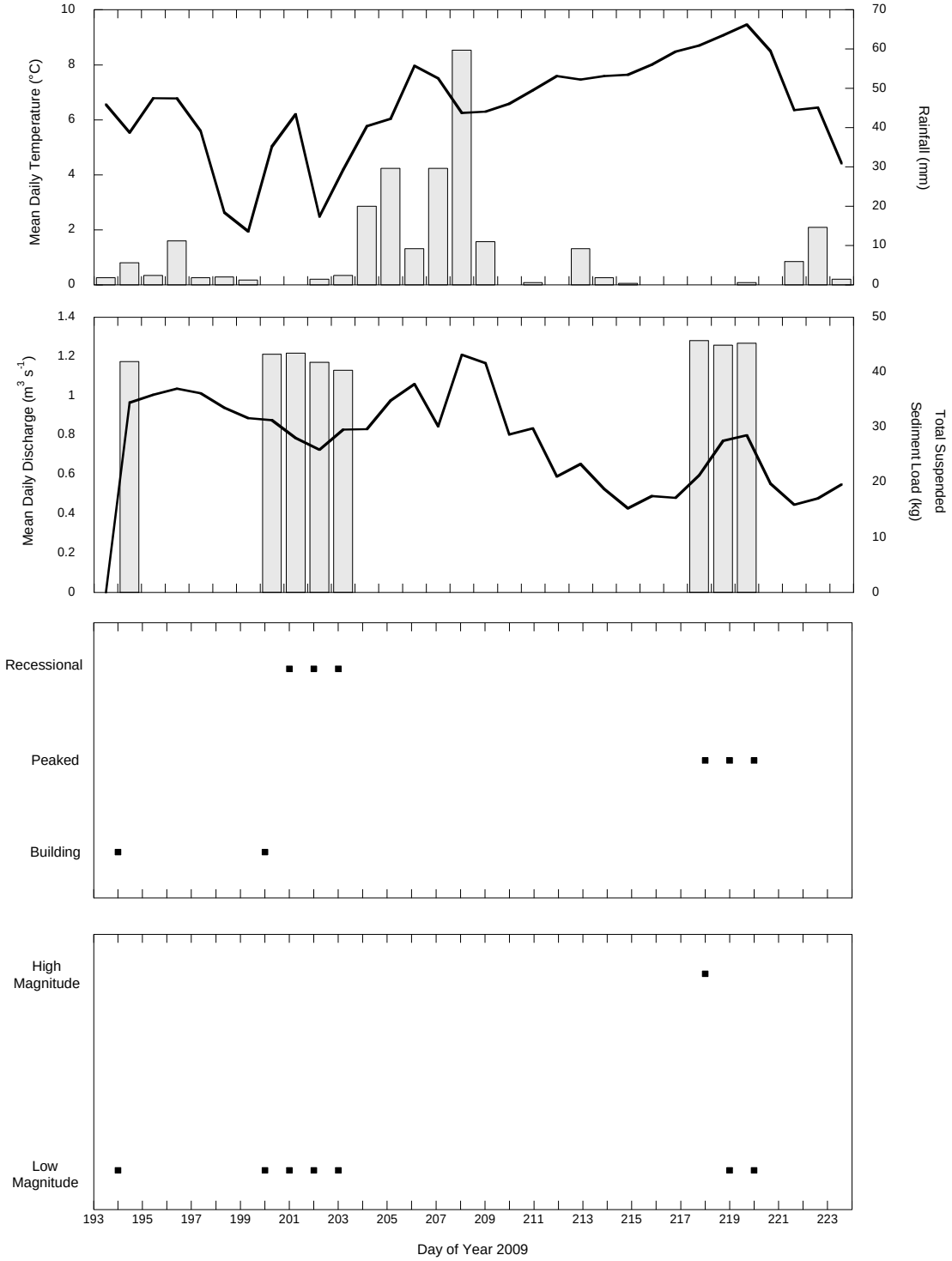


**Figure 5.3. Composite daily suspended sediment response shape and magnitude plot for the Sydjåkk gauging site during the 2009 ablation season. N.B. Gaps in the total daily suspended sediment load plot are the result of missing data and do not indicate an absence of suspended sediment transport.**

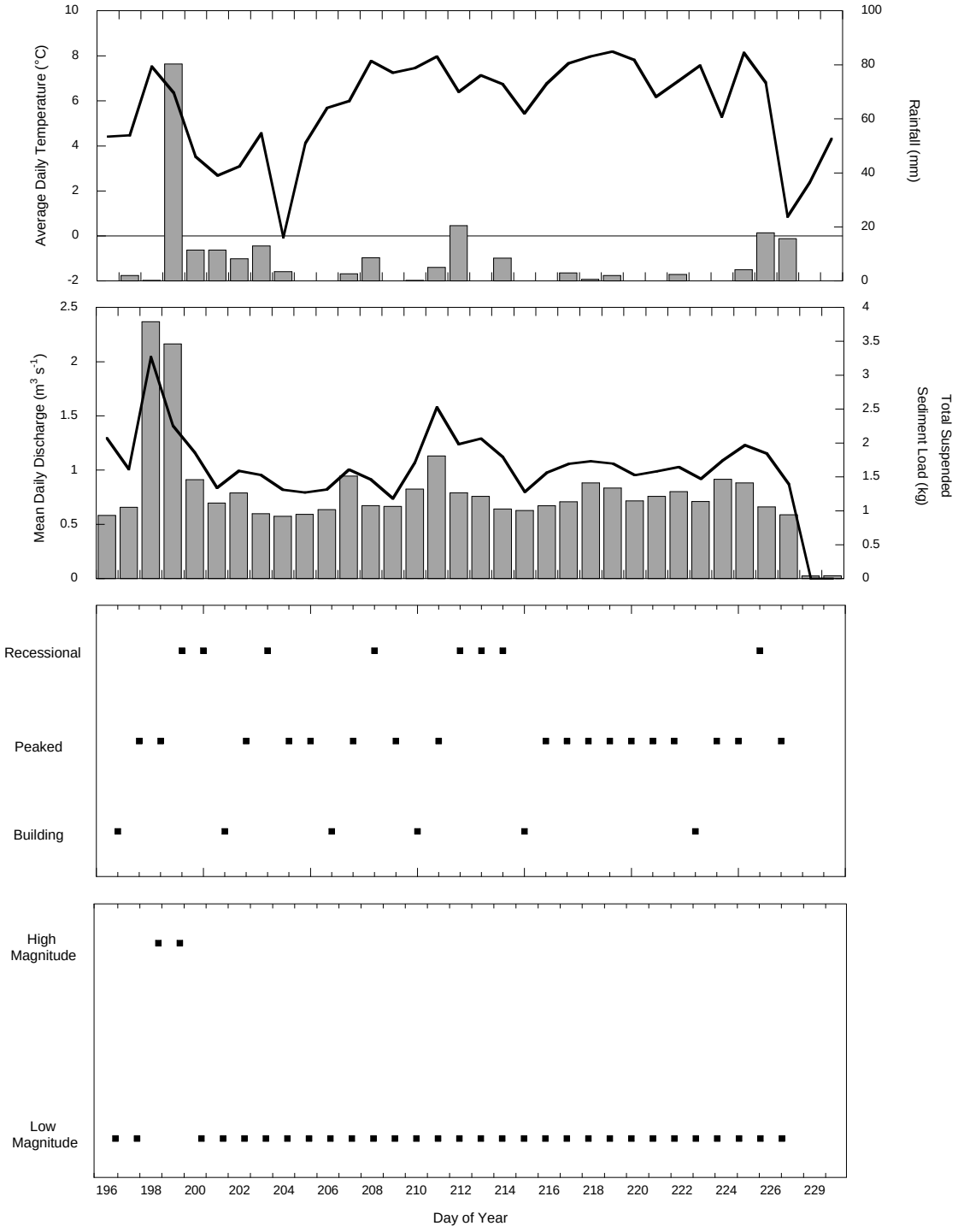


**Figure 5.4. Composite daily suspended sediment response shape and magnitude plot for the Nordjåkk gauging site during the 2010 ablation season.**

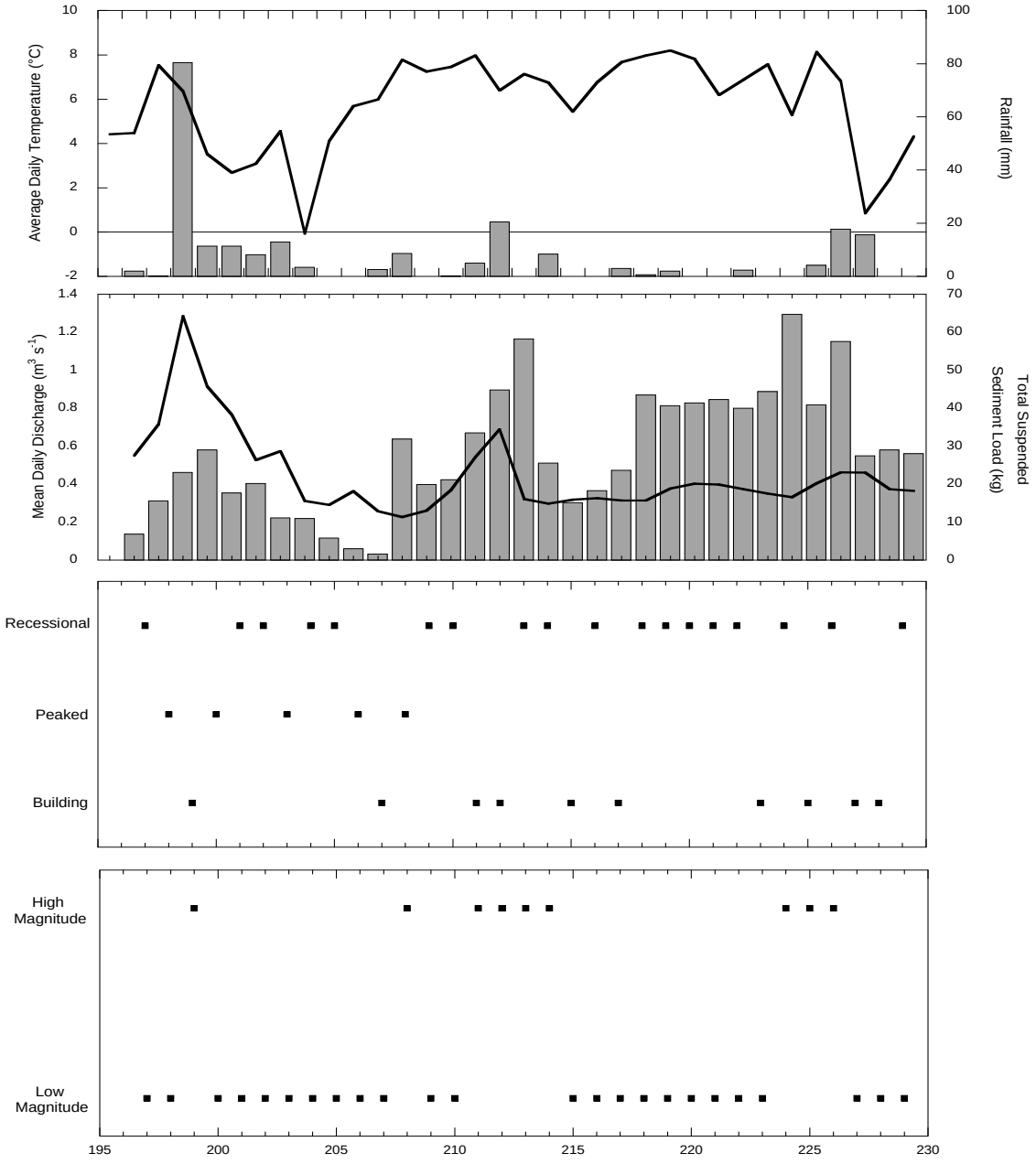


**Figure 5.5. Composite daily suspended sediment response shape and magnitude plot for the Sydjåkk gauging site during the 2010 ablation season.**

### 5.3.2. Description of Daily Suspended Sediment Magnitude

In both 2009 and 2010, principal component analysis of daily suspended sediment data retained two discrete components related to suspended sediment magnitude. These components were classified into 'high' and 'low' magnitude classes at both Nordjåkk and Sydjåkk gauging sites.

The greatest percentage of daily data at each site was classified as low magnitude. In 2009, 83.3% of days were classified as low magnitude compared with 16.7% classified as high magnitude. In 2010, 83.1% of the total measured days were classified as low magnitude, whilst 16.9% were classified as high magnitude. These data also reflect the difference between the relative suspended sediment load of both Nordjåkk and Sydjåkk. In 2009, Nordjåkk was responsible for the greatest percentage of high magnitude days (20%), whilst Sydjåkk was responsible for the greatest percentage of low magnitude days (87.5%). Comparatively, in 2010, Nordjåkk is responsible for the greatest percentage of low magnitude days (93.8%), whilst Sydjåkk is responsible for the greatest number of high magnitude days (27.3%). The greatest difference between Nordjåkk and Sydjåkk in terms of magnitude however, is the relative difference in suspended sediment data recorded in each class. In 2009, the mean suspended sediment concentration observed during low magnitude days at Nordjåkk ranges from 0.039 g $L^{-1}$ to 0.058 g $L^{-1}$. Conversely, the mean suspended sediment concentration observed during high magnitude days ranges from 0.064 g $L^{-1}$ to 0.090 g $L^{-1}$. At Sydjåkk, mean suspended sediment concentration at low magnitude ranges from 1.683 g $L^{-1}$ to 1.887 g $L^{-1}$. However in 2009, only one day was classified as high magnitude, with a mean suspended sediment concentration of 1.907 g $L^{-1}$. In 2010, the mean suspended sediment concentration observed during low magnitude days at Nordjåkk ranges from 0.038 g $L^{-1}$ to 0.075 g $L^{-1}$. Conversely, the mean suspended sediment concentration observed during high magnitude days ranges from 0.144 g $L^{-1}$ to 0.158 g $L^{-1}$. At Sydjåkk, mean suspended sediment concentration on low

magnitude days ranges from 0.068 g $L^{-1}$ to 1.850 g $L^{-1}$, whilst mean suspended sediment concentration at high magnitude ranges from 0.964 g $L^{-1}$ to 2.696 g $L^{-1}$.

### 5.3.3. Observed Associations between Daily Suspended Sediment Shape and Magnitude Response

Following the methods of Orwin and Smart (2004), suspended sediment shape and magnitude data for each gauging station were plotted alongside meteorological, discharge and suspended sediment concentration data (Figures 5.2 to 5.5). This enables events which produce distinctive suspended sediment shape and magnitude responses at each gauging site to be identified.

**2009**

Due to incomplete suspended sediment data from the 2009 ablation season (Figures 5.2 and 5.3), analysis of sediment response shape and magnitude is limited. However, the available data do allow recognition of patterns of association between variables.

At both gauging sites, high magnitude events appear to be predominantly associated with increased air temperature. Only days 204 and 205 of the Nordjåkk time series exhibit high magnitude response during notable periods of rainfall. During the 2009 ablation seasons, there appears to be a link between suspended sediment magnitude and response shape. Although only three high magnitude days occur across both streams during the season, two of these occur during 'peaked' sediment response days. The remaining high magnitude event (day 205, Nordjåkk) occurs during a 'recessional' suspended sediment response.

Therefore, it seems that suspended sediment response follows the general pattern of air temperature and stream discharge, with 'recessional' response following periods of 'peaked' response.

**2010**

At the Nordjåkk gauging site (Figure 5.4), high magnitude sediment response is exclusively associated with periods of high rainfall. The two high magnitude response days occur early in the season during a storm which produced ~ 80 mm of rain in 24 hours, and which resulted in the highest suspended sediment concentrations observed during the season. At the Sydjåkk gauging site however (Figure 5.5), high magnitude days appear to be associated with high air temperature, although as at Nordjåkk, Day 198 is associated with a high rainfall event. As a result, high magnitude sediment responses are more evenly spread through the whole of the ablation season, rather than during a short time period, as observed at Nordjåkk.

There is no obvious pattern of association between high magnitude sediment response, and changes in sediment response shape. At Nordjåkk, the two high magnitude days occur during and immediately following a period of high rainfall, and relatively high temperature. As a result, the sediment response shape is as expected, with Day 198 producing a peaked response, and Day 199 producing a recessional response as rainfall-associated runoff diminishes. The seven day period of sustained peaked response at Nordjåkk, coincides with a period of high air temperature, low rainfall, and slightly increasing suspended sediment concentration. In both seasons, sediment response shapes follow the general patterns of air temperature and stream discharge, peaked sediment response days are generally (although not exclusively) preceded by a building response shape, and followed by a recessional response shape.

### 5.3.4. Description of Daily Meteorological Components

Principal component analysis of daily meteorological indices retained four discrete components in 2009, and five discrete components in 2010 (as presented in Tables 5.3 and 5.4). The first four of these components were consistent at both gauging sites and were classified as:

- 'Warm' days. Days within this cluster typically exhibit maximum daily air temperature greater than 7°C. Days are mostly dry but may experience some limited rainfall.
- 'Cold' days. Days within this cluster display a minimum daily air temperature of less than 3°C. These days typically experience medium to high levels of rainfall.
- 'Wet' days. These days typically receive greater than 10 mm daily precipitation, although as little as 2 mm has been observed.
- 'Dry' days. These days typically receive less than 2 mm daily precipitation, in most cases experiencing no precipitation at all.

The remaining fifth component was observed only in 2010 and was classified as an extreme precipitation event. Only one day (day 199) was grouped into this class, during which 80.3 mm of rain was recorded. The distribution of each meteorological period during both ablation seasons is outlined in Tables 5.3 and 5.4, and Figures 5.6 and 5.7.

**Table 5.3. Summary statistics for meteorological periods identified using cluster analysis during the 2009 ablation season.**

| Meteorological Period | $T_{mean}$ (°C) | $T_{max}$ (°C) | $T_{min}$ (°C) | Mean Daily Precipitation (mm) | Cumulative Daily Solar Radiation (W $m^{-2}$) | Days | % of Total Days |
|---|---|---|---|---|---|---|---|
| Dry | 8.33 | 9.52 | 6.64 | 0.31 | 14947110.35 | 9 | 28.13 |
| Wet | 6.57 | 7.79 | 5.38 | 20.01 | 6735293.35 | 9 | 28.13 |
| Warm | 6.33 | 8.43 | 4.01 | 3.61 | 18309332.49 | 9 | 28.13 |
| Cold | 3.13 | 4.95 | 1.17 | 1.68 | 14116661.47 | 5 | 15.63 |

**Table 5.4 Summary statistics for meteorological periods identified using cluster analysis during the 2010 ablation season.**

| Meteorological Period | $T_{mean}$ (°C) | $T_{max}$ (°C) | $T_{min}$ (°C) | Mean Daily Precipitation (mm) | Cumulative Daily Solar Radiation (W $m^{-2}$) | Days | % of Total Days |
|---|---|---|---|---|---|---|---|
| Dry | 4.80 | 7.55 | 1.40 | 0.33 | 17308570.73 | 8 | 23.53 |
| Wet | 6.59 | 7.97 | 4.76 | 10.16 | 4509937.24 | 7 | 20.59 |
| Warm | 7.26 | 8.88 | 4.81 | 1.29 | 14991796.39 | 13 | 38.24 |
| Cold | 2.02 | 3.64 | 0.51 | 10.02 | 12356250.38 | 5 | 14.71 |
| Extreme Precipitation | 6.35 | 7.66 | 2.41 | 80.33 | 2704973.87 | 1 | 2.94 |

In both years, 'cold' days make up the smallest classes (excluding the extreme rainfall class) with 15.63% in 2009, and 14.71% in 2010 of the total days included. Conversely, in both years 'warm' days make up the largest classes, with 28.13% in 2009, and 38.24% in 2010 of the total days included. 'Dry' and 'wet' days contain similar numbers of days in both seasons. In 2010, 'dry' days explain slightly more of the total variance (23.53%) than 'wet' days (20.59%). However in 2009, 'warm, 'wet' and 'dry' days contain the same number of days, and hence each explain 28.13% each of the total population.

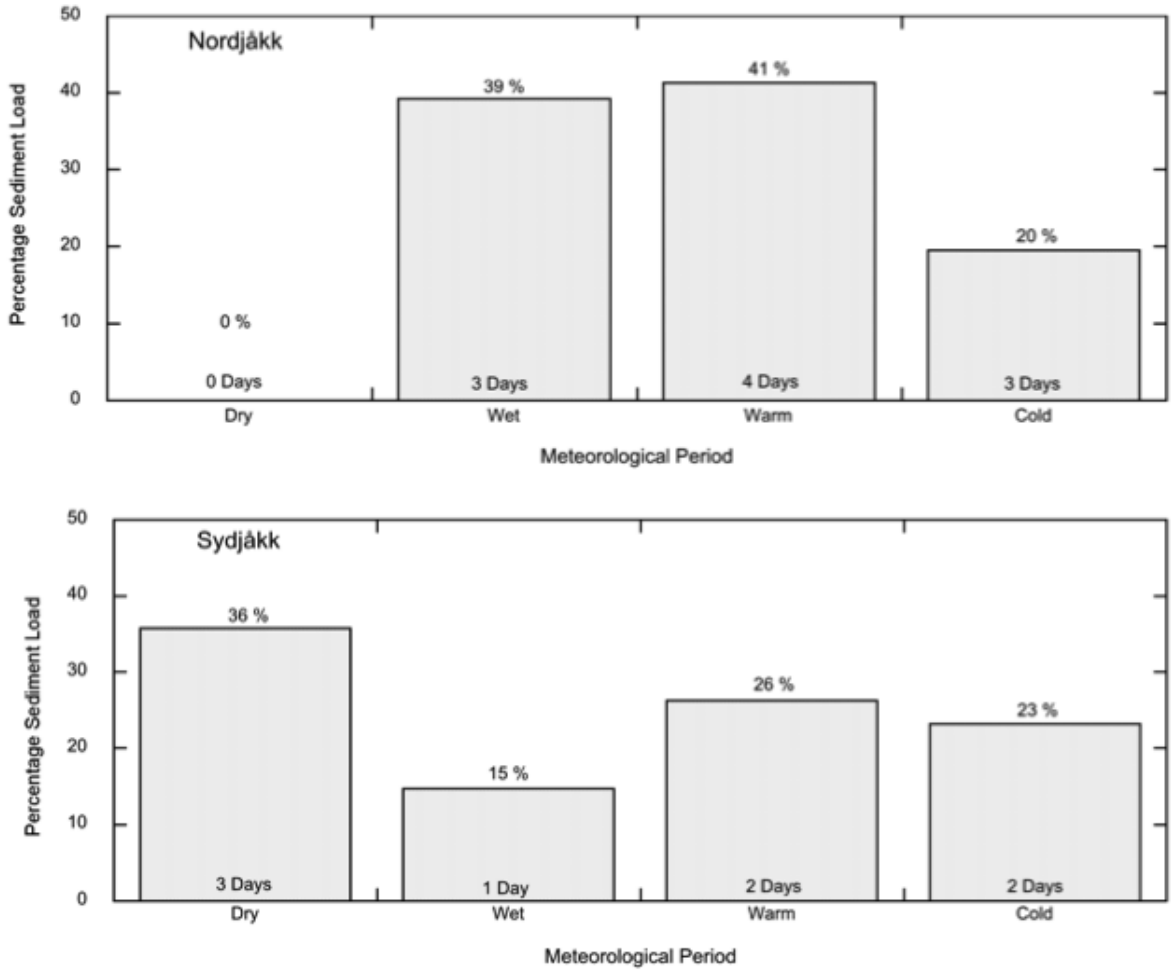


**Figure 5.6. Suspended sediment load patterns for each meteorological period during the 2009 ablation season.**

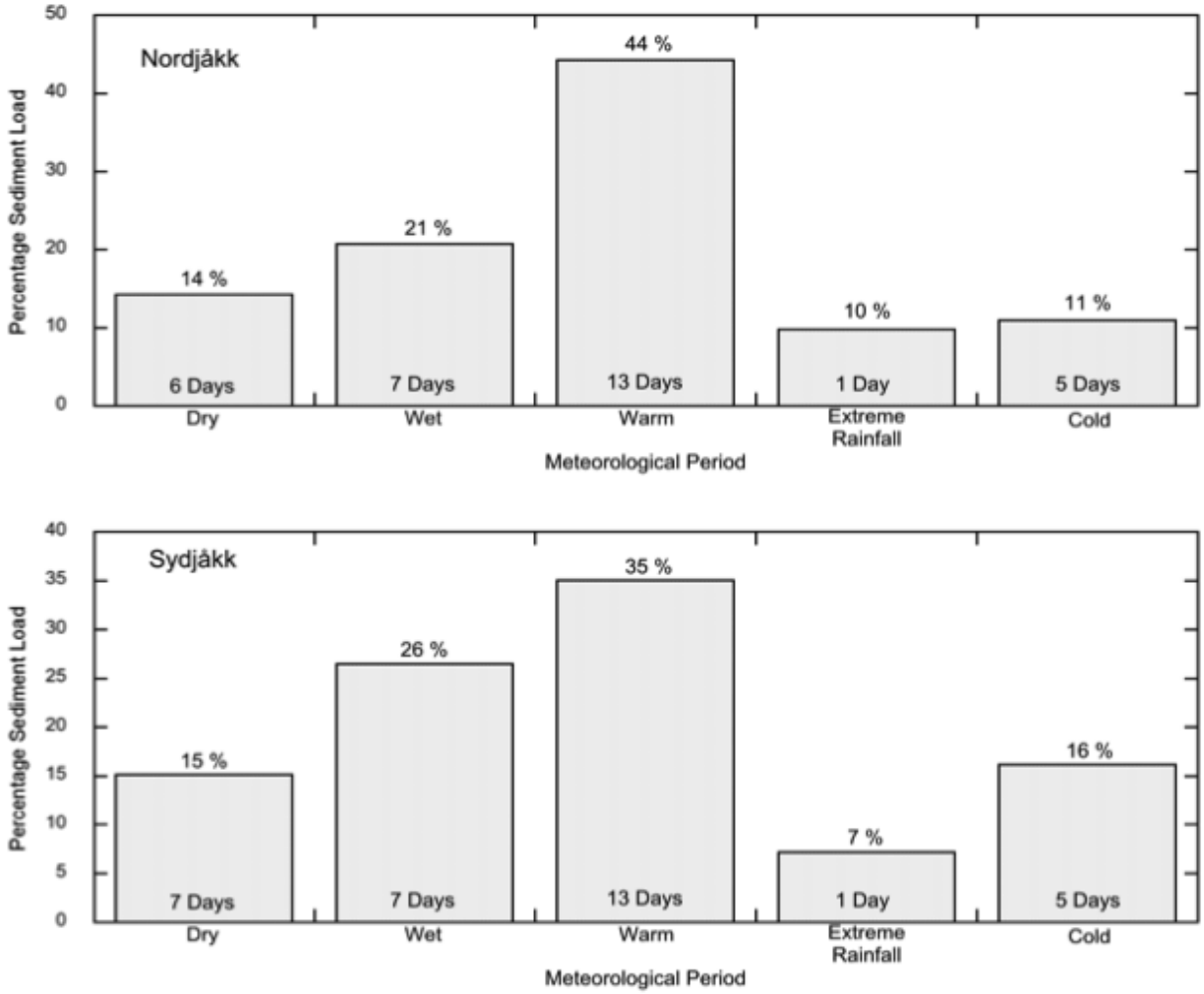


**Figure 5.7. Suspended sediment load patterns for each meteorological period during the 2010 ablation season.**

## 5.4. Discussion

As in Chapters 3 and 4 the interpretation and discussion below is based solely on the 2010 time series. Given the extensive missing data in the 2009 time series, it is difficult to assess the representativeness of the data in the context of a full glacier melt season and to make firm interpretations. However the data has been presented throughout the chapter for thoroughness and openness.

### 5.4.1. Composite Daily Suspended Sediment Shape and Magnitude Response

In order to assess patterns of suspended sediment transfer based on common response shapes, it is first necessary to interpret how each shape represents changes in the suspended sediment time series. 'Peaked' response shapes, exhibit a pronounced diurnal pattern, and are associated with periods of increased air temperature. It is suggested therefore, that 'peaked' suspended sediment shapes are indicative of sedimentary response to ablation-driven discharge. This is especially evident late in the 2010 ablation season at Nordjåkk, when a period of relatively stable discharge and high air temperatures is associated with seven consecutive days of 'peaked' response. 'Recessional' response shapes typically occur during periods of high suspended sediment variability, and during periods where suspended sediment concentration and discharge are independent of each other. This is supported by the high frequency of 'recessional' days towards the middle and end of the 2010 ablation season at Sydjåkk, when high suspended sediment variability is observed. Finally, 'building' response shapes frequently occur prior to increases in discharge, precipitation or air temperature. It is interpreted therefore, that they reflect changes in the nature of factors which drive sediment mobilisation, and therefore high suspended sediment concentrations. As a result, it is expected that 'building' response shapes precede suspended sediment peaks. This is the case at both Nordjåkk and Sydjåkk, where 'building' shapes are observed prior to or during high magnitude days.

The magnitude of suspended sediment transfer is dependent on meteorological variables, although these differ between the two streams. High magnitude suspended sediment transfer occurs in response to rainfall in Nordjåkk, and predominantly due to increased air temperature in Sydjåkk. It is inferred that this difference reflects the routing characteristics of both streams. Given that meltwater routed through Nordjåkk has little or no residence time at the glacier bed, ablation-controlled discharge is unlikely to substantially increase suspended sediment entrainment. However, it is possible that fine sediment flushed into Nordjåkk from the stream banks and from ice-marginal slopes increased the volume of suspended sediment in transport (Hodson *et al*., 1998; Orwin and Smart, 2004). The opposite is true of Sydjåkk, given the increased residence time of the stream at the glacier bed (Hock and Hooke, 1993). Ablation-driven discharge is able to entrain a greater volume of suspended sediment from within the subglacial drainage system, increasing suspended sediment transfer.

Similar results were observed by Orwin and Smart (2004) at Small River Glacier, suggesting that that high magnitude suspended sediment events occurred in response to different meteorological variables at different streams. However, Orwin and Smart (2004) also suggested that such events were associated with 'irregular' response shapes. Due to differences in the methodologies of this study and that of Orwin and Smart (2004), the classification of shape here does not distinguish between 'regular' and 'irregular' shapes. For the purposes of comparison however, it is assumed that 'regular' refers to a diurnal pattern resembling that of ablation-driven discharge. As described above, such patterns are represented in this study by 'peaked' suspended sediment response shapes which occur predominantly during periods of high air temperatures, suggesting ablation-dominated discharge. In this case, Sydjåkk appears to correspond with the results of Orwin and Smart (2004), with most high magnitude days associated with 'building' or 'recessional' days. It is therefore interpreted that suspended sediment transfer increases during non-'peaked' days, suggesting that ablation-driven discharge may be less influential in mobilising suspended sediment than precipitation during events of high magnitude.

### 5.4.2. Temporal Patterns of Suspended Sediment Shape Response

As discussed in the previous section (Section 5.4.1), events classified as high magnitude occur infrequently throughout the ablation seasons monitored during this study, and are typically driven by a change in either precipitation or air temperature. This can be identified based on changes in suspended sediment response shape. However, such changes can also be used to identify temporal changes in suspended sediment delivery during low magnitude suspended sediment concentrations.

During the 2010 ablation season, the occurrence of 'peaked' days increases later in the season at Nordjåkk, whilst 'recessional' days decrease. 'Recessional' days have been interpreted as suggesting variable suspended sediment delivery. It is therefore speculated that the number of 'recessional' days early in the season infer high suspended sediment availability. As a result, suspended sediment mobilisation responds quickly to changes in discharge or meteorological variables, resulting in rapid changes in suspended sediment concentration. It is also suggested that the increasing number of 'peaked' days later in the season, whilst suggesting a more ablation-driven pattern of discharge, infers a decrease in the availability of sediment. As a result suspended sediment concentration remains relatively stable during this period, requiring the increased erosive potential of a high magnitude event to increase suspended sediment concentrations.

The pattern of suspended sediment response shapes at Sydjåkk is less clear. 'Peaked' response occurs only early in the season, whilst 'recessional' response is frequent throughout. The high frequency of 'recessional' days suggests that suspended sediment transport is variable, and later in the season may occur as a result of ice-marginal sediment sources becoming more active. The lack of 'peaked' days may suggest that high variability in suspended sediment concentrations simply masks underlying patterns of ablation-driven discharge which result in 'peaked' response.

### 5.4.3. Meteorological Components: Implications for Suspended Sediment Transport

In order to assess the impact of changing meteorological conditions on suspended sediment transport, daily suspended sediment load data were classified into the relevant meteorological period as outlined in Section 5.3.4. Total suspended sediment load was determined for each period, and subsequently calculated as a percentage of the total seasonal sediment load. This allows the influence of each meteorological period on suspended sediment transport to be assessed throughout the ablation season, and at each gauging site.

During the 2010 ablation season (Figure 5.7), both Nordjåkk and Sydjåkk show similar patterns of suspended sediment response during meteorological component periods. In both streams 'warm' days account for the greatest percentage of total suspended sediment load transported (Nordjåkk, 44%; Sydjåkk, 35%). 'Warm' days account for the largest meteorological component (13 days), suggesting that suspended sediment transport increases during periods of increased ablation. As a result, suspended sediment in transport during this period is likely to be entrained by high, ablation-driven discharge. Conversely, reduced sediment transport during 'cold' days (Nordjåkk, 11%; Sydjåkk, 16%) indicates reduced ablation driven discharge due to colder air temperatures and hence, reduced suspended sediment entrainment. At both gauging sites, 'cold' and 'dry' days exhibit a similar percentage of suspended sediment load transported. Although 'dry' days are considerably warmer and dryer than 'cold' days, it is possible that these days still do not experience favourable conditions for significant ablation to occur. At both stream sites, 'wet' days account for the second greatest percentage of the total suspended sediment load moved (Nordjåkk, 21%; Sydjåkk, 26%), although this is still substantially less than that of 'warm' days. That this component accounts for over 20% of the total transferred suspended sediment load at both gauging sites reflects the dominance of precipitation (specifically rainfall) on discharge patterns, and hence, sediment entrainment. The significance of rainfall on suspended sediment transport can be further observed in the percentage of sediment load

moved during the 'extreme rainfall' period. In spite of only one day of the season being classified into this component, extreme rainfall accounted for the transport of 10% and 7% respectively of the total seasonal suspended sediment load of Nordjåkk and Sydjåkk. As suggested by Willis *et al*. (1996), it may be possible that the short distance from the glacier terminus to the gauging stations in this study (~20 m) has reduced the influence of rainfall on suspended sediment transfer. Periods of rainfall can result in the mobilisation of ice-marginal sediment which is able to enter the fluvial system (Hodson *et al*., 1998) and also facilitate release of suspended sediment from in-channel sources as a result of increased discharge. Reduction of the distance over which such processes can occur will substantially limit the volume of sediment entrained through rainfall events, and therefore, limit the role of rainfall as a geomorphic agent. Jansson *et al*. (2005) suggest that the influence of precipitation of sediment transport in the Tarfala valley is ambiguous, with highly variable patterns observed over two seasons. Whilst this may be a result of interannual variability, both seasons monitored in this study both suggest that precipitation ('wet' days) act as an important geomorphic agent, entraining over 45% of the total suspended sediment load mobilised in each ablation season.

## 5.5. Summary

Based on the interpretations discussed in Section 5.4, the following conclusions can be drawn regarding patterns of suspended sediment delivery at Storglaciären:

- Suspended sediment response shapes differ between both Nordjåkk and Sydjåkk. Response shapes at Nordjåkk are typically 'peaked' reflecting sediment mobilisation as a result of ablation-driven discharge. Conversely, response shapes at Sydjåkk are typically recessional, suggesting high variability in suspended sediment delivery, and disconnection with the discharge time series. This itself suggests that precipitation or ice-marginal processes may be more influential geomorphic agents than ablation-driven discharge.

- Suspended sediment magnitude also varies between the two streams. At Nordjåkk, high magnitude suspended sediment events are instigated by rainfall, whereas at Sydjåkk, they are caused by air temperature. It is suggested that this reflects the hydrological routing of each stream, with ablation-driven discharge able to entrain greater volumes of suspended sediment in the more subglacially routed Sydjåkk during high magnitude events.

- 'Warm' and 'wet' days appear to be responsible for the greatest volumes of suspended sediment entrained. In 2010 'warm' days are dominant at both streams, although 'wet' days appear to hold more influence at Sydjåkk than Nordjåkk, reflecting the first point above.

*Chapter 6*

# Modelling of Meltwater Routing and Suspended Sediment Transfer

## 6.1. Introduction

Glaciers provide complex and challenging settings in which to undertake instrumented monitoring of glacier hydrology. The inaccessibility of sub- and englacial environments complicate data collection, with access generally only possible via boreholes (e.g. Hubbard *et al*., 1995; Gordon *et al*., 1998; Rose *et al*., 2009), or rarely, through speleological exploration of glacial cavities (e.g. Holmlund, 1988b; Gulley and Benn, 2007; Gulley *et al*., 2009). As a result, analyses of hydrological outputs are often used to infer details of the glacial drainage system in place of direct observations (Hodgkins *et al*., 2013). These data can be used to inform models which provide a conceptualised representation of the glacial drainage system (such as linear reservoir models), allowing drainage pathways to be assessed further in the context of water routing and seasonal drainage system evolution.

As well as modelling glacier hydrology, predicting suspended sediment transfer in glacial basins has become an important tool in the management and use of meltwater (e.g. Østrem, 1975; Bezinge *et al*., 1987; Bogen, 1989), and in studies of fluvial and glacial processes (e.g. Gurnell *et al*., 1992a; Clifford *et al*., 1995; Hodgkins, 1996; Willis *et al*., 1996; Hodson and Ferguson, 1999; Swift *et al*, 2002; 2005). This is typically performed using statistical (e.g. Gurnell and Fenn, 1984; Hodgkins, 1999) or physical models (e.g. Clarke, 1996a; Jones and Arnold, 1999; Fausto *et al*., 2012). Physical models are less developed than statistical models (Hodgkins, 2011) and therefore it is imperative that such

techniques are advanced, allowing more accurate and effective predictions to be undertaken.

### 6.1.1. Aims of the Chapter

This chapter aims to elucidate patterns of water routing through Storglaciären using a combination of flow-recession analysis and linear-reservoir modelling. This will be complemented by a suspended sediment transfer model, which will enable suspended sediment concentration to be predicted in response to changing hydrological and physical processes.

There are three specific objectives:

- To evaluate the nature of the drainage system of Storglaciären using flow recession analysis and linear reservoir modelling.

- To identify episodes of drainage system evolution which represent a rationalisation of glacial drainage.

- To assess the applicability of a physically-based sediment transfer model in predicting suspended sediment delivery in the Storglaciären basin.

## 6.2. Methods

### 6.2.1. Linear Reservoir Modelling

Glacierized areas exhibit markedly different runoff responses to non-glacierized areas as a consequence of the storage and release of water within the glacier (Jansson *et al*., 2003). As a result, it is important that glacier hydrological models give consideration to the routing and delaying of meltwater and precipitation through the glacier system (Jansson *et al*., 2003). Glacier linear-reservoir models achieve this by assuming that the glacier system is represented by two (or more) principal hydrological reservoirs (flow pathways) whose storage is linearly related to the rate of outflow (Chow *et al*., 1998). Linear reservoir models are therefore conceptual (rather than physical), in that physical components and interactions within the glacier are not explicitly represented. Instead, processes within the drainage system, reservoir state and reservoir outflow are intrinsically linked to retain the most important characteristics of the major drainage pathways. For example, in a glacier undergoing rapid melt with fast reservoir flow and high magnitude outflow, the cascade from melt to runoff is entirely integrated (Hodgkins *et al*., 2013).

Linear-reservoir models usually include a fast reservoir accommodating high flows, and a slow reservoir accommodating low flows (Hodgkins *et al*., 2013). From a glaciological perspective, the fast reservoir would typically represent meltwater drained through an efficient, channelised system; whilst the slow reservoir would typically represent meltwater drained through an inefficient, distributed system (Raymond *et al*., 1995; Fountain and Walder, 1998; Hodgkins *et al*., 2013). Reservoirs can be coupled in series, whereby one reservoir provides the inflow for another (e.g. Van de Wal and Russell, 1994), or in parallel, whereby the outflow of each reservoir at each time step yields the total glacier discharge (e.g. Baker *et al*. 1982). The number of reservoirs used in a model can vary depending on the purpose of the modelling exercise.

For example, Moore (1993) used a single reservoir to model streamflow in the Lillooet River drainage basin, British Columbia, changing the values of the reservoir coefficients on a daily basis to account for the seasonal evolution of the glacial drainage system. Comparatively, Hock and Noetzli (1997) used three reservoirs to model discharge at Storglaciären, each accounting for flow through a different glacier surface media: snow, ice and firn.

The linear-reservoir approach is based on relating stored water volume, $V$, to the rate of outflow, $Q$ (Chow *et al*., 1998; Hodgkins *et al*., 2013). This can be represented through the equation:

$$V_t = KQ_t \qquad (6.1)$$

where $t$ is the model time step, and $K$ is a storage constant. As suggested by Hodgkins *et al*. (2013), the term 'reservoir coefficient' is preferred to storage constant as it more clearly describes the role of $K$ in the model, and as a result, will be used for the remainder of this thesis. A diagrammatic representation of Equation 6.1. and its application to glacier melt water routing is given in Figure 6.1.

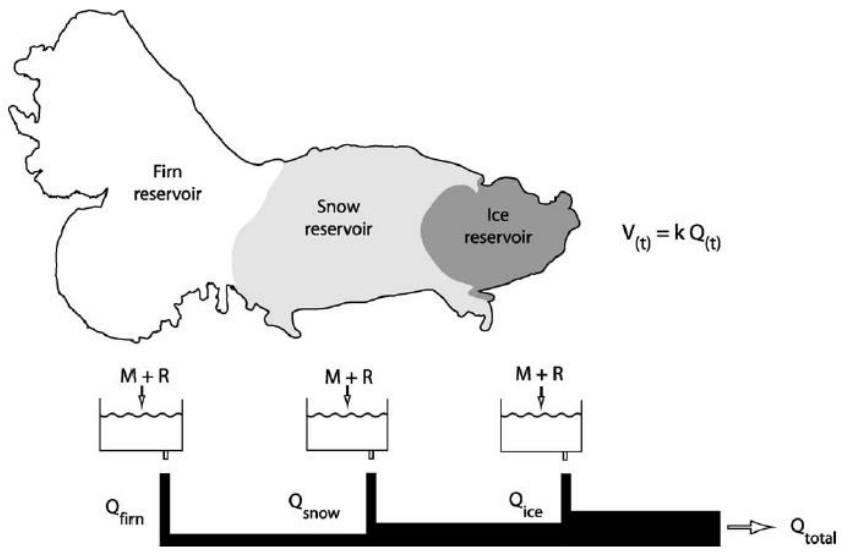


**Figure 6.1 Concept of three parallel linear reservoirs as applied to Storglaciären (Hock and Noetzli, 1997). The reservoirs are supplied by melt, *M*; and rain water, *R*: Outflow, *Q*; is proportional to reservoir volumes, *V*. (After Jansson *et al*., 2003).**

The continuity equation is therefore:

$$\frac{dQ}{dt} = I_t - Q_t \qquad (6.2)$$

where $I$ is the rate of inflow into the drainage system. The equation therefore indicates that the rate of change of water storage is equal to the difference between the rates of inflow and outflow. Water storage occurs when inflow exceeds outflow (Hodgkins *et al.*, 2013). Combining equations 1 and 2 gives:

$$K\frac{dQ}{dt} = I_t - Q_t \qquad (6.3)$$

which rewrites storage in terms of outflow and the reservoir coefficient. When integrated, this gives expressions for recession flow and recharge flow. In order to ascertain how much of a delay each reservoir imposes on the inflow, a reservoir coefficient is specified for each reservoir. The combined effect of the number of reservoirs and their coefficients defines the temporal pattern of outflow, expressed in the form of the hydrograph (Hodgkins *et al.*, 2013). Reservoir coefficients may be obtained either by tuning (i.e. maximising the agreement between modelled and measured glacier outflow) (Hock and Noetzli (1997; Klok *et al.*, 2001), or by flow recession analysis (e.g. Gurnell, 1993; Hannah and Gurnell, 2001). Although both methods have merits and limitations, recession analysis is advantageous in that it is isolated from the modelling procedure and that therefore estimates of reservoir coefficients are independently derived (Hodgkins *et al.*, 2013). This study combines the two techniques with reservoir coefficients derived in the first instance using flow recession analysis, and subsequently tuned using the Microsoft Excel™ function 'Solver' in order to maximise the fit of the modelled discharge to observed values. Flow recession analysis is discussed in greater detail in Section 6.2.2.

Having defined the reservoir coefficient, recession flow from the reservoir can be calculated using Equation 6.4.

$$Q_t = Q_0 exp \frac{-(t-t_0)}{\mathrm{K}} \quad (6.4)$$

where $t_0$ is the time step preceding time $t$, and $Q_0$ is the discharge preceding $Q_t$. This represents the output of the glacier if all hydrological inputs ceased (melting and otherwise). Ongoing inputs into the glacier and the total glacier output can be calculated by the addition of a recharge flow. This can be defined as:

$$Q_t = I_t[1 - exp] \frac{-(t-t_0)}{\mathrm{K}} \quad (6.5)$$

This equation has the same exponent as the reservoir flow (Equation 6.4), but depends on inflow at the current time step, rather than outflow at the previous time step (Hodgkins *et al*., 2013). The final linear-reservoir model of glacier drainage can be obtained by combining Equations 6.4 and 6.6, representing the reservoir flow plus the recharge flow for a single reservoir:

$$Q_t = Q_0 exp \frac{-(t-t_0)}{\mathrm{K}} + I_t[1 - exp] \frac{-(t-t_0)}{\mathrm{K}} \quad (6.6)$$

As discussed in Section 6.2.1. glacier linear-reservoir models typically employ two or more reservoirs, as is the case in this study.

During the study, this was completed using discharge data recorded at both the Nordjåkk and Sydjåkk gauging sites during the 2010 melt season. Discharge from each stream was simulated with two parallel reservoirs, and therefore the steps described above are undertaken twice in order to calculate the recession and recharge flow for both reservoirs. Due to the frequent missing data gaps in data collected in the 2009 melt season (as discussed in earlier chapters) these data were considered too fragmented to analyse and were therefore disregarded in this chapter.

### 6.2.2. Flow Recession Analysis

As discussed in Section 6.2.1, flow recession analysis was used to calculate linear reservoir coefficients (*K*). The reservoir coefficient essentially describes the delay imposed on the outflow by each reservoir, and the combined effect of these values and the number of reservoirs defines the temporal pattern of outflow (Hodgkins *et al.*, 2013). By isolating and analysing recession curves of the glacier hydrograph (as exemplified in Figure 6.2) the residence time of water within the glacial system can be estimated (Gurnell, 1993). Although comparison of reservoir coefficients is difficult, especially in glaciers with differing thermal regimes, a range of published reservoir coefficients is displayed in Table 6.1.

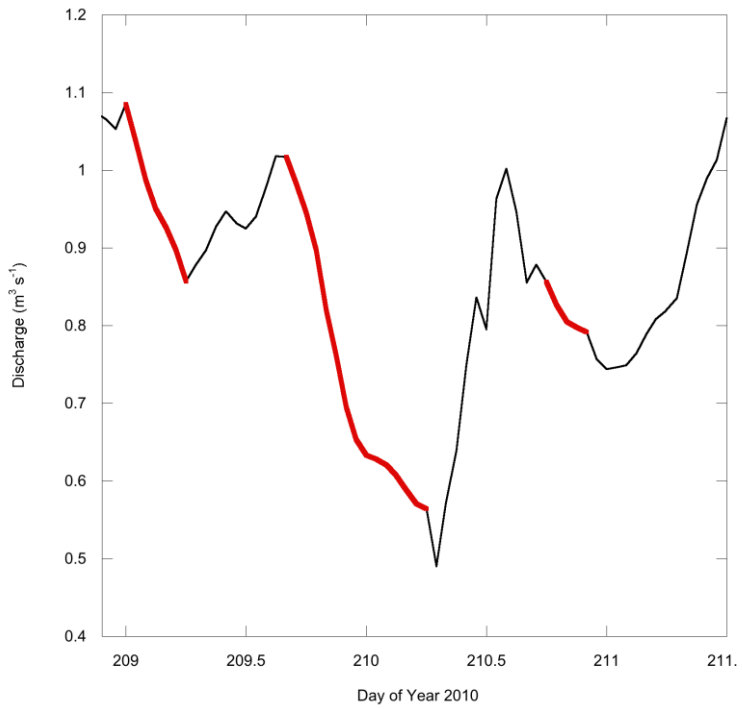


**Figure 6.2 Three example flow recessions from discharge data recorded at Nordjakk during the 2010 melt season. Linear regression statistics (slope/intercept/$r^2$) where Day of Year is the independent variable and *lnQ* is the dependent variable for each recession are: (Day 209) Reservoir 1: -1.07/224.71/0.99; Reservoir 2: -0.93/195.14/0.98. (Day 210) Reservoir 1: -1.59/334.29/0.98; Reservoir 2: -0.51/106.38/0.97. (Day 211) Reservoir 1: -0.74/155.2/0.99 Reservoir 2: -0.62/129.55/0.93.**

Once flow recessions have been identified, analysis is performed on the assumption that each period of recessional flow represents the outflow from a linear reservoir. As discussed in Section 6.2.1, if there is no recharge flow into the reservoir (i.e. new inflow), then the discharge at a given time ($Q_t$) can be expressed as a function of the proceeding recession flow ($Q_0$).

$$Q_t = Q_0 exp \frac{-(t-t_0)}{\mathrm{K}} \tag{6.4}$$

Equation 6.4 also implies that during periods of recession flow, the value of $K$ can be estimated from the slope of a semilogarithmic plot of discharge over time (Gurnell, 1993). Recessions generated by outflow from a linear reservoir will plot as a straight line. Breaks of slope can be recognized as the presence of more than one linear component (Gurnell, 1993; Hodgkins *et al.*, 2013). The point in the recession where the break of slope occurs therefore represents the break in recession between a number of different reservoirs with different reservoir coefficients (as shown in Figure 6.3).

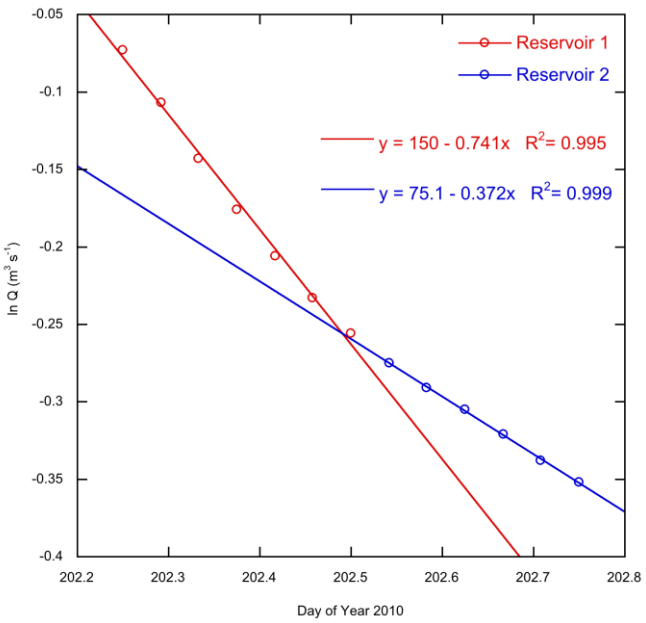


**Figure 6.3 Example of a period of flow recession separated into two reservoirs. Circles represent the hourly natural logarithm (*ln*) discharge; lines represent the linear regression of each reservoir. Reservoir 1 (fast) is represented in red; Reservoir 2 (slow) is represented in blue.**

The *K* value of a reservoir can be calculated using the equation:

$$K = \frac{-(t-t_0)}{\ln(Q_t - Q_0)} \quad (6.7)$$

*K* values estimated in this way represent aggregates of all the reservoirs contributing to the plotted recession. In order for reservoir specific *K* values to be estimated, the recessions from each reservoir require separation (Gurnell, 1993). Separation is straightforward if the linear reservoirs occur in parallel (i.e. both contribute directly to the total glacier outflow) as a linear extension of the slower reservoir can be used to separate the faster reservoir (as exemplified in Figure 6.3). As the two outlet streams at Storglaciären, Nordjåkk and Sydjåkk both emerge at the glacier terminus and deliver the bulk of the glacier discharge, a parallel configuration of reservoirs at Storglaciären appears to be applicable. Reservoir coefficients vary considerably between glaciers and, as such, it is difficult to undertake comparisons, especially in glaciers with differing thermal regimes. A range of published reservoir coefficients is displayed in Table 6.1.

During the analysis, every flow recession of four hours in duration or greater was examined. Given the hourly resolution of the times series, shorter periods were considered too brief from which to draw valid inferences due to the fact that regressions would have been estimated based on only two or three data points (Hodgkins *et al*., 2013). As reservoir coefficients were only determined for periods of flow recession, a continuous hourly time series was required to enhance the model setup. This was accomplished by interpolating a continuous series using the 'Interpolate' function of Synergy Software's Kaleidagraph™ v. 4.1.3 (Synergy Software, 2010). As Hodgkins *et al*. (2013) note, this technique is only an estimate, although the interpolation is constrained by known reservoir coefficients derived from flow-recession analysis.

**Table 6.1 Storage constants used in various glacier melt-runoff modelling studies employing the concept of parallel linear-reservoirs for water routing through the glacier. In order to aid comparison between studies, storage constants, *K*, are labelled in ascending order, rather than as defined by the original authors. Therefore, $K_1$ represents the fastest reservoir, $K_2$ the next fastest, and so on. All storage constants are given in hours. Adapted from Hock and Jansson (2005) and Hannah *et al*. 2001. *As cited in Oerter *et al*. (1981). ‡Mean K values over a 30 year period. †Area given is the total glacierized area. [a]Data from the 1999 melt season. [b]Data from the 2000 melt season**

| Site (basin size, glacierization %) | $K_1$ (h) | $K_2$ (h) | $K_3$ (h) | $K_4$ (h) | Source | Reference |
|---|---|---|---|---|---|---|
| Vernagtferner (11.4 km$^2$, 81%) | 4.5 | 28.75 | 244 | - | - | Hibsch (1979)* |
| Vernagtferner (11.4 km$^2$, 81%) | 4 | 30 | 430 | ∞ | Recession Analysis | Oerter *et al*. (1981) |
| Vernagtferner (11.1 km$^2$, 81%) | 4 | 30 | 430 | - | Recession Analysis | Baker *et al*. (1982) |
| Gornergletscher (82 km$^2$, 84%) | 11.5 | - | - | - | Recession Analysis | Collins (1982) |
| Haut Glacier d'Arolla (6.7 km$^2$, 54%) | 3 | 8 | 24 | - | Recession Analysis | Gurnell (1993) |
| Storglaciären (4.4 km$^2$, 70%) | 16 | 30 | 350 | - | Tuning | Hock & Noetzli (1997) |
| Vernagtferner (11.1 km$^2$, 81%) | 6 | 40-80 | 430 | - | Tuning | Escher-Vetter (2000) |
| Taillon Glacier (0.22 km$^2$, 61%) | 13 | 45 | - | - | Recession Analysis | Hannah *et al*. (2001) |
| Rhonegletscher (39 km$^2$, 48%) | 45 | 120 | 350 | - | Tuning | Klok *et al*. (2001) |
| Kesselwandferner (98 km$^2$, 48%)‡ | 0.71 | 12.8 | - | - | Tuning | Span & Kuhn (2003) |
| Rieperbreen/Foxfonna (4.05 km$^2$)† | 63 | 193 | 331 | - | Recession Analysis | Rutter *et al*. (2011) |
| Finsterwalderbreen (44 km$^2$, 80%)[a] | 16 | 41 | - | - | Recession Analysis | Hodgkins *et al*. (2013) |
| Finsterwalderbreen (44 km$^2$, 80%)[b] | 54 | 114 | - | - | Recession Analysis | Hodgkins *et al*. (2013) |

### 6.2.3. Implied Linear Reservoir Model Input

Having defined the characteristics of each reservoir within a linear reservoir model, an initial value of runoff and an input series are required in order to complete the simulation of runoff (Hodgkins *et al*., 2013). This input series should comprise the total surface melt of the glacier, plus any other hydrological inputs (e.g. rainfall). Meteorological data collected at the Tarfala research station (approximately 1 km north of Storglaciären) by Stockholm University have been used in other areas of this study to provide an overview of the prevailing meteorological conditions. However, as these data are not collected on the glacier itself, any melt modelling undertaken would suffer from high levels of uncertainty. Therefore, a best estimate of the input series is used, referred to as implied input (Hodgkins *et al*., 2013), in order to complete the model setup.

Implied input consists of glacier melt plus rainfall, but also reflects any changes in meltwater storage that may have taken place, particularly the release of snowmelt stored earlier in the summer (Jansson *et al*., 2003; Hodgkins *et al*., 2013). Unlike other studies which employ linear reservoir modelling (e.g. Hock and Noetzli, 1997), distributions of snow, ice and firn are unavailable as detailed measurements of the glacier snow line were not collected. Therefore, following the methodology of Hodgkins *et al*. (2013), this study uses a lumped approach, evaluating the effects of reservoir characteristics, rather than the characteristics of different media.

To calculate implied input, the reservoir coefficients from each flow recession and the flow fraction to each reservoir are used. Flow fraction is established by assessing the proportional contribution of the flow decrease in each reservoir to the total flow decrease observed during the flow recession, and is therefore determined with a simple percentage calculation. However, as flow fractions are only determined for periods of flow recession, a continuous hourly time series is synthesised using interpolation. This was accomplished using the 'Interpolate' function of Synergy Software's Kaleidagraph™ v. 4.1.3 (Synergy

Software, 2010). As Hodgkins *et al*. (2013) note, this technique is only an estimate, although the interpolation is constrained by known fractions derived from flow-recession analysis. The flow fractions (*f*) used during modelling at Both Nordjåkk and Sydjåkk are shown in Figures 6.4 and 6.5.

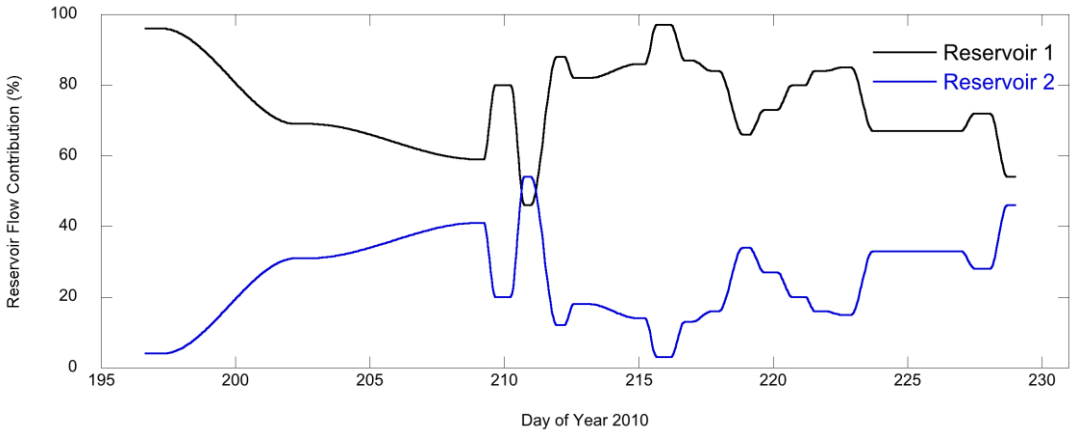


**Figure 6.4. Plot showing the percentage contribution of flow to each reservoir at Nordjåkk.**

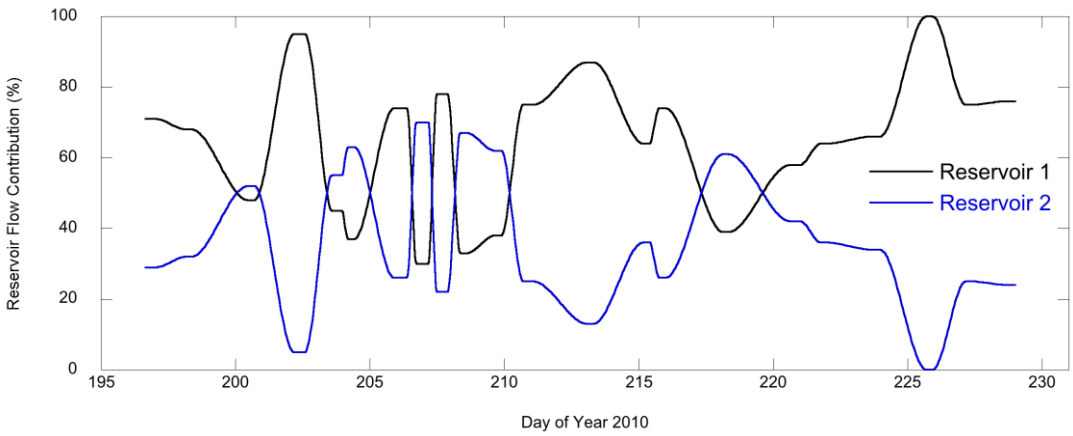


**Figure 6.5. Plot showing the percentage contribution of flow to each reservoir at Sydjåkk..**

The full equation for the calculation of implied input is presented in Equation 6.8. This assumes that two parallel reservoirs are present, although modification can be made to allow for more reservoirs if required.

$$Q_t = fQ_0 exp\frac{-(t-t_0)}{\mathrm{K}_1} + fI_t\left\{[1-exp]\frac{-(t-t_0)}{K_1}\right\}$$
$$+(1-f)Q_0 exp\frac{-(t-t_0)}{\mathrm{K}_2} + (1-f)I_t\left\{[1-exp]\frac{-(t-t_0)}{K_2}\right\} \quad (6.8)$$

### 6.2.4. Linear Reservoir Model Performance

Performance of the linear reservoir model was assessed in three ways. Firstly, Mean Error (ME) assesses the overall tendency of the modelled runoff (Q*) to overestimate or underestimate observed runoff (Q), and can be calculated using the equation:

$$ME = \frac{\Sigma(Q-Q^*)}{df} \quad (6.9)$$

where *df* is degrees of freedom, determined by *N-P-1*, where *N* is the number within the sample, and P is the number of predictors. A positive ME value suggests a model overestimation, whereas a negative ME value suggests a model underestimation. Root Mean Square Error (RMSE) provides the standardized, mean error of modelled runoff:

$$RMSE = \sqrt{\frac{\Sigma(Q-Q^*)^2}{df}} \quad (6.10)$$

The Nash-Sutcliffe efficiency criterion, E, provides an assessment of the goodness-of-fit of the modelled to the observed time series:

$$E = 1 - \frac{\Sigma(Q-Q^*)^2}{\Sigma(Q-\bar{Q})^2} \quad (6.11)$$

where the range of E lies between 1.0 (a perfect fit), and -∞. An efficiency of less than zero indicates that the mean value of the observed time series would act as a better predictor than the modelled time series itself (Krause *et al*., 2005; Hodgkins *et al*., 2013).

### 6.2.5. Linear Reservoir Model Sensitivity

The responsiveness of the model to changing input variables was evaluated through a sensitivity analysis of the modelled time series. In these tests, $K_1$, $K_2$ and $f$ values were altered, while the remaining parameters were held equal to their nominal values. Reservoir coefficients were varied to reflect the range of $K$ values produced using flow recession analysis (Hodgkins *et al*., 2013). Therefore, at Nordjåkk, $K_1$ values ranged from 5 to 110 h, and $K_2$ values ranged from 1 to 260 h. At Sydjåkk, $K_1$ values ranged from 5 to 80 h, and $K_2$ values ranged from 2 to 200 h.

For $f$ values (i.e. the fraction of flow contributed by each reservoir), two different scenarios were tested: one where 100% of the total flow was contributed by Reservoir 1 (i.e. a single reservoir), and one where the contribution of flow was divided equally between two reservoirs.

In both $K$ and $f$ scenarios, the relative change in total modelled discharge and Root Mean Square Error act as an indicator of model sensitivity in response to changing parameters.

### 6.2.6. Suspended Sediment Transport Model

In order to model suspended sediment concentration at Storglaciären, a lumped-element model developed by Clarke (1996a) is used. This model treats the glacial drainage system as a series of idealized hydraulic circuit elements (Clarke, 1996b) which describe discharge and suspended sediment pathways through a glacier. The setup of the model is similar to that used by Clarke (1996a) and Fausto *et al*. (2012), although smaller in scope as only one

subglacial conduit is used, rather than a cascade of meltwater pathways from glacier surface to proglacial stream. It is assumed therefore, that the uptake and deposition of suspended sediment occurs beneath the glacier terminus in a channel with identical dimensions to those recorded in the proglacial area at Nordjåkk and Sydjåkk. All model values were calculated using an hourly time step.

For the purpose of constructing the model, suspended sediment is assumed to come from an inexhaustible source. Furthermore, it is assumed that the sediment source consists of permeable sediment with porosity $n$, and density $\rho_s$. The mass flux of sediment into fluid suspension ($F_e$) is calculated using the equation:

$$F_e = \rho_s(1-n)k_E(\tau_0 - \tau^*)^N \qquad (6.12)$$

where $k_E$ is the erosion rate constant, $\tau^*$ is the threshold stress for bed erosion which must be exceeded for erosion to commence, $\tau_0$ is the shear stress exerted by the flow onto the conduit walls and bed, and $N$ is an exponent of erosion law. The erosion rate constant, $k_E$, is based on Allen (1970) which assumes that the sediment undergoing erosion is both cohesionless, and constructed of similar particles. According to Clarke (1996a), the critical boundary stress, $\tau^*$, is dependent on grain size, and in extremely small particles (e.g. silt) is approximately equal to zero. For the purpose of the model, the mean recorded particle size diameter across both streams was used ($1.67 \times 10^{-6}$ m). Maintaining a constant particle size diameter is considered appropriate, as Fenn and Gomez (1989) suggest that sediment size distribution in a glacial stream is typically unimodal with a predominantly silt composition. $1.67 \times 10^{-6}$ m can be considered a very fine silt, and therefore, using a mean silt size is sufficient for modelling suspended sediment concentration. The shear stress, $\tau_0$, is calculated assuming turbulent flow within the channel using the equation:

$$\tau_0 = \frac{f\rho_w v^2}{8} \qquad (6.13)$$

where $v$ is the flow velocity, $f$ is the Darcy-Weisbach Coefficient, and $\rho_w$ is the density of water, 1000 kg m$^{-3}$. It is assumed that Stokes' Law governs the sedimentation rate of suspended sediment as follows:

$$v_s = \frac{(\rho_s - \rho_w) g {D_p}^2}{18\mu} \quad (6.14)$$

where $v$ is the settling velocity of spherical grains of diameter $D_p$ and density $p_s$, within a fluid of viscosity $\mu$ and density $p_w$. Based on similar models, both the density of sediment particles (2700 kg m$^{-3}$) and the viscosity of water (1.787 × 10$^{-3}$ Pa s) are considered to remain constant throughout the study (Clarke, 1996a; Fausto *et al*., 2012). The mass flux of sedimentation is therefore represented as:

$$F_s = c_s v_s = \frac{(\rho_s - \rho_w) g {D_p}^2}{18\mu} \quad (6.15)$$

where $c_s$ is the suspended sediment concentration. In an idealised hydrological conduit system, the conservation of mass relates to changes in mass of suspended sediment concentration to the suspended sediment concentration input flux ($F_{in}$) and output flux ($F_{out}$) together with sediment erosion ($F_e$) and deposition ($F_s$) over time (Fausto *et al*., 2012). As a result, the conservation of mass can be represented using the equation:

$$\frac{dM}{dt} = F_{in} + F_{out} + F_e + F_s \quad (6.16)$$

where $M$ is the mass of suspended sediment. In the final suspended sediment balance equation, the lumped-element assumptions of Equations 6.11 to 6.15 are applied with suspended sediment mass, $M$, substituted for observed suspended sediment concentration, $c_s$. Furthermore, following Clarke (1996), the volume within the channel is assumed to remain constant with time in order to simplify the system of equations. The final suspended sediment balance is therefore represented:

$$\frac{dc_s}{dt} = \frac{1}{V[{c_s}^{in}Q^{in} - {c_s}^{out}Q^{out} + A(F_e - F_s)]} \quad (6.17)$$

where $Q$ is the water discharge and $A$ is the bottom area of the channel. However, this study differs from those of Clarke (1996a) and Fausto *et al*. (2012) in that detailed knowledge of the dimensions of glacial conduits, and suspended sediment inputs are not known. Therefore, Clarke's (1996a) sediment balance equation is modified thus:

$$\frac{dc_s}{dt} = \frac{1}{V[{c_s}^{in}Q^{in} + A(F_e - F_s)]} \quad (6.18)$$

Whilst this is not a true sediment balance equation, it still takes into account the channel dimensions and the factors which influence sediment erosion and sedimentation at each time step.

An overview of the physical parameters used in the sediment model is presented in Table 6.2.

**Table 6.2. Physical parameters used in the suspended sediment concentration model setup (after: Clarke, 1996a; Fausto *et al*., 2012). *Note that the parameters *n*, *N* and *f* are dimensionless.**

| Property | Value |
|---|---|
| Water density ($p_w$) | 1000 kg m$^{-3}$ |
| Sediment density ($\rho_s$) | 2700 kg m$^{-3}$ |
| Gravitational acceleration ($g$) | 9.82 m s$^{-2}$ |
| Viscosity of water ($\mu$) | 1.787 x 10$^{-3}$ Pa s |
| Sediment particle diameter ($D_p$) | 1.67 x 10$^{-6}$ m |
| Porosity of sediment load ($n$) | 0.35* |
| Threshold stress for erosion ($\tau^*$) | 0 Pa |
| Exponent for erosion law ($N$) | 1.5* |
| Erosion rate constant ($k_E$) | 5 x 10$^{-9}$ m s$^{-1}$ Pa$^{-N}$ |
| Darcy-Weisbach Coefficient ($f$) | 0.25* |

Performance of the suspended sediment model was assessed using the same three methods as the linear reservoir model: Mean Error, Root Mean Square Error, and the Nash-Sutcliffe efficiency criterion. These are described in more detail in Section 6.2.4.

### 6.2.7. Suspended Sediment Transport Model Sensitivity

The responsiveness of the model to changing input variables was evaluated through a sensitivity analysis of the modelled suspended sediment concentration time series. Clarke's (1996a) suspended sediment model utilizes a range of empirical constants and parameterizations in order to simulate the nature of the glacier drainage system. Following the methods of Jones and Arnold (1999) and Fausto *et al*. (2012), the sensitivity of the model output to variations in the parameters $N$ (exponent for erosion law), $k_E$ (erosion rate constant) and $\tau^*$ (threshold stress for erosion) was assessed using a range of values identical to those used in Fausto *et al*. (2012). In each case, one parameter was kept constant in order to determine the range of solutions for the model.

## 6.3. Results

### 6.3.1. Flow-Recession Analysis & Reservoir Coefficients

Reservoir coefficients derived using flow recession analysis and employed in the setup of the linear reservoir model are presented in Figure 6.6 (Nordjåkk) and Figure 6.7 (Sydjåkk). Flow recession statistics for both Nordjåkk and Sydjåkk are presented in Table 6.3

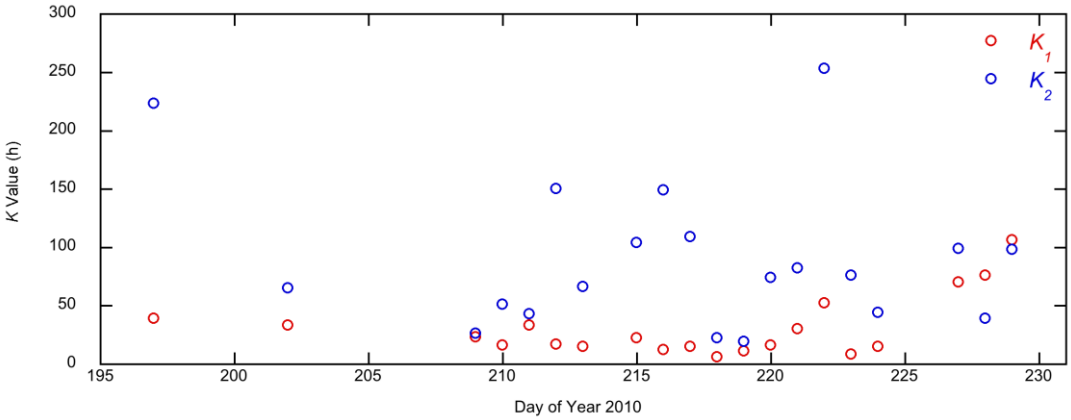


**Figure 6.6 Variation of reservoir coefficients over time during the 2010 field season at Nordjåkk.**

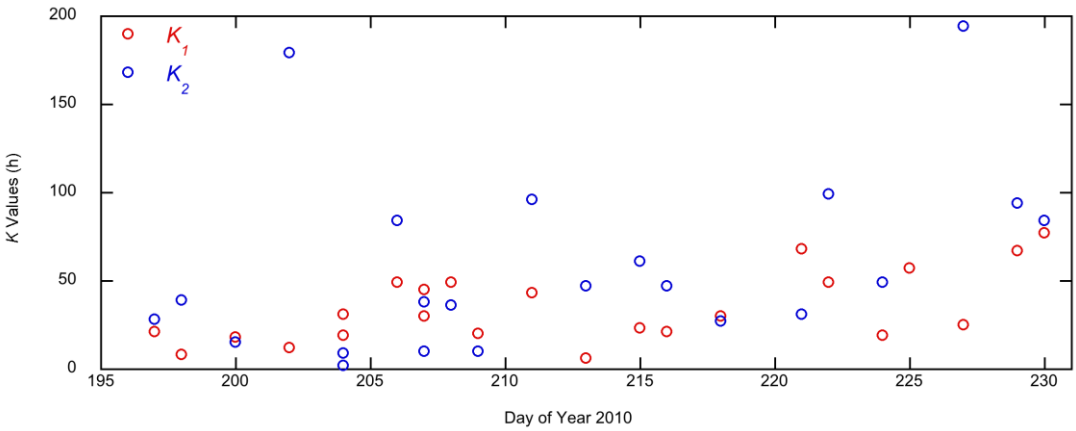


**Figure 6.7 Variation of reservoir coefficients over time during the 2010 field season at Sydjåkk.**

**Table 6.3 Summary of flow recession statistics from the 2010 field season. $\Delta Q$ represents the change in reservoir discharge during a flow recession. For range values, maximum and minimum values are shown, and the calculated range given in brackets.**

| | Nordjåkk | Sydjåkk |
|---|---|---|
| **Reservoir 1** | | |
| Number of Flow Recessions | 20 | 23 |
| Mean Duration (h) | 5 | 4 |
| Maximum Duration (h) | 11 | 9 |
| $\Delta Q$ Mean ($m^3 s^{-1}$) | -0.29 | -0.08 |
| $\Delta Q$ Range ($m^3 s^{-1}$) | -0.79 to -0.04 (0.75) | -0.22 to -0.02 (0.20) |
| $K_1$ Mean (h) | 31 | 34 |
| $K_1$ Range (h) | 6 to 106 (100) | 6 to 77 (71) |
| Flow Proportion Mean (%) | 76 | 63 |
| **Reservoir 2** | | |
| Number of Flow Recessions | 20 | 22 |
| Mean Duration (h) | 3 | 2 |
| Maximum Duration (h) | 7 | 4 |
| $\Delta Q$ Mean ($m^3 s^{-1}$) | -0.05 | -0.03 |
| $\Delta Q$ Range ($m^3 s^{-1}$) | -0.13 to -0.01 (0.12) | -0.11 to -0.002 (0.12) |
| $K_2$ Mean (h) | 90 | 58 |
| $K_2$ Range (h) | 19 to 253 (234) | 2 to 194 (192) |
| Flow Proportion Mean (%) | 24 | 37 |

From Figures 6.6 and 6.7 it appears that $K_1$ values increase as the season progresses at both Nordjåkk and Sydjåkk. However, whilst the relationship between $K_1$ and day of year at Sydjåkk is statistically significant at a confidence level of 95% ($R^2 = 0.32$; $p = 0.01$), this is not the case for Nordjåkk. Toward the middle of the season at Nordjåkk, $K_1$ values appear to decline slightly, yielding a season minimum reservoir coefficient (Day 218). However this pattern is quickly reversed, with the seasonal maximum reservoir coefficient reached in Day 229. At Sydjåkk, $K_1$ appears to fluctuate more, in spite of the significance of the increasing trend. The seasonal minimum $K_1$ value occurs on Day 213,

whilst the seasonal maximum occurs almost concurrently with that at Nordjåkk on Day 230. $K_1$ values are similar at both Nordjåkk and Sydjåkk in terms of the mean values and the proportion of flow observed. However, the change in discharge during flow recessions is notably higher at Nordjåkk, both in terms of mean (-0.29) and range (0.75). Comparison of the mean $K_1$ values suggest that flow through Reservoir 1 at Nordjåkk is marginally faster than that at Sydjåkk, although only by three hours.

In terms of $K_2$ values, a similar pattern of increasing reservoir coefficients is also observed in the data collected at Sydjåkk. Values appear to be at their lowest early in the season (with the exception of Day 202 which exhibits a $K_2$ value of 197 hours) and increase steadily towards the end of the season. No clear pattern of $K_2$ change over time is evident at Nordjåkk. Comparison of $K_2$ statistics between Nordjåkk and Sydjåkk in Table 6.3 suggest that in many regards, the two streams have similar Reservoir 2 coefficients. However, mean $K_2$ values at Nordjåkk are considerably higher (32 hours) than at Sydjåkk, in spite of similar ranges between the two streams. Furthermore, Reservoir 2 at Sydjåkk on average carries a greater proportion of flow than that at Nordjåkk (0.37 compared with 0.24).

Plots representing the relationship between discharge and reservoir coefficients are presented in Figures 6.8 and 6.9. At Nordjåkk, no clear predictive relationship between discharges at the start of each flow recession ($Q_{start}$) and either $K_1$ or $K_2$ is apparent. However, both plots indicate clustering of values at low $K$ values and low $Q_{start}$ values. A similar relationship is observed between $K_2$ values and the change in discharge during flow recession ($\Delta Q$). A power curve can be fitted to the relationship between $K_1$ and $\Delta Q$, indicating a clear decline in $K_1$ values with greater change in discharge during flow recession.

At Sydjåkk, relationships between $K_1$ values and both $Q_{start}$ and $\Delta Q$ exhibit significant ($p>0.05$) decreasing trends. A power curve can be fitted to the relationship between $K_1$ and $\Delta Q$ ($r^2 = 0.71$). In terms of $K_2$ values, slight

negative relationships are observed between $K_2$ and both $\Delta Q$ *and* $Q_{start}$. However both relationships are significant, and both are weakened by high reservoir coefficients (early and late in the season for $\Delta Q$, and mid-season for $Q_{start}$). Similarly to $K_2$ values observed at Nordjåkk, both relationships are largely represented as a cluster of values at lower start discharges and changes in discharge.

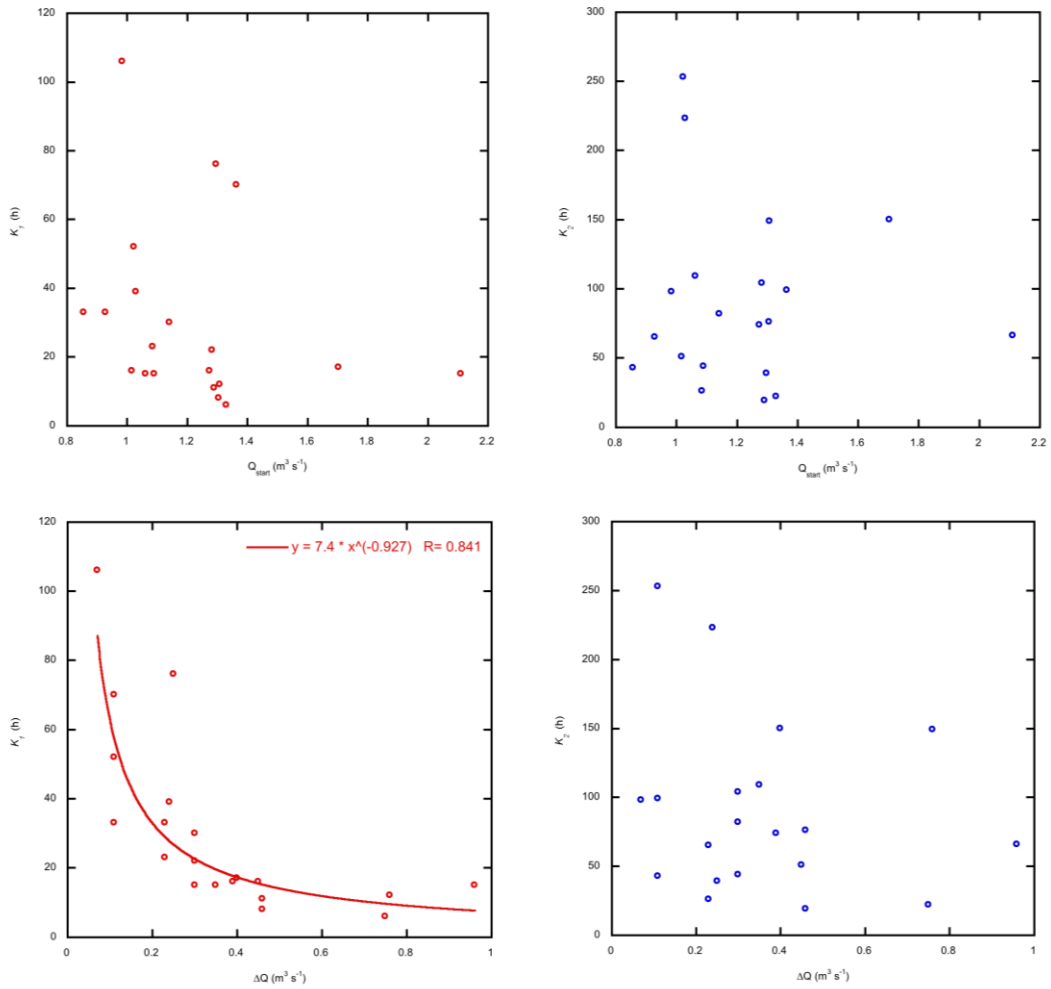


**Figure 6.8 Plots showing the variation of reservoir coefficients with discharge at the start of the flow recession ($Q_{start}$) and discharge change over the duration of the flow recession ($\Delta Q$) during the 2010 field season at Nordjåkk. Plots comparing $K_1$ values are on the left (red), and plots comparing $K_2$ values are on the right (blue).**

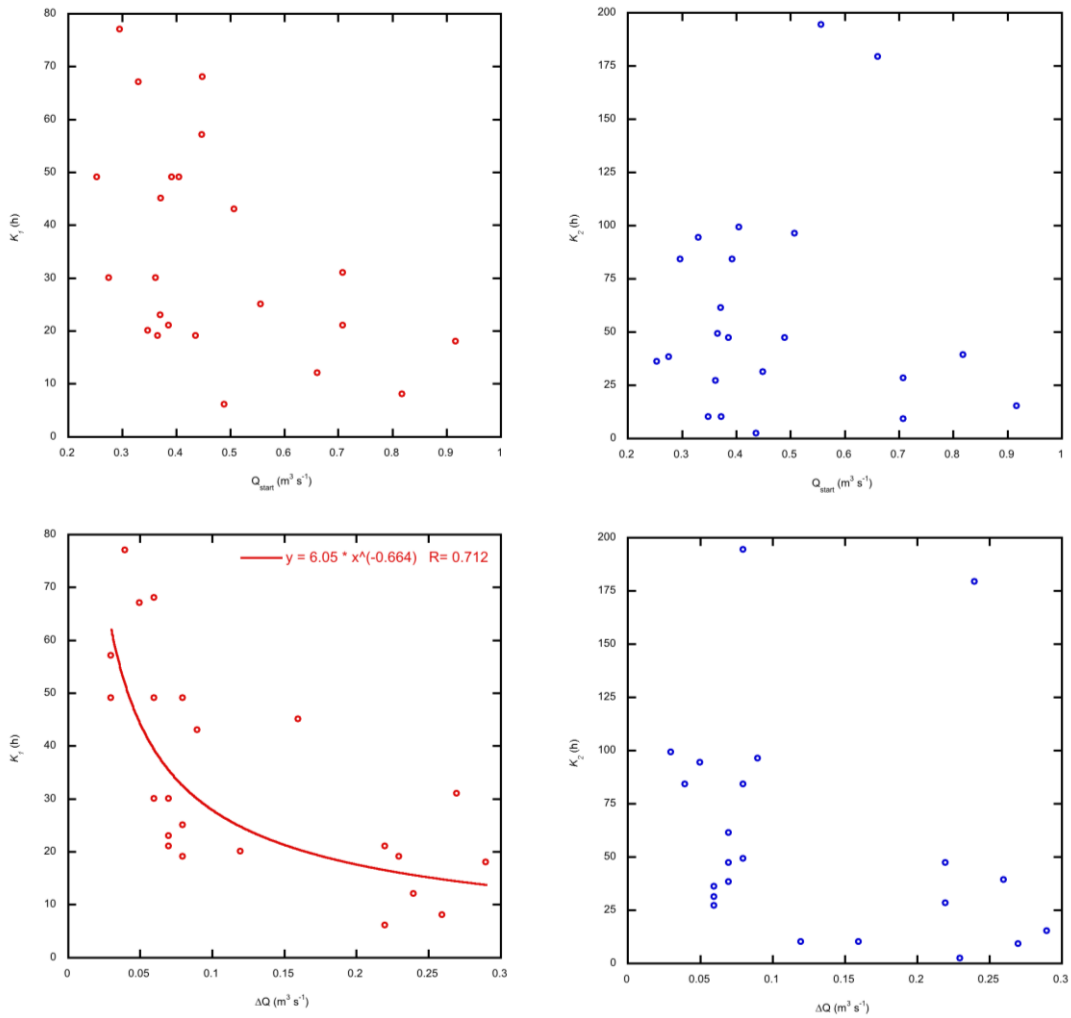


**Figure 6.9 Plots showing the variation of reservoir coefficients with discharge at the start of the flow recession ($Q_{start}$) and discharge change over the duration of the flow recession ($\Delta Q$) during the 2010 field season at Sydjåkk. Plots comparing $K_1$ values are on the left (red), and plots comparing $K_2$ values are on the right (blue).**

### 6.3.2. Linear Reservoir Model Time Series

#### 6.3.2.1. Nordjåkk

Composite plots containing time series of implied input, modelled discharge, recession and recharge flows from Nordjåkk are presented in Figure 6.10.

Implied input into the glacier drainage system is steady for the duration of the melt season, save for periods of high discharge driven by high rainfall events (as discussed in earlier chapters). For example, whilst the seasonal average implied input is approximately 0.16 mm $h^{-1}$, an input of approximately 5 mm $h^{-1}$ is observed on Day 199 corresponding with the seasonal maximum discharge.

It is clear from comparing the total reservoir output with the recession output in Figure 6.10, that recession flow contributes the greatest volume of discharge in both Reservoir 1 and Reservoir 2. As expected, recession flow from Reservoir 1 is the greatest contributor with a mean discharge of 0.75 $m^3$ $s^{-1}$, compared with 0.26 $m^3$ $s^{-1}$ from Reservoir 2. The proportion of recession flow contributed by Reservoir 1 and Reservoir 2 generally remains consistent, although on Days 199 and 212 (when high discharge events occur) flow from Reservoir 1 is considerably higher. Between Days 205 and 211, the recession flow contributions from Reservoirs 1 and 2 are close to equal, and on Days 210 and 211, discharge from Reservoir 2 briefly surpasses Reservoir 1. From approximately Day 216, recession flow from Reservoir 2 appears to increase steadily, and again almost equalises with Reservoir 1 on Day 229.

Whilst recharge flow from both reservoirs is low, the Reservoir 1 time series exhibits a number of notable peaks, in conjunction with high discharge events on Days 199 and 212, and on Day 218. Recharge flow from Reservoir 2 is considerably lower than that from Reservoir 1, with a mean discharge of 0.01 $m^3$ $s^{-1}$ (compared with 0.05 $m^3$ $s^{-1}$ from Reservoir 1). As observed in the recession flow time series, the two reservoirs equalise between Days 205 and

211, and again on Days 228 and 229, periods where there is little implied input in the glacier drainage system.

#### 6.3.2.2. Sydjakk

Composite plots containing time series of implied input, modelled discharge, recession and recharge flows from Sydjåkk are presented in Figure 6.11.

Implied input into Sydjåkk is lower than that into Nordjåkk with a mean of 0.07 mm $h^{-1}$ (compared with 0.16 mm $h^{-1}$ into Nordjåkk). Although these mean inputs are not considerably distant, the greatest difference is observed around Days 199 and 200, where input into Nordjåkk approximates 5 mm $h^{-1}$, whilst input into Sydjåkk reaches a maximum of 1 mm $h^{-1}$. In spite of this discrepancy, the implied input series into Sydjåkk during this period does suggest more variable and sustained input, as opposed to a single high magnitude input as seen at Nordjåkk.

As observed in the Nordjåkk data, recession flow is the dominant contributor to total glacier output in both reservoirs. Reservoir 1 is the dominant contributor of runoff with a mean discharge of 0.28 $m^3$ $s^{-1}$. However, recession flow from Reservoir 2 is greater than that observed at Nordjåkk, with a mean discharge of 0.15 $m^3$ $s^{-1}$. Whilst flow from Reservoir 1 is most dominant during high discharge events (e.g. Day 213), Reservoir 2 is steadier throughout, although a seasonal maximum (~0.9 $m^3$ $s^{-1}$) is observed on Day 200 during such an event. Whilst Reservoir 2 recession flow surpasses that of Reservoir 1 briefly at Nordjåkk, this occurs several times at Sydjåkk, including a two day period between Days 208 and 210.

Recharge flow from Reservoir 1 shows similarity with that of Nordjåkk, as discharge is typically low (with a mean of 0.02 $m^3$ $s^{-1}$), but appears very responsive during high discharge events (e.g. a seasonal maximum discharge of 0.33 $m^3$ $s^{-1}$ on Day 213). Recharge flow from Reservoir 2 also exhibits differences to that at Nordjåkk, although it is remains low (mean = 0.01 $m^3$ $s^{-1}$).

However, early in the season it is highly variable, surpassing recharge flow from Reservoir 1 on several occasions, often considerably. For example, on Day 204, recharge flow from Reservoir 1 averages ~0.1 $m^3$ $s^{-1}$, whereas Reservoir 2 peaks at ~0.12 $m^3$ $s^{-1}$.

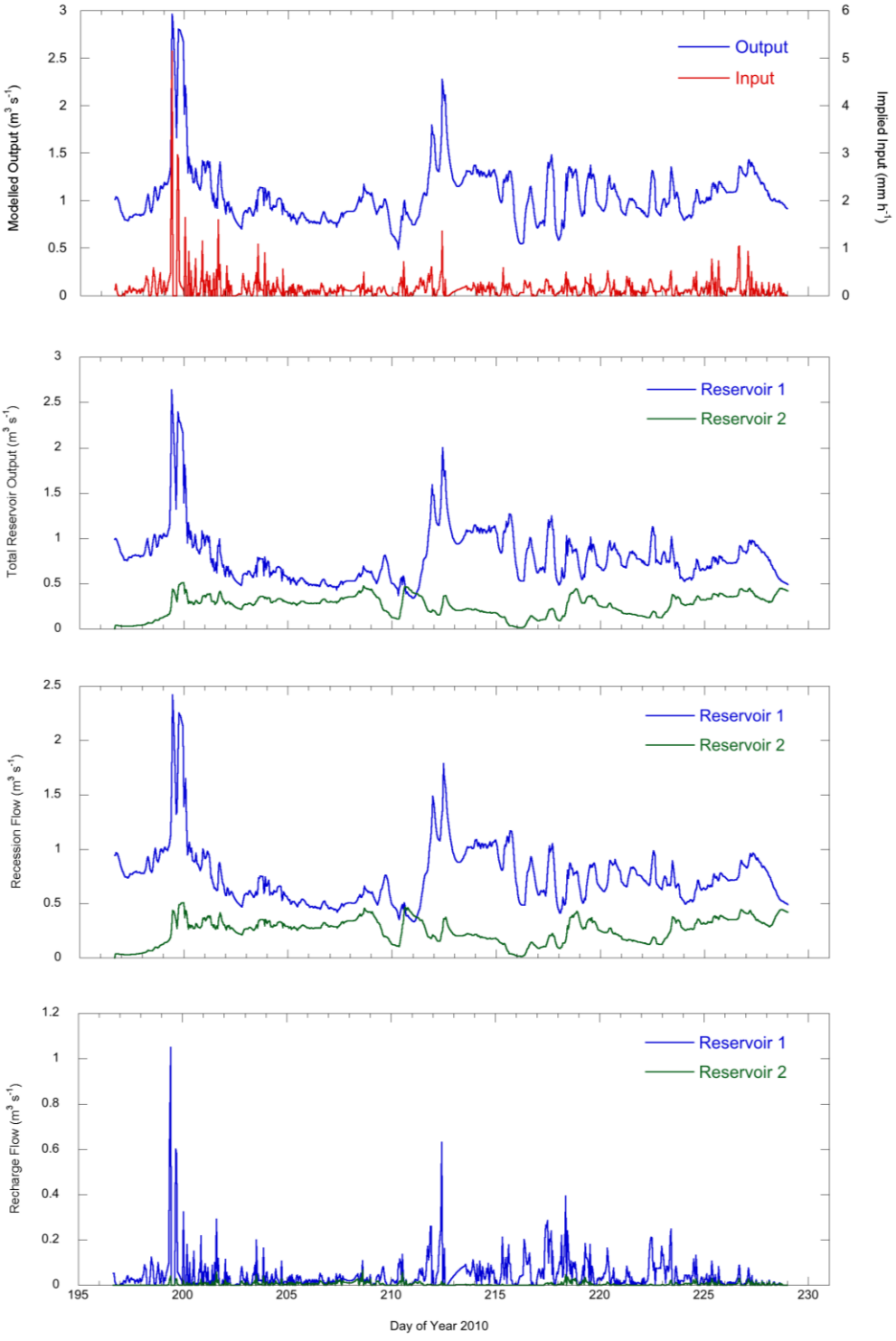


**Figure 6.10 Linear reservoir models for the 2010 melt season at Nordjåkk: implied input and output (top), total flow from each reservoir, recession flow from both reservoirs (middle), and recharge flow from both reservoirs (bottom).**

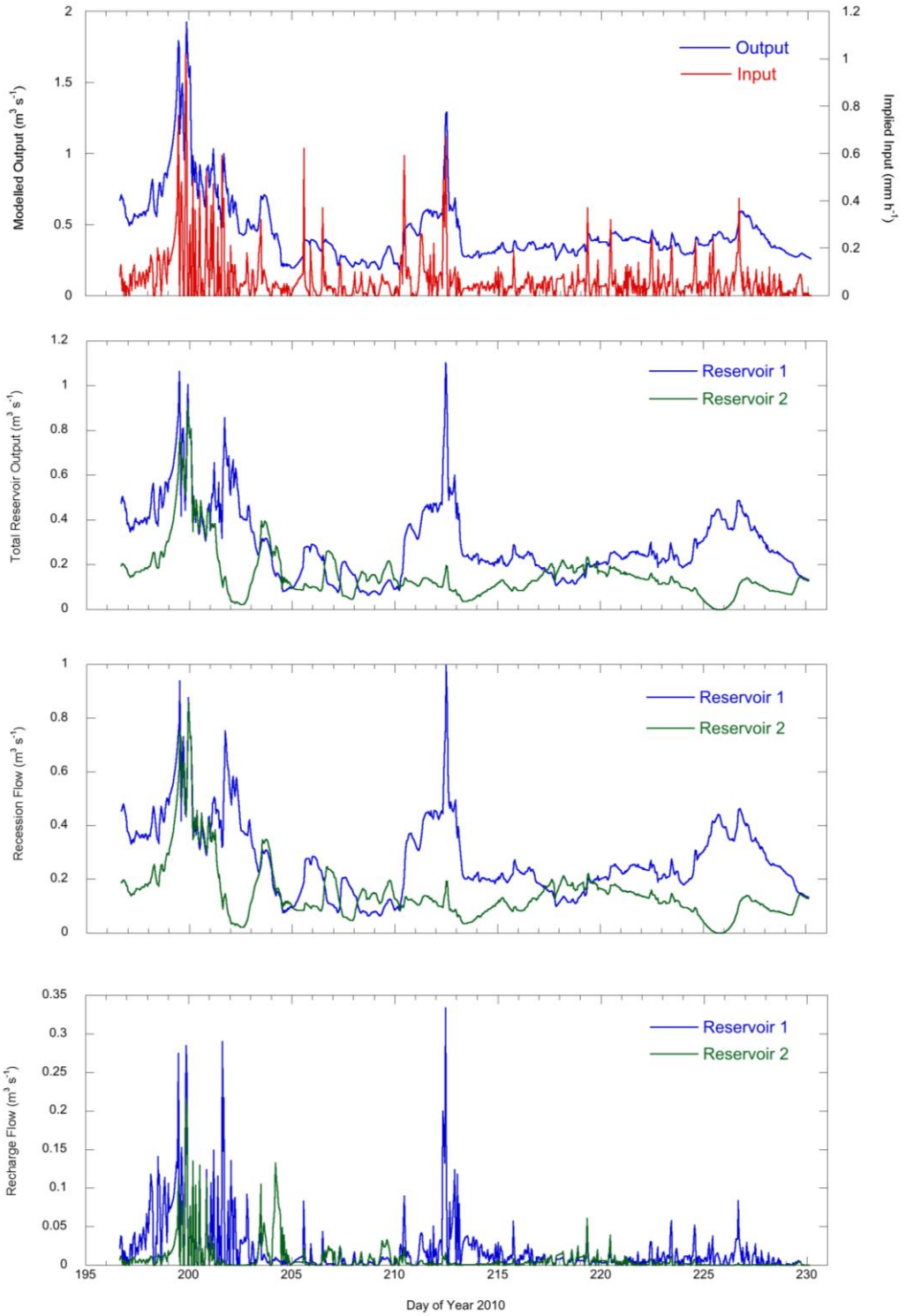


**Figure 6.11 Linear reservoir models for the 2010 melt season at Sydjåkk: implied input and output (top), total flow from each reservoir, recession flow from both reservoirs (middle), and recharge flow from both reservoirs (bottom).**

### 6.3.3. Linear Reservoir Model Performance

Time series of observed discharge data compared with linear-reservoir modelled discharge are presented in Figures 6.12 (for Nordjåkk), and 6.13 (for Sydjåkk).

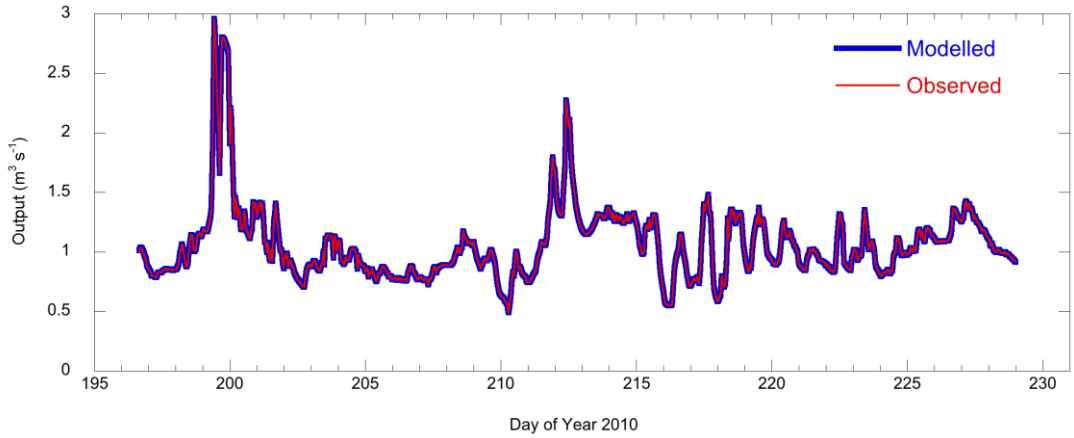


**Figure 6.12 Comparison of observed discharge recorded at the Nordjåkk gauging station during the 2010 field season with linear-reservoir modelled output.**

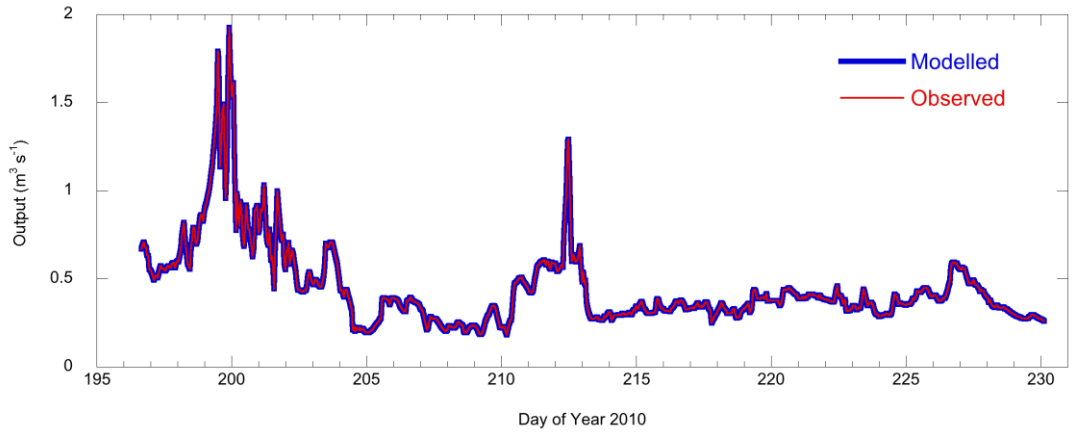


**Figure 6.13 Comparison of observed discharge recorded at the Nordjåkk gauging station during the 2010 field season with linear-reservoir modelled output.**

It is clear from Figures 6.12 and 6.13 that visually, the modelled discharge data compares favourably with the observed discharge data for both Nordjåkk and Sydjåkk. This is supported using the performance indicators Mean Error (*ME*), Root Mean Square Error (*RMSE*), and the Nash-Sutcliffe efficiency criterion (*E*)

as described in Section 6.2.3. Results of these statistics are presented in Table 6.4.

**Table 6.4 Performance statistics comparing observed and total modelled discharge. Mean Error, Root Mean Square Error and the Nash-Sutcliffe efficiency criterion (*E*) are calculated relative to observed values (i.e. the goodness of fit to non-modelled data).**

| | Nordjåkk Total Modelled Flow ($m^3 s^{-1}$) | Nordjåkk Observed Discharge ($m^3 s^{-1}$) | Sydjåkk Total Modelled Flow ($m^3 s^{-1}$) | Sydjåkk Observed Discharge ($m^3 s^{-1}$) |
|---|---|---|---|---|
| Mean | 1.06 | 1.06 | 0.46 | 0.46 |
| St. Dev. | 0.32 | 0.32 | 0.24 | 0.24 |
| *ME* | 0.00 | - | 0.00 | - |
| *RMSE* | 0.00 | - | 0.00 | - |
| *E* | 1.00 | - | 1.00 | - |

It is likely that the model performance is somewhat improved by the use of implied input, as this is determined using the observed discharge data from each stream gauging site. As Hodgkins *et al.* (2013) point out, the use of other forms of melt input would likely result in lower *E* values. However, since the model input values for the $K_1$ and $K_2$ reservoir coefficients were tuned using the Microsoft Excel function 'Solver' this also increases the fit between the observed and modelled data. In order to demonstrate the performance of the model prior to tuning taking place, the 'pre-tuning' performance statistics are presented in Table 6.5.

**Table 6.5 Performance statistics comparing observed and total modelled discharge prior to model tuning taking place. Mean Error, Root Mean Square Error and the Nash-Sutcliffe efficiency criterion (*E*) are calculated relative to observed values (i.e. the goodness of fit to non-modelled data).**

| | Nordjåkk Total Modelled Flow ($m^3 s^{-1}$) | Nordjåkk Observed Discharge ($m^3 s^{-1}$) | Sydjåkk Total Modelled Flow ($m^3 s^{-1}$) | Sydjåkk Observed Discharge ($m^3 s^{-1}$) |
|---|---|---|---|---|
| Mean | 1.04 | 1.06 | 0.46 | 0.46 |
| St. Dev. | 0.33 | 0.32 | 0.24 | 0.24 |
| *ME* | 0.00 | - | 0.00 | - |
| *RMSE* | 0.03 | - | 0.03 | - |
| *E* | 0.98 | - | 0.99 | - |

Comparing the data in Tables 6.4 and 6.5 it is apparent that the fit of modelled to observed data prior to tuning (i.e. using only the recession coefficient values obtained from flow-recession analysis) is very high. Modelled discharge at Sydjåkk exhibits a very slightly increased fit with observed data compared to that at Nordjåkk (Sydjåkk $E$ = 0.99, Nordjåkk $E$ = 0.98). Nonetheless it can be concluded that model tuning in this case yielded only a small improvement in the model performance.

### 6.3.4. Linear Reservoir Model Sensitivity

The results of the model sensitivity to variations in reservoir coefficients are presented in Figures 6.14 to 6.17. Model sensitivity to $f$ is described in Table 6.6.

**Table 6.6. Response of modelled discharge and Root Mean Square Error to variation in *f* values. *f* values are presented as percentage contributions to the total discharge. *Results obtained using original *f* values.**

| | $K_1$ | $K_2$ | *f (%)* | Modelled Total Discharge ($m^3\ s^{-1}$) | *RMSE* |
|---|---|---|---|---|---|
| Nordjåkk | 39 | 223 | 94* | 0.830 | 0.0002 |
| Nordjåkk | 39 | 223 | 100 | 0.830 | 0.0001 |
| Nordjåkk | 39 | 223 | 50 | 0.835 | 0.0032 |
| Sydjåkk | 21 | 28 | 71* | 0.515 | $8.67 \times 10^{-6}$ |
| Sydjåkk | 21 | 28 | 100 | 0.514 | 0.0005 |
| Sydjåkk | 21 | 28 | 50 | 0.516 | 0.0004 |

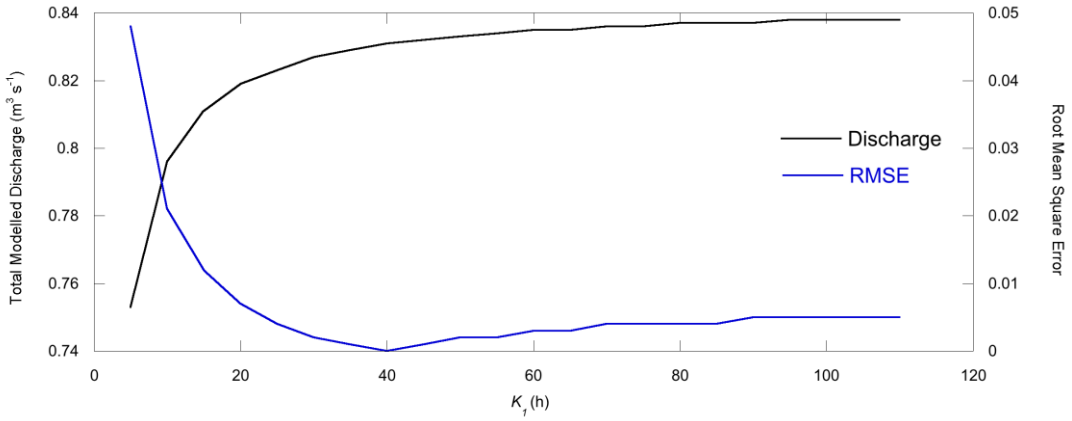


**Figure 6.14. Response of Nordjåkk modelled discharge and Root Mean Square Error to variation in $K_1$ values. Original $K_1$ value = 39.**

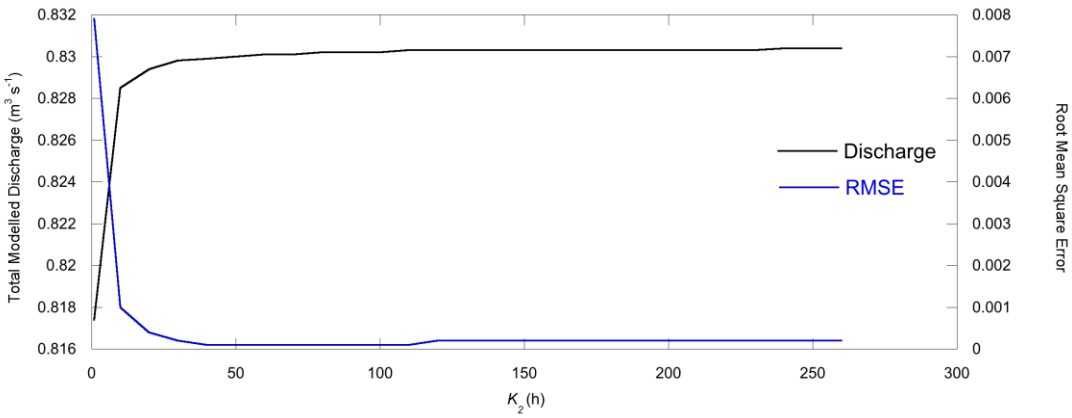


**Figure 6.15. Response of Nordjåkk modelled discharge and Root Mean Square Error to variation in $K_2$ values. Original $K_2$ value = 223.**

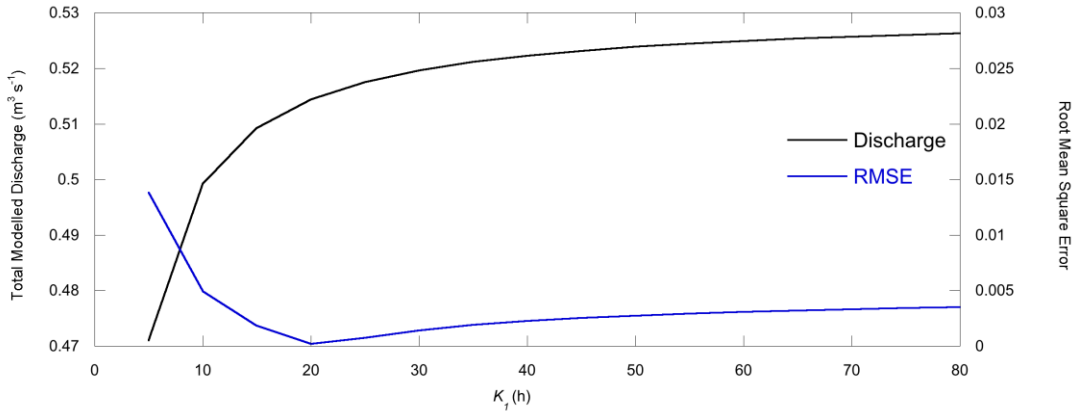


**Figure 6.16. Response of Sydjåkk modelled discharge and Root Mean Square Error to variation in $K_1$ values. Original $K_1$ value = 21.**

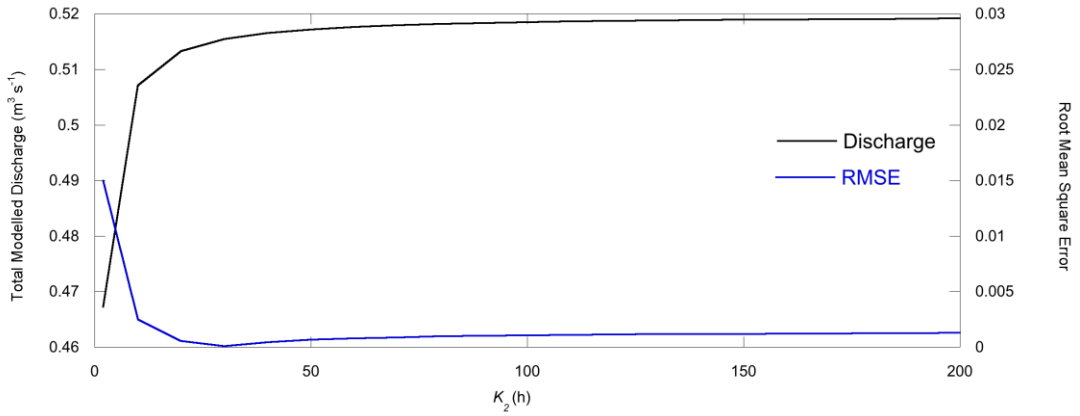


**Figure 6.17. Response of Sydjåkk modelled discharge and Root Mean Square Error to variation in $K_2$ values. Original $K_2$ value = 28.**

The response of modelled discharge to variations in $K_1$ and $K_2$ values appear to be similar at both Nordjåkk and Sydjåkk. Regardless of stream or reservoir, the main variation is observed at lower $K$ values, resulting in the greatest change in modelled discharge and RMSE. As $K$ values increase, modelled discharge at RMSE appears to reach a plateau, responding only subtly to subsequent variations.

The sensitivity of the model to changes in flow fraction differs between the two streams. Simulating discharge with a single reservoir at Nordjåkk has little effect on either the total modelled discharge, or the RMSE. A two-reservoir

system split evenly does result in a change, albeit small (an ~0.005 $m^3$ $s^{-1}$ in discharge. At Sydjåkk, the difference between a single reservoir (a decrease of ~0.001 $m^3$ $s^{-1}$) and an evenly divided drainage system (and increase of ~0.001 $m^3$ $s^{-1}$) is even smaller. Changing the fraction of flow contribution to each reservoir therefore, does not appear to significantly influence the modelled time series.

### 6.3.5. Suspended Sediment Model Time Series

Suspended sediment model output for both Nordjåkk and Sydjåkk is presented in Figures 6.18 and 6.19. Model performance statistics are presented in Table 6.7.

#### 6.3.5.1. Nordjåkk

The suspended sediment model run at Nordjåkk appears to successfully simulate temporal changes in suspended sediment concentration. However, the modelled suspended sediment time series consistently underestimates suspended sediment concentration. This is clearly exemplified by the mean suspended sediment concentration for each time series: 0.056 g $L^{-1}$ for the observed series, and 0.027 g $L^{-1}$ for the modelled series, and represented by a Mean Error of -0.03. The only exception to this underestimation is during a high suspended sediment event on Day 213, where the modelled series exceeds the observed series, albeit by less than 0.01 g $L^{-1}$. The modelled mass suspended sediment flux (i.e. erosion) and the flux of sedimentation (i.e. deposition) series are negligible, both with mean values less than 0.01 g $L^{-1}$ (0.006 and 0.001 g $L^{-1}$ respectively). Whilst peaks in these time series (predictably) concur with those in the modelled and observed time series, there appears to be very little erosion occurring on Day 207, an occasion which coincides with an increase in suspended sediment concentration.

### 6.3.5.2. Sydjåkk

Similarly to the Nordjåkk time series, the modelled suspended sediment concentration series largely underestimates the observed time series although not as consistently. Between Days 206 and 208 for example, the modelled series equals, and at one point exceeds the observed series. However, the underestimation is most noticeable during high suspended sediment events, for example during the middle and end of the season where the model underestimation can reach up to 2 g $L^{-1}$.

As in the Nordjåkk time series, mass suspended sediment flux is negligible (mean = 0.03 g $L^{-1}$) throughout the season, other than during the high magnitude suspended sediment peak early in the season and, to a lesser degree, at the mid-point of the season. The flux of sedimentation is also small (mean = 0.03 g $L^{-1}$), although the time series is more dynamic than that of the mass suspended sediment flux.

**Table 6.7. Performance comparing observed and modelled suspended sediment concentration data. Mean Error, Root Mean Square Error and the Nash-Sutcliffe efficiency criterion (*E*) are calculated relative to observed values (i.e. the goodness of fit to non-modelled data).**

| | Nordjåkk Total Modelled SSC (g $L^{-1}$) | Nordjåkk Observed SSC (g $L^{-1}$) | Sydjåkk Total Modelled SSC (g $L^{-1}$) | Sydjåkk Observed SSC (g $L^{-1}$) |
|---|---|---|---|---|
| Mean | 0.03 | 0.06 | 0.58 | 1.18 |
| St. Dev. | 0.04 | 0.04 | 0.50 | 0.88 |
| *ME* | -0.03 | - | -0.60 | - |
| *RMSE* | 0.03 | - | 0.81 | - |
| *E* | 0.45 | - | 0.42 | - |

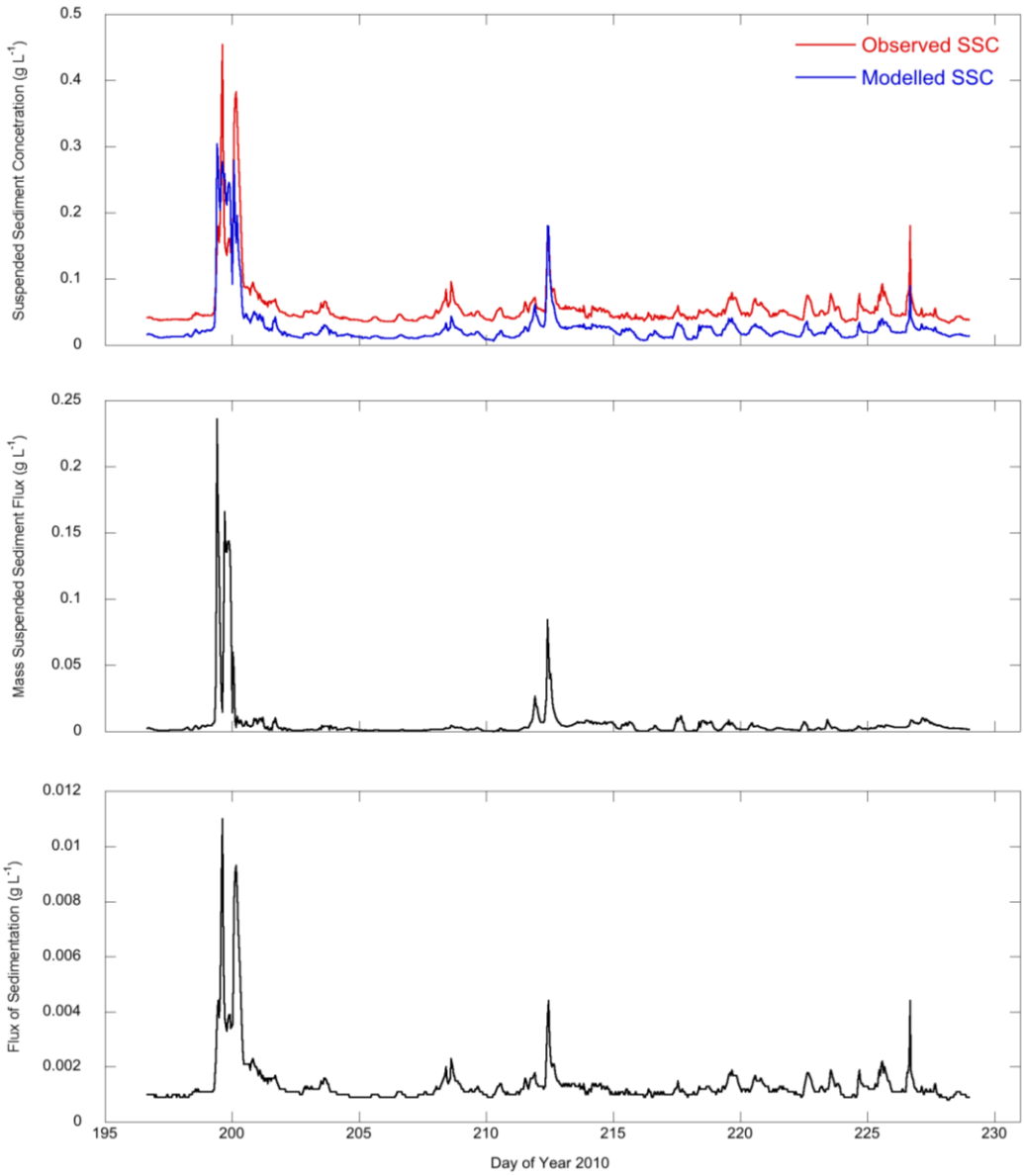


**Figure 6.18. Suspended sediment model output for the 2010 melt season at Nordjåkk: modelled and observed SSC (top); mass flux of sediment into suspension (middle); flux of suspended sediment deposition (bottom).**

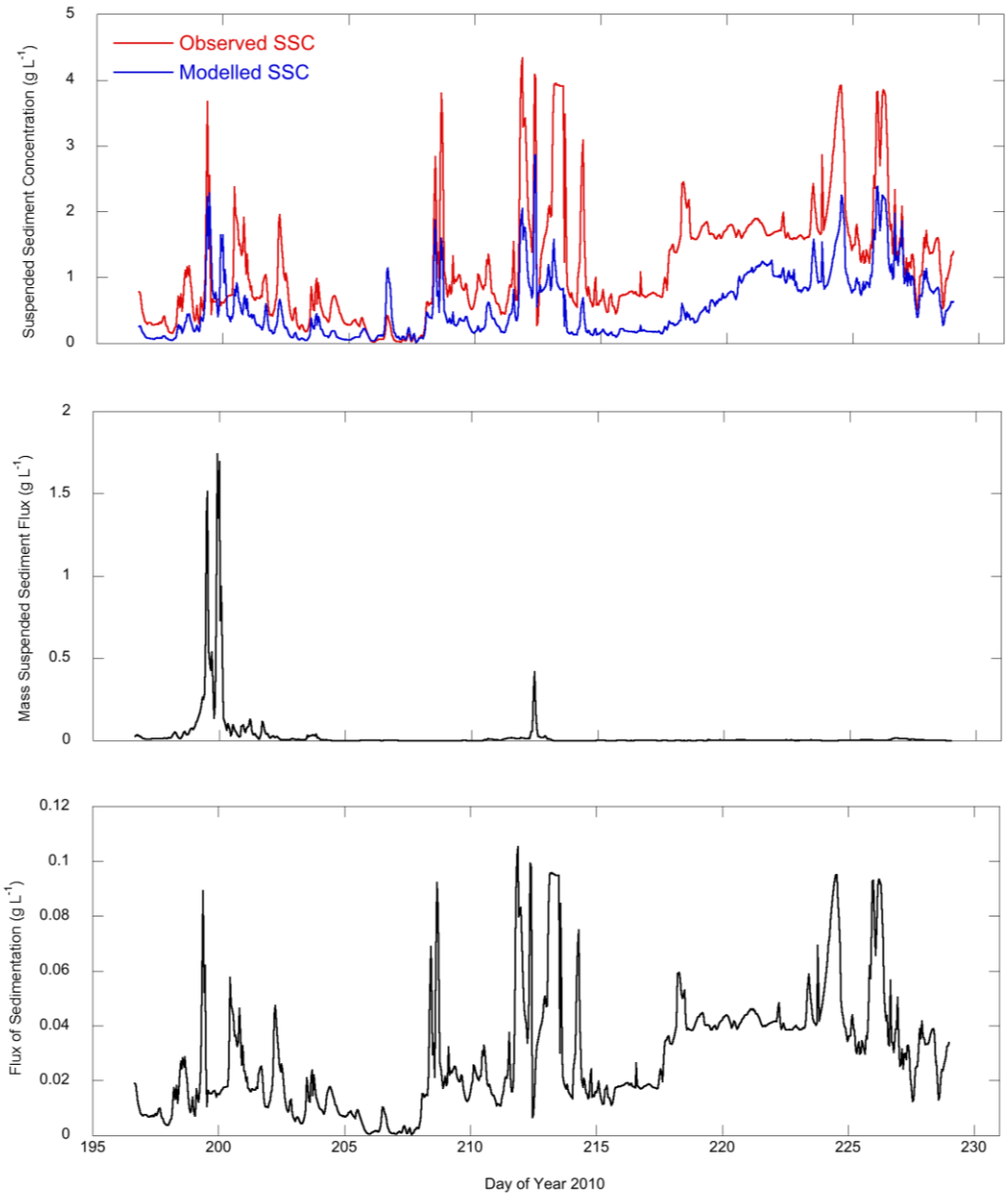


**Figure 6.19. Suspended sediment model output for the 2010 melt season at Sydjåkk: modelled and observed SSC (top); mass flux of sediment into suspension (middle); flux of suspended sediment deposition (bottom).**

### 6.3.6. Suspended Sediment Model Sensitivity

The results of the model sensitivity to different model constants are presented in Figures 6.20 to 6.25. Descriptive statistics of each time series are presented in Tables 6.8 and 6.9.

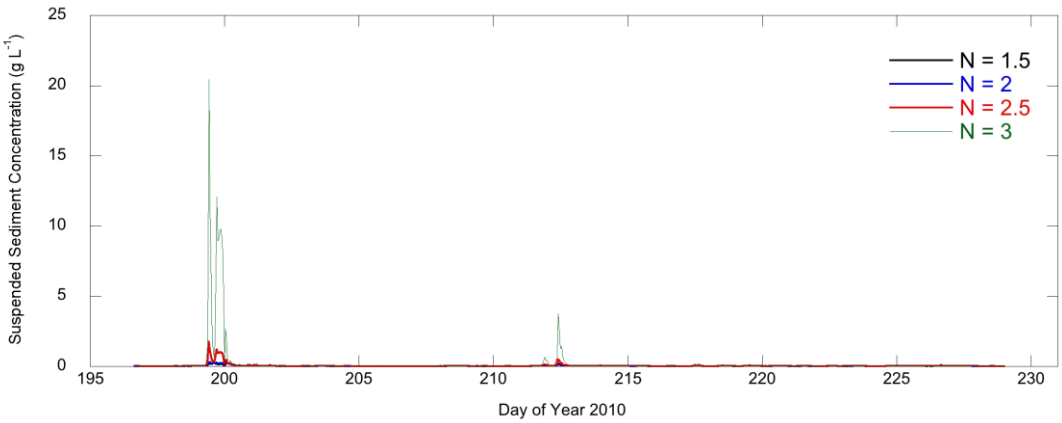


**Figure 6.20. Modelled suspended sediment concentration time series for Nordjåkk using four different values of *N*.**

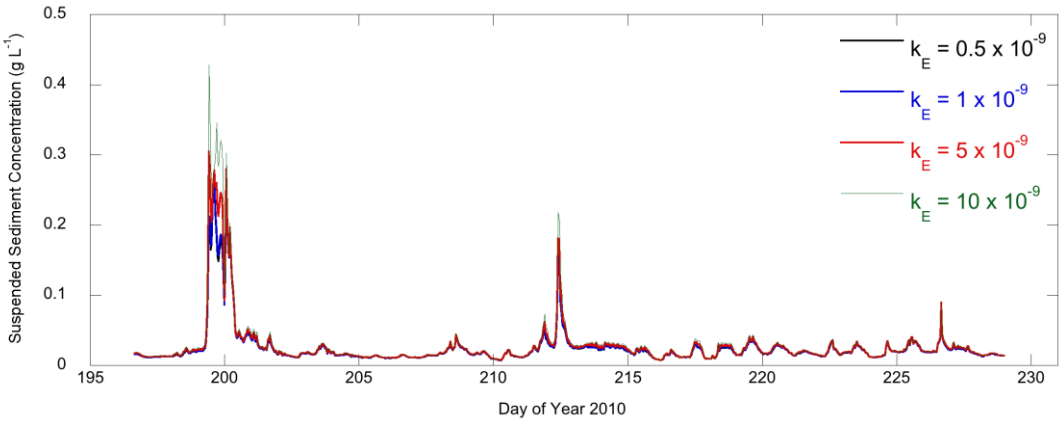


**Figure 6.21. Modelled suspended sediment concentration time series for Nordjåkk using four different values of $k_E$.**

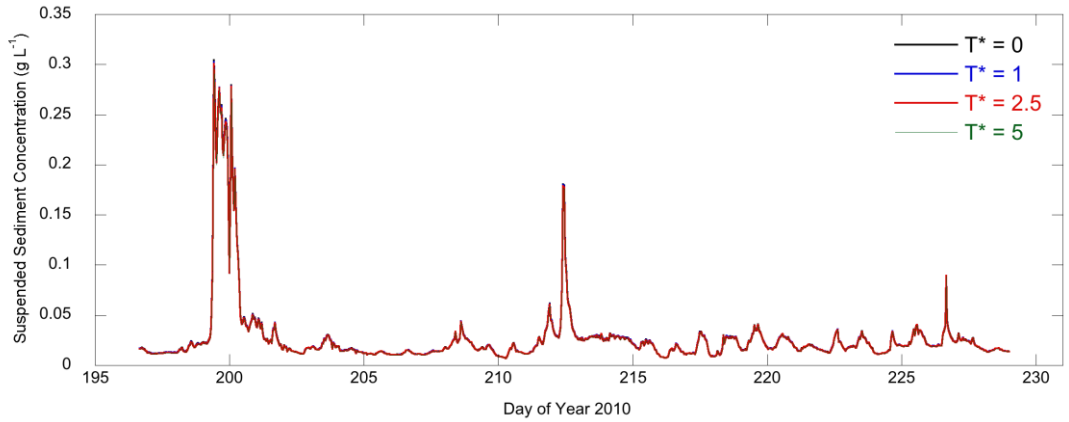


**Figure 6.22. Modelled suspended sediment concentration time series for Nordjåkk using four different values of $\tau$.**

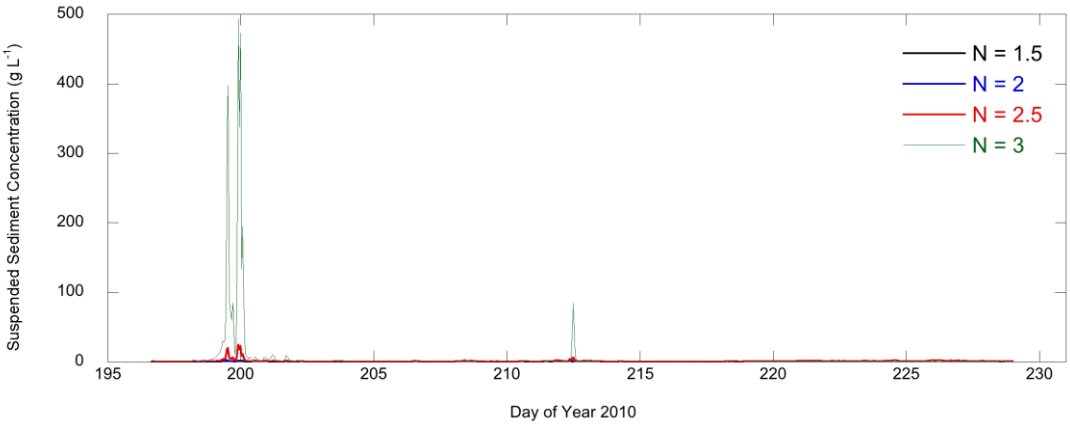


**Figure 6.23. Modelled suspended sediment concentration time series for Sydjåkk using four different values of $N$.**

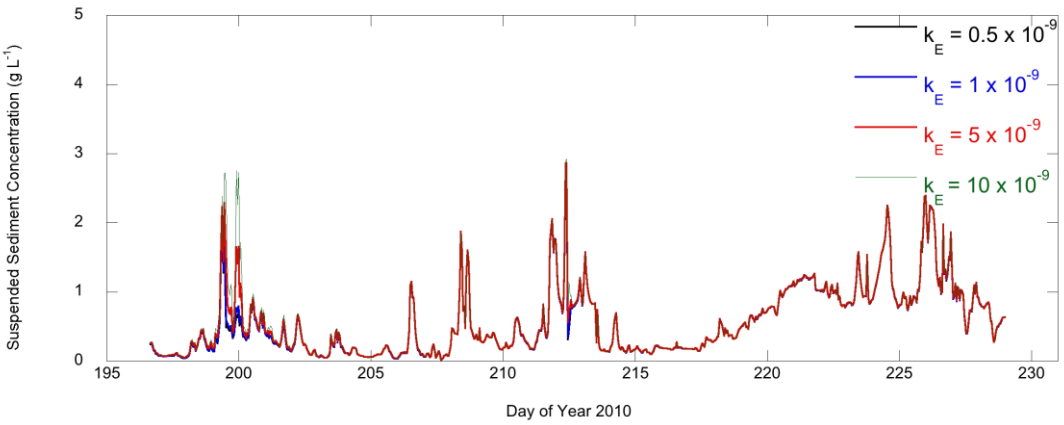


**Figure 6.24. Modelled suspended sediment concentration time series for Sydjåkk using four different values of $k_E$.**

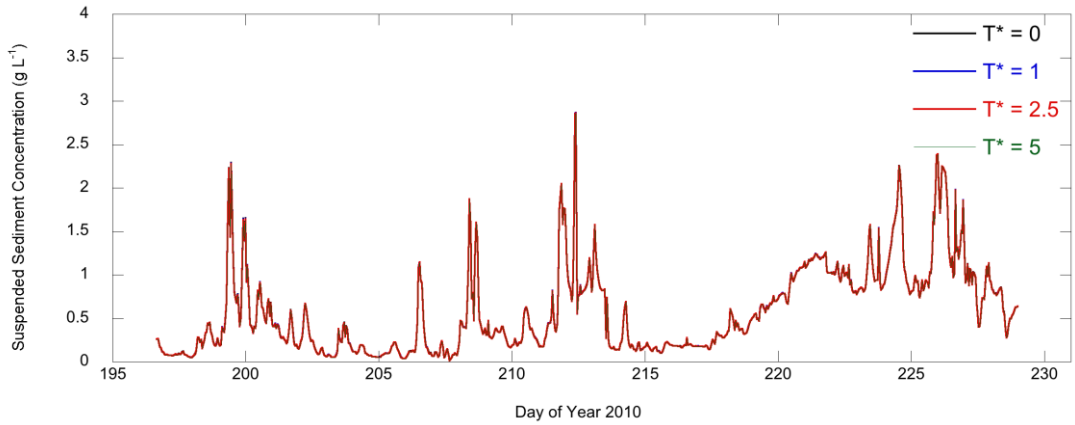


**Figure 6.25. Modelled suspended sediment concentration time series for Sydjåkk using four different values of $\tau$.**

Many of the parameters used in the model are based on the results of laboratory experiments which do not recreate the conditions observed in subglacial environments (Clarke, 1996a; Jones and Arnold, 1999). It is therefore prudent to evaluate the effects of changing variables on the model output. Based on the results presented in Figures 6.20 to 6.25 it appears that the modelled suspended sediment concentration time series change very little in response to changing model components. Varying threshold stress for erosion ($\tau^*$) for example has almost no effect on the suspended sediment time series, producing identical time series. Similarly, changing the erosion rate constant ($k_E$) has little effect on modelled suspended sediment concentration at either Nordjåkk or Sydjåkk, although some variations were apparent during peak events. At Nordjåkk (Figure 6.21) changing $k_E$ to 10 x $10^{-9}$ produces an overestimation of approximately 0.1 g $L^{-1}$, whilst a value of 1 x $10^{-9}$ produces an underestimation of approximately 0.5 g $L^{-1}$. The degree of overestimation is slightly less at Sydjåkk (approximately 0.5 g $L^{-1}$ when $k_E$ = 10 x $10^{-9}$) (Figure 6.24), although the general fit between the time series is similar to that observed at Nordjåkk. The greatest variation of suspended sediment concentration time series is observed in response to changes of the exponent for erosion law ($N$). Whilst little variation is observed with $N$ values of between 1.5 and 2.5, a value of 3 results in unreasonable model overestimation during peak events. At Nordjåkk (Figure 6.20), the overestimation around Day 199, the seasonal maximum is approximately 18 g $L^{-1}$, far above the observed

suspended sediment concentration for both Nordjåkk and Sydjåkk combined. At Sydjåkk (Figure 6.23), the overestimation on Day 199 is approximately 500 g $L^{-1}$. Jones and Arnold (1999) observed similar changes as a result of varying the value of $N$ above 1.6, describing the increase in both the mean and diurnal range of suspended sediment concentration as exponential. However, Jones and Arnold (1999) and Fausto *et al*. (2012) both recorded greater sensitivity to changes in $k_E$ and ($\tau^*$) than observed in this study.

**Table 6.8. Descriptive statistics of modelled suspended sediment concentration time series for Nordjåkk for each constant changed during sensitivity analysis. *Indicates values used in the original model run for comparison.**

| | $N$ = 1.5 | $N$ = 2* | $N$ = 2.5 | $N$ = 3 | $k_E$ = 0.5 x $10^{-9}$ | $k_E$ = 1 x $10^{-9}$ | $k_E$ = 5 x $10^{-9}$* | $k_E$ = 10 x $10^{-9}$ | $\tau^*$ = 0* | $\tau^*$ = 1 | $\tau^*$ = 2.5 | $\tau^*$ = 5 |
|---|---|---|---|---|---|---|---|---|---|---|---|---|
| Mean | 0.025 | 0.027 | 0.046 | 0.219 | 0.025 | 0.025 | 0.027 | 0.030 | 0.027 | 0.027 | 0.027 | 0.027 |
| Maximum | 0.271 | 0.304 | 1.764 | 20.460 | 0.270 | 0.271 | 0.304 | 0.428 | 0.304 | 0.303 | 0.301 | 0.297 |
| Minimum | 0.007 | 0.007 | 0.007 | 0.007 | 0.007 | 0.007 | 0.007 | 0.007 | 0.007 | 0.007 | 0.007 | 0.007 |
| St. Dev. | 0.029 | 0.036 | 0.129 | 1.279 | 0.029 | 0.030 | 0.036 | 0.044 | 0.036 | 0.036 | 0.036 | 0.036 |

**Table 6.9. Descriptive statistics of modelled suspended sediment concentration time series for Sydjåkk for each constant changed during sensitivity analysis. *Indicates values used in the original model run for comparison.**

| | $N$ = 1.5 | $N$ = 2* | $N$ = 2.5 | $N$ = 3 | $k_E$ = 0.5 x $10^{-9}$ | $k_E$ = 1 x $10^{-9}$ | $k_E$ = 5 x $10^{-9}$* | $k_E$ = 10 x $10^{-9}$ | $\tau^*$ = 0* | $\tau^*$ = 1 | $\tau^*$ = 2.5 | $\tau^*$ = 5 |
|---|---|---|---|---|---|---|---|---|---|---|---|---|
| Mean | 0.555 | 0.575 | 0.852 | 5.381 | 0.555 | 0.558 | 0.575 | 0.596 | 0.575 | 0.574 | 0.574 | 0.572 |
| Maximum | 2.815 | 2.865 | 23.862 | 492.963 | 2.815 | 2.820 | 2.865 | 2.921 | 2.865 | 2.864 | 2.862 | 2.858 |
| Minimum | 0.012 | 0.013 | 0.016 | 0.025 | 0.012 | 0.012 | 0.013 | 0.015 | 0.013 | 0.013 | 0.012 | 0.012 |
| St. Dev. | 0.491 | 0.501 | 1.854 | 35.342 | 0.491 | 0.491 | 0.501 | 0.528 | 0.501 | 0.501 | 0.501 | 0.500 |

## 6.4. Discussion

### 6.4.1. Drainage System Structure

Whilst linear reservoir models offer conceptual representations of the glacial drainage system, studies employing them often attempt to apply a physical interpretation to the reservoir themselves e.g. Hannah and Gurnell (2001), Hodgkins *et al*. (2013). There is clear evidence in the results of the linear reservoir model that Reservoir 1 represents a fast reservoir, whilst Reservoir 2 represents a slow reservoir in both outlet streams. Throughout the flow recession analysis, only one recession was characterised by a single reservoir. This suggests that an interpretation of the drainage system of Storglaciären based on bipartite parallel reservoirs (as concluded by Nilsson and Sundblad, 1975 and Hock and Noetzli, 1997) is appropriate. Furthermore, the concept of parallel reservoirs in polythermal glaciers is supported by evidence from Finsterwalderbreen (Hodgkins *et al*., 2013) and Hannabreen (Vatne *et al*., 1996). As Hodgkins *et al*. (2013) suggest, parallel reservoirs may be an appropriate approximation of drainage in polythermal glaciers generally.

Reservoir 1 at both Nordjåkk and Sydjåkk exhibits lower (faster) mean reservoir coefficients than Reservoir 2, and the maximum $K$ values observed in Reservoir 2 far exceed those observed in Reservoir 1. Furthermore, Reservoir 1 is the greatest contributor to the total discharge from both streams with a mean contribution of 76% of the total output, at Nordjåkk, and a mean contribution of 63% at Sydjåkk. The dominance of Reservoir 1 to total output is further supported by the results of the sensitivity analysis. These suggest that both discharge and RMSE change very little in response to variation in $K_2$ values in comparison with variation of $K_1$ values.

In comparing the two streams, it appears that Reservoir 1 at Nordjåkk is marginally faster that that at Sydjåkk (31 h and 34 h mean $K_1$ values

respectively). However, Reservoir 2 at Nordjåkk is considerably slower than that at Sydjåkk, exhibiting greater mean and maximum $K_2$ values. As described above however, the volume of meltwater routed through Reservoir 2 is consistently very small, and therefore higher $K_2$ values may have little effect on the overall residence time of water draining into Nordjåkk. A number of studies suggest that meltwater entering Nordjåkk is routed en- and supraglacially from the accumulation area, whilst Sydjåkk is largely routed subglacially (Östling and Hooke, 1986; Seaberg *et al*., 1988; Hock and Hooke, 1993; Hooke and Pohjola, 1994), which may explain the relative time differences in water routing between the two streams. The relationship between Reservoir 1 and Reservoir 2 at Sydjåkk is more complex, with a much greater volume of water routed though Reservoir 2, and periods where Reservoir 2 discharge exceeds that of Reservoir 1 (discussed further in Section 6.4.2.2).

### 6.4.2. Drainage System Evolution

#### 6.4.2.1. Nordjåkk

Low $K_1$ values (mean = 31 h) throughout the season at Nordjåkk indicate that drainage through the fast reservoir is relatively consistent. Despite this consistency, decline in $K_1$ values is apparent between Days 215 and 218, at which point the season minimum (6 h) is observed. This is consistent with the early-August establishment of Storglaciären's late-season drainage configuration, as suggested by Hock and Hooke (1993). The season minimum is immediately followed by a clear, although non-linear increase in $K_1$, reaching a season maximum on Day 229 (106 h). This decline is in keeping with similar studies (e.g. Collins, 1982; Hannah and Gurnell, 2001; Hodgkins *et al*., 2013), as is the end-of-season increase in $K_1$ values observed during the 2000 melt season at Finsterwalderbreen by Hodgkins *et al*. (2013). This trend is suggestive of a gradual, but slow increase in the efficiency of drainage through Nordjåkk. As discharge draining via Nordjåkk consists largely of meltwater

routed en- and supraglacially from the accumulation area (Hock and Hooke, 1993; Hooke and Pohjola, 1994), this could be attributed to the gradual retreat of the glacier snowline. Since snow and firn have naturally high residence times (Colbeck, 1972; Campbell *et al*., 2006; de Woul *et al*., 2006), removal of these slow flow pathways (e.g. through snowline retreat) limits meltwater delay through these media, and exposes larger areas of bare ice, facilitating rapid flow. This may also explain both the faster mean $K_1$ values at Nordjåkk compared to Sydjåkk (which is predominantly subglacially routed), and the slower mean $K_2$ values compared to Sydjåkk (resulting from the delay imposed by the snow and firn reservoirs).

$K_2$ values at Nordjåkk are more variable, showing no obvious increase or decline. However, given the small contributions to the total glacier discharge by Reservoir 2, this is likely to have little impact on the overall efficiency of the drainage system. The increase in $K_1$ towards the end of the season is attributed to a reduced input into the drainage system. As a result, this is unlikely to indicate any significant drainage system changes, but may suggest the release of water from storage as inputs decline, delaying the cessation of discharge (Fountain and Walder, 1998).

#### 6.4.2.2. Sydjåkk

Both $K_1$ and $K_2$ values at Sydjåkk are observed to increase as the melt season progresses, suggesting that both reservoirs are draining more slowly towards the end of the melt season. This is somewhat surprising given the presumed subglacial routing of Sydjåkk, as a change in the nature of subglacial conduits could be expected (e.g Nienow *et al*., 1998; Swift *et al*., 2002), increasing flow efficiency and reducing residence time. However, as glacier melt had already commenced before the monitoring period began, it is possible that the subglacial drainage system had already evolved, and was not substantially changed thereafter. Alternatively, it is possible that given the relatively low discharges observed in Sydjåkk and the lower relative contribution of meltwater to the total glacier discharge that meltwater inputs are insufficient

to allow significant evolution of the drainage system to occur. This is supported by the relationship between $Q_{start}$ and $K_1$ (Figure 6.9) which suggests that the reservoir coefficient increases at lower discharges. As noted in earlier chapters, discharge late in the 2010 season at Sydjåkk is close to the season minimum, and certainly below the seasonal mean discharge (0.45 $m^3s^{-1}$). The pattern of low or declining discharge may therefore either prevent or mask any drainage system evolution, especially as $K_1$ values appear to decline around Days 206 and 207 as discharge increases.

A number of periods in the modelled data (e.g. Days 207 to 210 and Days 217 to 219) suggest that Reservoir 2 surpasses Reservoir 1 as the main contributor of discharge in Sydjåkk. These periods coincide with decreases in $K_2$ values (often reflecting faster drainage than $K_1$ values). These periods may reflect some shifts in the configuration of the drainage system (e.g. Bartholomew *et al*., 2011), although it may be more likely that they occur due to the periodic release of water from storage. This is supported by the fact that during these periods, both discharge and inputs are low. This is a similar pattern to that observed by Willis *et al*. (1993) at Midtalsbreen, Norway, where the release of water from storage occurred in response to declining meltwater input.

### 6.4.3. Suspended Sediment Transfer

The degree to which the sediment transfer model systematically underestimates suspended sediment concentration at both Nordjåkk and Sydjåkk suggests that the application of the model has not been successful. Whilst the relative temporal pattern of suspended sediment concentration is well simulated, the greatest failing of the model lies in the simulation of magnitude. Sensitivity analysis suggests that the model is largely insensitive to the variation of constant parameters (other than that of $N$) and therefore changing these does not 'improve' the model output. Despite these

shortcomings, there are however a number of interesting points to be taken from the modelled data.

The model fit for Sydjåkk is the weaker of the two streams (the observed series mean is almost double that of the modelled series). Sydjåkk carries a considerably greater sediment load than Sydjåkk (mean = 1.17 g $L^{-1}$ compared with 0.06 g $L^{-1}$ at Nordjåkk). As the difference between the observed and modelled time series at Sydjåkk appears to be at its least during periods of lower suspended sediment concentration variability, it may be possible that the model performs better in streams with lower, less dynamic sediment loads (such as Nordjåkk).

The relatively low levels of erosion combined with the model underestimation may be indicative of non-glacial sediment contributions. Results in previous chapters have suggested the possibility of ice-marginal sediment transfer as an important geomorphic process at Storglaciären, particularly on the southern margin of the glacier drained by Sydjåkk. Although the model uses the observed suspended sediment concentration time series as an input, modifying it to account for erosion and sedimentation within the stream channel, sediment input along the entire channel reach is not accounted for. This may suggest that model underestimation during certain periods (e.g. late in the 2010 melt season at Sydjåkk) is the result of sediment fluxes which are not parameterised in the model setup.

## 6.5. Summary

Based on the interpretations discussed in Section 6.4, the following conclusions can be drawn regarding the nature of the drainage system and suspended sediment transfer at Storglaciären.

- The drainage system at Storglaciären can be characterized by two parallel reservoirs: one fast and one slow. The faster reservoir (Reservoir 1) is likely to principally act as a flow pathway for

supraglacial and englacial meltwater, whilst the slower reservoir (Reservoir 2) acts a flow pathway for subglacially routed meltwater. Reservoir 1 is the dominant pathway at both Nordjåkk and Sydjåkk, whilst Reservoir 2 contributes only a small proportion of the total discharge.

- Analysis of flow recession data from Nordjåkk indicates that drainage system evolution does occur at Storglaciären, with a marked decline of reservoir coefficient values apparent towards the middle of the season. A similar pattern is not observed at Sydjåkk, although this is attributed either to drainage system evolution occurring at Sydjåkk prior to the monitoring period commencing, or to low discharge data 'masking' evidence of evolution due to their influence on *K* values.

- The application of a sediment transfer model to Storglaciären provides time series which accurately simulate the temporal change in, but systematically underestimate suspended sediment concentration. Sensitivity analysis suggests that the model is insensitive to changing parameters, and the underestimation cannot therefore be explained by the model setup. However it is suggested that the model may respond better when applied to streams with lower, less dynamic suspended sediment concentrations. Furthermore, underestimation may occur due to the role of ice-marginal sediment transfer, which is not accounted for in the model setup.

*Chapter 7*

# Synthesis and Discussion

## 7.1. Introduction

### 7.1.1. Aims of Chapter

This chapter draws together the results from preceding chapters into a synthesising discussion of patterns of discharge and suspended sediment delivery to the proglacial area of Storglaciären. Section 7.1.2 summarises the aims of the study introduced in Chapter 1, Section 7.2 reviews the approaches and techniques employed for each chapter of the thesis, and Section 7.3 describes the main findings of the chapters.

### 7.1.2. Review of Study Aims

The purpose of this study was to contribute to the understanding of suspended sediment transfer in glacierised basins through the investigation of patterns of suspended sediment delivery to the proglacial area of Storglaciären, a small polythermal valley glacier located in the Tarfala valley, arctic Sweden. The specific objectives of the study were:

i. To identify key meteorological drivers of discharge generation in the Storglaciären basin

ii. To assess the variability of discharge between two proglacial outlet streams of Storglaciären: Nordjåkk and Sydjåkk.

iii. To assess seasonal-scale variability in suspended sediment delivery to the proglacial area of Storglaciären

iv. To investigate the nature of the drainage system of Storglaciären and identify periods of drainage system evolution.

v. To understand the underlying factors which influence suspended sediment transport at Storglaciären.

vi. To assess the applicability of physically based sediment transfer model in predicting suspended sediment delivery in the Storglaciären basin.

It was anticipated that realisation of these objectives would enable important information to be gained on the processes by which suspended sediment in the Storglaciären basin is entrained and transported, and how these respond to changing patterns of discharge and meteorological variables.

## 7.2. Review of Approaches and Thesis Structure

### Chapter 3 – Patterns of Proglacial Discharge Variability

The aims of this chapter were to investigate discharge patterns in the proglacial area of Storglaciären and the factors which influence them. The chapter outlined the methods used to collect and prepare discharge data from two outlet streams during two summer field seasons (2009 and 2010). Principal component analysis using discharge time series and meteorological variables as inputs allowed drivers of discharge generation at Storglaciären to be identified. Further analysis of the discharge time series enabled differences in discharge delivery to the proglacial area to be assessed.

### Chapter 4 - Temporal Patterns of Suspended Sediment Transfer

The aims of this chapter were to assess seasonal suspended sediment delivery to the proglacial area of Storglaciären through analysis of the diurnal relationship between stream discharge and suspended sediment concentration. The chapter outlined the methods used to collect suspended sediment and continuous turbidity

data at Storglaciären during the 2009 and 2010 field seasons, and details of techniques used to fill gaps in the data were explained. Hysteresis and linear regression techniques were used to identify changes in the seasonal suspended sediment time series which may indicate changes in processes which influence suspended sediment delivery.

**Chapter 5 – Drivers of Suspended Sediment Transport**

The aim of this chapter was to utilise techniques of principal component analysis and hierarchical cluster analysis to more closely examine patterns in the suspended sediment time series collected at Storglaciären during the 2009 and 2010 ablation seasons. The chapter described the statistical techniques used to identify changes in suspended sediment time series shape and magnitude, and to classify periods of similar meteorological response. These data were then used to identify factors which influence suspended sediment delivery to the proglacial area of Storglaciären.

**Chapter 6 - Modelling of Meltwater Routing and Suspended Sediment Transfer**

The aim of this chapter was to elucidate patterns of water routing through Storglaciären using a combination of flow-recession analysis and linear-reservoir modelling. The chapter also assess the applicability of a physically based suspended sediment transfer model which will allow suspended sediment concentration to be predicted in response to changing hydrological and physical processes. These data were used to identify the nature of the glacial drainage system, and periods of drainage system evolution and rationalisation.

## 7.3. Summary of Major Findings

Based on the results presented in Chapter 3 it is suggested that the primary control on discharge generation at Storglaciären is ablation. However, there is a marked difference in the precise drivers at each proglacial outlet stream monitored in this study. Discharge at Sydjåkk is dominated by precipitation (specifically rainfall), whereas discharge at Nordjåkk appears not to have a primary driver, but responds equally to forcing by ablation and precipitation.

Based on the results presented in Chapter 4 it is interpreted that suspended sediment transfer in the proglacial area of Storglaciären differs between Nordjåkk and Sydjåkk. It is well established that Sydjåkk carries a greater suspended sediment load than Nordjåkk (e.g. Seaberg *et al*., 1988; Hooke and Pohjola, 1994), and this is reflected in the data collected with the mean suspended sediment concentration at Sydjåkk exceeding that at Nordjåkk by an order of magnitude in both 2009 and 2010. However it also appears that suspended sediment transport at Sydjåkk is more complex than at Nordjåkk. Periods of highly variable suspended sediment concentration which occur independently of discharge indicate shifts in the subglacial drainage system towards the middle of the season, and mobilisation of ice-marginal sediment sources late in the season. Both streams exhibit patterns of suspended sediment supply exhaustion, but these are relatively short lived, suggesting that new sediment sources are quickly tapped, recharging the glacial drainage system.

Based on the results presented in Chapter 5, it is suggested that patterns of suspended sediment transfer differ greatly between Nordjåkk and Sydjåkk. Under 'normal' conditions (i.e. days not classified as containing high magnitude suspended sediment transport by hierarchical cluster analysis), the principal driver of suspended sediment transport at Nordjåkk is ablation-driven discharge. Conversely, the principal driver of suspended sediment transport at Sydjåkk is rainfall, possibly as a result of mobilisation of material from ice-marginal sources.

However, this pattern is reversed during periods of high magnitude suspended sediment transport, with high suspended sediment concentrations instigated by rainfall at Nordjåkk, and ablation-driven discharge at Sydjåkk. In both the 2009 and 2010 ablation seasons, principal component and hierarchical cluster analyses suggest that the greatest volumes of suspended sediment are entrained and transported during 'warm' and 'wet' meteorological periods. 'Warm' days are the dominant driver of suspended sediment transport at both streams, although 'wet' days appear to have a greater influence at Sydjåkk than at Nordjåkk.

Based on the results presented in Chapter 6, it is suggested that the drainage system of Storglaciären is best characterised by two linear reservoirs acting in parallel, as suggested by Nilsson and Sundblad (1975) and Hock and Noetzli (1997). The two reservoirs take the forms of a fast and a slow reservoir, the faster responsible for the routing of supra- and englacial meltwater, and the slow reservoir responsible for subglacial drainage. The relative dominance of each reservoir at Nordjåkk and Sydjåkk, indicates that previous suggestions of the source of meltwater draining into each stream (e.g. Östling and Hooke, 1986; Seaberg *et al*., 1988; Hock and Hooke, 1993; Hooke and Pohjola, 1994) are correct. Meltwater contribution into Nordjåkk is therefore primarily snow and ice melt routed supraglacially or through the englacial drainage system, whilst Sydjåkk is primarily subglacial. The drainage system of Storglaciären does exhibit patterns of subglacial evolution through the course of the melt season as observed in a number of studies (e.g. Nienow *et al*., 1998; Cowton *et al*., 2013). However, this evidence is only observed at Nordjåkk, suggesting that evidence of evolution at Sydjåkk is either masked, or occurred outside of the study monitoring period. A sediment transfer model was applied to assess its applicability in predicting suspended physically-based sediment concentration at Storglaciären. Ultimately this was unsuccessful, although the model may have been limited by its inability to account for ice-marginal sediment transfer.

### 7.3.1. Suspended Sediment Transport in the Storglaciären Basin

The findings summarised above and presented in Chapters 4 and 5 are suggestive of a complex system of suspended sediment transfer. Both patterns of suspended sediment delivery to the proglacial area, and the processes that influence them vary widely across the glacier terminus. Variations between proglacial streams are not uncommon (e.g. Orwin and Smart, 2004), although at Storglaciären such variations appear to reflect the nature of the bipartite glacial drainage system as described by Stenborg (1973). Data from both Nordjåkk and Sydjåkk suggest that peak suspended sediment availability occurs early in the ablation season. This is typical of temperate glaciers, where increasing meltwater production reopens subglacial drainage networks following their closure during winter (Bogen, 1991; Lawson, 1993). However, whilst Nordjåkk exhibits a trend of progressively decreasing suspended sediment response to discharge as the ablation season progresses, suspended sediment concentration on Sydjåkk increases towards the end of the season, almost equalling the earlier season maximum. This has been interpreted as the result of ice-marginal suspended sediment mobilisation possibly from an ice-cored moraine. These patterns of suspended sediment transport are suggestive of two discrete suspended sediment transfer regimes: one typical of polythermal glaciers as observed by (e.g.) Repp (1988), Bogen (1991), Hodgkins (1996) and Hodson and Ferguson (1999), and one typical of temperate glaciers as observed by (e.g.) Richards (1984) and Gurnell (1987). As a result, it could be speculated that suspended sediment transport at Storglaciären may be a hybrid of both temperate and non-temperate processes. In this hybrid model, Sydjåkk exemplifies a non-temperate sub-aerial glacial stream, where contributions of ice-marginal sediment are high, and Nordjåkk typifies a temperate glacial stream with high early season suspended sediment availability, and an increasing pattern of sediment supply exhaustion. However, it is not clear whether this occurs as a result of the thermal regime of Storglaciären, or whether it indicates discontinuous processes on both ice-margins, e.g. little or no significant ice-marginal sediment mobilisation at the northern ice margin. Gusmeroli (2010) suggests that continued slow and persistent thinning of the cold surface layer of Storglaciären due to warming air temperatures may cause the thermal regime of

the glacier to shift from polythermal to fully temperate, although further research would be required to fully assess the implications for glacier drainage and subsequently, suspended sediment transport. Under a warming climate, thermal regime evolution of glaciers is increasingly possible (Vincent *et al*., 2007; Huggel, 2009) and the nature of the drainage system of Storglaciären as described above may become increasingly common in polythermal glaciers, influencing patterns of suspended sediment transport in high-latitudes.

Based on IPCC model projections (Meehl *et al*., 2007) mean annual air temperatures in northern Europe are predicted to increase at a rate above the global mean. Under this scenario, northern Europe will see a twenty-year mean temperature increase of between 2 – 5.3°C. Furthermore, regions above 55°N are predicted to receive increased precipitation, and a shortened snow season. (Meehl *et al*., 2007). Under these conditions, the Tarfala valley is likely to see earlier snow line retreat due to both reduced winter snow cover, larger bare ice areas and increasing air temperatures, both of which will increase the production of meltwater. The results presented in Chapter 5 suggest that throughout the ablation season, Sydjåkk increasingly responds to precipitation (as a driver for ice-marginal sediment mobilisation), and Nordjåkk increasingly responds to ablation. Earlier snow line retreat and production of bare ice areas will increase the speed of supraglacial runoff, further contributing to the delivery of water to the glacier bed and proglacial area. As a result, short term suspended sediment yield from both the northern and southern terminus are likely to increase, since the dominant drivers of suspended sediment entrainment and transport will be facilitated by a changing climate (Knight and Harrison, 2012; Keiler *et al*., 2013). It is speculated that the greatest implications of such increases will be felt downstream of the Tarfala Valley, where the Tarfalajåkk feeds into the larger Láddjujohka, and ultimately the lakes Láddjujávri and Lakkujärvi. Increased sediment yield from the Tarfala valley may result in increased fluvial deposition of fine sediment in these water bodies, decreasing channel (or lake) depth and increasing flood risk (Østrem and Olsen, 1987; Keiler *et al*., 2013). Furthermore, fish spawning may be negatively affected by changes in oxygen and nutrient levels, and by diminished

light transmission through the water column as a result of increased sediment transport (Sear, 1993; Wood and Armitage, 1997; Petticrew and Rex, 2006; Kemp *et al*., 2011). In March 2012, a plane crash into the west-facing wall of the Kebnekaise range resulted in the distribution of Jet A fuel over Rabots Glaciär, Bjorlings Glaciär and Storglaciären. This increases the possibility that meltwater and, as a result, suspended sediment delivered downstream of the Tarfala valley may be contaminated with hydrocarbons, further damaging habitats, and providing a health risk for local residents (Lipiatou and Saliot, 1991; Dauvalter and Rognerud, 2001; MacDonald *et al*., 2002; Bogdal *et al*., 2009). Settlements such as Nikkaluokta are likely to bear the brunt of these changes, adversely affecting the lives of the local Sami population. On a broader scale, the results of this study are likely to be of interest to the hydroelectric power industry. Although no hydroelectric dams are situated directly downstream of Storglaciären, hydroelectric power accounts for ~45% of Sweden's total electricity generation, and a number of large scale (>10 MW) hydropower stations are located in northern Sweden (Rudberg, 2013) where glacially derived fluvial suspended sediment is abundant. Whilst these schemes themselves have considerable influence on local fluvial geomorphology (Gurnell, 1983; *et al*., 1990) they are also vulnerable to changes in fluvial suspended sediment transport which can reduce channel or reservoir volume behind the structure, and damage intakes and turbines through abrasion (Bogen, 1989; Padhy and Saini, 2008).

In spite of these projections, it is possible however, that increased meltwater or rainfall input to the glacier bed may result in much more rapid suspended sediment evacuation, causing the glacial drainage system to become exhausted much more quickly. This study suggests that periods of exhaustion are currently short-lived, and that sediment sources are recharged quickly. However, if the rate of sediment evacuation is greater than the rate of recharge over a sustained period, this may no longer be possible, and may result in a seasonal pattern of exhaustion similar to that observed in temperate glacier basins (Østrem, 1975; Bogen, 1995; Collins, 1990; Hammer and Smith, 1983; Leistøl, 1967; Hooke *et al*., 1985).

## 7.4. Limitations of the Study

The greatest limitation faced in this study was the lack of complete data sets from the 2009 ablation season. Gaps in the 2010 ablation season data were filled using a combination of interpolation and linear-regression technique. However, it was felt that to replicate these processes in 2009 given the proportion of missing data would not have yielded any advantage, and may have limited the accuracy of the seasonal data set. As a result, analyses were applied as much as possible, although comparison with the 2010 data was hindered, and true interannual variability of discharge and suspended sediment processes was difficult to assess. For this reason, no interpretations of the 2009 data sets were attempted in the thesis, although analyses in the form of plots and tables were included for the sake of openness and completeness. Therefore, further research may be necessary to fully understand annual variability in proglacial meltwater and suspended sediment delivery at Storglaciären.

*Chapter 8*

# Conclusions and Future Research

## 8.1. Conclusions

This study has shown that suspended sediment transfer at Storglaciären is strongly influenced by both meteorological conditions and the nature of the glacial drainage network. As previously stated by several studies, patterns of suspended sediment delivery differ across the glacier terminus, with the northern outlet stream, Nordjåkk, carrying a relatively small concentration of suspended sediment compared with the southern outlet stream, Sydjåkk. However, both streams also differ in terms of the suspended sediment-discharge hysteretic relationship. Whilst Nordjåkk exhibits evidence of a decreasing suspended sediment response to discharge peaks as the season progresses (and hence exhaustion), Sydjåkk shows a trend of increasing suspended sediment concentration late in the ablation season, and large-scale increases in suspended sediment concentration independent of discharge. This has led to speculation that the two streams have each assumed characteristics typical of different models of glacier drainage: Nordjåkk, a temperate glacier stream experiencing progressively decreasing suspended sediment concentrations throughout the ablation season; and Sydjåkk, a sub-aerial non-temperature glacier stream receiving considerable suspended sediment contributions from ice-marginal (non-glacial) sources. However, whether this occurs as the result of the thermal regime of the glacier or the bipartite glacial drainage system is unclear, and warrants further research in order to better understand the glaciological implications.

The differences in suspended sediment transport between the two streams are compounded by differences in how suspended sediment transport is influenced meteorologically. Deconstruction of suspended sediment time series into discrete

classes of diurnal sedigraph shape and magnitude suggests that suspended sediment transport at Nordjåkk increases when discharge is ablation driven. Conversely, suspended sediment at Sydjåkk increases due to rainfall. These differences are interpreted as a consequence of routing, where rainfall entrains greater volumes of non-glacial suspended sediment into Sydjåkk, and rapid supraglacial runoff over bare ice areas augments discharge in Nordjåkk, thereby increasing the stream erosive capacity. However, these differences are reversed during high magnitude events, with ablation driving suspended sediment transport at Sydjåkk, and rainfall driving suspended sediment transport at Nordjåkk. This is interpreted as reflecting the routing characteristics of each stream, especially the subglacially routed Sydjåkk as greater volumes of water access the glacier bed in response to increased meltwater generation. Nonetheless, data from both streams suggest that ablation is still the primary driver of suspended sediment transport at Storglaciären, with the greatest percentage of total seasonal suspended sediment load transport occurring during days classified as 'warm'. In a warming climate, this is likely to have a significant effect on the volume of suspended sediment transported, and the patterns of delivery to the proglacial area. For example, Stott and Mount (2007) found that suspended sediment load delivery to the proglacial area of Glacier Noir, France, was approximately three to four times higher in July 2003 (a European heatwave year [Beniston, 2004; Black *et al*., 2004]) than in July 2004 (a comparatively 'normal' year).

Hydrologically, the results collected during the study suggest that ablation is the dominant control upon discharge generation at Storglaciären. However, similarly to the stream-specific patterns of suspended sediment transport, the dominant meteorological driver of discharge differs at both stream gauging sites. Sydjåkk is driven principally by precipitation-generated discharge, whilst Nordjåkk is not influenced by one specific meteorological variable, and responds equally to precipitation and ablation. It is concluded here that these differences reflect the routing characteristics of each stream, with supraglacial runoff over bare ice areas possibly explaining that lack of a specific driver at Nordjåkk. These routing characteristics are confirmed by flow-recession analysis and linear reservoir

modelling, which suggest that meltwater routing is performed by two parallel reservoirs, one faster than the other.

## 8.2. Suggestions for Future Research

Whilst this study has advanced our understanding of the nature of discharge generation and suspended sediment transport in the Storglaciären basin, a number of further investigations may provide further information on the mechanisms of sediment evacuation.

Firstly, whilst a number of studies focusing on the drainage system of Storglaciären have previously been conducted (e.g. Stenborg, 1973; Kohler, 1995; Holmlund, 1988) the differences in suspended sediment delivery and discharge drivers between Nordjåkk and Sydjåkk warrant that this area is revisited. Specifically, dye tracing of the area downstream of the riegel would allow differences in the lag times between Nordjåkk and Sydjåkk to be better understood. It may also be possible to use tracers to monitor non-glacial sediment mobilization (e.g. Collins *et al*., 1998; Walling *et al*., 1999; Owens *et al*., 2005; Navratil *et al*., 2012; D'Haen *et al*., 2013), although this would require careful planning to ensure that any tracer used only entered the stream channel in conjunction with suspended sediment.

Secondly, as stated in Section 8.1, mean patterns of diurnal discharge during the 2009 ablation season exhibit a pattern which suggests considerable lags in peak discharge. Whilst tracing techniques as mentioned above may reveal delays in glacier drainage, an initial analysis of previous years data may be a productive first step. Discharge data from the Rännan gauging station is likely to contain similar patterns to that collected for Nordjåkk and Sydjåkk, and the creation of mean diurnal hydrographs would suggest whether the data collected during the 2009 ablation season represents an anomalous single year, or is indicative of as yet unknown larger scale processes.

Thirdly, the temperate/non-temperate models of glacier drainage observed at Nordjåkk and Sydjåkk could be further investigated in relation to the thermal

regime of the glacier. As the evolution of glacier thermal regimes from polythermal to temperate has already been observed (e.g. Vincent *et al.*, 2007; Huggel, 2009), understanding the implications for meltwater production, routing and sediment transport is of key importance. Winter ground penetrating radar surveys of the area around the stream outlets may reveal the nature of the cold surface layer across the terminus, and deployment of thermistors during the ablation season would allow seasonal englacial temperature changes to be monitored.

# *References*


Alley, R. B., Cuffey, K. M., Evenson, E. B., Strasser, J. C, Lawson, D. E. and Larson, G. J. 1997. How glaciers entrain and transport basal sediment: physical constraints. *Quaternary Science Reviews* **19** (9), 1017-1038.

Alley, R. B., Lawson, D. E., Evenson, E. B., Strasser, J. C., and Larson, G. J. 1998. Glaciohydraulic supercooling: a freeze-on mechanism to create stratified, debris-rich basal ice: II. Theory. *Journal of Glaciology.* **44**, 563–569.

Alley, R. B., Lawson, D. E., Evenson, E. B., and Larson, G. J. 2003. Sediment, glaciohydraulic supercooling, and fast glacier flow. *Annals of Glaciology*, **36**, 135-141.

Alley, R. B., Dupont, T. K., Parizek, B. R. and Anandakrishnan, S. 2005. Access of surface meltwater to beds of sub-freezing glaciers: preliminary insights. *Annals of Glaciology* **40**, 8-14.

Andreassen, L. M., Van Den Broeke, M. R., Giesen, R. H. and Oerlemans, J. 2008. A 5 year record of surface energy and mass balance from the ablation zone of Storebreen, Norway. *Journal of Glaciology* **54** (185), 245-258.

Andréasson, P. and Gee, D. 1989. Bedrock geology and morphology of the Tarfala area, Kebnekaise Mts., Swedish Caledonides. *Geografiska Annaler. Series A. Physical Geography* **71** (3), 235–239.

Aschwanden, A. and Blatter, H. 2009. Mathematical modeling and numerical simulation of polythermal glaciers. *Journal of Geophysical Research. F. Earth Surface*, **114** (F1), F01027.

Baird, G. B. 2005. On the bedrock geology of the Tarfala Valley: Preliminary results of 2003 and 2004 fieldwork. In: Jansson, P. (Ed). *Tarfala Research Station Annual Report, 2003-2004* **2B**(1), 1-5.

Baker, D., Escher-Vetter, H., Moser, H., Oerter, H. and Reinwarth, O. 1982. A glacier discharge model based on results from field studies of energy balance, water storage and flow. *International Association of Hydrological Sciences Publication* **138**, 103-112.

Barry, R. G. 2006. The status of research on glaciers and global glacier recession: a review. *Progress in Physical Geography* **30** (3), 285-306.

Bartholomew, I., Niewnow, P., Sole, A., Mair, D., Cowton, T., Palmer, S. and Wadham, J. 2011. Supraglacial forcing of subglacial drainage in the ablation zone of the Greenland Ice Sheet. *Geophysical Research Letters* **38**, L08502, doi:10.1029/2011GL047063.

Beniston, M. 2004. The 2003 heat wave in Europe: A shape of things to come? An analysis based on Swiss climatological data and model simulations. *Geophysical Research Letters* **31**, 2022–2026, L02202. doi:10.1029/2003GL018857.

Bezinge, A. 1987. Glacial meltwater streams, hydrology and sediment transport: The case of the Grande Dixence hydroelectricity scheme. In: Gurnell, A.M and Clark, M.J. (Eds.), *Glacio–fluvial sediment transfer: An Alpine perspective*. Wiley, Chichester, 473–498.

Bhattacharyya, P. and Hudleston, P. 2001. Strain in ductile shear zones in the Caledonides of northern Sweden: a three-dimensional puzzle. *Journal of Structural Geology* **23** (10), 1549–1565.

Bindschadler, R., Choi, H. 2007. Increased water storage at ice-stream onsets: a critical mechanism? *Journal of Glaciology* **53** (181), 163-171.

Black, E, Blackburn, M., Harrison, G., Hoskins, B. and Methven, J. 2004. Factors contributing to the summer 2003 European heatwave. *Weather* **59** (8), 217-223.

Blyth, S., Groombridge, B., Lysenko, I., Miles, L. and Newton, A. 2002. Mountain Watch. *Environmental Change and Sustainable Development in Mountains*. UNEP World Conservation Monitoring Centre, Cambridge.

Björnsson, H. 1981. Radio-echo sounding maps of Storglaciären, Isfallsglaciären and Rabots Glaciär, northern Sweden. *Geografiska Annaler. Series A. Physical Geography* **63** (3), 225–231.

Bogdal, C., Schmid, P., Zennegg, M., Anselmetti, F.S., Scheringer, M. and Hungerbühler, K. 2009. Blast from the Past: Melting Glaciers as a Relevant Source for Persistent Organic Pollutants. *Environmental Science and Technology* ***43*** (21), 8173-8177.

Bogen, J. 1980. The hysteresis effect of sediment transport systems. *Norsk Geografisk Tidsskrift-Norwegian Journal of Geography* **34** (1), 45–54.

Bogen, J. 1989. Glacial sediment production and development of hydro-electric power in glacierized areas. *Annals of Glaciology* **13**, 6-11.

Bogen, J. 1991. Erosion and sediment transport in Svalbard. In: Gjessing, Y., Hagen, J. O., Hassel, K. A., Sand, K. and Wold, B. (Eds), Arctic Hydrology. Present and Future Tasks, *Norwegian National Committee for Hydrology Report* **23**, Oslo, 1991, 147–158.

Bogen, J. 1996. Erosion rates and sediment yields of glaciers. *Annals of Glaciology* **22**, 48-52.

Boon, S. and Sharp, M. 2003. The role of hydrologically-driven ice fracture in drainage system evolution on an Arctic glacier. *Geophysical Research Letters* **30** (18), 4.

Brabets, T. P., March, R. S. and Trabant, D. C. 2004. Glacial history and runoff components of the Tlikakila river basin, Lake Clark National Park and Preserve, Alaska. *U.S. Geological Survey, Scientific Investigations Report* – 5057.

Braithwaite, R. 2002. Glacier mass balance: the first 50 years of international monitoring. *Progress in Physical Geography* **26** (1), 76-95.

Braithwaite, R. and Zhang, Y. 1999. Modelling changes in glacier mass balance that may occur as a result of climate changes. *Geografiska Annaler Series A. Physical Geography* **81** (4), 489–496.

Brock, B., Willis, I. & Sharp, M.J. 2000. Measurement and parameterization of albedo variations at Haut Glacier d'Arolla, Switzerland. *Journal of Glaciology* **46** (155), 675–688.

Bronge, C. 1996. The Excavation of the Storglaciären trough during the Quaternary. *Geografiska Annaler. Series A. Physical Geography* **78** (2), 163–169.

Bronge, C. and Openshaw, A. 1996. New instrument for measuring water discharge by the salt dilution method. *Hydrological Processes* **10** (3), 463–470.

Brugman, M.M. 1986. *Water flow at the base of a surging glacier*, California Institute of Technology, Pasadena, CA, USA, 267pp.

Campbell, F., Nienow, P. and Purves, R. 2006. Role of the supraglacial snowpack in mediating meltwater delivery to the glacier system as inferred from dye tracer investigations. *Hydrological Processes* **20** (4), 969–985.

Carrivick, J. L. and Brewer, T. 2004. Improving local estimations and regional trends of glacier equilibrium line altitudes. *Geografiska Annaler. Series A. Physical Geography* **86** (1), 67–79.

Chen, C., 1991. Unified theory on power laws for flow resistance. *Journal of Hydraulic Engineering* **117** (3), 371–389.

Chen, J. and Ohmura, A. 1990. On the influence of Alpine glaciers on runoff. Hydrology in Mountainous Regions I. *Hydrological Measurements; The Water Cycle*. Lausanne Symposia, 117–125.

Chin, A. 2002. The periodic nature of step-pool mountain streams. *American Journal of Science* **302** (2), 144.

Chow, V., Maidment, D. and Mays, L. 1998. *Applied Hydrology*, McGraw-Hill, New York.

Church, M. and Gilbert, R. 1975. Proglacial fluvial and lacustrine environments. In *Glaciofluvial and Glaciolacustrine Sedimentation*, Special Publication **23**. 22-100.

Clarke, G.K.C. 1996a. Lumped-element model for subglacial transport of solute and suspended sediment. *Annals of Glaciology* **22**, 152-159.

Clarke, G.K.C. 1996b. Lumped-element analysis of subglacial hydraulic circuits. *Journal of Geophysical Research* **101** (B8), 17,547-17,559.

Clifford, N.J., Richards, K. S., Brown, R. A., Lane, S. N. 1995. Laboratory and field assessment of an infrared turbidity probe and its response to particle size and variation in suspended sediment concentration. *Hydrological Sciences Journal* **40** (6), 771–791.

Colbeck, S. C. 1972. A theory of water percolation in snow. *Journal of Glaciology* **11** (63), 369-385.

Colbeck, S. C. 1973. Theory of metamorphism of wet snow. U.S. *Cold Regions Research and Engineering Laboratory Research Report* **313**.

Collins, A.L., Walling, D.E., and Leeks, G.J.L. 1998. Use of composite fingerprints to determine the provenance of the contemporary suspended sediment load transported by rivers. *Earth Surface Processes and Landforms* **23** (1), 31-52.

Collins, D. N. 1979a. Quantitative determination of the subglacial hydrology of two alpine glaciers. *Journal of Glaciology* **23** (29): 347-362.

Collins, D. N. 1979b. Sediment concentration in melt waters as an indicator of erosion processes beneath an alpine glacier. *Journal of Glaciology* **23**, 247-257.

Collins, D. 1982. Water storage in an Alpine glacier. *International Association of Hydrological Sciences Publication* **138**, 113–122.

Collins, D. N. 1989. Seasonal development of subglacial drainage and suspended sediment delivery to meltwaters beneath an Alpine glacier. *Annals of Glaciology* **13**, 45-50.

Collins, D. N. 1990. Seasonal and annual variations of suspended sediment transport in meltwaters draining from an Alpine glacier. *International Association of Hydrological Sciences Publication* **193**, 439-446.

Collins, D. 1998. Outburst and rainfall-induced peak runoff events in highly glacierized Alpine basins. *Hydrological Processes* **12** (15), 2369–2381.

Cooper, R. J. 2003. Chemical Denudation in the proglacial zone of Finsterwalderbreen, Svalbard. Unpublished Ph.D. Thesis, University of Bristol, School of Geographical Sciences. U.K.

Cowton, T., Nienow, P., Sole, A., Wadham, J., Lis, G., Bartholomew, I., Mair, D. and Chandler, D. 2013. Evolution of drainage system morphology at a land-terminating Greenlandic outlet glacier. *Journal of Geophysical Research: Earth Surface* **118**, 29-41.

Cunderlik, J.M. and Ouarda, T.B.M.J. 2009. Trends in the timing and magnitude of floods in Canada, *Journal of Hydrology* **375** (3–4), 471-480.

Cutler, P. 1998. Modelling the evolution of subglacial tunnels due to varying water input. *Journal of Glaciology* **44** (148), 485–497.

D'Haen, K., Dusar,B., Verstraeten, G., Degryse, P., and De Brue, H. 2013. A sediment fingerprinting approach to understand the geomorphic coupling in an eastern Mediterranean mountainous river catchment, *Geomorphology* **197**, 64-75.

Dahlke, H. E., Lyon, S. W., Stedinger, J. R., Rosqvist, G. and Jansson, P. 2012. Contrasting trends in floods for two sub-arctic catchments in northern Sweden – does glacier presence matter*?* *Hydrology and Earth System Sciences* **16**, 2123-2141.

Das, S.B., Joughin, I., Behn, M.D., Howat, I.M., King, M.A., Lizarralde, D., and Bhatia, M.P. 2008. Fracture Propagation to the Base of the Greenland Ice Sheet During Supraglacial Lake Drainage. *Science* **320**, 778-781.

Dauvalter, V. and Rognerud, S. 2001. Heavy metal pollution in sediments of the Pasvik River drainage. *Chemosphere* **42** (1), 9-18.

Dewart, G. 1966. Moulins on Kaskawulsh Glacier, Yukon Territory. *Journal of Glaciology* **6** (44), 320-321.

de Woul, M. and Hock, R. 2005. Static mass-balance sensitivity of Arctic glaciers and ice caps using a degree-day approach. *Annals of Glaciology* **42** (1), 217–224.

de Woul, M., Hock, R., Braun, M., Thorsteinsson, T., Jóhannesson, T. and Halldórsdóttir, S. 2006. Firn layer impact on glacial runoff: a case study at Hofsjökull, Iceland. *Hydrological Processes* **20** (10), 2171-2185.

Dyurgerov, M. and Meier, M. 1999. Analysis of winter and summer glacier mass balances. *Geografiska Annaler. Series A. Physical Geography* **81** (4), 541–554.

Eriksson, M., Björnsson, H., Herzfeld, U. C., and Holmlund, P. 1993. The bottom topography of Storglaciären: a new map based on old and new ice depth measurements, analysed with geostatistical methods. *Forskningsrapport* STOU-NG 95, Department of Physical Geography, Stockholm University, Stockholm.

Escher-Vetter, H. 2000. Modelling meltwater production with a distributed energy balance method and runoff using a linear reservoir approach – results from Vernagtferner, Oetzal Alps, for the ablation seasons 1992 to 1995. *Zeitschrift für Gletscherkunde and Glazialgeologie* **36**, 119-150.

Etienne, J., Glasser, N.F. and Hambrey, M.J. 2003. Proglacial Sediment—Landform Associations of a Polythermal Glacier: Storglaciären, Northern Sweden. *Geografiska Annaler. Series A. Physical Geography* **85** (2), 149–164.

Evenson, E.B. and Clinch, J.M., 1987. Debris transfer mechanisms of active Alpine glaciers: Alaskan case studies. In: K. Kugansuu and M. Saarnisto (Eds.), *INQUA Till Symposium, Finland 1985. Geological Survey of Finland Special Paper* **3**, 111–136.

Fausto, R.S., Mernild, S.H., Hasholt, B., Ahlstrøm, A.P. and Knudsen, N.T. 2012. Modeling suspended sediment concentration and transport, Mittivakkat Glacier, Southeast Greenland. *Arctic, Antarctic, and Alpine Research* **44** (3), 306-318.

Fenn, C.R. and Gomez, B. 1989. Particle size analysis of the suspended sediment in a proglacial stream: Glacier de Tsidjiore Nouve, Switzerland. *Hydrological Processes* **3**, 123-135.

Flowers, G.E. 2008. Subglacial modulation of the hydrograph from glacierized basins. *Hydrological Processes* **22** (19), 3903–3918.

Fountain, A. 1989. The storage of water in, and hydraulic characteristics of, the firn of South Cascade Glacier, Washington State USA. *Annals of Glaciology* **13**, 69–75.

Fountain, A.G. 1992. Subglacial water flow inferred from stream measurements at South Cascade Glacier, Washington, U.S.A. *Journal of Glaciology* **38** (128), 1–14.

Fountain, A.G. 1993. Geometry and flow conditions of subglacial water at South Cascade Glacier, Washington State, U.S.A. *Journal of Glaciology* **39**, 143–156.

Fountain, A. 1996. Effect of snow and firn hydrology on the physical and chemical characteristics of glacial runoff. *Hydrological Processes* **10** (4), 509–521.

Fountain, A.G. and Tangborn, W.V. 1985. The effect of glaciers on streamflow variations, *Water Resources Research* **21** (4), 579-586.

Fountain, A. and Walder, J. 1998. Water flow through temperate glaciers. *Reviews of Geophysics* **36** (3), 299–328.

Fountain, A.G., Jacobel, R.W., Schlichting, R. and Jansson, P. 2005. Fractures as the main pathways of water flow in temperate glaciers. *Nature* **433** (7026), 618–621.

Fowler, A.C. 1984. On the transport of moisture in polythermal glaciers. *Geophysics, Astrophysics and Fluid Dynamics* **28**, 99-140.

Gee, D.G. 1975. A tectonic model for the central part of the Scandinavian Caledonides. *American Journal of Science* **275A**, 468-515.

González, J., Melching, C. & Oberg, K. 1996. Analysis of open-channel velocity measurements collected with an acoustic Doppler current profiler. *Proceedings from the 1st International Conference on New/Emerging Concepts for Rivers* - RiverTech96, IWRA, Chicago, Illinois, **2**, 838–845.

Goodfellow, B., Stroeven, A. P., Hättestrand, C., Kleman, J., Jansson, P. 2008. Deciphering a non-glacial/glacial landscape mosaic in the northern Swedish mountains. *Geomorphology* **93** (3-4), 213–232.

Gordon, S., Sharp, M., Hubbard, B., Smart, C., Ketterling, B. and Willis, I. 1998. Seasonal reorganization of subglacial drainage system of Haut Glacier d'Arolla, Valais, Switzerland, inferred from measurements in boreholes, *Hydrological Processes* **12**, 105 - 133.

Greenspan Analytical, 2007. Turbidity Sensor TS100 User Manual. 3rd Edition, 26pp.

Gregory, K. J. and Walling, D. E. 1973. *Drainage Basin Form and Process: A geomorphological approach*. Edward Arnold, London.

Gulley, J. D., and Benn, D.I. 2007, Structural control of englacial drainage systems in Himalayan debris-covered glaciers. *Journal of Glaciology* **53**, 299-312.

Gulley, J.D., Benn, D.I., Müller, D. and Luckman, A. 2009. A cut-and-closure origin for englacial conduits in uncrevassed regions of polythermal glaciers. *Journal of Glaciology* **55** (189), 66-79.

Gulley, J. D., Grabiec, M., Martin, J. B., Jania, J., Catania, G. and Glowacki, P. 2012. The effect of discrete recharge by moulins and heterogeneity in flow-path efficiency at glacier beds on subglacial hydrology. *Journal of Glaciology* **58** (211), 926-940.

Gurnell, A.M. 1982. The dynamics of suspended sediment concentration in an Alpine pro-glacial stream network. In: Hydrological aspects of alpine and high mountain areas. Proceedings of the Exeter Symposium, July 1982. *International Association of Hydrological Sciences Publication* **138**, 319-30.

Gurnell, A.M. 1983. Downstream channel adjustments in response to water abstraction for hydro-electric power generation from alpine glacial melt-water streams. *The Geographical Journal* **149**, 342-354.

Gurnell, A.M. 1987. Suspended sediment. In: *Glaciofluvial Sediment Transfer: An Alpine Perspective* (Ed. Gurnell, A.M. & Clark, M.J.), 305-354. Wiley, Chichester, UK.

Gurnell, A.M. 1993. How many reservoirs? An analysis of flow recessions from a glacier basin. *Journal of Glaciology* **39**, 409-414.

Gurnell, A. M. 1995. Sediment yield from alpine glacier basins. In: *Sediment and Water Quality in River Catchments* (Ed. Foster, I. D. L., Gurnell, A. M. and Webb, B. W.) 407-435, Wiley, Chichester, U.K.

Gurnell, A.M. and Fenn, C.R., 1984. Box-Jenkins transfer function models applied to suspended sediment concentration–discharge relationships in a proglacial stream. *Arctic and Alpine Research* **16**, 93-106.

Gurnell, A.M. and Warburton, J. 1990. The significance of suspended sediment pulses for estimating suspended sediment load and identifying suspended sediment sources in Alpine glacier basins. *Hydrology in Mountainous Regions I. Hydrological Measurements; The Water Cycle. Lausanne Symposia*, **1**, 463–470.

Gurnell, A.M., Clark, M.J. and Hill, C.T. 1990. The geomorphological impact of modified river discharge and sediment transport regimes downstream of hydropower scheme meltwater intake structures. *International Association of Hydrological Sciences Publication* **194**, 165-170.

Gurnell, A. M., Clark, M. J., Tranter, M., Brown, G. H. and Hill, C. T. 1991. Alpine glacier hydrology inferred from a proglacial river monitoring programme. *Proceedings of the British Hydrological Society National Symposium* **5**, 9-5.

Gurnell, A. M., Clark, M. J. and Hill, C. T. 1992. Analysis and interpretation of patterns within and between hydroclimatological time series in an Alpine glacier basin. *Earth Surface Processes and Landforms* **17**, 821-829.

Gurnell, A. M., Hodson, A., Clark, M. J., Bogen, J., Hagen, J. O. and Tranter, M. 1994. Water and sediment discharge from glacier basins: an arctic and alpine comparison. In *Variability in Stream Erosion and Sediment Transport*. Symposium at Canberra. *International Association of Hydrological Sciences Publication* **224**, 325-334.

Gusmeroli, A. 2010. Polythermal glacier dynamics at Storglaciären, Arctic Sweden, inferred using in situ geophysical techniques. Unpublished PhD Thesis, University of Swansea, UK.

Gusmeroli, A., Murray, T., Jansson, P., Pettersson, R., Aschwanden, A. and Booth, A. D. 2010. Vertical distribution of water within the polythermal Storglaciären, Sweden. *Journal of Geophysical* Research F. Earth Surface **115** (F04002). doi: 10.1029/2009JF001539.

Haag, I. and Westrich, B. 2002. Processes governing river water quality identified by principal component analysis. *Hydrological Processes* **16** (16), 3113–3130.

Hagen, J.O., Kohler, J., Melvold, K. and Winther, J.G. 2003. Glaciers in Svalbard: mass balance, runoff and freshwater flux. *Polar Research* **22** (2), 145-159.

Haakensen, N. 1986. Glacier mapping to confirm results from mass-balance measurements. *Annals of Glaciology* **8**, 73-77.

Haeberli, W., Cihlar, J., and Barry, R. 2000. Glacier monitoring within the global climate observing system. *Annals of Glaciology* **31**, 241 – 246.

Haefeli, R. 1970. Changes in the behaviour of the Unteraargletscher in the last 125 years. *Journal of Glaciology* **16**, 205-217.

Hallet, B., and Anderson, R.S. 1980. Detailed glacial geomorphology of a proglacial bedrock area at Castleguard Glacier, Alberta, Canada. *Zeitschrift fur Gletscherkunde und Glazialgeologie* **16**, 171-183.

Hallet, B., Hunter, L., and Bogen, J. 1996, Rates of erosion and sediment evacuation by glaciers: A review of field data and their implications: *Global and Planetary Change* **12**, 213–235.

Hambrey, M.J. 1977. Supraglacial drainage and its relationship to structure, with particular reference to Charles Rabots Bre, Okstindan, Norway. *Norsk Geografisk Tidsskrift* **31**, 69-78.

Hammer, K.M. and Smith, N.D. 1983. Sediment production and transport in a proglacial stream: Hilda Glacier, Alberta, Canada. *Boreas* **12** (2), 91-106.

Hannah, D., Gurnell, A.M. & McGregor, G. 1999. A methodology for investigation of the seasonal evolution in proglacial hydrograph form. *Hydrological Processes* **13** (16), 2603–2621.

Hannah, D. M., Smith, B. P. G., Gurnell, A. M. and McGregor, G. R. 2000. An approach to hydrograph classification. *Hydrological Processes* **14** (2), 317–338.

Hannah, D. and Gurnell, A.M. 2001. A conceptual, linear reservoir runoff model to investigate melt season changes in cirque glacier hydrology. *Journal of Hydrology* **246** (1-4), 123–141.

Harbor, J., Warburton, J. 1993. Relative rates of glacial and nonglacial erosion in alpine environments. *Arctic and Alpine Research* **25** (1), 1-7.

Harper, J.T. and Humphrey, N.F. 1995. Borehole video analysis of a temperate glacier's englacial and subglacial structure: implications for glacier flow models. *Geology* **23**, 901-904.

Hibsch, G. (1979). Abfluβmodelle für vergletscherte Einzugsgebiete, dargestellt am Beispeil des Vernagtferners. *Sonderforschungsberiech* **81** TU München, Vortragsveranstaltung 26.6.79, 5-26.

Hock, R. 2005. Glacier melt: a review of processes and their modelling. *Progress in Physical Geography* **29** (3), 362.

Hock, R. and Hooke, R.LeB. 1993. Evolution of the internal drainage system in the lower part of the ablation area of Storglaciären, Sweden. *Bulletin of the Geological Society of America* **105** (4), 537.

Hock, R. and Jansson, P. 2005. Modelling glacier hydrology. In: Anderson, M. (Ed), *Encyclopaedia of Hydrological Sciences*. 2647-2655.

Hock, R., Iken, A. and Wangler, A. 1999. Tracer experiments and borehole observations in the over- deepening of Aletschgletscher, Switzerland, *Annals of Glaciology* **28**. 253-260.

Hock, R., Jansson, P. and Braun, L.N., 2005. Modelling the response of mountain glacier discharge to climate warming. In: Huber, U.M., Bugmann, H.K.M. and Reasoner, M.A. (Eds). Global Change and Mountain Regions. Springer, Dordrecht. 243–252.

Hock, R. and Noetzli, C. 1997. Areal melt and discharge modelling of Storglaciären, Sweden. *Annals of Glaciology* **24**, 211–216.

Hodgkins, R. 1996. Seasonal trend in suspended-sediment transport from an Arctic glacier, and implications for drainage-system structure. *Annals of Glaciology* **22**, 147–151.

Hodgkins, R. 1997. Glacier hydrology in Svalbard, Norwegian high arctic. *Quaternary Science Reviews* **16** (9), 957–973.

Hodgkins, R. 1999. Controls on suspended-sediment transfer at a High-Arctic glacier, determined from statistical modelling. *Earth Surface Processes and Landforms* **24** (1), 1–21.

Hodgkins, R. 2001. Seasonal evolution of meltwater generation, storage and discharge at a non-temperate glacier in Svalbard. *Hydrological Processes* **15** (3), 441–460.

Hodgkins, R. 2011. Sediment transfer modelling. In: Singh, V.P., Singh, P. and Haritashya, U.K. (Eds). *Encyclopaedia of Snow, Ice and Glaciers*. Springer, 659pp.

Hodgkins, R., Hagen, J. O., Hamran, S. E. 1999. Twentieth-century mass balance and thermal regime change at Scott Turnerbreen Svalbard. *Annals of Glaciology* **28** (1), 216-220.

Hodgkins, R., Cooper, R., Wadham, J. and Tranter, M. 2003. Suspended sediment fluxes in a high-Arctic glacierised catchment: implications for fluvial sediment storage. *Sedimentary Geology* **162** (1-2), 105–117.

Hodgkins, R., Cooper, R., Tranter, M. and Wadham, J. 2013. Drainage-system development in consecutive melt seasons at a polythermal, Arctic glacier, evaluated by flow-recession analysis and linear-reservoir simulation. *Water Resources Research* **49**, 1-14.

Hodson, A. J., Gurnell, A. M., Washington, R., Tranter, M., Clark, M. J. and Hagen, J. O. 1998. Meteorological and runoff time-series characteristics in a small, high-Arctic glaciated basin, Svalbard. *Hydrological Processes* **12** (3), 509–526.

Hodson, A.J. and Ferguson, R. 1999. Fluvial suspended sediment transport from cold and warm-based glaciers in Svalbard. *Earth Surface Processes and Landforms* **24** (11), 957–974.

Holmlund, P. and Hooke, R. LeB. 1983. High water-pressure events in moulins, Storglaciären, Sweden. *Geografiska Annaler* **65A** (1-2), 19-25.

Holmlund, P. 1987. Mass balance of Storglaciären during the 20th century. *Geografiska Annaler. Series A. Physical Geography* **69** (3), 439–447.

Holmlund, P. 1988a. An application of two theoretical melt water drainage models on Storglaciären and Mikkaglaciären, Northern Sweden. *Geografiska Annaler. Series A. Physical Geography* **70**, 1–7.

Holmlund, P. 1988b. Internal geometry and evolution of moulins. Storglaciären, Sweden. *Journal of Glaciology* **34**, 242–248.

Holmlund, P. 1988c. Is the longitudinal profile of Storglaciären, northern Sweden, in balance with the present climate? *Journal of Glaciology* **34** (118), 269–273.

Holmlund, P. and Eriksson, M. 1989. The Cold Surface Layer on Storglaciären. *Geografiska Annaler. Series A, Physical Geography* **71** (3/4), 241-244.

Holmlund, P. and Jansson, P. 1999. The Tarfala mass balance program. *Geografiska. Annaler Series A. Physical Geography* **81** (4), 621–631.

Holmlund, P., Karlén, W. and Grudd, H. 1996a. Fifty years of mass balance and glacier front observations at the Tarfala Research Station. *Geografiska Annaler. Series A. Physical Geography* **78** (2), 105–114.

Holmlund, P., Burman, H. and Rost, T., 1996b. Sediment-mass exchange between turbid meltwater streams and proglacial deposits of Storglaciaren, northern Sweden. *Annals of Glaciology* **22**, 1–5.

Holmlund, P. and Jansson, P. 2002. Glaciological Research at Tarfala Research Station. ISBN 91-7540-141x. 48.

Holmlund, P., Jansson, P. and Pettersson, R. 2005. A re-analysis of the 58 year mass-balance record of Storglaciaren, Sweden. *Annals of Glaciology* **42** (1),.389–394.

Hooke, R.LeB. 1984. On the role of mechanical energy in maintaining subglacial water conduits at atmospheric pressure. *Journal of Glaciology* **30** (105), 180–187.

Hooke, R. LeB. 1989. Englacial and subglacial hydrology: a qualitative review. *Arctic and Alpine Research* **21** (3), 221-233.

Hooke, R. LeB. 1991. Positive feedbacks associated with erosion of glacial cirques and overdeepenings. *Geological Society of America Bulletin* **103** (8), 1104-1108.

Hooke, R. LeB., Gould, J.E. and Brozozowski, J. 1983. Near-surface temperatures near and below the equilibrium line on polar and subpolar glaciers. *Zeitschrift fiir Gletscherkunde und Glazialgeologie* **19**, 1-25.

Hooke, R. LeB., Holmlund, P. and Iverson, N.R. 1987. Extrusion flow demonstrated by borehole deformation measurements over a riegel, Storglaciären, Sweden. *Journal of Glaciology* **33** (113), 72–78.

Hooke, R. LeB., Wold, B., and Hagen, J.O. 1985. Subglacial hydrology and sediment transport at Bondhusbreen, southwest Norway. *Geological Society of America Bulletin* **96** (3), 388-397.

Hooke, R. LeB., Miller, S. & Kohler, J. 1988. Character of the englacial and subglacial drainage system in the upper part of ablation area of Storglaciären, Sweden. *Journal of Glaciology* **34**, 117.

Hooke, R. LeB. & Pohjola, V. A. 1994. Hydrology of a segment of a glacier situated in an overdeepening, Storglaciaren, Sweden. *Journal of Glaciology* **40** (134), 140–148.

Hubbard, B. and Nienow, P. 1997. Alpine subglacial hydrology. *Quaternary Science Reviews* **16**, 939- 955.

Hubbard, B., Sharp, M., Willis, I., Nielsen, M. and Smart, C. 1995. Borehole water-level variations and the structure of the subglacial drainage system of Haut Glacier d'Arolla, Valais, Switzerland, *Journal of Glaciology* **41** (139), 572 – 583.

Hudson, P.F. 2003. Event sequence and sediment exhaustion in the lower Panuco Basin, Mexico. *Catena* **52**, 57-76.

Huggel, C. 2009. Recent extreme slope failures in glacial environments: effects of thermal perturbation. *Quaternary Science Reviews* **28**, 1119–1130.

Humphrey, N., Raymond, C.F. & Harrison, W.D. 1986. Discharges of turbid water during mini-surges of Variegated Glacier, Alaska. *Journal of Glaciology* **32** (111), 195–207.

Huss, M., Farinotti, D., Bauder, A. and Funk, M. 2008. Modelling runoff from 69 highly glacierized alpine drainage basins in a changing climate. *Hydrological Processes* **22**, 3888-3902.

Iken, A. and Bindschadler, R.A. 1986. Combined Measurements of Subglacial Water Pressure and Surface Velocity of Findelengletscher, Switzerland: Conclusions about Drainage System and Sliding Mechanism. *Journal of Glaciology* **32** (110) 101-119.

IPCC (Intergovernmental Panel on Climate Change). 1996. *Climate Change 1995*, Chapter 6: Climate models – projections of future climate. Cambridge University Press, Cambridge, U.K. 572.

IPCC (Intergovernmental Panel on Climate Change). 2001. *Climate Change 2001: The scientific basis*. Houghton, J. T., Ding, Y., Griggs, D. J., Noguer, M., Van der Linden, P. J., Dai, X., Maskell, K. and Johnson, C. A. (Eds). Cambridge University Press, Cambridge, 881.

Irvine-Fynn, T.D.L., Moorman, B.J., Sjogren, D., Walter, F. S. A., Willis, I. C., Hodson, A. J., Williams, J. L. M., Mumford, P. N. 2005a. Cryological processes implied in Arctic proglacial stream sediment dynamics using principal components analysis and regression. *Geological Society London Special Publications* **242** (1), 83.

Irvine-Fynn, T.D.L., Moorman, B.J., Willis, I., Sjogren, D., Hodson, A. J., Mumford, P. N., Walter, F. S. A., Williams, J. L. M. 2005b. Geocryological processes linked to High Arctic proglacial stream suspended sediment dynamics: examples from Bylot Island, Nunavut, and Spitsbergen, Svalbard. *Hydrological Processes* **19** (1), 115–135.

Irvine-Fynn, T.D.L. 2008. *Modelling runoff from the maritime Arctic cryosphere: Water storage and routing at Midtre Lovénbreen*. Unpublished Ph.D. Thesis, University of Sheffield. 359.

Jansson, P. 1995. Water pressure and basal sliding on Storglaciären, northern Sweden. *Journal of Glaciology* **41** (138), 232–240.

Jansson, P. 1996. Dynamics and hydrology of a small polythermal valley glacier. *Geografiska Annaler. Series A. Physical Geography* **78** (2), 171–180.

Jansson, P. 1997. Longitudinal coupling in ice flow across a subglacial ridge. *Annals of Glaciology* **24**, 169–174.

Jansson, P. and Hooke, R. LeB. 1989. Short-term variations in strain and surface tilt on Storglaciaren, Kebnekaise, Northern Sweden. *Journal of Glaciology* **35**, 120.

Jansson, P., Jacobson, D. and Hooke, R. LeB. 1993. Playa areas in southern California and adjacent part of Nevada. *Earth Surfaces Processes and Landforms* **18** (2), 109–119.

Jansson, P., Richardson, C. and Jonsson, S. 1999. Assessment of requirements for cirque formation in northern Sweden. *Annals of Glaciology* **28**, 16–22.

Jansson, P**.,** Hock, R. and Schneider, T. 2003. The concept of glacier storage – A review. *Journal of Hydrology* **282** (1–4), 116–129.

Jansson, P., Rosqvist, G. and Schneider, T., 2005. Glacier fluctuations, suspended sediment flux and glacio-lacustrine sediments. *Geografiska Annaler. Series A. Physical Geography* **87** (1), 37–50.

Jansson, P. and Pettersson, R. 2007. Spatial and temporal characteristics of a long mass balance record, Storglaciären, Sweden. *Arctic, Antarctic, and Alpine Research* **39** (3), 432–437.

Jansson, P. and Näslund, J.O. 2009. *Spatial and temporal variations in glacier hydrology on Storglaciären, Sweden*. SKB TR-09-13, Swedish Nuclear Waste management Company. 53 pp.

Jolliffe, I. T. 1990. Principle components analysis: A beginners guide I: introduction and application. *Weather* **45**, 375-382.

Jolliffe, I. T. 1993. Principle components analysis: A beginners guide II: pitfalls, myths and extensions. *Weather* **48**, 246-253.

Jones, H. and Arnold, N. 1999. Modelling the entrainment and transport of suspended sediment in subglacial hydrological systems. *Glacial Geology and Geomorphology* **rp09**, 1-19.

Jonsell, U., Hock, R. and Holmgren, B. 2003. Spatial and temporal variations in albedo on Storglaciaren, Sweden. *Journal of Glaciology* **49** (164), 59–68.

Kamb, B. 1987. Glacier surge mechanism based on linked cavity configuration of the basal water conduit system. *Journal of Geophysical Research* **92**, 9083-9100.

Kamb, B., Raymond, C.F., Harrison, W.D., Engelhardt, H.F., Echelmeyer, K.A., Humphrey, N., Brugman, M.M. and Pfeffer, T. 1985. Glacier surge mechanism: 1982-1983 surge of Variegated Glacier, Alaska. *Science* **227**, 469-479.

Kane, D. L., McNamara , J. P., Yang, D., Olsson, P. Q. and Gieck, R. E. 2003. An extreme rainfall/runoff event in Arctic Alaska. *Journal of Hydrometeorology* **4** (6), 1220-1228.

Keiler, M., Knight, J., and Harrison, S. 2013. Climate change and geomorphological hazards in the eastern European Alps. *Philosophical Transactions of the Royal Society A*. **368** (1919), 2461-2479.

Kemp, P., Sear, D., Collins, A., Naden, P. and Jones, I. 2011. The impacts of fine sediment on riverine fish. *Hydrological Processes* **25**, 1800–1821.

Kirkbride, M.P. (1995). Processes of transportation. In: J. Menzies (Ed.), *Modern Glacial Environments: Processes, Dynamics and Sediments*. Butterworth–Heinemann, Oxford, 261–292

Kleman, J. and Stroeven, A.P. 1997. Preglacial surface remnants and Quaternary glacial regimes in northwestern Sweden. *Geomorphology* **19** (1-2), 35-54.

Klok, E.J., Jasper, K., Roelofsma, K.P., Gurtz, J. and Badoux, A. 2001. Distruibuted hydrological modelling of a heavily glaciated Alpine river basin. *Hydrological Sciences Journal* **46** (4), 553-570.

Knight, J. and Harrison, S. 2012. Evaluating the impacts of global warming on geomorphological systems. *AMBIO: A Journal of the Human Environment* **41** (2), 206-210.

Knighton, A.D. 1981. Channel form and flow characteristics of supraglacial streams, Austre Okstindbreen, Norway. *Arctic and Alpine Research* **13** (3), 295-306.

Knighton, A.D. 1985. Channel form adjustment in supraglacial streams, Austre Okstindbreen, Norway. *Arctic and Alpine Research* **17** (4), 451-466.

Koblet, T., Gärtner-Roer, I., Zemp, M., Jansson, P., Thee, P., Haeberli, W., Holmlund, P. 2010. Reanalysis of multi-temporal aerial images of Storglaciären, Sweden (1959–99)–Part 1: Determination of length, area, and volume changes. *The Cryosphere* **4**, 333–343.

Kohler, J., 1995. Determining the extent of pressurized flow beneath Storglaciären, Sweden, using results of tracer experiments and measurements of input and output discharge. *Journal of Glaciology* **41** (138), 217–231.

Krause, P., Boyle, D. and Bäse, F. 2005. Comparison of different efficiency criteria for hydrological model assessment. *Advances in Geosciences* **5**, 89-97.

Lang, H. 1967. Relations between glacier runoff and meteorological factors observed on and outside the glacier. IUGG General Assembly, International

Association of Scientific Hydrology: *International Association of Hydrological Sciences Publication* **79**, 429-439.

Lang, H. 1973. Variations in the relation between discharge and meteorological elements. *International Association of Hydrological Sciences Publication* **95**, 85-96.

Lang, H. 1987. Forecasting meltwater runoff from snow-covered areas and from glacier basins. In: Kraijenhoff, D. A. and Moll, J.R. (Eds.), *River Flow Modelling and Forecasting*, Reidel, Dordrecht, 99–127

Lawler, D., McGregor, G. and Phillips, I. 2003. Influence of atmospheric circulation changes and regional climate variability on river flow and suspended sediment fluxes in southern Iceland. *Hydrological Processes* **17** (16), 3195–3223.

Lawson, D. E. 1993. Glaciohydrologic and glaciohydraulic effects on runoff and sediment yield in glacierized basins, Monogram 93-2, 108 pp., Cold Regions Research and Engineering Laboratory, U.S. Army Corps of Engineers, Hanover, New Hampshire.

Lecce, S.A. 1993. *Fluvial response to spatial and temporal variations of stream power, Blue River, Wisconsin*. Unpublished PhD Thesis, Department of Geography, University of Wisconsin, Madison, WI, 244 pp.

Le Coz, J., Pierrefeu, G., and Paquier, A. 2008. Evaluation of river discharges monitored by a fixed side-looking Doppler profiler. *Water Resources Research* **44**, W00D09, doi:10.1029/2008WR006967.

Leistøl, O. 1967. Storbreen glacier in Jotunheimen, Norway. *Norsk Polarinstitutt Skrifter* **141**. 63pp.

Lipiatou, E. and Saliot, A. 1991. Hydrocarbon contamination of the Rhone delta and western Mediterranean. *Marine Pollution Bulletin* **22** (6), 297-304.

Lliboutry, L. 1968. General theory of subglacial cavitation and sliding of temperate glaciers. *Journal of Glaciology* **7**, 21-58.

Lliboutry, L. 1971. Permeability, brine content and temperature of temperate ice, *Journal of Glaciology* **10**, 15–30.

Lliboutry, L.A. 1983. Modifications to the theory of intraglacial waterways f or the case of subglacial ones. *Journal of Glaciology* **29** (102), 216-26.

Lliboutry, L. 1996. Temperate ice permeability, stability of water veins and percolation of internal meltwater. *Journal of Glaciology*, **42** (141), 201-211.

Lukas, S., Nicholson, L.I., Ross, F.H. and Humlum, O. 2005. Formation, meltout processes and landscape alteration of High-Arctic ice-cored moraines – examples from Nordenskiöld Land, central Spitsbergen. *Polar Geography* **29** (3), 157-187.

MacDonald, D.D., Ingersoll, C.G., Smorong, D.E., Lindskoog, R.A., Sparks, D.W., Smith, J.R., Simon, T.P. and Hanacek, M.A. 2002. An assessment of injury to sediments and sediment-dwelling organisms in the Grand Calumet River and Indiana Harbor area of concern, USA. *Archives of Environmental Contamination and Toxicology* **43** (2), 141-155.

Marren, P. 2005. Magnitude and frequency in proglacial rivers: a geomorphological and sedimentological perspective. *Earth-Science Reviews* **70** (3-4), 203–251.

Marsh, P. 2005. Water flow through snow and firn. In: Anderson, M.G.(Ed). *The Encyclopedia of Hydrological Sciences*. Volume 4. John Wiley & Sons, Ltd. Chichester. Meier, M. F. and Tangborn, W. V. 1961. Distinctive characteristics of glacier runoff. *U.S. Geological Survey Professional Paper* **424B**, 14–16

Marsh, P. and Woo, M. 1984. Wetting front advance and freezing of meltwater within a snow cover: 1. Observations in the Canadian Arctic. *Water Resources Research* **20** (12), 1853.

Marston, R.A. 1983. Supraglacial stream dynamics on the Juneau Icefield. *Annals of the Association of American Geographers* **73**, 597-608.

Meehl, G.A., Stocker, T.F., Collins, W.D., Friedlingstein, P., Gaye, A.T., Gregory, J.M., Kitoh, A., Knutti, R., Murphy, J.M., Noda, A., Raper, S.C.B., Watterson, I.G., Weaver,

A.J. and Zhao, Z.-C. 2007. Global Climate Projections. In 'Climate Change 2007: The Physical Science Basis. Contribution of Working Group I to the Fourth Assessment Report of the Intergovernmental Panel on Climate Change'. (Eds Solomon, S., Qin, D., Manning, M., Chen, Z., Marquis, M., Averyt, K.B., Tignor, M., and Miller, H.L.). 747-845. Cambridge University Press: Cambridge, United Kingdom and New York, NY, USA.

Moore, R.D. 1993. Application of a conceptual streamflow model in a glacierized drainage basin. *Journal of Hydrology* **150**, 151-168.

Moore, P. L., Iverson, N. R., Brugger, K. A., Cohen, D., Hooyer, T. S., Jansson, P. 2011. Effect of a cold margin on ice flow at the terminus of Storglaciären, Sweden: implications for sediment transport. *Journal of Glaciology* **57** (201), 77–87.

Munro, D. S. and Young, G. J. 1982. An operational net shortwave radiation model for glacier basins. *Water Resources Research* **18** (2), 220.

Navratil, O., Evrard, O., Esteves, M., Legout, C., Ayrault, S., Némery, J., Mate-Marin, A., Ahmadi, M., Lefèvre, I., Poirel, A. and Bonté, P. 2012. Temporal variability of suspended sediment sources in an alpine catchment combining river/rainfall monitoring and sediment fingerprinting. *Earth Surface Processes and Landforms* **37**, 828–846.

Nienow P. 1997. Hydrological influences on basal flow dynamics in valley glaciers. *Final report, NERC Research Fellowship GT5/93/AAPS/1*.

Nienow, P., Sharp, M., and Willis, I. 1998. Seasonal changes in the morphology of the subglacial drainage system, haut Glacier d'Arolla, Switzerland. *Earth Surface Processes and Landforms* **23** (9), 825–843.

Nihei, Y., and Kimizu, A. 2008. A new monitoring system for river discharge with horizontal acoustic Doppler current profiler measurements and river flow simulation. *Water Resources Research* **44**, W00D20, doi: 10.1029/2008WR006970.

Nilsson, J. and Sundblad, B. 1975. The internal drainage of Storglaciären and Isfallsglaciären described by an autoregressive model. *Geografiska Annaler* **57A** (1-2), 73-98.

Nye, J.F. 1953. The flow law of ice from measurements in glacier tunnels, laboratory experiments, and the Jungfraufirn borehole experiment. *Proceedings of the Royal Society of London A.* **219** (1139), 477-89.

Nye, J. F. 1970. Glacier sliding without cavitation in a linear viscous approximation, *Proceedings of the Royal Society London A.* **315**, 381– 403.

Nye, J.F., 1973. Water flow at the bed of glaciers. *International Association of Hydrological Sciences Publication* **95**, 189-194.

Nye, J.F. 1976. Water flow in glaciers: jökulhlaups, tunnels and veins. *Journal of Glaciology* **17** (76), 181–207.

Nye, J.F. and Frank, F.C. 1973. Hydrology of the intergranular veins in a temperate glacier. *International Association of Hydrological Sciences Publication* **95**, 157-161.

Oerlemans, J. 2000. Analysis of a 3 year meteorological record from the ablation zone of Morteratschgletscher, Switzerland: energy and mass balance. *Journal of Glaciology* **46** (155), 571–579.

Oerter, H., Baker, D., Moser, H., and Reinwarth, O. 1981. Glacial-hydrological investigations at the Vernagtferner Glacier as a basis for a discharge model. *Nordic Hydrology* **12** (4), 335–348.

Orwin, J. F. and Smart, C. C. 2004. Short-term spatial and temporal patterns of suspended sediment transfer in proglacial channels, small River Glacier, Canada. *Hydrological Processes* **18** (9), 1521–1542.

Östling, M. and Hooke, R.L. 1986. Water storage in Storglaciären, Kebnekaise, Sweden. *Geografiska Annaler* **68A**, 279-29.

Østrem, G. 1973. Runoff forecasts for highly glacierized basins. In: *The Role of Snow and Ice in Hydrology*. Proceedings of Banff symposium, September 1972: International Association of Hydrological Sciences Publication **107** (2), 1111-1132

Østrem, G. 1975. Sediment Transport in glacial meltwater streams. In Jopling, A. V. and MacDonald, B. C. (Eds.), *Glaciofluvial and Glaciolacustrine Sedimentation,* Society of Economic Palaeontologists and Mineralogists Special Publication **23**, 101-122.

Østrem, G. and Olsen, H.C. 1987. Sedimentation in a glacier lake. *Geografiska Annaler* **69A** (1), 123-138.

Østrem, G. and Brugman, M. 1991. Glacier mass-balance measurements. A manual for field and office work. *National Hydrology Research Institute (NHRI) Publication Science Report **4***. Saskatoon, Canada.

Østrem, G. and Haakensen, N. 1999. Map comparison or traditional mass-balance measurements: which method is better? *Geografiska Annaler: Series A, Physical Geography* **81** (4), 703-711.

Owens, P. N., Batalla, R. J., Collins, A. J., Gomez, B., Hicks, D. M., Horowitz, A. J., Kondolf, G. M., Marden, M., Page, M. J., Peacock, D. H., Petticrew, E. L., Salomons, W. and Trustrum, N. A. 2005. Fine-grained sediment in river systems: environmental significance and management issues. *River Research and Applications* **21**, 693–717.

Padhy, M.K. and Saini, R.P. 2008. A review on silt erosion in hydro turbines. *Renewable and Sustainable Energy Reviews* **12** (7), 1974-1987.

Pälli, A., Moore, J.C., Jania, J., Kolondra, L. and Glowacki, P. 2003. The drainage pattern of Hansbreen and Werenskioldbreen, two polythermal glaciers in Svalbard. *Polar Research* **22** (2), 355-371.

Paterson, W. S. B. 1994. *The Physics of Glaciers*, 3rd Ed. Pargamon, Oxford.

Pattyn, F. 2008. Investigating the stability of subglacial lakes with a full Stokes model. *Journal of Glaciology* **54** (185), 353-361.

Pettersson, R., Jansson, P. and Holmlund, P. 2003. Cold surface layer thinning on Storglaciären, Sweden, observed by repeated ground penetrating radar surveys. *Journal of Geophysical Research. F. Earth Surface* **108** (F1), 6004.

Pettersson, R., Jansson, P., Huwald, H., Blatter, H. 2007. Spatial pattern and stability of the cold surface layer of Storglaciären, Sweden. *Journal of Glaciology* **53** (180), 99–109.

Petticrew, E.L. and Rex, J.F. 2006*. The importance of temporal changes in gravel-stored fine sediment on habitat conditions in a salmon spawning stream. In: Sediment Dynamics and the Hydromorphology of Fluvial Systems* (Eds. Rowan, J.S., Duck, R.W., and Werritty, A.) *International Association of Hydrological Sciences Publication* **306,** 434-441.

Pohjola, V. A. 1994. TV-video observations of englacial voids in Stroglaciaren, Sweden. *Journal of Glaciology* **40** (135), 231-240.

Porter, P., Vatne, G., NG, F., Irvine-Fynn, T. D. L. 2010. Ice-marginal sediment delivery to the surface of a high-Arctic glacier: Austre Brøggerbreen, Svalbard. *Geografiska Annaler. Series A. Physical Geography* **92** (4), 437–449.

Radić, V. and Hock, R. 2006. Modeling future glacier mass balance and volume changes using ERA-40 reanalysis and climate models: A sensitivity study at Storglaciären, Sweden. *Journal of Geophysical research* **111** (F03003). doi:10.1029/2005JF000440.

Raymond, C.F. and Harrison, W.D. 1975. Some observations on the behaviour of the liquid and gas phases in temperate glacier ice. *Journal of Glaciology* **14**, 213-233.

Raymond, C. F., Benedict, R. J., Harrison, W. D., Echelmeyer, K. A. and Sturn, M. 1995. Hydrological discharges and motion of Fels and Black Rapids Glaciers, Alaska, USA: implications for the structure of their drainage systems. *Journal of Glaciology* **41**, 290-304.

Repp, K. 1988. The Hydrology of Bayelva, Spitsbergen. Nordic Hydrology. Ribstein, P. *et al*., 1995. Tropical climate and glacier hydrology: a case study in Bolivia. *Journal of Hydrology* **165** (1-4), 221–234.

Richards, K. S. 1984. Some observations on suspended sediment dynamics in Storbregrova, Jotunheim', *Earth Surface Processes and Landforms* **9**, 101-112.

Richards, K. S., Sharp, M., Arnold, N., Gurnell, A., Clark, M., Tranter, M., Nienow, P., Brown, G., Willis, I., Lawson, W. 1996. An integrated approach to modelling hydrology and water quality in glacierized catchments. *Hydrological Processes* **10** (4), 479–508.

Rippin, D., Willis, I., Arnold, N., Hodson, A., Moore, J., Kohler, J. and Bjornsson, H. 2003. Changes in geometry and subglacial drainage of Midre Lovenbreen, Svalbard, determined from digital elevation models. *Earth Surface Processes and Landforms* **28** (3), 273-298.

Robin, G. de Q. 1974. Depth of water filled crevasses that are closely spaced. *Journal of Glaciology* **16**, 543

Röthlisberger, H. 1972. Water pressure in intra- and subglacial channels. *Journal of Glaciology* **11**, 177-203.

Röthlisberger, H. and Lang, H. 1987. Glacial hydrology. In *Glacio-fluvial Sediment Transfer: An Alpine Perspective.* Eds: Gurnell, A.M. and Clark, M.J. 207-284. Wiley, Chichester.

Rose, K.C., Hart, J.K. and Martinez, K. 2009. Seasonal changes in basal conditions at Briksdalsbreen, Norway: the winter-spring transition. *Boreas* **38**, 579-590.

Rudberg, P. 2013. Sweden's evolving hydropower sector: Renovation, restoration and concession change. *Stockholm Environment Institute Project Report* **2013-01**. 46pp.

Rutter, N. 2002. Subglacial water storage in an Alpine glacier: Including hydrometeorological and glaciological influences on flooding in Alpine glacierised basins. Unpublished PhD Thesis, University of Oxford, UK.

Rutter, N., Hodson, A., Irvine-Fynn, T. and Solås, M.K. 2011. Hydrology and hydrochemistry of a deglaciating high-Arctic catchment, Svalbard. *Journal of Hydrology* **410**, 39-50.

Sawada, M. & Johnson, P. 2000. Hydrometeorology, suspended sediment and conductivity in a large glacierized basin, Slims River, Yukon Territory, Canada (1993-94). *Arctic* **53** (2), 101.

Schneider, T. and Bronge, C. 1996. Suspended sediment transport in the Storglaciären drainage basin. *Geografiska Annaler. Series A. Physical Geography* **78** (2), 155–161.

Schuler, T. and Fischer, U.H., 2009. Modeling the diurnal variation of tracer transit velocity through a subglacial channel. *Journal of Geophysical Research F. Earth Surface* **114** (F4), F04017.

Schytt, V. 1947. Glaciologiska arbeten i Kebnekajse. *Ymer* **67** (1), 118-142.

Schytt, V. 1968. Notes on glaciological activities in Kebnekaise, Sweden during 1966 and 1967. Geografiska Annaler **50A** (2), 111-120.

Seaberg, S. Z., Seaberg, J. Z., Hooke, R. LeB. and Wiberg, D. W. 1988. Character of the englacial and subglacial drainage system in the lower part of the ablation area of Storglaciären, Sweden, as revealed by dye-trace studies. *Journal of Glaciology* **34**, 217–227.

Sear, D. A. 1993. Fine sediment infiltration into gravel spawning beds within a regulated river experiencing floods: Ecological implications for salmonids. *Regulated Rivers: Research and Management* **8**, 373–390.

Shreve, R., 1972. Movement of water in glaciers. *Journal of Glaciology* **11** (62), 205–214.

Shreve, R. L. 1985. Esker characteristics in terms of glacier physics, Katahdin esker system, Maine, *Geological Society of America Bulletin* **96**, 639–646.

Solyom, Z., Andréasson, P. G. and Johansson, I. 1979. Geochemistry of amphibolites from Mt. Sylarna, Central Scandinavian Caledonides. *Geologiska Föreningens i Stockholm Förhandlingar* **101**, 17-25.

SonTek YSI, 2002. Argonaut Internal Flow Theoretical Modeling Firmware Ver. 9.0, SonTek/YSI. San Diego, California.

SonTek YSI, 2007. Argonaut Acoustic Doppler Current Meter, Technical Documentation. SonTek/YSI, San Diego, California.

Span, N. and Kuhn, M. 2003. Simulating annual glacier flow with a linear reservoir model. *Journal of Geophysical Research* **108** (D10), 4313, doi:10.1029/2002JD002828.

Statham, I. 1977. *Earth Surface Sediment Transport*. Clarendon Press, Oxford, UK, 184.

Stenborg, T. 1965. Problems concerning winter run-off from glaciers. *Geografiska Annaler. Series A. Physical Geography* **47A** (3), 141–184.

Stenborg, T. 1968. Glacier drainage connected with ice structures. *Geografiska Annaler* **50A** (1), 25-53.

Stenborg, T. 1969. Studies of the internal drainage of glaciers. *Geografiska Annaler. Series A. Physical Geography*, **51A** (1-2), 13–41.

Stenborg, T. 1973. Some viewpoints on the internal drainage of glaciers. *International Association of Scientific Hydrology Publication* **95** (Hydrology of Glaciers). 117-129.

Stott, T. and Mount, N., 2007. Alpine proglacial suspended sediment dynamics in warm and cool ablation seasons: Implications for global warming. *Journal of Hydrology* **332** (3-4), 259–270.

Swift, D.A., Nienow, P.W., Spedding, N., and Hoey, T.B. 2002. Geomorphic implications of subglacial drainage configuration: rates of basal sediment evacuation controlled by seasonal drainage system evolution. *Sedimentary Geology* **149**, 5-19

Swift, D.A., Nienow, P. W., Hoey, T. B., Mair, D. W. F. 2005. Seasonal evolution of runoff from Haut Glacier d'Arolla, Switzerland and implications for glacial geomorphic processes. *Journal of Hydrology* **309** (1-4), 133-148.

Synergy Software, 2010. *Kaleidagraph* (4th Edition), Synergy Software, Reading, Pennsylvania.

Syvitski, J.P.M. (Ed.). 1991. *Principles, Methods and Application of Particle Size Analysis*. Cambridge: Cambridge University Press.

Tangborn, W., Krimmel, R. and Meier, M. 1975. A comparison of glacier mass balance by glaciological, hydrological and mapping methods, South Cascade Glacier, Washington. *International Association of Hydrological Sciences* Publication **104**, 185–196.

Theakstone, W. and Knudsen, N. 1981. Dye tracer tests of water movement at the glacier Austre Okstindbreen, Norway. *Norsk Geografisk Tidsskrift-Norwegian Journal of Geography* **35** (1), 21–28.

Tranter, M. and Raiswell, R. 1991. The composition of the englacial and subglacial components in bulk meltwaters draining the Gornergletscher, *Journal of Glaciology* **125**, 59-66.

van der Veen, C.J. 1998. Fracture mechanics approach to penetration of bottom crevasses on glaciers. *Cold Regions Science and Technology* **27**, 213-223.

van de Wal, R.S.W., Oerlemans, J. and van der Hage, J. 1992. A study of ablation variations on the tongue of Hintereisferner, Austrian Alps. *Journal of Glaciology* **38** (130), 319–324.

van de Wal, R.S.W. and Russell, A.J. 1994. A comparison of energy balance calculations, measured ablation and meltwater runoff near Søndre Strømfjord, West Greenland. *Global Planetary Change* **9** (1/2), 29-38.

Vatne, G., 2001. Geometry of englacial water conduits, Austre Brøggerbreen, Svalbard. *Norsk Geografisk Tidsskrift* **55**, 24-33.

Vatne, G., Etzelmüller, B., Ødegård, R. and Sollid. J. L. 1992. Water-budget and glaciofluvial sediment transfer of a subpolar glacier, Erikbreen. Svalbard. *Stuttgarter Geographische Studien **117**,* 253-266.

Vatne, G., Etzelmüller, B., Ødegård, R.S. and Sollid, J.L. 1996. Meltwater routing in a high arctic glacier: Hannabreen, northern Spitsbergen. *Norsk Geografisk Tidsskrift*, **50**, 67-74.

Vincent, C., E. LeMeur, D. Six, P. Possenti, E. Lefebvre, and M. Funk. 2007. Climate warming revealed by englacial temperatures at Col du Dome (4250 m, Mont Blanc area), *Geophysical Research Letters* **34**. doi: 10.1029/2007GL029933.

Walder, J.S., and Hallet, B. 1979. Geometry of former subglacial water channels and cavities. *Journal of Glaciology* **23** (89), 335-346.

Walling, D.E. 1974. Suspended sediment and solute yields from a small catchment prior to urbanization. In: *Fluvial Processes in Instrumented Watersheds* (Ed. Gregory, K.J. & Walling, D.E.). Institute of British Geography Special Publication **6**, 169-192.

Walling, D. E. 1995. Suspended sediment yields in a changing environment. In: Gurnell, A.M., Petts, G.E. (Eds.), *Changing River Channels*. Wiley, Chichester, 149–176.

Walling, D.E., Owens, P.N., and Leeks, G.J.L. 1999. Fingerprinting suspended sediment sources in the catchment of the River Ouse, Yorkshire, UK. *Hydrological Processes* **13** (7), 955-975.

Ward, J. H. 1963. Hierarchical groupings to optimize an objective function. *Journal of the American Statistical Society* **58**, 236-244.

Weertman, J. 1969. Water lubrication mechanism of glacier surges, *Canadian Journal of Earth Science* **6**, 929–942.

Weertman, J. 1972. General theory of water flow at the base of a glacier or ice sheet. *Reviews of Geophysics and Space Physics* **10**, 287-333.

Weertman, J. 1973. Can a water filled crevasse reach the bottom surface of a glacier. *International Association of Hydrological Sciences Publication* **95,** 139-145.

Willis I.C., Sharp, M.J., Richards, K.S. 1993. Studies of the water balance of Midtdalsbreen, Hardangerjøkulen, Norway. II. Water storage and runoff prediction. *Zeitschrift für Gletscherkunde und Glazialgeologie* **27/28,** 117–138.

Willis, I. 2005. Hydrology of glacierised basins. In: Anderson, M. G. and McDonnal, J. J. (Eds) *Encyclopaedia of Hydrological Sciences*. Wiley, Chichester. UK.

Willis, I. and Bonvin, J. M. 1995. Climate change in mountain environments. *Geography* **80** (3), 247–261.

Willis, I., Richards, K.S. and Sharp, M.J. 1996. Links between proglacial stream suspended sediment dynamics, glacier hydrology and glacier motion at Midtdalsbreen, Norway. *Hydrological Processes* **10** (4), 629–648.

Willis, I., Arnold, N. and Brock, B. 2002. Effect of snowpack removal on energy balance, melt and runoff in a small supraglacial catchment. *Hydrological Processes* **16** (14), 2721–2749.

Wood, P.J. and Armitage, P.D. 1997. Biological effects of fine sediment in the lotic environment. *Environmental Management* **21** (2), 203-217.

Zemp, M., Jansson, P., Holmlund, P., Gärtner-Roer, I., Koblet, T., Thee, P., Haeberli, W. 2010. Reanalysis of multi-temporal aerial images of Storglaciären, Sweden

(1959–99)–Part 2: Comparison of glaciological and volumetric mass balances. *The Cryosphere* **4**, 345–357.

Zimmerer, S. 1987. A study of the englacial and subglacial hydrology of Storglaciären, northern Sweden. Unpublished M.Sc. Dissertation. Department of Geology and Geophysics, University of Minnesota, USA.

Zimmermann, A. and Church, M. 2001. Channel morphology, gradient profiles and bed stresses during flood in a step-pool channel. *Geomorphology* **40**, 311–327.

Zwally, H.J., Abdalati, W., Herring, T., Larson, K., Saba, J. and Steffen, K. 2002. Surface melt-induced acceleration of Greenland Ice-Sheet flow. *Science* **297**, 218-222.